Complete electroweak $\mathcal{O}(N_c^2)$ two-loop contributions to the Higgs boson masses in the MSSM and aspects of two-loop renormalisation

Dissertation

zur Erlangung des Doktorgrades
an der Fakultät für Mathematik,
Informatik und Naturwissenschaften
Fachbereich Physik
der Universität Hamburg

vorgelegt von

Daniel Meuser

aus

Heinsberg, Deutschland

Hamburg

2023

Gutachter/innen der Dissertation:	Prof. Dr. Georg Weiglein Prof. Dr. Geraldine Servant
Zusammensetzung der Prüfungskommission:	Prof. Dr. Georg Weiglein Prof. Dr. Geraldine Servant Prof. Dr. Michael Potthoff Prof. Dr. Timo Weigand Prof. Dr. Christian Schwanenberger
Vorsitzende/r der Prüfungskommission:	Prof. Dr. Michael Potthoff
Datum der Disputation:	23.08.2023
Vorsitzender Fach-Promotionsausschuss PHYSIK:	Prof. Dr. Günter H. W. Sigl
Leiter des Fachbereichs PHYSIK:	Prof. Dr. Wolfgang J. Parak
Dekan der Fakultät MIN:	Prof. Dr.-Ing. Norbert Ritter

Zusammenfassung

Das MSSM ist eine der vielversprechendsten Erweiterungen des SM. Im MSSM können die Massen der Higgs-Bosonen in Abhängigkeit der anderen Modellparameter vorhergesagt werden. In dieser Arbeit untersuchen wir zum ersten Mal die vollen elektroschwachen Zwei-Schleifen-Beiträge der $\mathcal{O}\left((\alpha_{\text{em}} + \alpha_q)^2 N_c^2\right)$ zu den Massen der MSSM Higgs-Bosonen unter Benutzung eines Feynman-diagrammatischen Ansatzes und unter voller Berücksichtigung der Abhängigkeit vom externen Impuls. Wir erwarten, dass diese Korrekturen den dominanten Anteil der noch fehlenden Zwei-Schleifen-Korrekturen ausmachen. Da wir auf $\mathcal{O}\left(N_c^2\right)$ arbeiten, zerfallen die relevanten Zwei-Schleifen-Selbstenergien in Produkte von Ein-Schleifen-Integralen, was es uns erlaubt, die analytische Struktur der Selbstenergien detailliert zu studieren.
Um endliche Werte für die Vorhersage der Higgs-Boson-Massen zu erhalten, renormieren wir den Higgs-Eich-Sektor des MSSM auf dem Zwei-Schleifen-Niveau und den Quark-Squark-Sektor auf dem Ein-Schleifen-Niveau für den allgemeinen Fall komplexer Modellparameter. Wir erweitern eine häufig verwendete Relation zwischen Zwei-Schleifen-Massencountertermen von skalaren Bosonen und Vektorbosonen auf den Fall nicht verschwindender elektroschwacher Eichkopplungen und zu allen Ordnungen der Störungstheorie. Dies ist ein wesentlicher Bestandteil für die Renormierung der neutralen und geladenen Higgs-Boson-Selbstenergien.
Wir vergleichen OS und $\overline{\text{DR}}$ Renormierungsschemata für $\tan(\beta)$, das Verhältnis der Vakuumerwartungswerte. Wir untersuchen, wie die Wahl des Renormierungsschemas das Auftreten von $\mathcal{O}(\varepsilon)$-Teilen von Schleifenintegralen in der Vorhersage für die Higgs-Boson-Masse beeinflusst. Aus dieser Analyse können wir ableiten, unter welchen Bedingungen Berechnungen mit unterschiedlichen Renormierungsschemata mittels einer einfachen Reparametrisierung miteinander verglichen werden können.
In unserer numerischen Analyse vergleichen wir die neuen Korrekturen mit bereits bekannten Zwei-Schleifen-Beiträgen und der experimentellen Unsicherheit der Masse des beobachteten Higgs-Bosons. Wenngleich die neu berechneten Beiträge kleiner als die bereits bekannten Zwei-Schleifen-Anteile sind, so sind sie in ihrer Größe mit der experimentellen Unsicherheit vergleichbar. In einem Szenario mit starker Teilchen-Mischung können die Effekte von generationsmischenden Beiträgen sogar die experimentelle Unsicherheit um eine Größenordnung übersteigen. Dies unterstreicht die Relevanz der bisher noch nicht bekannten Terme der elektroschwachen Zwei-Schleifen-Beiträge.

Abstract

The MSSM is one of the most promising extensions of the SM. In the MSSM, the masses of the Higgs bosons can be predicted in terms of the other model parameters. In this thesis, we calculate for the first time the full electroweak two-loop contributions of $\mathcal{O}\Big((\alpha_{\text{em}} + \alpha_q)^2 N_c^2\Big)$ to the MSSM Higgs boson masses using a Feynman-diagrammatic approach including the full dependence on the external momentum. These corrections are expected to constitute the dominant part of the two-loop corrections that were still missing up to now. As a consequence of working at $\mathcal{O}\Big(N_c^2\Big)$, the relevant two-loop self-energies decompose into products of one-loop integrals, allowing us to study the analytic structure of the self-energies and their renormalisation in detail.

In order to get finite values for the Higgs boson mass prediction, we renormalise the Higgs-gauge sector of the MSSM at the two-loop level and the quark-squark sector at the one-loop level for the general case of complex input parameters. We extend a well-known relation between two-loop mass counterterms of scalar and vector bosons to the case of non-vanishing electroweak gauge couplings and to all orders in perturbation theory. This is a crucial ingredient for the renormalisation of the neutral and charged Higgs boson self-energies.

We compare OS and $\overline{\text{DR}}$ renormalisation schemes for $\tan(\beta)$, the ratio of the vacuum expectation values. We examine how the choice of renormalisation scheme affects the appearance of $\mathcal{O}(\varepsilon)$ parts of loop integrals in the Higgs boson mass prediction. From this analysis, we infer under which conditions calculations with different renormalisation schemes can be compared with each other using a simple reparametrisation.

In our numerical analysis, the new corrections are compared against already known two-loop contributions and the experimental uncertainty of the mass of the observed Higgs boson. While smaller than the already known two-loop parts, the new terms are comparable in size to the experimental uncertainty. In a scenario with strong particle mixing, the effects of generation-mixing contributions can exceed the experimental uncertainty by an order of magnitude. This underlines the relevance of the so-far unknown electroweak two-loop contributions.

Contents

1 Introduction **1**

2 Regularisation and renormalisation **5**

2.1 Regularisation 6

2.1.1 Wick rotation 6

2.1.2 Cut-off regularisation 8

2.1.3 Pauli-Villars regularisation 8

2.1.4 Dimensional regularisation 9

2.1.5 Dimensional reduction 10

2.1.6 Other regularisation schemes 11

2.2 Renormalisation 12

2.2.1 On-shell renormalisation 12

2.2.2 General momentum-subtraction scheme 15

2.2.3 Minimal subtraction schemes 16

2.3 Minimal subtraction schemes at the two-loop level 20

2.3.1 Defining the $\widetilde{\text{DR}}$ renormalisation scheme 21

2.3.2 Defining the $\overline{\text{DR}}$ renormalisation scheme at higher orders . . . 25

3 The pole mass of a particle **27**

3.1 The Feynman propagator and vertex functions 28

3.1.1 Correlation functions 28

3.1.2 Generating functionals 31

3.1.3 Two-point function and propagator at higher orders 33

3.2 Calculating the pole mass 34

3.2.1 Unstable particles and the complex pole 34

3.2.2 Particle mixing and the vertex function matrix 36

3.2.3 The fixed-order method 37

3.2.4 The fixed-point iteration 38

4 Renormalisation of the MSSM **41**
4.1 The quark and squark sector of the MSSM 41
4.1.1 Tree-level 42
4.1.2 Renormalisation at the one-loop level 45
4.1.3 $\overline{\text{DR}}$ renormalisation of μ and A_q 51
4.2 The Higgs and gauge sector of the MSSM 53
4.2.1 Tree-level 53
4.2.2 Renormalisation at the one-loop level 59
4.2.3 Renormalisation at the two-loop level 68
4.3 Renormalisation of $\tan(\beta)$ 76
4.3.1 The DCPR scheme 77
4.3.2 $\overline{\text{DR}}$ renormalisation via the AZ transition 78
4.3.3 OS renormalisation via the decay $A \to \tau^-\tau^+$ 79

5 Calculation of electroweak $\mathcal{O}\left(N_c^2\right)$ terms to the Higgs boson masses **87**
5.1 Current status of the MSSM Higgs boson mass prediction 88
5.2 The structure of the self-energies 90
5.3 Algebraic calculation of the two-loop self-energies 93
5.4 The cancellation of $\mathcal{O}(\varepsilon)$ parts of one-loop integrals and counterterms 97

6 Algebraic expressions for the leading $\mathcal{O}(N_c)$ one-loop terms **103**
6.1 The gaugeless limit and further approximations 104
6.2 The leading one-loop contributions to the neutral Higgs-boson self-energies 105
6.3 The difference between the $\mathcal{CP}$-odd and the charged self-energy in the cMSSM 109

7 Numerical analysis of the full electroweak $\mathcal{O}\left(N_c^2\right)$ two-loop results **111**
7.1 Scenario 1: The dependence of M_h on the scale M_S for $A_q = 0$ 115
7.2 Scenario 2: The dependence of M_h on the scale M_S for $A_q = -2M_S$. 118
7.3 Scenario 3: The dependence of M_h on the trilinear coupling A_q 122
7.4 Scenario 4: The dependence of M_H on the SUSY scale M_S 126
7.5 Scenario 5: The Higgs boson masses in the M_h^{125} scenario with strong mixing 130

8 Conclusions and outlook **135**

A One- and two-loop field and parameter counterterms **141**
A.1 One-loop counterterms . . . 141
A.1.1 One-loop mass counterterms . . . 141
A.1.2 One-loop field counterterms . . . 142
A.1.3 One-loop DR counterterms at $\mathcal{O}(N_c)$ . . . 143
A.2 Two-loop counterterms . . . 144
A.2.1 Two-loop mass counterterms . . . 144
A.2.2 Two-loop field counterterms . . . 146

B Slavnov-Taylor identities for scalar-vector mixing **147**

C Renormalisation of the mass M_W **149**
C.1 Calculating the pole mass M_W . . . 149
C.2 The on-shell counterterms . . . 151

D One-loop integrals **153**
D.1 Definitions . . . 153
D.2 Reducing the integrals . . . 155
D.2.1 The scalar integrals . . . 155
D.2.2 The B_0' function . . . 156
D.2.3 The tensor coefficients . . . 157
D.3 Analytic formulae for A_0 and the massless B_0 . . . 159

E The package `ColorSimp.m` **161**

F Generation of plots **163**

Bibliography **167**

1 Introduction

In 2012, a scalar particle with a mass of approximately 125 GeV has been discovered at the *Large Hadron Collider* (LHC) at the *European Organisation for Nuclear Research* (CERN) [1–3]. The observed properties of this particle are in agreement with the properties of the Higgs boson predicted by the *Standard Model of Particle Physics* (SM) within the current experimental and theoretical uncertainties [4–6]. The combination of most recent measurements yields an observed Higgs boson mass of $M_h = 125.25 \pm 0.17$ GeV [7]. While this observation elucidates the mechanism through which the massive vector bosons and charged fermions obtain a mass, there are still many open questions with respect to the nature of *electroweak symmetry breaking* (EWSB) that are left to be answered.

Despite its great success, the Standard Model is not without shortcomings; it e.g. fails to provide a suitable *Dark Matter* (DM) candidate. The existence of Dark Matter, while not proven by direct-detection experiments, is widely accepted. It is therefore desirable that a more complete theory of Nature should provide a candidate particle for Dark Matter.

Moreover, the Standard Model describes neutrinos as massless, weakly interacting particles. It has been experimentally observed that neutrinos oscillate whilst propagating through space-time. For neutrinos to be able to oscillate, they need to be massive. As we know from experimentally determined upper bounds, their masses are much smaller than the masses of the other SM particles. So far, the origin of neutrino masses is unclear.

The Standard Model also fails to explain the *baryon asymmetry of the Universe*, the observed overabundance of matter over antimatter in the Universe. For a model to be able to explain the baryon asymmetry, baryon number violation and $\mathcal{CP}$-symmetry violation must be present, and the Universe must have been out of thermal equilibrium for the period of baryogenesis. While the SM provides sources for baryon number violation as well as $\mathcal{CP}$-symmetry violation, the latter is far too weak to describe the observations correctly. The SM also lacks a strong first-order phase transition for the observed value of the Higgs boson mass, which could otherwise put the early Universe out of thermal equilibrium.

From a theoretical point of view, it is appealing to regard the Standard Model as a low-energy version of a more fundamental theory, like for instance a *Grand Unified Theory* (GUT). A GUT is a theory which combines the electroweak and the strong force into a single, unified force. In a GUT, the gauge couplings take the same value at a high energy scale M_X, the GUT scale. This feature is called the *gauge coupling unification*. In the SM, the running gauge couplings g, g' and g_s do not unify at a high energy scale.

The fermion and gauge boson masses of the Standard Model are protected from receiving large radiative corrections by chiral and gauge symmetry, respectively. For the scalar SM Higgs boson, however, no such symmetry exists. While not a problem within the Standard Model itself, we know that it can at most be valid up to the Planck scale ($M_P \approx 10^{19}$ GeV) since it does not incorporate gravity. Once a more complete theory introduces new physics at e.g. the aforementioned GUT scale or the Planck scale (both considerably larger than the observed Higgs boson mass), the lack of symmetry protection for the Higgs boson becomes an issue. Quantum corrections will drive the unprotected Higgs boson mass to the highest energy scale in the theory. This discrepancy between the Planck scale and the observed value of the Higgs boson mass, which is of the same order of magnitude as the electroweak scale, is known as the *hierarchy problem*.

A commonly studied extension of the SM is the *Minimal Supersymmetric Standard Model* (MSSM) [8,9]. *Supersymmetry* (SUSY) is a space-time symmetry whose generators transform bosons into fermions and vice versa. As a consequence, the MSSM contains a SUSY partner for each SM particle, differing in spin by $\frac{1}{2}$. If supersymmetry was an exact symmetry of Nature, the SM particles and their superpartners would be mass degenerate. No superpartners of known particles have been observed so far, so supersymmetry cannot be exact. In the MSSM, the supersymmetry breaking is soft and explicit.

The MSSM addresses many of the aforementioned problems of the SM. If R-parity is conserved, the *lightest supersymmetric particle* (LSP) is stable and can hence provide a candidate for Dark Matter. The introduction of additional particles alters the running of the gauge couplings in such a way that they take a very similar value at the same energy scale, hinting at the MSSM arising from a GUT. Furthermore, supersymmetry protects the Higgs boson mass from obtaining large loop corrections due to a cancellation taking place between bosonic and fermionic degrees of freedom. Naturally, the MSSM cannot address all of the aforementioned problems of the SM. It should also be noted that the issues listed above are not a full account of the Standard Model's shortcomings.

The MSSM is a *two-Higgs-doublet model* (2HDM) with five physical Higgs bosons, three neutral ones and a charged pair. At the tree-level, the Higgs boson masses are fully determined by (experimentally known) SM parameters and two additional parameters, one of which is a Higgs boson mass. The remaining MSSM Higgs boson masses can therefore be predicted. In the SM, on the other hand, no such prediction is possible as the Higgs boson mass is an input parameter of the theory.
The tree-level mass of the lightest MSSM Higgs boson is bounded from above by the mass of the Z boson [10] ($M_Z \approx 91$ GeV), and it is therefore not in agreement with the observed value. The large size of the quantum corrections shifts the predicted value closer to the observed one, rendering a precision calculation crucial in order to profit from the high experimental accuracy. Predicting the masses of the MSSM Higgs bosons and restricting the parameter space of the theory to match experimental observations provides an important test of the model. For this reason, the prediction of the MSSM Higgs boson masses is the focal point of this thesis.
In an interacting, four-dimensional theory, the full pole mass of a particle cannot be calculated without approximations. For this reason, different limiting cases and methods have to be used in order to make a prediction for the MSSM Higgs boson masses. For a SUSY scale M_S not much larger than the electroweak scale, the calculation of Higgs boson self-energies in terms of *Feynman diagrams* (FD) in a (sufficiently high) fixed order of perturbation theory yields a reliable result [11–80]. For a large SUSY scale, the appearance of large logarithms spoils the accuracy of the prediction. These large logarithms are resummed by making use of the *renormalisation group* (RG) in a so-called *effective field theory* (EFT) [31, 32, 81–127]. The hybrid approach combines the FD ansatz with the EFT method by interpolating the predictions for intermediate values of M_S [90, 111, 115, 128–139]. An overview of the different approaches is given in Ref. [140].
In this thesis, we pursue a Feynman-diagrammatic approach with focus on electroweak two-loop terms of the form $\mathcal{O}\Big((\alpha_{\text{em}} + \alpha_q)^2 N_c^2\Big)$, where α_{em} is the fine-structure constant, and α_q is any product of the top and bottom Yukawa couplings. N_c is the number of quark colours in the theory. The gauge group of the MSSM is $\text{SU}(3)_c \times \text{SU}(2)_L \times \text{U}(1)_Y$ and hence identical to the SM gauge group; the number of colours is $N_c = 3$. We take into account the full momentum dependence of the self-energies, allowing for a prediction in the case of large mixing between the lowest-order mass eigenstates as well. For the first time, we perform a two-loop prediction including pure gauge contributions in combination with an on-shell renormalisation scheme. We expect these contributions to be the dominant electroweak corrections beyond the ones that are already known.

To obtain the desired contributions, we have to perform a complete renormalisation of the MSSM Higgs-gauge sector at the two-loop level under the full inclusion of electroweak effects. This leads to more complicated relations between the two-loop counterterms in comparison to what has been encountered up to now. These relations have to be taken into account in order to obtain a finite result in the general case where the fine-structure constant is kept non-vanishing. From our analysis of the structure of the two-loop self-energies, we can infer under which conditions two calculations can be compared by employing a simple reparametrisation. We will also show that our newly calculated contributions are larger than the experimental uncertainty of the mass of the observed Higgs boson, and hence they should be included in any prediction in order to further improve the theoretical precision.

This thesis is structured as follows: In Ch. 2, we recall the well-known concepts of regularisation and renormalisation, and we explain how a minimal subtraction scheme can consistently be defined at the two-loop order. We introduce the most important quantities appearing in a pole mass calculation at the beginning of Ch. 3. Subsequently, we define the pole mass also in the presence of particle mixing and for the case of unstable particles. We conclude the chapter by comparing the fixed-order method and the fixed-point iteration, which are used to determine a particle pole mass, in the case of two-particle mixing.

In Ch. 4, we discuss the renormalisation of the quark-squark sector and the Higgs-gauge sector of the MSSM at the one- and two-loop level, respectively. We provide an overview of the renormalised expressions for all relevant self-energies and we explain the renormalisation of each parameter and field entering our calculation. In particular, we derive an on-shell renormalisation prescription for the MSSM parameter $\tan(\beta)$. We discuss the analytical structure of our self-energies at the beginning of Ch. 5. Subsequently, we give an overview of the programs and codes we used, and we explain how the computation was performed at each step. We conclude the chapter by analysing how the choice of renormalisation scheme influences which parts of loop integrals enter the final prediction. This is important in understanding under which circumstances calculations with different renormalisation schemes can be compared with each other using a simple reparametrisation.

In Ch. 6, we give analytical expressions for the leading one-loop m_t^4 contributions to the MSSM Higgs boson masses for the case of complex parameters. In Ch. 7, we investigate how our newly calculated contributions influence the Higgs boson mass prediction in five different MSSM scenarios. We compare their size with already known contributions as well as with the experimental uncertainty of the Higgs boson mass. We sum up the results of this thesis and draw our conclusions in Ch. 8.

2 Regularisation and renormalisation

We start this chapter by briefly summarising the well-established concepts of regularisation and renormalisation. Subsequently, we will motivate a prescription which allows us to introduce a separate renormalisation scale for each parameter which is defined in a minimal subtraction scheme.

A quantum field theory (QFT) is a framework that combines quantum mechanics [141–143] and special relativity [144, 145] with classical field theory methods. Quantum field theories in four space-time dimensions cannot be solved exactly, so different approximations need to be performed in order to carry out a calculation in the model discussed in the present work. A very common approach is the so-called perturbative expansion. Thereby, the interaction part of the theory's Lagrangian is treated as a perturbation to the free, non-interacting theory. As long as the coupling constants in the theory are sufficiently small, this approximation allows for the accurate prediction of physical observables. Such a calculation is usually organised in terms of Feynman diagrams, which provide a nice visual representation of the perturbative expansion. Hence, we also refer to the perturbative approach as the Feynman-diagrammatic (FD) approach.

Typically, the lowest order prediction for an observable is obtained from a tree-level amplitude.[1] In diagrams contributing to such an amplitude, the momentum of each internal propagator is fully determined by the momenta of the external particles.

At higher orders of perturbation theory, diagrams contain propagators whose momenta are undetermined; we integrate over these momenta, which potentially leads to a divergent expression. If these singularities stem from high-energy momenta, we call them "ultraviolet" (UV) divergence; we call them "infrared" (IR) if they arise from the integrand's behaviour at the lower bound of integration. While IR divergences drop out in a sufficiently inclusive calculation, UV divergences are treated by renormalising the parameters (and in general also the fields) of the theory. To this end, we distinguish between the "bare" and the renormalised value of a parameter. The renormalised parameters can be related to physical observables and so they are finite quantities; the bare parameters absorb the infinities from the divergent loop

[1] There are exceptions, such as the decay of a Higgs boson into two photons; its lowest order contribution starts at the one-loop level.

integrals and are, therefore, divergent quantities themselves. We call the difference between the bare and the renormalised value the parameter's counterterm, which typically diverges as well.
To obtain meaningful expressions for the aforementioned divergent quantities, the theory has to be regularised before the renormalisation can be carried out. It is advantageous in this context if the regularisation prescription respects the symmetries of the theory. Therefore, several different types of regularisation are used in practice depending on the theory considered.

2.1 Regularisation

The idea of regularisation is to make the divergent part of an amplitude mathematically meaningful by introducing a *regulator*, or "cut-off". In the case of integration over loop momenta, this can for example be done by adding an artificial upper limit of integration. We are now able to assign an analytic expression to the divergent integral, allowing us to perform subtractions and other algebraic manipulations with it. This is necessary, as otherwise subtracting infinite expressions from one another is not a well-defined mathematical operation. In the prediction of a physical observable, all divergences need to cancel. After this cancellation has happened, the regulator is removed, yielding the final expression for the considered quantity.
At first glance, this seems to allow for a wide variety of different regularisation schemes. In most cases, however, it is convenient to choose a regularisation that as much as possible preserves the symmetries of the theory as it avoids the need for symmetry-restoring counterterms, resulting in a small set of regularisation schemes employed in practice. We will introduce the most important ones used in perturbative calculations in the following.

2.1.1 Wick rotation

In a general one-loop integral, we integrate over the four components of a four-vector $(q^\mu) = (q^0, \vec{q})$. Each component takes values in the interval $(-\infty, +\infty)$ and so the Minkowski inner product $q^2 \equiv \eta_{\mu\nu} q^\mu q^\nu$ is indefinite. To make use of the well-established techniques of multi-dimensional Euclidean integrals, we perform a so called *Wick rotation*. Let us consider the one-loop integral

$$\int \mathrm{d}^4 q \, \frac{f(q^2)}{q^2 - m^2 + \mathrm{i}\epsilon}, \tag{2.1}$$

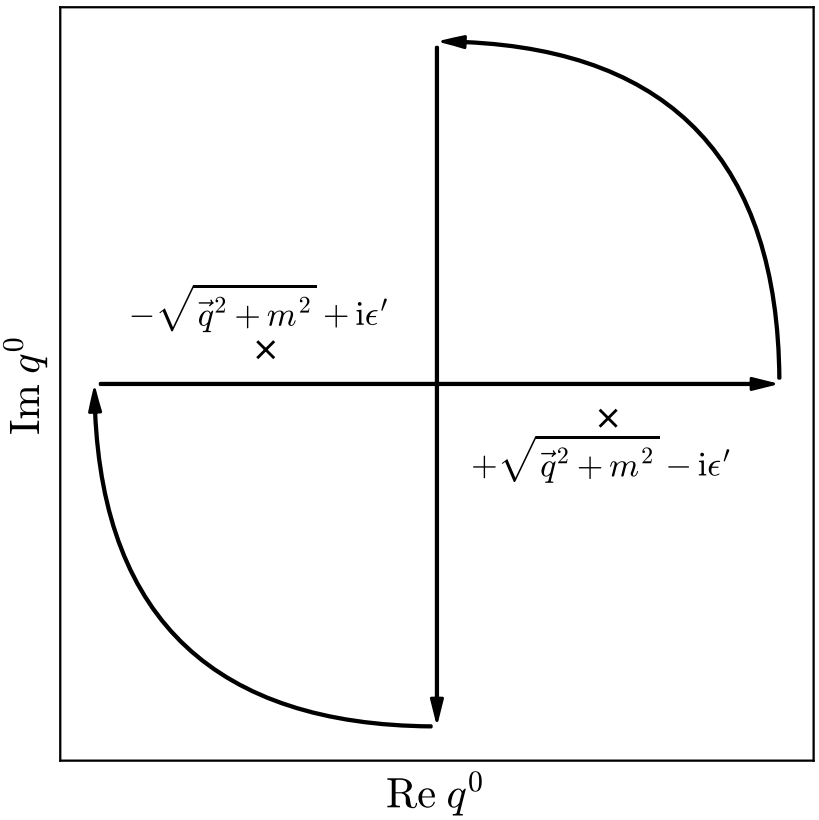

Figure 2.1: The Wick contour integral in the complex q^0 plane. The two crosses denote the location of the complex poles of the integrand in Eq. (2.1). $\epsilon' > 0$ is a regulator like ϵ but with a different mass dimension.

where f is a holomorphic function of the Lorentz scalar q^2 and $\epsilon > 0$ is an infinitesimally small quantity that is included to give the correct Feynman propagator prescription. In the following, the limit $\epsilon \to 0$ is always implied. The Wick rotation is simply a change of variables

$$(q_E^m) = \begin{pmatrix} q_E^0 \\ \vec{q_E} \end{pmatrix} \equiv \begin{pmatrix} -\mathrm{i}q^0 \\ \vec{q} \end{pmatrix}. \tag{2.2}$$

The Euclidean scalar product

$$q_E^2 \equiv q_E^m q_E^m = (q_E^0)^2 + \vec{q_E} \cdot \vec{q_E} = -(q^0)^2 + \vec{q} \cdot \vec{q} = -q^2 \tag{2.3}$$

is a positive-definite quantity in terms of the new variables q_E^0 and $\vec{q_E}$.
Let us consider the q^0 direction of the four-dimensional integral in Eq. (2.1). We close the q^0-integration contour in the complex plane as shown in Fig. 2.1. The contour is chosen such that the poles lie in the exterior of the curve. By virtue of Cauchy's residue theorem, the contour integral vanishes. Since the integration along

the two quarter circles does not contribute, we find

$$\int_{-\infty}^{+\infty} \mathrm{d}q^0 \, \frac{f(q^2)}{q^2 - m^2 + \mathrm{i}\epsilon} + \int_{+\mathrm{i}\infty}^{-\mathrm{i}\infty} \mathrm{d}q^0 \, \frac{f(q^2)}{q^2 - m^2 + \mathrm{i}\epsilon} = 0. \tag{2.4}$$

Using the Wick rotation for the integration along the imaginary line, we can write

$$\int_{-\infty}^{+\infty} \mathrm{d}q^0 \, \frac{f(q^2)}{q^2 - m^2 + \mathrm{i}\epsilon} = -\mathrm{i} \int_{-\infty}^{+\infty} \mathrm{d}q_E^0 \, \frac{f(-q_E^2)}{-q_E^2 - m^2 + \mathrm{i}\epsilon}. \tag{2.5}$$

The propagator poles are located in the vicinity of the real axis, so we are able to take the limit $\epsilon \to 0$ (which is equivalent to $\epsilon' \to 0$ in Fig. 2.1) on the right-hand side of the equation. Adding the integration over the spatial directions, we get

$$\int \mathrm{d}^4 q \, \frac{f(q^2)}{q^2 - m^2 + \mathrm{i}\epsilon} = \mathrm{i} \int \mathrm{d}^4 q_E \, \frac{f(-q_E^2)}{q_E^2 + m^2}. \tag{2.6}$$

The integral over the Euclidean four-momentum can now be further evaluated using four-dimensional spherical coordinates.

2.1.2 Cut-off regularisation

The idea of cut-off regularisation is to regularise momentum integrals by restricting the components of the loop four-momentum. A Lorentz-invariant condition, like $q^2 \leq \Lambda^2$, fails to achieve this, as the 0-component remains unrestricted [146]. We thus require

$$q_E^2 \leq \Lambda^2 \Leftrightarrow |q_E| = \sqrt{q_E^2} \leq \Lambda \tag{2.7}$$

after the Wick rotation discussed above. With this, the above integral is replaced by

$$\int \mathrm{d}^4 q \, \frac{f(q^2)}{q^2 - m^2 + \mathrm{i}\epsilon} \to \mathrm{i} \int\limits_{|q_E| \leq \Lambda} \mathrm{d}^4 q_E \, \frac{f(-q_E^2)}{q_E^2 + m^2}. \tag{2.8}$$

The cut-off parameter Λ has mass dimension one, and the unregularised expression is recovered in the limit $\Lambda \to \infty$. This prescription, however, breaks Lorentz invariance and is thus rarely used in practise.

2.1.3 Pauli-Villars regularisation

This method of regularisation goes back to Wolfgang Pauli and Felix Villars [147]. It is most commonly applied in the abelian QFT of quantum electrodynamics (QED),

by replacing the photon propagator

$$\frac{1}{q^2 + \mathrm{i}\epsilon} \to \frac{1}{q^2 + \mathrm{i}\epsilon} - \frac{1}{q^2 - \Lambda^2 + \mathrm{i}\epsilon}. \tag{2.9}$$

As in cut-off regularisation, the parameter Λ has mass dimension one, and the limit $\Lambda \to \infty$ has to be taken at the end of the calculation. The term with the regulator can be interpreted as originating from the extra term

$$\mathcal{L}_{\mathrm{PVR}} = \frac{1}{2\Lambda^2} \partial_\mu F^{\mu\rho} \partial^\nu F_{\nu\rho} \tag{2.10}$$

in the QED Lagrangian. As the field strength tensor $F^{\mu\nu}$ is a gauge-invariant quantity in a local $U(1)$ theory, this regularisation scheme does not break gauge invariance in QED. On the other hand, $F^{\mu\nu}$ is only gauge covariant in a non-abelian gauge theory, rendering the above approach gauge symmetry violating in the case of quantum chromodynamics (QCD). A gauge-invariant non-abelian generalisation of Pauli-Villars regularisation can be useful in the renormalisation of chiral theories, as it avoids the ambiguity of defining γ^5 in D space-time dimensions [148].

2.1.4 Dimensional regularisation

Dimensional regularisation (DREG) was introduced by Gerard 't Hooft and Martinus Veltman to prove the renormalisability of Yang-Mills gauge theories in 1972 [149]. They also showed that the theory will remain renormalisable even if the underlying gauge symmetry is spontaneously broken. This regularisation scheme is often used for calculations within the framework of the SM, which utilises the Higgs mechanism to give mass to its elementary particles.

The idea of DREG is to perform a calculation in $D = 4 - 2\varepsilon \in \mathbb{C}$ space-time dimensions instead of the 4 dimensions of the Minkowski space-time. If a momentum integral UV-diverges in 4 dimensions, it converges in D dimensions when $\mathrm{Re}(D)$ is chosen sufficiently small. Allowing D to be complex, we are able to utilise techniques (like analytical continuation) from complex analysis to evaluate Feynman diagrams. The unregularised expression is obtained upon taking the limit $D \to 4$ (or, equivalently, $\varepsilon \to 0$).

Defining a theory in D and not in 4 dimensions brings with it some interesting consequences; as the action

$$S[\varphi_i] = \int \mathrm{d}^D x \, \mathcal{L}(\varphi_i, \partial^\mu \varphi_i) \tag{2.11}$$

has to be a dimensionless quantity when working with natural units $c = \hbar = 1$, the

Lagrangian $\mathcal{L}$ needs to have mass dimension D. This alters the mass dimension of fields and couplings; while gauge and Yukawa couplings are dimensionless quantities in 4 dimensions, in a D dimensional calculation, they have mass dimension ε. To keep working with dimensionless couplings, the *regularisation scale* μ_{D} has to be introduced. In some cases it is instructive to work with multiple regularisation scales [150], as it enables us to deal with far-apart physical scales without the need to use effective field theory (EFT) methods.

To demonstrate the procedure, let us discuss the one-loop Feynman diagram contributing to a self-energy in ϕ^4 theory with coupling λ. In 4 dimensions, it is of the form

$$\Sigma_4^{(1)} = -\frac{\mathrm{i}\lambda}{2}\int \frac{\mathrm{d}^4 q}{(2\pi)^4}\frac{1}{q^2-m^2}. \tag{2.12}$$

In D dimensions, λ has mass dimension 2ε. In order to work with a dimensionless coupling, we substitute $\lambda \to \lambda\mu_{\mathrm{D}}^{2\varepsilon}$, where the new λ has mass dimension zero. At the same time, the mass dimension of the integration variable changes. We write

$$\begin{aligned}\Sigma_D^{(1)} &= -\frac{\mathrm{i}\lambda}{2}\mu_{\mathrm{D}}^{2\varepsilon}\int \frac{\mathrm{d}^D q}{(2\pi)^D}\frac{1}{q^2-m^2} \\ &= \frac{\lambda}{32\pi^2}\left(\frac{16\pi^2}{\mathrm{i}}\mu_{\mathrm{D}}^{2\varepsilon}\int \frac{\mathrm{d}^D q}{(2\pi)^D}\frac{1}{q^2-m^2}\right) \\ &\equiv \frac{\lambda}{32\pi^2}A_0(m^2,\varepsilon,\mu_{\mathrm{D}}).\end{aligned} \tag{2.13}$$

The loop integral A_0 has an integer mass dimension of 2. When expanding such an expression around $\varepsilon = 0$, all the appearing logarithms will have dimensionless arguments. For this reason, the definition of A_0 encompasses the regularisation scale μ_{D}. The imaginary unit is included so that it can be absorbed when Wick rotating. As these are both desirable properties, the above logic will be the foundation of all one-loop integrals defined in the present thesis. In what follows, we will almost always suppress the ε and μ_{D} dependence in notation. Had we defined the above expression in Pauli-Villars regularisation instead, A_0 would depend on m^2 and Λ. The scale Λ would simultaneously serve as a regulator and a regularisation scale.

2.1.5 Dimensional reduction

Fully defining a theory in D dimensions, however, leads to issues when working with a supersymmetric theory; a mismatch between the number of degrees of freedom of a gauge field A^μ and its associated gauginos spoils multiplicative renormalisation, and supersymmetry-restoring counterterms have to be introduced [151]. This

problem can be circumvented by modifying the regularisation scheme such that it respects supersymmetry. This idea led to the introduction of *dimensional reduction* (DRED) by Warren Siegel in 1979 [152]. Unlike in DREG, vector fields A^μ, gamma matrices γ^μ, and $\epsilon^{\mu\nu\rho\sigma}$ are still treated as four-dimensional tensors in DRED. Only loop-momenta live in D dimensions in order to regularise divergent integrals. While this unequal treatment of Lorentz tensors leads to additional mathematical inconsistencies [151], we will use DRED in this "naive" formulation throughout the entirety of this thesis. A mathematically consistent but more technical formulation is given in Ref. [151]. The different formulations yield the same results for the quantities considered in this thesis. Apart from these differences, DRED is very similar to DREG. As the momenta are defined in D dimensions, the four-dimensional limit is obtained by taking $\varepsilon \to 0$.

2.1.6 Other regularisation schemes

Of the regularisation schemes mentioned so far, DREG and DREG are the ones used most commonly in a perturbative calculation.

If the coupling constant, with respect to which the series expansion is performed, is too large, a non-perturbative approach has to be taken. A regularisation scheme suited for this kind of calculation is the *lattice regularisation*, in which the QFT is defined on a four-dimensional grid of lattice points. In this scheme, the lattice spacing a serves both as a regulator and as a regularisation scale with mass dimension -1. The continuum limit is recovered when taking $a \to 0$. While local gauge invariance is relatively simple to maintain within lattice regularisation, Poincaré invariance is reduced to a discrete group [153]. Poincaré symmetry is restored once the continuum limit is taken.

In curved spacetime [154], *zeta function regularisation* is used to assign finite values to path integrals for fields [155]. This method introduces a dimensionless regulator s and an arbitrary parameter μ with mass dimension 1, which is necessary from dimensional considerations [156]. In this regularisation scheme, a generalised zeta function $\zeta(s)$ is formed from the eigenvalues of a differential operator. The determinant of the operator is then defined to be $\exp\big(-\zeta'(0)\big)$.

We close this section with an important statement: **The process of regularisation introduces both a regulator and a regularisation scale into the theory.** Those quantities can be identical as in the case of Pauli-Villars and lattice regularisation, or they can be separate quantities, as is the case in DREG/DRED and zeta function regularisation. The regulator and the regularisation scale are unphysical and drop out in the relation between physical observables at any given order.

2.2 Renormalisation

The idea of renormalisation is to absorb the aforementioned infinities from the loop integrals into the parameters of the theory. It is very important to be precise when specifying the renormalisation procedure, as only then different calculations can be compared in a meaningful sense. We will introduce the most important renormalisation schemes used in practice in what follows. For all purposes, we work with a multiplicative renormalisation scheme. This means that a theory's bare and renormalised parameters are related via

$$p_B = Z_p\, p = p + \delta p = p + \sum_{i=1}^{\infty} \delta^{(i)} p, \tag{2.14}$$

where p_B is the bare parameter, Z_p is the renormalisation constant, p is the renormalised parameter, and δp is the counterterm, which is expanded up to the desired loop order. Additionally, we renormalise fields as well. If multiple fields carry identical quantum numbers, the renormalisation needs to account for loop-induced mixing. For the case of two fields, this is done by a 2×2 matrix:

$$\begin{pmatrix} \varphi_{1,B} \\ \varphi_{2,B} \end{pmatrix} = \begin{pmatrix} \sqrt{Z_{\varphi_1\varphi_1}} & \frac{1}{2}\delta Z_{\varphi_1\varphi_2} \\ \frac{1}{2}\delta Z_{\varphi_2\varphi_1} & \sqrt{Z_{\varphi_2\varphi_2}} \end{pmatrix} \begin{pmatrix} \varphi_1 \\ \varphi_2 \end{pmatrix}. \tag{2.15}$$

The diagonal renormalisation constant and the off-diagonal counterterm have a similar loop expansion as the parameters:

$$Z_{\varphi_i\varphi_i} = 1 + \delta Z_{\varphi_i\varphi_i}, \tag{2.16a}$$

$$\delta Z_{\varphi_i\varphi_j} = \sum_{i=1}^{\infty} \delta^{(i)} Z_{\varphi_i\varphi_j}. \tag{2.16b}$$

In the subsequent chapters, we will express the relation between bare and renormalised quantities in the form of a renormalisation transformation

$$p \to p + \delta p\,(= p_B). \tag{2.17}$$

2.2.1 On-shell renormalisation

The *on-shell renormalisation* scheme (OS) directly relates parameters to physical observables. If a mass parameter is renormalised in the OS scheme, its renormalised value is identical to the pole mass of the particle. The pole mass of a particle is

defined via the equation

$$p^2 - m^2 + \hat{\Sigma}^{\text{eff}}(p^2) = 0 \quad \text{at } p^2 = \mathcal{M}^2 \equiv M^2 - \mathrm{i}M\Gamma, \tag{2.18}$$

where m is the tree-level mass, M is the physical pole mass, and $\mathcal{M}^2$ is the complex pole. $\hat{\Sigma}^{\text{eff}}$ is the renormalised effective self-energy. We will derive this equation in Ch. 3. At the one-loop level, the effective self-energy is identical to the usual self-energy $\hat{\Sigma}$. The renormalised one-loop self-energy is of the form

$$\hat{\Sigma}^{(1)}(p^2) = \Sigma^{(1)}(p^2) + \delta^{(1)}Z(p^2 - m^2) - \delta^{(1)}m^2, \tag{2.19}$$

where $\delta^{(1)}Z$ is the field counterterm and $\delta^{(1)}m^2$ is the mass counterterm. To demonstrate the renormalisation procedure, we give an example with a scalar one-loop self-energy. Let

$$\Sigma^{(1)}(p^2) = \alpha A_0(m^2) + \beta p^2 B_0(p^2, m_1^2, m_2^2), \tag{2.20}$$

where α and β are real, dimensionless constants. The one-loop integrals A_0 and B_0 are defined in Eqs. (D.1). In a general self-energy, other loop functions might appear and, in the case of a charged self-energy, the coefficients can be complex.
The on-shell scheme is now defined by requiring that the squared tree-level mass m^2 coincides with the real part of the complex pole M^2. At the one-loop level, this leads to the renormalisation condition

$$\operatorname{Re}\hat{\Sigma}^{(1)}(m^2) \stackrel{!}{=} 0. \tag{2.21}$$

The one-loop mass counterterm is then

$$\begin{aligned} \delta^{(1)}m^{2,\text{OS}} &= \operatorname{Re}\Sigma^{(1)}(m^2) \\ &= \alpha A_0(m^2) + \beta m^2 \operatorname{Re}B_0(m^2, m_1^2, m_2^2). \end{aligned} \tag{2.22}$$

A mass counterterm defined in such a way typically has both a divergent and a finite part. Additionally, there are also parts proportional to higher powers of ε (when working with e.g. DRED, which we will always assume from here on). While this part vanishes in the limit $\varepsilon \to 0$ and does not contribute in any one-loop calculation, it becomes very important in a two-loop calculation and has to be included.
Just like mass parameters, field counterterms can be defined in an OS way as well. To this end, we require the propagator to have unit residue, which gives us the

renormalisation condition

$$\frac{\partial}{\partial p^2}\hat{\Sigma}^{(1)}(p^2)\bigg|_{p^2=m^2} \equiv \partial\hat{\Sigma}^{(1)}(m^2) \stackrel{!}{=} 0. \tag{2.23}$$

From this, we infer the OS counterterm

$$\begin{aligned}\delta^{(1)}Z^{\mathrm{OS}} &= -\partial\Sigma^{(1)}(m^2)\\ &= -\beta m^2\partial B_0(m^2,m_1^2,m_2^2) - \beta B_0(m^2,m_1^2,m_2^2).\end{aligned} \tag{2.24}$$

Let us now check the structure of $\hat{\Sigma}^{(1)}$ with OS counterterms as above. Its divergent part is

$$\begin{aligned}\hat{\Sigma}^{(1)}(p^2)\Big|_{\mathrm{div}} &= \Sigma^{(1)}(p^2)\Big|_{\mathrm{div}} + \delta^{(1)}Z^{\mathrm{OS}}\Big|_{\mathrm{div}}(p^2-m^2) - \delta^{(1)}m^{2,\mathrm{OS}}\Big|_{\mathrm{div}}\\ &= \frac{\alpha m^2+\beta p^2}{\varepsilon} + \frac{-\beta}{\varepsilon}(p^2-m^2) - \frac{\alpha m^2+\beta m^2}{\varepsilon}\\ &= 0.\end{aligned} \tag{2.25}$$

We see that the field counterterm is necessary to get a finite self-energy also for off-shell momenta $p^2 \neq m^2$. To analyse the finite structure of the renormalised self-energy, we set $m_1^2 = m_2^2 = 0$ for simplicity. We use

$$A_0^{\mathrm{fin}}(m^2)/m^2 = 1 + \log(4\pi) - \gamma_E + \log\left(\frac{\mu_{\mathrm{D}}^2}{m^2}\right), \tag{2.26a}$$

$$B_0^{\mathrm{fin}}(p^2,0,0) = 2 + \log(4\pi) - \gamma_E + \log\left(-\frac{\mu_{\mathrm{D}}^2}{p^2}\right). \tag{2.26b}$$

For the renormalisation constants we find

$$\begin{aligned}\delta^{(1)}m^{2,\mathrm{OS,fin}} &= \alpha m^2\left[1+\log(4\pi)-\gamma_E+\log\left(\frac{\mu_{\mathrm{D}}^2}{m^2}\right)\right]\\ &\quad+\beta m^2\left[2+\log(4\pi)-\gamma_E+\mathrm{Re}\log\left(-\frac{\mu_{\mathrm{D}}^2}{m^2}\right)\right],\end{aligned} \tag{2.27a}$$

$$\delta^{(1)}Z^{\mathrm{OS,fin}} = -\beta m^2\left(-\frac{1}{m^2}\right) - \beta\left(2+\log(4\pi)-\gamma_E+\log\left(-\frac{\mu_{\mathrm{D}}^2}{m^2}\right)\right). \tag{2.27b}$$

Putting everything together, we get

$$\begin{aligned}\hat{\Sigma}^{(1)}(p^2) &\stackrel{\mathrm{OS}}{=} \beta p^2\left[1+\log\left(-\frac{\mu_{\mathrm{D}}^2}{p^2}\right)-\log\left(-\frac{\mu_{\mathrm{D}}^2}{m^2}\right)\right]\\ &\quad-\beta m^2\left[1+\mathrm{Re}\log\left(-\frac{\mu_{\mathrm{D}}^2}{m^2}\right)-\log\left(-\frac{\mu_{\mathrm{D}}^2}{m^2}\right)\right]+\mathcal{O}(\varepsilon).\end{aligned} \tag{2.28}$$

Assuming $\mu_{\mathrm{D}}, m > 0$, we get

$$\hat{\Sigma}^{(1)}(p^2) \overset{\mathrm{OS}}{=} \beta p^2 \left[1 + \log\left(-\frac{m^2}{p^2}\right) - \mathrm{i}\pi\right] - \beta m^2(1 - \mathrm{i}\pi) + \mathcal{O}(\varepsilon). \tag{2.29}$$

From this simple result we see that the renormalised one-loop self-energy does not depend on the regularisation scale μ_{D} anymore. For this cancellation to happen, the finite parts of both $\delta^{(1)}m^2$ and $\delta^{(1)}Z$ need to be taken into account. In a momentum-subtraction scheme this always happens, while in a minimal subtraction scheme it does not. We explain these schemes in Sects. 2.2.2 and 2.2.3.

2.2.2 General momentum-subtraction scheme

The previously introduced OS scheme is an example of a so-called momentum-subtraction (MOM) scheme. A MOM scheme is a renormalisation scheme where renormalisation conditions are imposed at a specific energy scale (as opposed to a minimal subtraction scheme, where we only require finiteness). This energy scale is called the *renormalisation scale*. We modify the OS renormalisation conditions to

$$\operatorname{Re}\hat{\Sigma}^{(1)}(Q_m^2) \overset{!}{=} 0, \tag{2.30a}$$

$$\partial\hat{\Sigma}^{(1)}(Q_Z^2) \overset{!}{=} 0, \tag{2.30b}$$

where Q_m and Q_Z are the mass and field renormalisation scales, respectively. The MOM counterterms now depend on the renormalisation scales

$$\delta^{(1)}m^{2,\mathrm{MOM}} = \operatorname{Re}\Sigma^{(1)}(Q_m^2) + \operatorname{Re}\delta^{(1)}Z^{\mathrm{MOM}}(Q_m^2 - m^2), \tag{2.31a}$$

$$\delta^{(1)}Z^{\mathrm{MOM}} = -\partial\Sigma^{(1)}(Q_Z^2). \tag{2.31b}$$

The counterterms read

$$\begin{aligned}\delta^{(1)}m^{2,\mathrm{MOM}} = {} & \alpha A_0(m^2) + \beta Q_m^2 \operatorname{Re}B_0(Q_m^2, m_1^2, m_2^2) - (Q_m^2 - m^2) \\ & \times \beta\left[Q_Z^2 \operatorname{Re}\partial B_0(Q_Z^2, m_1^2, m_2^2) + \operatorname{Re}B_0(Q_Z^2, m_1^2, m_2^2)\right],\end{aligned} \tag{2.32a}$$

$$\delta^{(1)}Z^{\mathrm{MOM}} = -\beta Q_Z^2 \partial B_0(Q_Z^2, m_1^2, m_2^2) - \beta B_0(Q_Z^2, m_1^2, m_2^2). \tag{2.32b}$$

We see that the mass counterterm now depends on the field renormalisation. As the divergent part of the one-loop counterterms is always scheme independent, the

renormalised self-energy is still finite

$$\begin{aligned}\hat{\Sigma}^{(1)}(p^2)\Big|_{\text{div}} &= \Sigma^{(1)}(p^2)\Big|_{\text{div}} + \delta^{(1)}Z^{\text{MOM}}\Big|_{\text{div}}(p^2-m^2) - \delta^{(1)}m^{2,\text{MOM}}\Big|_{\text{div}} \\ &= \frac{\alpha m^2+\beta p^2}{\varepsilon} + \frac{-\beta}{\varepsilon}(p^2-m^2) - \frac{\alpha m^2+\beta Q_m^2-\beta(Q_m^2-m^2)}{\varepsilon} \\ &= 0.\end{aligned} \tag{2.33}$$

The finite MOM self-energy reads

$$\begin{aligned}\hat{\Sigma}^{(1)}(p^2) \overset{\text{MOM}}{=}\ & \beta p^2\left[1+\log\left(-\frac{\mu_{\text{D}}^2}{p^2}\right)-\log\left(-\frac{\mu_{\text{D}}^2}{Q_Z^2}\right)\right] \\ & -\beta Q_m^2\left[1+\text{Re}\log\left(-\frac{\mu_{\text{D}}^2}{Q_m^2}\right)-\text{Re}\log\left(-\frac{\mu_{\text{D}}^2}{Q_Z^2}\right)\right] \\ & -\beta m^2\left[\text{Re}\log\left(-\frac{\mu_{\text{D}}^2}{Q_Z^2}\right)-\log\left(-\frac{\mu_{\text{D}}^2}{Q_Z^2}\right)\right]+\mathcal{O}(\varepsilon).\end{aligned} \tag{2.34}$$

Assuming $\mu_{\text{D}}, Q_m, Q_Z > 0$, we can simplify

$$\begin{aligned}\hat{\Sigma}^{(1)}(p^2) \overset{\text{MOM}}{=}\ & \beta p^2\left[1+\log\left(-\frac{Q_Z^2}{p^2}\right)-\text{i}\pi\right]-\beta Q_m^2\left[1+\log\left(\frac{Q_Z^2}{Q_m^2}\right)\right] \\ & +\beta m^2\times\text{i}\pi+\mathcal{O}(\varepsilon).\end{aligned} \tag{2.35}$$

We see that the μ_{D} dependence drops out again and it is replaced by a dependence on both Q_m and Q_Z. The choice $Q_m^2 = Q_Z^2 = m^2$ yields the OS results from the previous section.

2.2.3 Minimal subtraction schemes

In a *minimal subtraction* scheme, counterterms are chosen to have only a divergent part. By this choice, renormalised self-energies are still rendered finite, but with a different finite part in comparison to momentum-subtraction schemes. In practice, we calculate the desired counterterm in any MOM scheme and simply discard its finite parts. This method defines the MS scheme in DREG and the DR scheme in DRED. As we work with the DRED regularisation scheme exclusively, we will here focus on the DR scheme. All results carry over to the MS scheme when using DREG instead. The mass and field counterterms are

$$\begin{aligned}\delta^{(1)}m^{2,\text{DR}} &\equiv \delta^{(1)}m^{2,\text{OS}}\Big|_{\text{div}} \\ &= \frac{\alpha m^2+\beta m^2}{\varepsilon},\end{aligned} \tag{2.36a}$$

$$\begin{aligned}\delta^{(1)}Z^{\mathrm{DR}} &\equiv \left.\delta^{(1)}Z^{\mathrm{OS}}\right|_{\mathrm{div}} \\ &= -\frac{\beta}{\varepsilon}.\end{aligned} \tag{2.36b}$$

With this, the renormalised self-energy is

$$\begin{aligned}\hat{\Sigma}^{(1)}(p^2) \overset{\mathrm{DR}}{=} \beta p^2 \left[2 + \log(4\pi) - \gamma_E + \log\left(-\frac{\mu_{\mathrm{D}}^2}{p^2}\right)\right] \\ + \alpha m^2 \left[1 + \log(4\pi) - \gamma_E + \log\left(\frac{\mu_{\mathrm{D}}^2}{m^2}\right)\right] + \mathcal{O}(\varepsilon).\end{aligned} \tag{2.37}$$

To get rid of the irrational constants 4π and γ_E, one often uses the *modified minimal subtraction* schemes $\overline{\mathrm{MS}}$ and $\overline{\mathrm{DR}}$, where additional finite terms are added to the counterterms:

$$\delta^{(1)}m^{2,\overline{\mathrm{DR}}} = (\alpha + \beta)\, m^2 \left(\frac{1}{\varepsilon} + \log(4\pi) - \gamma_E + \mathcal{O}(\varepsilon)\right), \tag{2.38a}$$

$$\delta^{(1)}Z^{\overline{\mathrm{DR}}} = -\beta \left(\frac{1}{\varepsilon} + \log(4\pi) - \gamma_E + \mathcal{O}(\varepsilon)\right). \tag{2.38b}$$

The $\mathcal{O}(\varepsilon)$ parts do not matter in a one-loop calculation and are often not spelled out in literature. In Sect. 2.3, we will explain why they are needed in higher-order calculations and we will extend the expressions above to incorporate them. With this choice of counterterms, the renormalised self-energy is

$$\hat{\Sigma}^{(1)}(p^2) \overset{\overline{\mathrm{DR}}}{=} \beta p^2 \left[2 + \log\left(-\frac{\mu_{\mathrm{D}}^2}{p^2}\right)\right] + \alpha m^2 \left[1 + \log\left(\frac{\mu_{\mathrm{D}}^2}{m^2}\right)\right] + \mathcal{O}(\varepsilon). \tag{2.39}$$

In both the DR and the $\overline{\mathrm{DR}}$ scheme, the renormalised self-energy depends on μ_{D}. At first glance, this dependence seems to carry over to the prediction of observables like the pole mass. This does not happen, however, as the DR/$\overline{\mathrm{DR}}$ parameters $m^{2,\mathrm{DR}/\overline{\mathrm{DR}}}(\mu_{\mathrm{D}})$ and $Z^{\mathrm{DR}/\overline{\mathrm{DR}}}(\mu_{\mathrm{D}})$ are scale dependent themselves. The *renormalisation group* (RG) ensures that the scale dependence drops out order by order in relations between physical observables, and the specific energy at which the pole mass is calculated, the so-called *pole mass scale* [137, 157], does not matter at any given order.

The renormalisation group The renormalisation group describes how the properties of a physical system change when varying the energy scale at which it is described. This holds in particular for $\overline{\mathrm{DR}}$ parameters, which are regularisation

scale dependent. We start from the relation

$$m^{2,\mathrm{OS}} + \delta m^{2,\mathrm{OS}} = m_B^2 = m^{2,\overline{\mathrm{DR}}} + \delta m^{2,\overline{\mathrm{DR}}}. \tag{2.40}$$

We take its derivative with respect to μ_{D}^2 and get

$$0 + \frac{\partial}{\partial \mu_{\mathrm{D}}^2}\delta m^{2,\mathrm{OS}} = \frac{\partial m^{2,\overline{\mathrm{DR}}}}{\partial \mu_{\mathrm{D}}^2} + 0, \tag{2.41}$$

as the OS mass is an observable and as such scale independent, and the $\overline{\mathrm{DR}}$ counterterm contains no scale. We define the *mass anomalous dimension*

$$\gamma_{m^2}^{\overline{\mathrm{DR}}} \equiv -\frac{\mu_{\mathrm{D}}^2}{m^{2,\overline{\mathrm{DR}}}}\frac{\partial m^{2,\overline{\mathrm{DR}}}}{\partial \mu_{\mathrm{D}}^2} = -\frac{\partial \log m^{2,\overline{\mathrm{DR}}}}{\partial \log \mu_{\mathrm{D}}^2}. \tag{2.42}$$

Similarly, we define the *beta function* of a coupling constant g via

$$\beta_g^{\overline{\mathrm{DR}}} \equiv \mu_{\mathrm{D}}^2 \frac{\partial g^{\overline{\mathrm{DR}}}}{\partial \mu_{\mathrm{D}}^2} = \frac{\partial g^{\overline{\mathrm{DR}}}}{\partial \log \mu_{\mathrm{D}}^2}. \tag{2.43}$$

For our current analysis, we require only the mass anomalous dimension $\gamma_{m^2}^{\overline{\mathrm{DR}}}$; we insert Eq. (2.27a) into Eq. (2.41) and use definition (2.42) to find

$$\gamma_{m^2}^{\overline{\mathrm{DR}}} = -(\alpha + \beta) + \mathcal{O}\Big(k^2\Big). \tag{2.44}$$

Here, k is the loop counting factor. We integrate Eq. (2.42) between two fixed but arbitrary scales Q_1 and Q_2 to find

$$\begin{aligned} m^{2,\overline{\mathrm{DR}}}(Q_2^2) &= m^{2,\overline{\mathrm{DR}}}(Q_1^2)\left(\frac{Q_2^2}{Q_1^2}\right)^{-\gamma_{m^2}^{\overline{\mathrm{DR}}}} + \mathcal{O}\Big(k^2\Big) \\ &= m^{2,\overline{\mathrm{DR}}}(Q_1^2) + (\alpha+\beta)m^{2,\overline{\mathrm{DR}}}\log\left(\frac{Q_2^2}{Q_1^2}\right) + \mathcal{O}\Big(k^2\Big). \end{aligned} \tag{2.45}$$

We have omitted the energy scale argument in terms where its impact is of higher order and we will continue to do so below.

We now use this result to demonstrate that the pole mass M^2 is indeed independent of the specific value of μ_{D} at which it is calculated. In the $\overline{\mathrm{DR}}$ scheme, the one-loop pole mass differs from the unphysical $\overline{\mathrm{DR}}$ mass by a finite shift. For the first

prediction we make the choice $\mu_{\mathrm{D}} = Q_1$:

$$\begin{aligned} M^2(Q_1^2) &= m^2(Q_1^2) - \operatorname{Re}\hat{\Sigma}^{(1)}(m^2) + \mathcal{O}\Big(k^2\Big) \\ &= m^2(Q_1^2) - \beta m^2\left[2 + \log\left(\frac{Q_1^2}{m^2}\right)\right] - \alpha m^2\left[1 + \log\left(\frac{Q_1^2}{m^2}\right)\right] + \mathcal{O}\Big(k^2\Big) \end{aligned} \tag{2.46}$$

Here and in the following equation, m^2 denotes the $\overline{\mathrm{DR}}$ mass. In the second and third term, the energy at which we evaluate m^2 matters only beyond one-loop order, so we omit the argument here.
For the second prediction, we set $\mu_{\mathrm{D}} = Q_2$:

$$\begin{aligned} M^2(Q_2^2) &= m^2(Q_2^2) - \beta m^2\left[2 + \log\left(\frac{Q_2^2}{m^2}\right)\right] - \alpha m^2\left[1 + \log\left(\frac{Q_2^2}{m^2}\right)\right] + \mathcal{O}\Big(k^2\Big) \\ &= m^2(Q_1^2) + (\alpha+\beta)m^2\log\left(\frac{Q_2^2}{Q_1^2}\right) - \beta m^2\left[2 + \log\left(\frac{Q_2^2}{m^2}\right)\right] \\ &\quad - \alpha m^2\left[1 + \log\left(\frac{Q_2^2}{m^2}\right)\right] + \mathcal{O}\Big(k^2\Big) \\ &= m^2(Q_1^2) - \beta m^2\left[2 + \log\left(\frac{Q_1^2}{m^2}\right)\right] - \alpha m^2\left[1 + \log\left(\frac{Q_1^2}{m^2}\right)\right] + \mathcal{O}\Big(k^2\Big) \\ &= M^2(Q_1^2) + \mathcal{O}\Big(k^2\Big). \end{aligned} \tag{2.47}$$

In the second step, we have made use of Eq. (2.45) and in the third we combined the logarithms to cancel Q_2. We have thus demonstrated that if we make a one-loop prediction for an observable at two different energies Q_1 and Q_2, the calculations will agree up to the one-loop level but differ at the two-loop order and beyond. We can hence vary the pole mass scale to estimate the size of missing higher-order terms.
Eq. (2.47) also tells us how to interpret the parameter μ_{D} in a minimal subtraction scheme. As we have seen, a $\overline{\mathrm{DR}}$ counterterm does not contain a scale that could be understood as a renormalisation scale. Instead, we identify the regularisation scale μ_{D} with the renormalisation scale at which the parameter is defined. For this reason, μ_{D} is often called the renormalisation scale although it is—strictly speaking—introduced at the step of regularisation. When working with $\overline{\mathrm{DR}}$ parameters, we always give the value of a parameter at its renormalisation scale. The RG allows us to calculate the parameter value at any other scale.

2.3 Minimal subtraction schemes at the two-loop level

If two or more parameters are defined in a minimal subtraction scheme, their renormalisation scales—i.e. the energy scales at which the parameters are defined—might be different. In this case, it is not clear which value for the regularisation scale μ_D should be used in the calculation. In the standard approach, we first employ the renormalisation group to evolve the parameters to the same scale, then we set μ_D to that value.

To illustrate this procedure, let us consider a calculation with two $\overline{\text{DR}}$ parameters, p_1 and p_2, which are defined at the renormalisation scales Q_1 and Q_2, respectively. On the one hand, we can evolve p_1 from Q_1 to Q_2, and since p_2 is already defined at Q_2, we also set $\mu_D = Q_2$. On the other hand, we can also evolve p_2 from Q_2 to Q_1 instead and set $\mu_D = Q_1$. As a third option, we can also evolve both parameters to a new scale Q_3 and set $\mu_D = Q_3$. In any n-loop calculation, all three methods yield results which agree to order n but differ by terms of order $(n+1)$. In a pole mass calculation, we can thus vary the pole mass scale to estimate the size of the missing higher-order terms.

This method has two shortcomings. First, we need to determine the beta functions for all $\overline{\text{DR}}$ couplings and anomalous dimensions for masses and fields defined in a minimal subtraction scheme up to the required loop order. Secondly, we are not able to tell how much each parameter contributes to the uncertainty due to missing higher orders. In this section, we want to introduce a different prescription, called the $\widetilde{\overline{\text{DR}}}$ renormalisation scheme. It avoids the need to calculate beta functions when several $\overline{\text{DR}}$ parameters are defined at different scales; in this way we circumvent the first issue. If the beta functions are known, however, we can use the $\widetilde{\overline{\text{DR}}}$ scheme to investigate the scale uncertainty which is introduced by each minimally defined parameter separately. Furthermore, our prescription naturally leads to a generalisation of the $\overline{\text{DR}}$ scheme to the two-loop order. This is important as—starting at the two-loop level—the definition of modified minimal subtraction is no longer unique [158, 159].

To illustrate the non-uniqueness of modified minimal subtraction at higher orders, let us look at the one-loop integrals A_0 and B_0, which are defined in Eqs. (D.1). A_0 and the massless B_0 have the neat property that they can be put in a closed expression without the need to expand the integrand in ε first, see Eqs. (D.22). As we can see from their definitions, all one-loop integrals are proportional to $\mu_D^{2\varepsilon}$, owing to the way the regularisation scale is introduced. The factor of $(4\pi)^\varepsilon$ always

appears in the same fashion as well, as it stems from a combination of the prefactor C of the integrals and the angular integral in D dimensions. The combination of Gamma functions, however, depends on the considered integral. Therefore, different definitions of the modified regularisation scale $\bar{\mu}_{\mathrm{D}}$ and, hence, the $\overline{\mathrm{DR}}$ scheme exist. The following conventions, among others, are found in the literature:

$$\bar{\mu}_{\mathrm{D}}^{2\varepsilon} = \left(4\pi e^{-\gamma_E}\right)^{\varepsilon} \mu_{\mathrm{D}}^{2\varepsilon} \text{ [46]}, \tag{2.48a}$$

$$\bar{\mu}_{\mathrm{D}}^{2\varepsilon} = \frac{(4\pi)^{\varepsilon}}{\Gamma(1-\varepsilon)} \mu_{\mathrm{D}}^{2\varepsilon} \text{ [158, 159]}, \tag{2.48b}$$

$$\bar{\mu}_{\mathrm{D}}^{2\varepsilon} = \frac{(4\pi)^{\varepsilon}\Gamma^2(1-\varepsilon)\Gamma(1+\varepsilon)}{\Gamma(1-2\varepsilon)} \mu_{\mathrm{D}}^{2\varepsilon} \text{ [160]}. \tag{2.48c}$$

All these conventions agree at $\mathcal{O}(\varepsilon)$. The second and third convention agree at $\mathcal{O}\left(\varepsilon^2\right)$, but differ from the first one at that order. At $\mathcal{O}\left(\varepsilon^3\right)$, all conventions differ. While all conventions are able to get rid of any $\log(4\pi)$ or γ_E terms, other irrational constants, which appear at higher orders, cannot be removed simultaneously by any choice. It can be shown, however, that differences of $\mathcal{O}\left(\varepsilon^2\right)$ in the definition of $\bar{\mu}_{\mathrm{D}}$ do not alter the value of a renormalised Green function after taking the limit $\varepsilon \to 0$ [159]. Therefore, the exact choice of how to define $\bar{\mu}_{\mathrm{D}}$ matters only for technical reasons.

2.3.1 Defining the $\widetilde{\mathrm{DR}}$ renormalisation scheme

When working with several parameters that are defined in a minimal subtraction scheme but at different energy scales, we have to evolve the parameters to the same energy scale via RG running. This would, however, mix loop orders. To avoid this mixing, we would have to expand the solution of the *renormalisation group equation* (RGE) up to the desired loop order.

This procedure is equivalent to adding a finite piece to the counterterm of the parameter; adding a logarithm of μ_{D} over the renormalisation scale Q_p for each parameter p replaces the μ_{D} dependence of the renormalised parameter by a dependence on the renormalisation scale. Now the renormalisation scales of the parameters can be set to their respective values and a prediction can be made. To illustrate this simple procedure, we start with the DR counterterm of the parameter p. It will be of the general form

$$\delta^{(1)} p^{\mathrm{DR}} = \frac{A}{\varepsilon}. \tag{2.49}$$

In a $\overline{\text{DR}}$ scheme, we have

$$\delta^{(1)} p^{\overline{\text{DR}}} = A \left(\frac{1}{\varepsilon} + \log(4\pi) - \gamma_E + \mathcal{O}(\varepsilon) \right). \tag{2.50}$$

This prescription removes the irrational constants for any linear combination of integrals at the one-loop level as they appear in the same combination with the divergence $\frac{1}{\varepsilon}$ for all one-loop integrals. If a parameter is renormalised in a MOM scheme (like e.g. an OS scheme), its one-loop counterterm will contain the same combination of divergence and irrational constants as the $\overline{\text{DR}}$ counterterm.
To get rid of the μ_{D} in the end result as well, we have to further extend the $\overline{\text{DR}}$ counterterm to the form

$$\delta^{(1)} p^{\overline{\text{DR}}} \to \delta^{(1)} p^{\widetilde{\text{DR}}} = A \left(\frac{1}{\varepsilon} + \log(4\pi) - \gamma_E + \log\left(\frac{\mu_{\text{D}}^2}{Q_p^2} \right) + \mathcal{O}(\varepsilon) \right), \tag{2.51}$$

where Q_p is the (renormalisation) scale at which p is defined. This form was obtained from comparison with an OS counterterm. The $\widetilde{\text{DR}}$ counterterm now has the same μ_{D} dependence as an OS counterterm:

$$\frac{\partial}{\partial \mu_{\text{D}}^2} \delta^{(1)} m^{2,\widetilde{\text{DR}}} = \frac{\partial}{\partial \mu_{\text{D}}^2} \delta^{(1)} m^{2,\text{OS}}. \tag{2.52}$$

An OS parameter is regularisation scale independent; this statement also holds for a $\widetilde{\text{DR}}$ parameter:

$$\frac{\partial m^{2,\widetilde{\text{DR}}}}{\partial \mu_{\text{D}}^2} = \frac{\partial m^{2,\text{OS}}}{\partial \mu_{\text{D}}^2} + \frac{\partial}{\partial \mu_{\text{D}}^2} \delta^{(1)} m^{2,\text{OS}} - \frac{\partial}{\partial \mu_{\text{D}}^2} \delta^{(1)} m^{2,\widetilde{\text{DR}}} = 0, \tag{2.53}$$

which follows from

$$m^{2,\text{OS}} + \delta m^{2,\text{OS}} = m^{2,\widetilde{\text{DR}}} + \delta m^{2,\widetilde{\text{DR}}}. \tag{2.54}$$

Of course, a $\widetilde{\text{DR}}$ parameter still depends on its renormalisation scale Q_p:

$$\frac{\partial m^{2,\widetilde{\text{DR}}}}{\partial Q_p^2} = -\frac{\partial}{\partial Q_p^2} \delta^{(1)} m^{2,\widetilde{\text{DR}}} = \frac{\partial}{\partial \mu_{\text{D}}^2} \delta^{(1)} m^{2,\widetilde{\text{DR}}} = \frac{\partial m^{2,\overline{\text{DR}}}}{\partial \mu_{\text{D}}^2} \neq 0. \tag{2.55}$$

The first equality holds as the bare parameter m_B^2 is independent of Q_p, the second one from the definition of the $\widetilde{\text{DR}}$ counterterm, and the third one from

$$m^{2,\overline{\text{DR}}} + \delta m^{2,\overline{\text{DR}}} = m^{2,\widetilde{\text{DR}}} + \delta m^{2,\widetilde{\text{DR}}}. \tag{2.56}$$

To understand how we can extend this procedure to the two-loop level, let us consider

a calculation where all parameters are defined in a MOM scheme. A renormalised two-loop self-energy is the sum of the unrenormalised self-energy and the two-loop counterterms. The unrenormalised self-energy comprises both diagrams with a genuine two-loop topology as well as one-loop diagrams with one-loop counterterm insertions. Each two-loop diagram is proportional to $\mu_{\mathrm{D}}^{4\varepsilon}$, while each one-loop diagram comes with a factor $\mu_{\mathrm{D}}^{2\varepsilon}$. The same holds for two- and one-loop counterterms, respectively, if they are defined in a MOM scheme. Thus, the renormalised two-loop self-energy will depend on μ_{D} merely through the overall factor $\mu_{\mathrm{D}}^{4\varepsilon}$. As the μ_{D}-independent part is finite through renormalisation, the scale μ_{D} cannot appear in the renormalised self-energy at $\mathcal{O}\left(\varepsilon^0\right)$. We want the same cancellation to take place when defining at least one parameter in a minimal subtraction scheme.
To this end, we define our own modified minimal subtraction scheme, the $\widetilde{\mathrm{DR}}$ scheme, as follows:

- The divergent part of a $\widetilde{\mathrm{DR}}$ counterterm agrees with its DR/$\overline{\mathrm{DR}}$ counterpart.
- For each $\widetilde{\mathrm{DR}}$ parameter p, we introduce a separate renormalisation scale Q_p.
- At every order of perturbation theory, the regularisation scale μ_{D} drops out at $D = 4$.
- All appearances of $\log(4\pi)$ and γ_E drop out for $D = 4$.

We work with the convention

$$\bar{\mu}_{\mathrm{D}}^2 = 4\pi e^{-\gamma_E} \mu_{\mathrm{D}}^2. \tag{2.57}$$

This replacement "hides" all appearances of $\log(4\pi)$ and γ_E in the newly defined regularisation scale $\bar{\mu}_{\mathrm{D}}$. If we can give a minimal subtraction prescription according to which all instances of $\bar{\mu}_{\mathrm{D}}$ disappear, the last two requirements of our $\widetilde{\mathrm{DR}}$ definition are simultaneously fulfilled. μ_{D} and the constant 4π always appear together, while the γ_E stems from the expansion of the gamma function. Explicit expressions of one-loop functions up to $\mathcal{O}(\varepsilon)$ as in Ref. [161] tell us that the above definition of $\bar{\mu}_{\mathrm{D}}$ indeed gets rid of all γ_E's as well. Any other aforementioned convention works as well and achieves the same.
We define a one-loop $\widetilde{\mathrm{DR}}$ counterterm from its DR counterpart via

$$\delta^{(1)} p^{\widetilde{\mathrm{DR}}} \equiv \left(\frac{\bar{\mu}_{\mathrm{D}}^2}{Q_p^2}\right)^{\varepsilon} \frac{\tilde{A}}{\varepsilon}, \tag{2.58}$$

where Q_p is the renormalisation scale of the $\widetilde{\mathrm{DR}}$ parameter p. The divergent part of the $\widetilde{\mathrm{DR}}$ counterterm has to agree with the divergence of the DR counterterm, giving

us the condition

$$\tilde{A} = A \tag{2.59}$$

for the coefficient of the divergence. This definition leads to

$$\delta^{(1)} p^{\widetilde{\mathrm{DR}}} = A \left(\frac{1}{\varepsilon} + \log\left(\frac{\bar{\mu}_\mathrm{D}^2}{Q_p^2}\right) + \frac{\varepsilon}{2} \log^2\left(\frac{\bar{\mu}_\mathrm{D}^2}{Q_p^2}\right) + \mathcal{O}\big(\varepsilon^2\big) \right) \tag{2.60}$$

with the same leading logarithms, $\varepsilon^n \log^{(n+1)}$, as a momentum-subtraction scheme and is therefore able to cancel all appearances of $\bar{\mu}_\mathrm{D}$. It also reproduces our previous expression in Eq. (2.51), but it now additionally includes a term of $\mathcal{O}(\varepsilon)$.
At the two-loop level, the procedure is very similar. A two-loop DR counterterm for the parameter p takes the form

$$\delta^{(2)} p^{\mathrm{DR}} = \frac{B}{\varepsilon^2} + \frac{C}{\varepsilon}. \tag{2.61}$$

Here, the coefficient B is independent from the renormalisation chosen at one-loop order, whereas C depends on the finite parts of the one-loop counterterms via sub-loop renormalisation.
We write the $\widetilde{\mathrm{DR}}$ counterterm as

$$\delta^{(2)} p^{\widetilde{\mathrm{DR}}} = \left(\frac{\bar{\mu}_\mathrm{D}^2}{Q_p^2}\right)^{2\varepsilon} \left(\frac{\tilde{B}}{\varepsilon^2} + \frac{\tilde{C}}{\varepsilon} \right). \tag{2.62}$$

$\tilde{B}$ and $\tilde{C}$ then need to be chosen such that the divergences of the DR counterterm are reproduced. The only possible choice is

$$\tilde{B} = B, \tag{2.63a}$$

$$\tilde{C} = C - 2B \log\left(\frac{\bar{\mu}_\mathrm{D}^2}{Q_p^2}\right). \tag{2.63b}$$

By construction, $\tilde{C}$ is $\bar{\mu}_\mathrm{D}$-independent while C is not. Re-expressing the $\widetilde{\mathrm{DR}}$ counterterm in terms of the DR coefficients and expanding in ε, we arrive at:

$$\delta^{(2)} p^{\widetilde{\mathrm{DR}}} = B \left(\frac{1}{\varepsilon^2} - 2\log^2\left(\frac{\bar{\mu}_\mathrm{D}^2}{Q_p^2}\right) + \mathcal{O}(\varepsilon) \right) + C \left(\frac{1}{\varepsilon} + 2\log\left(\frac{\bar{\mu}_\mathrm{D}^2}{Q_p^2}\right) + \mathcal{O}(\varepsilon) \right). \tag{2.64}$$

This prescription can easily be extended to higher loop orders. One must not forget to include $\mathcal{O}(\varepsilon)$ terms in counterterms of lower loop order. At the three-loop level, for example, we need to add an $\mathcal{O}(\varepsilon)$ part in the two-loop counterterm.
In the $\widetilde{\mathrm{DR}}$ scheme, the single scale μ_D or $\bar{\mu}_\mathrm{D}$ is replaced by one renormalisation scale

Q_p for each parameter p. By varying only one of the renormalisation scales, we can isolate the scale uncertainty stemming from the definition of the respective $\widetilde{\mathrm{DR}}$ parameter.

2.3.2 Defining the $\overline{\mathrm{DR}}$ renormalisation scheme at higher orders

We want to conclude this section by generalising the $\overline{\mathrm{DR}}$ scheme to the two-loop order as well. We can simply use the $\widetilde{\mathrm{DR}}$ prescription and set $Q_p = \mu_{\mathrm{D}}$:

$$\begin{aligned}\delta^{(1)}p^{\overline{\mathrm{DR}}} &\equiv \left(4\pi e^{-\gamma_E}\right)^{\varepsilon}\frac{\overline{A}}{\varepsilon} \\ &= A\left(\frac{1}{\varepsilon}+\log(4\pi)-\gamma_E+\frac{\varepsilon}{2}[\log(4\pi)-\gamma_E]^2+\mathcal{O}\left(\varepsilon^2\right)\right),\end{aligned} \tag{2.65a}$$

$$\begin{aligned}\delta^{(2)}p^{\overline{\mathrm{DR}}} &\equiv \left(4\pi e^{-\gamma_E}\right)^{2\varepsilon}\left(\frac{\overline{B}}{\varepsilon^2}+\frac{\overline{C}}{\varepsilon}\right) \\ &= B\left(\frac{1}{\varepsilon^2}-2[\log(4\pi)-\gamma_E]^2+\mathcal{O}(\varepsilon)\right) \\ &\quad + C\left(\frac{1}{\varepsilon}+2[\log(4\pi)-\gamma_E]+\mathcal{O}(\varepsilon)\right).\end{aligned} \tag{2.65b}$$

We determined $\overline{A}$, $\overline{B}$, and $\overline{C}$ again by comparing the divergent parts of DR and $\overline{\mathrm{DR}}$ counterterms, from which we obtained the relations

$$\overline{A} = A, \tag{2.66a}$$

$$\overline{B} = B, \tag{2.66b}$$

$$\overline{C} = C - 2B[\log(4\pi)-\gamma_E]. \tag{2.66c}$$

Similar as in the $\widetilde{\mathrm{DR}}$ scheme, the $\overline{\mathrm{DR}}$ constants $\overline{A}$, $\overline{B}$, and $\overline{C}$ do not contain the irrational constants $\log(4\pi)$ and γ_E. This prescription is in perfect agreement with the one found in Ref. [159] and was derived independently. In Ref. [159], the idea of adding one factor $S_\varepsilon = (4\pi e^{-\gamma_E})^\varepsilon$ for each loop in the counterterms is presented as well.[2]

[2] They use the different but equivalent convention $S_\varepsilon = (4\pi)^\varepsilon/\Gamma(1-\varepsilon)$.

3 The pole mass of a particle

In this chapter, we explain how the pole mass of a particle is determined in a perturbative, Feynman-diagrammatic calculation. The pole mass is a physical observable and so it can be used to compare the predictions of a given model with experimental observations. If a mass parameter is not renormalised in the OS scheme or if the parameter is not used an input parameter, we have to calculate the pole mass in terms of input parameters. The following analysis naturally leads to the definition of the OS scheme for masses at the two-loop level both for unstable particles and in the presence of particle mixing.

In the first section, we give definitions for several different types of correlation functions. Two of these—the Feynman propagator and the vertex function—play an important role in a pole mass calculation. We show how the correlators are obtained from generating functionals and that the Feynman propagator and the two-point vertex functions are inverse functions of each other. We demonstrate that inverting the two-point vertex function and performing a Dyson resummation of self-energies are equivalent and both result in the loop-corrected propagator.

In the second section, we discuss the issues of unstable particles and the mixing of particles; in the most general case, both effects play a role in a pole mass calculation. Subsequently, we give explicit one- and two-loop formulae from which the pole mass can be calculated in a fixed-order calculation. These formulae are the basis of a two-loop definition of the OS renormalisation scheme. In a two-loop prediction with particle mixing, resonance effects can enhance the loop corrections to the pole mass. This can be a problem within a fixed-order approach, which can be circumvented by numerically determining the exact location of the propagator pole via a fixed-point iteration. As the numerical approach mixes different loop orders, unphysical effects like a gauge-parameter dependence might affect the prediction. Therefore, depending on the scenario, one method might be more advantageous than the other.

3.1 The Feynman propagator and vertex functions

In this section, we give definitions of different correlation functions and generating functionals which appear in any interacting quantum field theory. For this discussion, we restrict ourselves to a scalar field theory with a single scalar field ϕ. The generalisation to the case of several different species of scalar particles is straightforward. The same concepts naturally exist for fields of higher spin—like fermions and gauge bosons—as well. In this thesis, however, we are solely interested in the prediction of scalar particle masses. Thus, the following definitions will turn out to be sufficient.

3.1.1 Correlation functions

The unrenormalised *Green function* is defined as the vacuum expectation value (VEV) of the time-ordered product of unrenormalised fields, each taken at a different space-time point:

$$G(x_1,\dots,x_n) \equiv \langle\Omega|\, T\phi_B(x_1)\dots\phi_B(x_n)\,|\Omega\rangle\,. \tag{3.1}$$

The renormalised Green function, on the other hand, is defined in terms of renormalised fields

$$\hat{G}(x_1,\dots,x_n) \equiv \langle\Omega|\, T\phi(x_1)\dots\phi(x_n)\,|\Omega\rangle = Z^{-\frac{n}{2}} G(x_1,\dots,x_n). \tag{3.2}$$

For practical applications, it is often easier to work in the momentum representation. Therefore, we introduce momentum-space Green functions via a continuous Fourier transform

$$\begin{aligned}\widetilde{G}(p_1,\dots,p_n) &\equiv \prod_i \left(\int \mathrm{d}^4x_i\, e^{\mathrm{i}p_i\cdot x_i}\right) G(x_1,\dots,x_n)\\ &\equiv (2\pi)^4\delta^{(4)}(p_1+\dots+p_n)G(p_1,\dots,p_n),\end{aligned} \tag{3.3a}$$

$$\begin{aligned}\hat{\widetilde{G}}(p_1,\dots,p_n) &\equiv \prod_i \left(\int \mathrm{d}^4x_i\, e^{\mathrm{i}p_i\cdot x_i}\right) \hat{G}(x_1,\dots,x_n)\\ &\equiv (2\pi)^4\delta^{(4)}(p_1+\dots+p_n)\hat{G}(p_1,\dots,p_n).\end{aligned} \tag{3.3b}$$

The Green functions without tilde are defined by pulling out a Dirac delta distribution which ensures the conservation of the overall four-momentum.
Removing external leg contributions by multiplying an n-point momentum-space

Green function with n inverse propagators is called *truncation*:

$$\widetilde{G}_{\text{trunc}}(p_1,\ldots,p_n) \equiv G^{-1}(p_1,-p_1)\ldots G^{-1}(p_n,-p_n)\widetilde{G}(p_1,\ldots,p_n), \tag{3.4a}$$

$$\hat{\widetilde{G}}_{\text{trunc}}(p_1,\ldots,p_n) \equiv \hat{G}^{-1}(p_1,-p_1)\ldots \hat{G}^{-1}(p_n,-p_n)\hat{\widetilde{G}}(p_1,\ldots,p_n). \tag{3.4b}$$

The relation between unrenormalised and renormalised truncated Green functions is

$$\hat{\widetilde{G}}_{\text{trunc}}(p_1,\ldots,p_n) = Z^{+\frac{n}{2}}\widetilde{G}_{\text{trunc}}(p_1,\ldots,p_n). \tag{3.5}$$

Note that the power of the field renormalisation constant in Eqs. (3.2) and (3.5) differs.

$\mathcal{S}$-matrix elements are just truncated on-shell Green functions supplemented with an appropriate normalisation

$$\begin{aligned}\langle -p_{s+1},\ldots,-p_n|\,\mathcal{S}\,|p_1,\ldots,p_s\rangle &= R^{\frac{n}{2}}\;\widetilde{G}_{\text{trunc}}(p_1,\ldots,p_n)\Big|_{p_i^2=M_i^2}\\ &= \hat{R}^{\frac{n}{2}}\;\hat{\widetilde{G}}_{\text{trunc}}(p_1,\ldots,p_n)\Big|_{p_i^2=M_i^2}.\end{aligned} \tag{3.6}$$

This equation is called the *LSZ formula*; the normalisation factors $R/\hat{R}$ are called *LSZ factors*. They are defined by

$$R \equiv\; -\mathrm{i}(p^2-M^2)\,G(p,-p)\Big|_{p^2=M^2}, \tag{3.7a}$$

$$\hat{R} \equiv\; -\mathrm{i}(p^2-M^2)\,\hat{G}(p,-p)\Big|_{p^2=M^2}, \tag{3.7b}$$

and related to one another by the field renormalisation constant:

$$\hat{R} = Z^{-1}R. \tag{3.8}$$

$\hat{R}$ is sometimes called a *wave-function normalisation factor*. R is renormalisation scheme independent while Z and hence $\hat{R}$ are not. If an OS renormalisation is chosen for Z, i.e. if $Z = R$, the wave-function normalisation $\hat{R}$ equals unity. When defining Z in a minimal subtraction scheme, a finite $\hat{R}$ needs to be included when calculating an $\mathcal{S}$-matrix element.

At tree-level, we do not need to distinguish between unrenormalised and renormalised quantities; the tree-level Green function in position space is given by

$$G^{(0)}(x_1,x_2) = \int \frac{\mathrm{d}^4p}{(2\pi)^4}\frac{\mathrm{i}}{p^2-m^2+\mathrm{i}\epsilon}e^{-\mathrm{i}p\cdot(x_1-x_2)}. \tag{3.9}$$

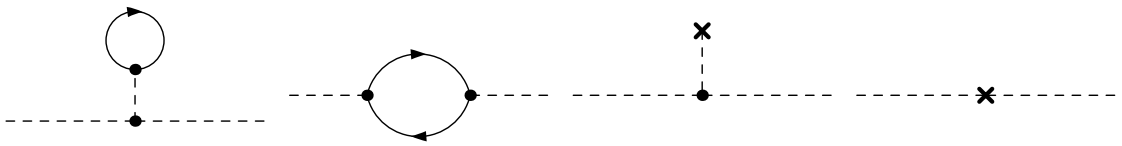

Top. 1 Top. 2 Top. 3 Top. 4

Figure 3.1: Four topologies that can contribute to a self-energy at the one-loop level. The first and third diagram are called tadpole contributions to the self-energy. The crosses in the third and fourth topology denote one-loop counterterm insertions. Not all possible one-loop topologies are shown here.

The ϵ (with $\epsilon > 0$) describes the correct deformation of the integration contour to ensure causality. From this expression, the momentum-space Green function is obtained by a continuous Fourier transform and subsequent removal of a Dirac delta distribution. The result is

$$G^{(0)}(p, -p) = \frac{\mathrm{i}}{p^2 - m^2 + \mathrm{i}\epsilon} \equiv \mathrm{i}\Delta^{(0)}(p^2), \tag{3.10}$$

where we defined the tree-level *Feynman propagator* $\Delta^{(0)}$ for scalar fields. It is worth noting that the imaginary unit is often included in the definition of the Feynman propagator and in these cases it coincides with the two-point Green function.
We conclude this section by motivating the concepts of both connected Green functions and vertex functions. We call a Green function *connected* if it consists only of fully-connected diagrams, i.e. diagrams that not contain any disconnected subgraphs. If we write the $\mathcal{S}$-matrix as

$$\mathcal{S} = \mathbb{1} + \mathrm{i}\mathcal{T}, \tag{3.11}$$

then only the connected Green functions contribute to the *transfer matrix* $\mathcal{T}$. We denote connected Green functions by the symbol G_{conn}.
Lastly, a *vertex function* Γ is a connected, fully truncated, one-particle irreducible (1PI) graph, multiplied by $-\mathrm{i}$.[3] A graph is one-particle irreducible if it decomposes into two graphs by cutting a single, momentum-carrying propagator.
It is important to note that this includes tadpole contributions in the definition of a vertex function. Tadpole contributions are diagrams where at least one propagator has vanishing momentum, see e.g. diagram 1 in Fig. 3.1. In an on-shell renormali-

[3] We include the imaginary unit here so that the vertex functions are derivatives of the effective action without any additional factors, see Sect. 3.1.2.

sation scheme for tadpoles, diagrams 1 and 3 would fully cancel each other. On the other hand, if a tadpole counterterm is not defined in an on-shell scheme, diagrams with tadpole insertions have to be included in the unrenormalised self-energy.

3.1.2 Generating functionals

In this section we briefly recall the definition of the most important *generating functionals* of Green and vertex functions. We give also the relation between the two-point Green and vertex functions and we thereafter derive an explicit expression for the lowest-order two-point vertex function.
Our starting point is the equation

$$Z[J] \equiv e^{-\mathrm{i}E[J]} \equiv \int \mathcal{D}\phi \exp\Big\{\mathrm{i}\int \mathrm{d}^4x \left[\mathcal{L}(\phi(x)) + J(x)\phi(x)\right]\Big\}, \tag{3.12}$$

where Z is the *partition function*,[4] E is the *energy functional*, and J an external source field. The functional derivative of E with respect to J defines the *classical field* in the presence of a source:

$$\frac{\delta}{\delta J(x)} E[J] = -\left\langle \Omega \right| \phi(x) \left| \Omega \right\rangle_J \equiv -\phi_{\mathrm{cl}}(x). \tag{3.13}$$

This definition sets us up to define the *effective action* as a Legendre transform of the energy functional:

$$\Gamma[\phi_{\mathrm{cl}}] \equiv -E[J] - \int \mathrm{d}^4x\, J(x)\phi_{\mathrm{cl}}(x). \tag{3.14}$$

The functional derivative of Γ is

$$\frac{\delta}{\delta \phi_{\mathrm{cl}}(x)} \Gamma[\phi_{\mathrm{cl}}] = -J(x). \tag{3.15}$$

An ordinary n-point Green function is obtained from the partition function by

$$G(x_1,\ldots,x_n) = \frac{1}{Z[0]} \left(-\mathrm{i}\frac{\delta}{\delta J(x_1)}\right) \ldots \left(-\mathrm{i}\frac{\delta}{\delta J(x_n)}\right) Z[J]\Big|_{J=0}. \tag{3.16}$$

If we use E instead of Z, we get the connected n-point Green functions

$$G_{\mathrm{conn}}(x_1,\ldots,x_n) = (-\mathrm{i}) \left(-\mathrm{i}\frac{\delta}{\delta J(x_1)}\right) \ldots \left(-\mathrm{i}\frac{\delta}{\delta J(x_n)}\right) E[J]\Big|_{J=0}. \tag{3.17}$$

[4] Strictly speaking, the partition function is a functional.

Lastly, the n-point vertex functions are obtained from the effective action Γ:

$$\Gamma(x_1,\ldots,x_n) = \left(\frac{\delta}{\delta\phi_{\mathrm{cl}}(x_1)}\right)\ldots\left(\frac{\delta}{\delta\phi_{\mathrm{cl}}(x_n)}\right)\Gamma[\phi_{\mathrm{cl}}]\bigg|_{\phi_{\mathrm{cl}}=0}. \tag{3.18}$$

Let us now derive a relation between the connected two-point Green function and the two-point vertex function (i.e. a vertex function with two external legs):

$$\begin{aligned}\delta^{(4)}(x_1-x_2) &= \frac{\delta J(x_1)}{\delta J(x_2)} \\ &= -\frac{\delta}{\delta J(x_2)}\frac{\delta}{\delta\phi_{\mathrm{cl}}(x_1)}\Gamma[\phi_{\mathrm{cl}}] \\ &= -\int \mathrm{d}^4x_3\,\frac{\delta\phi_{\mathrm{cl}}(x_3)}{\delta J(x_2)}\frac{\delta^2\Gamma[\phi_{\mathrm{cl}}]}{\delta\phi_{\mathrm{cl}}(x_3)\delta\phi_{\mathrm{cl}}(x_1)} \\ &= \int \mathrm{d}^4x_3\,\frac{\delta^2 E[J]}{\delta J(x_2)\delta J(x_3)}\frac{\delta^2\Gamma[\phi_{\mathrm{cl}}]}{\delta\phi_{\mathrm{cl}}(x_3)\delta\phi_{\mathrm{cl}}(x_1)}\end{aligned} \tag{3.19}$$

In the third step, we used the chain rule. Now, setting $J=\phi_{\mathrm{cl}}=0$, we get

$$\delta^{(4)}(x_1-x_2) = (-\mathrm{i})\int \mathrm{d}^4x_3\,G_{\mathrm{conn}}(x_2,x_3)\Gamma(x_3,x_1). \tag{3.20}$$

The two-point Green function is proportional to the propagator, so we can interpret the two-point vertex function as the *inverse propagator*. We now derive an expression for the vertex function in lowest order in two different ways. First, we Fourier transform the tree-level version of Eq. (3.20) by changing the variables $\{x_1,x_2\}\to\{p_1,p_2\}$. Performing the integrals over x_1 and x_2, we are left with

$$\begin{aligned}(2\pi)^4\delta^{(4)}(p_1+p_2) &= \Delta^{(0)}(p_2^2)\widetilde{\Gamma}^{(0)}(p_2,p_1) \\ &= (2\pi)^4\delta^{(4)}(p_1+p_2)\Delta^{(0)}(p_2^2)\Gamma^{(0)}(p_2,-p_2).\end{aligned} \tag{3.21}$$

In the last step we pulled out the Dirac delta distribution of total momentum conservation, leading to $p_1=-p_2$. We can read off the relation

$$\Gamma^{(0)}(p,-p) = \frac{1}{\Delta^{(0)}(p^2)} = p^2-m^2. \tag{3.22}$$

The same relation can alternatively be derived by taking functional derivatives of the effective action. To lowest order, the effective action agrees with the classical

action S and we get

$$\begin{aligned}\frac{\delta^2\Gamma^{(0)}[\phi_{\rm cl}]}{\delta\phi_{\rm cl}(x_1)\delta\phi_{\rm cl}(x_2)} &= \frac{\delta^2}{\delta\phi_{\rm cl}(x_1)\delta\phi_{\rm cl}(x_2)}\int \mathrm{d}^4x\left(\frac{1}{2}\partial_\mu\phi_{\rm cl}\partial^\mu\phi_{\rm cl}-\frac{1}{2}m^2\phi_{\rm cl}^2+\mathcal{L}_{\rm int}\right)\\ &= -(\Box_{x_1}+m^2)\delta^{(4)}(x_1-x_2)+\text{derivatives of }\mathcal{L}_{\rm int}.\end{aligned} \tag{3.23}$$

Setting $\phi_{\rm cl}=0$ removes the interaction terms and yields

$$\Gamma^{(0)}(x_1,x_2) = -(\Box_{x_1}+m^2)\delta^{(4)}(x_1-x_2). \tag{3.24}$$

Fourier transforming this expression as before leads to the known result

$$\Gamma^{(0)}(p,-p) = p^2-m^2. \tag{3.25}$$

3.1.3 Two-point function and propagator at higher orders

Beyond tree level, the two-point vertex function receives quantum corrections from loop diagrams:

$$\hat{\Gamma}(p,-p) = p^2-m^2+\hat{\Sigma}(p^2), \tag{3.26}$$

where $\hat{\Sigma}$ is the renormalised self-energy. $\hat{\Sigma}$ and $\hat{\Gamma}$ are one-particle irreducible. Taking the reciprocal of this expression yields the loop-corrected Feynman propagator

$$\hat{\Delta}(p^2) = \frac{1}{p^2-m^2+\hat{\Sigma}(p^2)}. \tag{3.27}$$

We can rewrite this equation as

$$\begin{aligned}\hat{\Delta}(p^2) &= \Delta^{(0)}(p^2)-\Delta^{(0)}(p^2)\hat{\Sigma}(p^2)\hat{\Delta}(p^2)\\ &= \Delta^{(0)}(p^2)-\hat{\Delta}(p^2)\hat{\Sigma}(p^2)\Delta^{(0)}(p^2).\end{aligned} \tag{3.28}$$

In this form, it is called the *Dyson equation* [162]. We can use this relation recursively to generate the Dyson series

$$\hat{\Delta} = \Delta^{(0)}-\Delta^{(0)}\hat{\Sigma}\Delta^{(0)}+\Delta^{(0)}\hat{\Sigma}\Delta^{(0)}\hat{\Sigma}\Delta^{(0)}-\Delta^{(0)}\hat{\Sigma}\Delta^{(0)}\hat{\Sigma}\Delta^{(0)}\hat{\Sigma}\Delta^{(0)}+\cdots, \tag{3.29}$$

where we have suppressed the momentum dependence of the propagators and self-energies. The Dyson series can be represented diagrammatically as we show in Fig. 3.2.

In this section, we have demonstrated that the loop-corrected propagator is simply the inverse of the loop-corrected two-point vertex function. This is an important

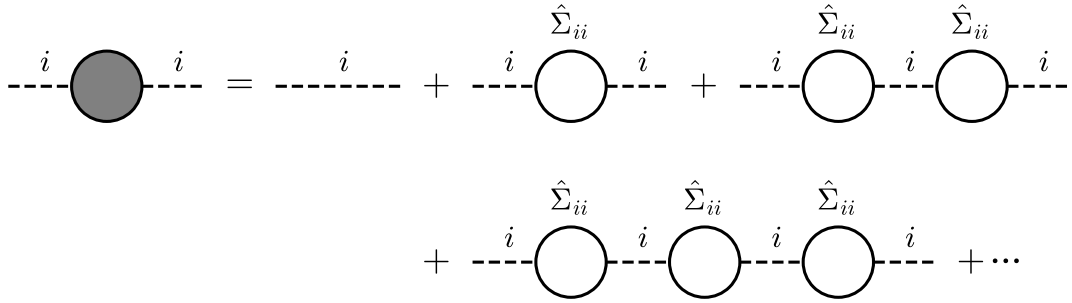

Figure 3.2: The loop-corrected propagator written as a Dyson series for a single particle species i. The grey blob denotes the full loop corrections to the propagator, the white blobs represent one-particle irreducible self-energies. The dashed lines are tree-level propagators.

result, as performing the resummation in the case of particle mixing becomes a non-trivial problem. In this situation, it is much more convenient to work with a matrix of vertex functions and invert it. We will show this explicitly in Sect. 3.2.2.

3.2 Calculating the pole mass

The *pole mass* is the real part of the simple pole of the Feynman propagator, which can be complex. Before we explain the different methods of determining the pole mass, we want to introduce two important concepts: Unstable particles and particle mixing.

3.2.1 Unstable particles and the complex pole

An unstable particle has a finite decay width. If the possible decay products appear in a diagram contributing to the self-energy of the unstable particle, said self-energy acquires a non-vanishing imaginary part for a sufficiently large external momentum. This is a consequence of the *optical theorem*, which is proven from the *unitarity* of the $\mathcal{S}$-matrix [146]. With a complex self-energy, the propagator and the location of its pole become complex quantities as well. We define the complex pole $\mathcal{M}^2$ as the solution of

$$p^2 - m^2 + \hat{\Sigma}(p^2)\Big|_{p^2=\mathcal{M}^2} = 0. \tag{3.30}$$

We split it into its real and imaginary part as

$$\mathcal{M}^2 = M^2 - \mathrm{i}M\Gamma, \tag{3.31}$$

where Γ is the total decay width of the particle. Whenever we talk about the physical pole mass of a particle in this thesis, we refer to the real part M^2 of the complex pole. As the complex pole is a gauge-invariant quantity, defining pole mass and decay width in this way yields a gauge-invariant prediction [163]. Furthermore, a mass counterterm δM^2 defined in the corresponding renormalisation scheme is gauge independent as well.

Of course, we could also define the pole mass as the pole of the real propagator. Let us call this mass $\widetilde{M}^2$. The difference between $\widetilde{M}^2$ and M^2 is gauge dependent and so is the counterterm $\delta\widetilde{M}^2$ [164]. For this reason, we do not use this prescription in the present thesis.

Sometimes, the pole mass is defined as the complex pole in its entirety, i.e. including both real and imaginary part. This leads to a complex mass counterterm $\delta\mathcal{M}^2$. Dependent couplings, for example the weak-mixing angle θ_w, then become complex quantities as well. While complex parameters in the Lagrangian seem to violate unitarity, unitarity still holds at each order of perturbation theory in the complex mass scheme. This happens because for any calculation at order n, the unitarity-violating terms are of order $n+1$ [165, 166]. For simplicity, we will also not follow this approach.

We close this section by addressing an issue which becomes relevant when working with unstable particles: the treatment of complex momenta. Solving the pole equation (3.30) requires evaluating the self-energy and hence loop functions at a complex value. In many cases, the loop integrals have been calculated assuming real arguments and we cannot compute them by simply inserting a complex value. Instead, we use an approximation; let us write the complex momentum as

$$p^2 = p_R^2 + \mathrm{i}p_I^2. \tag{3.32}$$

We then approximate the self-energy by

$$\hat{\Sigma}(p^2) = \hat{\Sigma}(p_R^2 + \mathrm{i}p_I^2) \approx \hat{\Sigma}(p_R^2) + \mathrm{i}p_I^2\partial\hat{\Sigma}(p_R^2). \tag{3.33}$$

Typically, the lowest order contribution to the real part of the pole appears at tree-level whereas the particle's decay width, which gives rise to the non-vanishing imaginary part, is at least a one-loop quantity. Therefore, the above approximation is understood to be a perturbative one. With it, we can evaluate a self-energy at any complex momentum while keeping the argument of any loop function real.

3.2.2 Particle mixing and the vertex function matrix

When two particles carry the same quantum numbers, a Green function containing both fields does not necessarily vanish. On the diagrammatic level, this leads to a non-vanishing mixing self-energy. Suppose we have two scalar particles ϕ_1 and ϕ_2 with identical quantum numbers and a non-vanishing mixing self-energy $\hat{\Sigma}_{12}$. These mixing effects start to play a role at two-loop order and have to be taken into account when making a prediction for the pole mass. Understanding how the propagator has to be resummed in the presence of several particle species is a non-trivial task. Instead, it is easier to invert the two-point vertex function. We can expand the inverse vertex function to show that it indeed takes into account the resummation correctly. As we have two species of particles, the vertex function becomes a 2×2 matrix, whose components read

$$(\Gamma(x_1,x_2))_{ij} = \left(\frac{\delta}{\delta\phi_{i,\mathrm{cl}}(x_1)}\right)\left(\frac{\delta}{\delta\phi_{j,\mathrm{cl}}(x_2)}\right)\Gamma[\phi_{\mathrm{cl}}]\Big|_{\phi_{\mathrm{cl}}=0}. \tag{3.34}$$

In momentum space, it reads

$$\hat{\Gamma}(p,-p) = \begin{pmatrix} p^2 - m_1^2 + \hat{\Sigma}_{11}(p^2) & \hat{\Sigma}_{12}(p^2) \\ \hat{\Sigma}_{21}(p^2) & p^2 - m_2^2 + \hat{\Sigma}_{22}(p^2) \end{pmatrix}. \tag{3.35}$$

We invert this matrix to obtain the loop-corrected propagator matrix

$$\hat{\Delta}(p^2) = \left(\hat{\Gamma}(p,-p)\right)^{-1}. \tag{3.36}$$

The components of the propagator read

$$\hat{\Delta}_{ii}(p^2) = \frac{p^2 - m_j^2 + \hat{\Sigma}_{jj}}{(p^2 - m_i^2 + \hat{\Sigma}_{ii})(p^2 - m_j^2 + \hat{\Sigma}_{jj}) - \hat{\Sigma}_{ij}\hat{\Sigma}_{ji}}, \tag{3.37a}$$

$$\hat{\Delta}_{ij}(p^2) = \frac{-\hat{\Sigma}_{ij}}{(p^2 - m_i^2 + \hat{\Sigma}_{ii})(p^2 - m_j^2 + \hat{\Sigma}_{jj}) - \hat{\Sigma}_{ij}\hat{\Sigma}_{ji}}, \tag{3.37b}$$

where $i \neq j$, and we left out the arguments of the self-energies to improve readability. We can further rewrite the diagonal terms by introducing the *effective self-energy*

$$\hat{\Sigma}_{ii}^{\mathrm{eff}}(p^2) \equiv \hat{\Sigma}_{ii}(p^2) - \frac{\hat{\Sigma}_{ij}(p^2)\hat{\Sigma}_{ji}(p^2)}{p^2 - m_j^2 + \hat{\Sigma}_{jj}(p^2)}, \tag{3.38}$$

which leaves us with

$$\hat{\Delta}_{ii}(p^2) = \frac{1}{p^2 - m_i^2 + \hat{\Sigma}_{ii}^{\mathrm{eff}}(p^2)}. \tag{3.39}$$

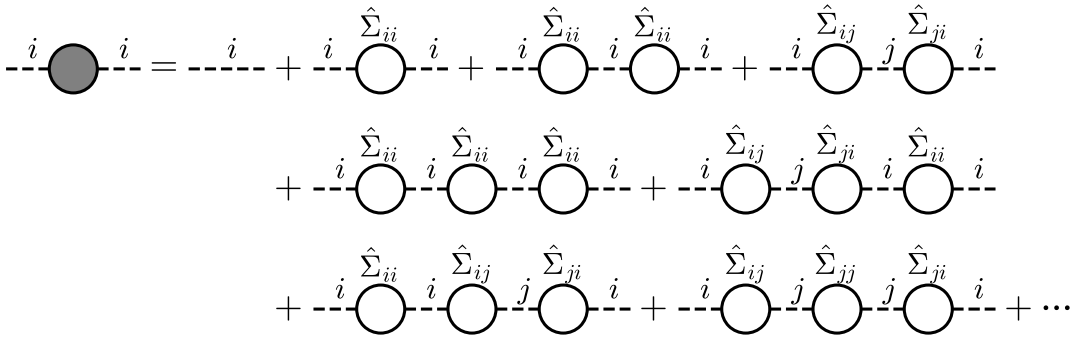

Figure 3.3: The loop-corrected propagator written as a Dyson series in the case of two-particle mixing between states i and j. The grey blob denotes the full loop corrections to the propagator, the white blobs represent one-particle irreducible self-energies. The dashed lines are tree-level propagators.

With the effective self-energy, the loop-corrected propagator is formally identical to the case of no mixing. We can expand the propagator, leading to an expression resembling the Dyson series in Eq. (3.29):

$$\begin{aligned}\hat{\Delta}_{ii} = {} & \Delta_{ii}^{(0)} - \Delta_{ii}^{(0)}\hat{\Sigma}_{ii}\Delta_{ii}^{(0)} + \Delta_{ii}^{(0)}\hat{\Sigma}_{ii}\Delta_{ii}^{(0)}\hat{\Sigma}_{ii}\Delta_{ii}^{(0)} + \Delta_{ii}^{(0)}\hat{\Sigma}_{ij}\Delta_{jj}^{(0)}\hat{\Sigma}_{ji}\Delta_{ii}^{(0)} \\ & - \Delta_{ii}^{(0)}\hat{\Sigma}_{ii}\Delta_{ii}^{(0)}\hat{\Sigma}_{ii}\Delta_{ii}^{(0)}\hat{\Sigma}_{ii}\Delta_{ii}^{(0)} - \Delta_{ii}^{(0)}\hat{\Sigma}_{ij}\Delta_{jj}^{(0)}\hat{\Sigma}_{ji}\Delta_{ii}^{(0)}\hat{\Sigma}_{ii}\Delta_{ii}^{(0)} \\ & - \Delta_{ii}^{(0)}\hat{\Sigma}_{ii}\Delta_{ii}^{(0)}\hat{\Sigma}_{ij}\Delta_{jj}^{(0)}\hat{\Sigma}_{ji}\Delta_{ii}^{(0)} - \Delta_{ii}^{(0)}\hat{\Sigma}_{ij}\Delta_{jj}^{(0)}\hat{\Sigma}_{jj}\Delta_{jj}^{(0)}\hat{\Sigma}_{ji}\Delta_{ii}^{(0)} + \cdots .\end{aligned} \tag{3.40}$$

The same expansion is shown in Fig. 3.3 in a diagrammatic form.
As we can see from Eqs. (3.37), all loop-corrected propagators have the same pole structure. This holds since each element of the propagator matrix is proportional to the inverse determinant of Eq. (3.35). Thus, each propagator, even the off-diagonal ones, can in practice be used to define the pole mass.
We now turn to two methods of calculating the pole mass in the presence of both unstable particles and particle mixing. We keep the number of scalar fields at two for simplicity. All concepts developed in this and the following sections are easily extended to the case of three or more particles mixing.

3.2.3 The fixed-order method

Our starting point for the fixed-order method (FO) is the pole equation

$$p^2 - m_i^2 + \hat{\Sigma}_{ii}^{\text{eff}}(p^2)\Big|_{p^2=\mathcal{M}_i^2} = 0, \tag{3.41}$$

where, as before,

$$\mathcal{M}_i^2 = M_i^2 - \mathrm{i}M_i\Gamma_i. \tag{3.42}$$

The one- and two-loop parts of the effective self-energy read

$$\hat{\Sigma}_{ii}^{\mathrm{eff},(1)} = \hat{\Sigma}_{ii}^{(1)}, \tag{3.43a}$$

$$\hat{\Sigma}_{ii}^{\mathrm{eff},(2)} = \hat{\Sigma}_{ii}^{(2)} - \frac{\hat{\Sigma}_{ij}^{(1)}\hat{\Sigma}_{ji}^{(1)}}{p^2 - m_j^2}, \tag{3.43b}$$

where $j \neq i$. We write the pole mass as the tree-level mass plus quantum corrections at different orders of perturbation theory:

$$M_i^2 = m_i^2 + \Delta^{(1)}M_i^2 + \Delta^{(2)}M_i^2. \tag{3.44}$$

For the one- and two-loop corrections we get

$$\Delta^{(1)}M_i^2 = -\operatorname{Re}\hat{\Sigma}_{ii}^{(1)}(m_i^2), \tag{3.45a}$$

$$\begin{aligned}\Delta^{(2)}M_i^2 = &-\operatorname{Re}\hat{\Sigma}_{ii}^{(2)}(m_i^2) + \operatorname{Re}\partial\hat{\Sigma}_{ii}^{(1)}(m_i^2)\operatorname{Re}\hat{\Sigma}_{ii}^{(1)}(m_i^2) \\ &- \operatorname{Im}\partial\hat{\Sigma}_{ii}^{(1)}(m_i^2)\operatorname{Im}\hat{\Sigma}_{ii}^{(1)}(m_i^2) + \operatorname{Re}\frac{\hat{\Sigma}_{ij}^{(1)}(m_i^2)\hat{\Sigma}_{ji}^{(1)}(m_i^2)}{m_i^2 - m_j^2}.\end{aligned} \tag{3.45b}$$

Demanding $\Delta^{(n)}M_i^2 = 0$ at each loop order n defines the renormalised mass $m_i^2 = M_i^2$ in an OS scheme. We see from Eq. (3.45b) that at the two-loop level mixing effects and imaginary parts of self-energies have to be included in the two-loop mass counterterm, which enters through $\operatorname{Re}\hat{\Sigma}_{ii}^{(2)}(m_i^2)$, to ensure a proper OS definition of M_i^2.

3.2.4 The fixed-point iteration

If the difference of the tree-level masses m_i and m_j of two mixing particles becomes very small, the two-loop correction $\Delta^{(2)}M_i^2$ becomes very large, as we can see in Eq. (3.45b). In this case, the perturbative series breaks down and the fixed-order method no longer provides reliable results. Instead of expanding the effective self-energy up to the desired perturbative order, which is the approach we take in the fixed-order method, we perturbatively expand the two-point function given in Eq. (3.35) before inverting it. This leads to an effective self-energy in which all entries of the self-energy matrix are expanded up to the same order. This amounts to including mixing effects already at the one-loop level.

With this approximation for the effective self-energy, we have to find the exact

solution of Eq. (3.41), which does not suffer from the fixed-order resonance effects. A self-energy usually has a complicated dependence on the external momentum p^2, and we have to employ a numerical method to find the exact location of the pole. In this thesis, we utilise an iterative procedure to determine the precise location of the complex pole. We solve the pole equation (3.30) for its explicit p^2 dependence and obtain the fixed-point iteration

$$p_{k+1}^2 = m_i^2 + \hat{\Sigma}_{ii}^{\text{eff}}(p_k^2) \equiv f_i(p_k^2), \quad k \in \mathbb{N}_0, \tag{3.46}$$

where p_0^2 is the starting point of the iteration. If the iteration converges

$$\lim_{k\to\infty} p_k^2 = \lim_{k\to\infty} f_i(p_k^2) \equiv \mathcal{M}^2, \tag{3.47}$$

we have found the complex pole $\mathcal{M}^2$, which is a fixed-point of f_i. The iteration converges in most scenarios investigated in the framework of the thesis.
If two species of particles participate in the mixing, we get two functions f_1 and f_2 as well as two complex poles $\mathcal{M}_1^2$ and $\mathcal{M}_2^2$. Both poles are fixed points of either function:

$$\mathcal{M}_a^2 = f_i(\mathcal{M}_a^2) \quad \text{for } i,a \in \{1,2\}. \tag{3.48}$$

We denote a tree-level mass eigenstate by the label i and a loop-corrected mass eigenstate by a. As both poles can in principle be found with either pole equation, the identification of a tree-level eigenstate with a corresponding loop-corrected mass eigenstate is not unique [163]. We order the loop-corrected masses by size of their real parts, i.e.

$$\operatorname{Re}\mathcal{M}_1^2 = M_1^2 < M_2^2 = \operatorname{Re}\mathcal{M}_2^2. \tag{3.49}$$

Both poles are fixed points of the f_i, so we can in principle use either f_1 or f_2 in the iteration to find the poles. As it turns out, in the case of 2×2 mixing, each pole is usually an attractive fixed point of one of the f_i, and a repelling fixed point of the other one. For practical application this means that we need to perform the fixed-point iteration with f_1 and f_2 to find both poles.
We demonstrate this in an MSSM scenario where $\mathcal{CP}$ symmetry is conserved, i.e. in the Higgs sector we have 2×2 mixing between the $\mathcal{CP}$-even scalars h and H. The loop-corrected mass eigenstates are h_1 and h_2, where h_1 is the lighter one. $\mathcal{M}_{h_1}^2$ is, for our case, the attractive fixed point of f_h and the repelling fixed point of f_H. For $\mathcal{M}_{h_2}^2$, the opposite is true. This is shown in Fig. 3.4.
We can see that $\mathcal{M}_{h_1}^2$ is a repelling fixed point of f_H, and $\mathcal{M}_{h_2}^2$ of f_h. If we use the real part of the complex pole as starting value p_0^2 (red and cyan dashed curves), the

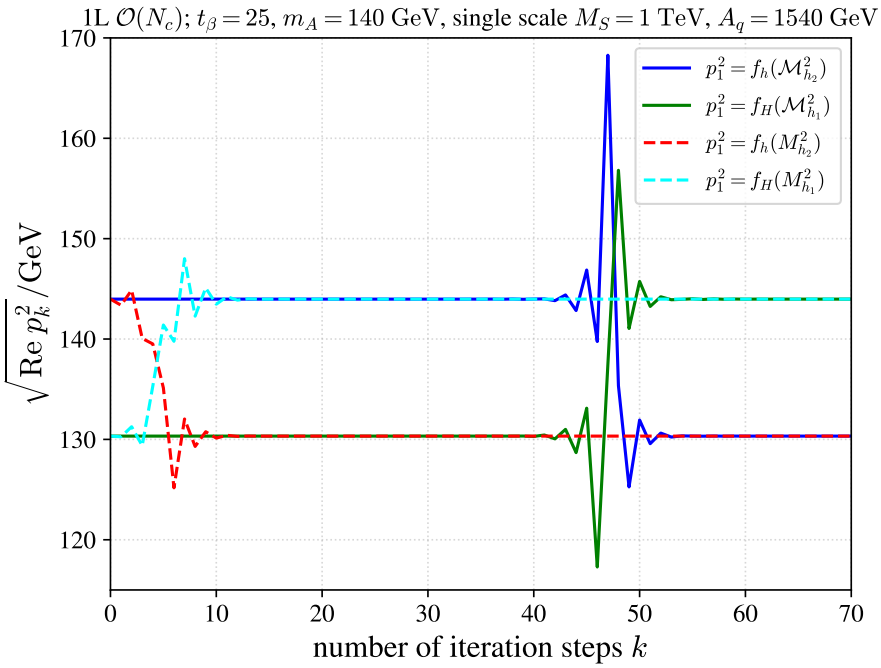

Figure 3.4: This figure shows how the iterative determination of the complex pole converges when choosing a starting value close to the repelling solution. k denotes the number of iteration steps, and p_k^2 is the momentum after k steps. As starting values p_0^2 we use both the full complex pole (blue and green curves) as well as the real part of the complex pole (red and cyan curves) of the respective repelling solution.

fixed-point iteration quickly reaches the opposite, attractive solution. If we use the full complex pole as starting value (solid blue and green curves), the iteration needs approximately 40 steps before it visibly moves away from the repelling solution, after which it quickly converges. Thus, we need both f_h and f_H to reliably find the two complex poles of the system.

We find a similar behaviour also in the case of a $\mathcal{CP}$-violating MSSM scenario with the same parameters as in Fig. 3.4 but $A_t = (1540 + 10\mathrm{i})$ GeV instead. In this case, the three scalars h, H, and A mix, giving rise to three functions f_h, f_H, and f_A. For each function, there are three fixed points, one of which is attractive and two are repelling. When plugging the solution found with f_A into f_h/f_H, the solver quickly converges and vice versa. The solution found with f_h lets the solver converge much more slowly when plugged into f_H and vice versa.

The fixed-point iteration, similar to other numerical methods that are used to determine the exact location of the pole of the propagator, mixes different orders of perturbation theory. As a consequence, such a prediction typically depends on the choice for the gauge-fixing parameters and the field counterterms. These unphysical, residual dependencies are e.g. studied in Refs. [79, 129, 130, 167].

4 Renormalisation of the MSSM

When predicting the Higgs boson masses in the MSSM at $\mathcal{O}\Big((\alpha_{\text{em}} + \alpha_q)^2 N_c^2\Big)$, two sectors of the model have to be renormalised; we need a renormalisation of the quark-squark sector at the one-loop level while the Higgs-gauge sector is renormalised up to two-loop order. For each sector, we first outline its structure at the tree-level. This gives an overview over the relevant model parameters, and we see how many input parameters are needed to perform a prediction, each corresponding to an independent renormalisation condition.
A renormalisation transformation tells us how a bare parameter or field is related to its renormalised value and its counterterm. The full set of transformations leads to expressions for renormalised self-energies in terms of unrenormalised self-energies and counterterms.
At the time and due to a lack of observation of SM superpartners, most MSSM parameters cannot be linked to measured physical observables. Thus, it is often not obvious which input parameters should be used for a calculation and which renormalisation schemes are appropriate for those parameters. In the quark-squark sector, we will present three different renormalisation schemes which differ both in the choice of input parameters and the renormalisation conditions. In the Higgs-gauge sector, the renormalisation of the parameter $\tan(\beta)$ plays an important role, and we will give two renormalisation prescriptions for it.
Parameters which do not serve as input parameters are dependent quantities; their values are calculated from the input parameters. Expressions for their counterterms are given in this chapter and in App. A.

4.1 The quark and squark sector of the MSSM

In this section, we fix the notation for the quark and squark sector in the MSSM. We give the renormalisation transformations and the resulting expressions for the renormalised squark self-energy diagrams up to the one-loop order. We present three different renormalisation schemes for the case of massive quarks and we illustrate how the renormalisation has to be modified in the massless case.

Throughout the whole thesis, we assume that mass terms do not mix quarks and squarks of different generations. This implies a unit CKM matrix and squark mass matrices which are diagonal in flavour space. The generalisation of our results to the case of non-zero mixing between the generations would easily be possible but is expected to not yield any new insights. Quartic interaction terms between squark flavours of different generations will nevertheless lead to Higgs self-energy diagrams with generation mixing.
The quark sector requires no renormalisation at our order of perturbation theory, so we focus solely on the squark sector of the MSSM.

4.1.1 Tree-level

The bilinear squark Lagrangian reads

$$\mathcal{L}^{\text{bil.}}_{\text{squark}} = \sum_{\tilde{q}} \left(\partial_\mu \tilde{q}_L^* \partial^\mu \tilde{q}_L + \partial_\mu \tilde{q}_R^* \partial^\mu \tilde{q}_R - \begin{pmatrix} \tilde{q}_L^* & \tilde{q}_R^* \end{pmatrix} \mathbf{M}^2_{\tilde{q}} \begin{pmatrix} \tilde{q}_L \\ \tilde{q}_R \end{pmatrix} \right), \tag{4.1}$$

where the sum runs over the squark flavors $\tilde{t}, \tilde{b}, \tilde{c}, \tilde{s}, \tilde{u}, \tilde{d}$. As we do not consider generation mixing, the squark mass matrices are flavour diagonal. We denote the elements of a squark mass matrix by

$$\mathbf{M}^2_{\tilde{q}} = \begin{pmatrix} \left(\mathbf{M}^2_{\tilde{q}}\right)_{LL} & \left(\mathbf{M}^2_{\tilde{q}}\right)_{LR} \\ \left(\mathbf{M}^2_{\tilde{q}}\right)_{RL} & \left(\mathbf{M}^2_{\tilde{q}}\right)_{RR} \end{pmatrix}. \tag{4.2}$$

The squark fields carry non-vanishing quantum numbers and are thus complex scalar fields; the mass matrices are, in the most general case, not symmetric but hermitian so that their eigenvalues—the physical squark masses—are real. The mass matrices for up- and down-type squarks read

$$\mathbf{M}^2_{\tilde{u}_g} = \begin{pmatrix} M^2_{\tilde{q}_g} + m^2_{u_g} + M_Z^2 \cos(2\beta)(\frac{1}{2} - \frac{2}{3}s^2_{\text{w}}) & m_{u_g} X^*_{u_g} \\ m_{u_g} X_{u_g} & M^2_{\tilde{u}_g} + m^2_{u_g} + \frac{2}{3} M_Z^2 \cos(2\beta) s^2_{\text{w}} \end{pmatrix}, \tag{4.3a}$$

$$\mathbf{M}^2_{\tilde{d}_g} = \begin{pmatrix} M^2_{\tilde{q}_g} + m^2_{d_g} + M_Z^2 \cos(2\beta)(-\frac{1}{2} + \frac{1}{3}s^2_{\text{w}}) & m_{d_g} X^*_{d_g} \\ m_{d_g} X_{d_g} & M^2_{\tilde{d}_g} + m^2_{d_g} - \frac{1}{3} M_Z^2 \cos(2\beta) s^2_{\text{w}} \end{pmatrix}. \tag{4.3b}$$

The index g labels the three generations of matter such that $m_{u_3} = m_t$ and $X_{d_2} = X_s$, for instance. We do not use this convention for the soft SUSY-breaking masses $M^2_{\tilde{q}_g}$, $M^2_{\tilde{u}_g}$, and $M^2_{\tilde{d}_g}$, i.e. there is no parameter $M^2_{\tilde{t}}$, so that we can distinguish between the

respective left- ($M^2_{\tilde{q}_3}$) and right-handed ($M^2_{\tilde{u}_3}$) mass terms. Moreover, we introduced the common abbreviations

$$X_{u_g} = A_{u_g} - \mu^* \cot(\beta), \tag{4.4a}$$

$$X_{d_g} = A_{d_g} - \mu^* \tan(\beta). \tag{4.4b}$$

The parameters $M^2_{\tilde{q}_g}, M^2_{\tilde{u}_g}, M^2_{\tilde{d}_g}, A_{u_g}, A_{d_g}$ break supersymmetry softly. In the most general scenario of SUSY breaking, they would be 3×3 matrices in generation space. In our calculation, as mentioned above, we neglect this mixing between generations and assume these matrices diagonal.

To change from the gauge eigenbasis to the mass eigenbasis, we introduce the unitary transformation

$$\begin{pmatrix} \tilde{q}_1 \\ \tilde{q}_2 \end{pmatrix} = \begin{pmatrix} c_{\tilde{q}} & -s_{\tilde{q}} e^{-\mathrm{i}\phi_{\tilde{q}}} \\ s_{\tilde{q}} e^{\mathrm{i}\phi_{\tilde{q}}} & c_{\tilde{q}} \end{pmatrix} \begin{pmatrix} \tilde{q}_L \\ \tilde{q}_R \end{pmatrix} \equiv U_{\tilde{q}} \begin{pmatrix} \tilde{q}_L \\ \tilde{q}_R \end{pmatrix} \tag{4.5}$$

for each squark flavor $\tilde{q}$. Here we introduced the abbreviations $c_{\tilde{q}} = \cos\left(\theta_{\tilde{q}}\right)$ and $s_{\tilde{q}} = \sin\left(\theta_{\tilde{q}}\right)$. The bilinear squark Lagrangian in terms of the mass eigenbasis reads

$$\mathcal{L}^{\text{bil.}}_{\text{squark}} = \sum_{\tilde{q}} \left(\partial_\mu \tilde{q}_1^* \partial^\mu \tilde{q}_1 + \partial_\mu \tilde{q}_2^* \partial^\mu \tilde{q}_2 - \begin{pmatrix} \tilde{q}_1^* & \tilde{q}_2^* \end{pmatrix} \mathbf{D}^2_{\tilde{q}} \begin{pmatrix} \tilde{q}_1 \\ \tilde{q}_2 \end{pmatrix} \right), \tag{4.6}$$

where

$$\mathbf{D}^2_{\tilde{q}} = U_{\tilde{q}} \mathbf{M}^2_{\tilde{q}} U^\dagger_{\tilde{q}} \equiv \begin{pmatrix} m^2_{\tilde{q}_1} & m^2_{\tilde{q}_{12}} \\ m^2_{\tilde{q}_{21}} & m^2_{\tilde{q}_2} \end{pmatrix}, \quad m^2_{\tilde{q}_{21}} = m^{2*}_{\tilde{q}_{12}}. \tag{4.7}$$

The angles $\theta_{\tilde{q}} \in [0, \frac{\pi}{2}]$ and $\phi_{\tilde{q}} \in (-\pi, \pi]$ are then determined by the conditions

$$m^2_{\tilde{q}_{12}} = 0 \quad \wedge \quad m^2_{\tilde{q}_1} \leq m^2_{\tilde{q}_2}. \tag{4.8}$$

To give explicit expressions for $\theta_{\tilde{q}}$ and $\phi_{\tilde{q}}$, we have to distinguish between the degenerate and the non-degenerate case. The two squark mass eigenvalues are degenerate if and only if the matrix $\mathbf{M}^2_{\tilde{q}}$ is proportional to the identity matrix, in which case no rotation is needed and $U_{\tilde{q}}$ can simply be chosen as unity. This happens when both $m_q X_q = 0$ and $\left(\mathbf{M}^2_{\tilde{q}}\right)_{LL} = \left(\mathbf{M}^2_{\tilde{q}}\right)_{RR}$ are fulfilled simultaneously. When working in the gaugeless limit, assuming a vanishing quark mass and a universal SUSY scale $M^2_{\text{SUSY}} = M^2_{\tilde{q}_g} = M^2_{\tilde{u}_g} = M^2_{\tilde{d}_g}$, this is always the case.

In the case of non-degenerate masses, the mass ordering ensures $m^2_{\tilde{q}_1} < m^2_{\tilde{q}_2}$, and we

can write

$$\exp\left(\mathrm{i}\phi_{\tilde{q}}\right) = \frac{X_q}{|X_q|}, \tag{4.9a}$$

$$\cos\left(2\theta_{\tilde{q}}\right) = \frac{\left(\mathbf{M}^2_{\tilde{q}}\right)_{RR} - \left(\mathbf{M}^2_{\tilde{q}}\right)_{LL}}{m^2_{\tilde{q}_2} - m^2_{\tilde{q}_1}}, \tag{4.9b}$$

$$\sin\left(2\theta_{\tilde{q}}\right) = \frac{2m_q|X_q|}{m^2_{\tilde{q}_2} - m^2_{\tilde{q}_1}}. \tag{4.9c}$$

The angles can then uniquely be determined from

$$\phi_{\tilde{q}} = \mathrm{Arg}(X_q), \qquad -\pi < \phi_{\tilde{q}} \leq \pi, \tag{4.10a}$$

$$\theta_{\tilde{q}} = \frac{1}{2}\arccos\frac{\left(\mathbf{M}^2_{\tilde{q}}\right)_{RR} - \left(\mathbf{M}^2_{\tilde{q}}\right)_{LL}}{m^2_{\tilde{q}_2} - m^2_{\tilde{q}_1}}, \qquad 0 \leq \theta_{\tilde{q}} \leq \tfrac{\pi}{2}. \tag{4.10b}$$

Mathematically, $\phi_{\tilde{q}}$ is undefined if X_q vanishes, and we set it to 0 for simplicity in this case.

The renormalisation transformations

For a full two-loop prediction of the Higgs boson masses, the one-loop renormalisation of the squark sector is needed. As we are only interested in electroweak corrections of $\mathcal{O}\left((\alpha_{\mathrm{em}} + \alpha_q)^2 N_c^2\right)$, no lepton/slepton/quark renormalisation constants are needed.
We renormalise the squark mass matrices and fields via

$$\mathbf{D}^2_{\tilde{q}} \to \mathbf{D}^2_{\tilde{q}} + \begin{pmatrix} \delta m^2_{\tilde{q}_1} & \delta m^2_{\tilde{q}_{12}} \\ \delta m^2_{\tilde{q}_{21}} & \delta m^2_{\tilde{q}_2} \end{pmatrix}, \tag{4.11a}$$

$$\begin{pmatrix} \tilde{q}_1 \\ \tilde{q}_2 \end{pmatrix} \to \begin{pmatrix} \sqrt{1+\delta Z_{\tilde{q}_{11}}} & \frac{1}{2}\delta Z_{\tilde{q}_{12}} \\ \frac{1}{2}\delta Z_{\tilde{q}_{21}} & \sqrt{1+\delta Z_{\tilde{q}_{22}}} \end{pmatrix} \begin{pmatrix} \tilde{q}_1 \\ \tilde{q}_2 \end{pmatrix}, \tag{4.11b}$$

$$\begin{pmatrix} \tilde{q}^*_1 \\ \tilde{q}^*_2 \end{pmatrix} \to \begin{pmatrix} \sqrt{1+\delta Z_{\tilde{q}_{11}}} & \frac{1}{2}\delta \bar{Z}_{\tilde{q}_{21}} \\ \frac{1}{2}\delta \bar{Z}_{\tilde{q}_{12}} & \sqrt{1+\delta Z_{\tilde{q}_{22}}} \end{pmatrix} \begin{pmatrix} \tilde{q}^*_1 \\ \tilde{q}^*_2 \end{pmatrix}. \tag{4.11c}$$

It should be noted that we introduce separate off-diagonal field counterterms for the squark and anti-squark fields. This follows the convention of Refs. [49, 50], where it enables the inclusion of absorptive contributions into the field counterterms. If the absorptive parts are left out, the off-diagonal field counterterms are related by $\delta \bar{Z}_{\tilde{q}_{ij}} = \delta Z^*_{\tilde{q}_{ji}}$.

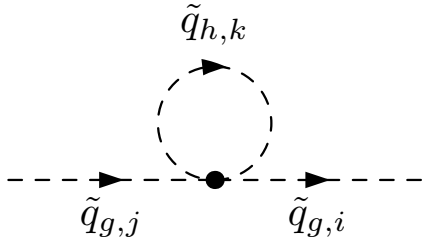

Figure 4.1: Unrenormalised one-loop squark self-energy $\Sigma^{(1)}_{\tilde{q}_{g,i}\tilde{q}_{g,j}}$. g and h are flavour labels, which we make explicit here since the squark in the loop, $\tilde{q}_h$, can have a different flavour than the external squark. i, j, and k label the two mass eigenstates. Note the convention for naming the self-energy, where the first label corresponds to the outgoing squark in the diagram.

4.1.2 Renormalisation at the one-loop level

In this section, we give an overview over the most important renormalisation schemes for the squark sector. We present expressions for the relevant one-loop renormalisation constants; they enter the prediction for the two-loop Higgs boson masses through the sub-loop part of two-loop Higgs self-energies.
With the renormalisation transformations given in the previous section, the renormalised one-loop squark self-energies read

$$\hat{\Sigma}^{(1)}_{\tilde{q}_1\tilde{q}_1}(p^2) = \Sigma^{(1)}_{\tilde{q}_1\tilde{q}_1}(p^2) + \delta^{(1)}Z_{\tilde{q}_{11}}(p^2 - m^2_{\tilde{q}_1}) - \delta^{(1)}m^2_{\tilde{q}_1}, \tag{4.12a}$$

$$\begin{aligned}\hat{\Sigma}^{(1)}_{\tilde{q}_1\tilde{q}_2}(p^2) = \Sigma^{(1)}_{\tilde{q}_1\tilde{q}_2}(p^2) &+ \frac{1}{2}\delta^{(1)}Z_{\tilde{q}_{12}}(p^2 - m^2_{\tilde{q}_1}) \\ &+ \frac{1}{2}\delta^{(1)}\bar{Z}_{\tilde{q}_{12}}(p^2 - m^2_{\tilde{q}_2}) - \delta^{(1)}m^2_{\tilde{q}_{12}},\end{aligned} \tag{4.12b}$$

$$\begin{aligned}\hat{\Sigma}^{(1)}_{\tilde{q}_2\tilde{q}_1}(p^2) = \Sigma^{(1)}_{\tilde{q}_2\tilde{q}_1}(p^2) &+ \frac{1}{2}\delta^{(1)}Z_{\tilde{q}_{21}}(p^2 - m^2_{\tilde{q}_2}) \\ &+ \frac{1}{2}\delta^{(1)}\bar{Z}_{\tilde{q}_{21}}(p^2 - m^2_{\tilde{q}_1}) - \delta^{(1)}m^2_{\tilde{q}_{21}},\end{aligned} \tag{4.12c}$$

$$\hat{\Sigma}^{(1)}_{\tilde{q}_2\tilde{q}_2}(p^2) = \Sigma^{(1)}_{\tilde{q}_2\tilde{q}_2}(p^2) + \delta^{(1)}Z_{\tilde{q}_{22}}(p^2 - m^2_{\tilde{q}_2}) - \delta^{(1)}m^2_{\tilde{q}_2}. \tag{4.12d}$$

The only topology contributing to the $\Sigma^{(1)}_{\tilde{q}_i\tilde{q}_j}$ self-energy at $\mathcal{O}(N_c)$ is shown in Fig. 4.1. These diagrams are independent of the external momentum, and no field renormalisation constants are needed to yield finite renormalised one-loop self-energies. Since in our calculation squarks appear as internal particles only, any finite part of their field renormalisation constants cancels in the sub-loop renormalisation of the

two-loop Higgs (and vector boson) self-energies, and we will set them to zero for simplicity:

$$\delta^{(1)} Z_{\tilde{q}_{ij}} = 0, \tag{4.13a}$$

$$\delta^{(1)} \bar{Z}_{\tilde{q}_{ij}} = 0. \tag{4.13b}$$

While this choice is not necessary, it simplifies the algebraic expressions and, if an on-shell renormalisation scheme is chosen for the squark masses, it lets the squark self-energies vanish for arbitrary external momenta.
By virtue of the momentum independence, the self-energies are free from absorptive contributions and they can only be complex because of the involved couplings. Consequently, the off-diagonal unrenormalised squark self-energies are related via

$$\Sigma^{(1)*}_{\tilde{q}_1\tilde{q}_2} \overset{\mathcal{O}(N_c)}{=} \Sigma^{(1)}_{\tilde{q}_2\tilde{q}_1}, \tag{4.14}$$

which holds for the renormalised self-energies as well. Whenever we set the symbol $\mathcal{O}(N_c)$ over an equal sign, the identity holds in our calculation at $\mathcal{O}(N_c)$ but not necessarily in a more inclusive one. Due to the absence of absorptive contributions, the diagonal self-energies are real.

Renormalisation conditions and counterterms for the massive case

In this thesis, unless explicitly stated otherwise, we work with a massive third generation of quarks, while the first two generations are treated as massless. For the third generation squark sector, we consider several different renormalisation schemes; an on-shell scheme (OS), a $\overline{\text{DR}}$ scheme, and a mixed scheme. In each of these schemes, we allow for either sbottom mass $m^2_{\tilde{b}_i}$ to be used as input parameter, which amounts to a total of six different renormalisation schemes for the third generation squark sector.
Regarding the choice of renormalisation conditions, it is useful to count the number of independent parameters first. A set of independent parameters in the stop-sbottom sector is for example given by $\{M^2_{\tilde{q}_3}, M^2_{\tilde{u}_3}, M^2_{\tilde{d}_3}, A_t, A_b\}$, of which the trilinear couplings can be complex. This requires us to impose seven (real) renormalisation conditions. Independent of the chosen renormalisation scheme for the squark sector, we require that

$$\mu,\ A_b \text{ are renormalised in the } \overline{\text{DR}} \text{ scheme.} \tag{4.15}$$

We derive the $\overline{\text{DR}}$ expressions for μ and A_b in Sect. 4.1.3.
In all schemes, the stop masses and one of the sbottom masses are used as indepen-

dent input parameters. We label the independent sbottom with n and the dependent sbottom with $f = 3-n$. In the case of the $\mathcal{O}\Big((\alpha_{\text{em}} + \alpha_q)^2 N_c^2\Big)$ contributions that are of interest to us, the quark sector is not renormalised. For the sake of completeness, we include the vanishing quark mass counterterms in the expressions below.

(i) OS scheme. We use on-shell definitions for the stop parameters and the nth sbottom mass:

$$\delta^{(1)} m^2_{\tilde{t}_i} = \operatorname{Re} \Sigma^{(1)}_{\tilde{t}_i \tilde{t}_i} \overset{\mathcal{O}(N_c)}{=} \Sigma^{(1)}_{\tilde{t}_i \tilde{t}_i}, \quad i \in \{1,2\}, \tag{4.16a}$$

$$\delta^{(1)} m^2_{\tilde{b}_n} = \operatorname{Re} \Sigma^{(1)}_{\tilde{b}_n \tilde{b}_n} \overset{\mathcal{O}(N_c)}{=} \Sigma^{(1)}_{\tilde{b}_n \tilde{b}_n}, \tag{4.16b}$$

$$\delta^{(1)} m^2_{\tilde{t}_{12}} = \widetilde{\operatorname{Re}}\, \Sigma^{(1)}_{\tilde{t}_1 \tilde{t}_2} \overset{\mathcal{O}(N_c)}{=} \Sigma^{(1)}_{\tilde{t}_1 \tilde{t}_2}, \tag{4.16c}$$

$$\delta^{(1)} m^2_{\tilde{t}_{21}} = \delta^{(1)} m^{2*}_{\tilde{t}_{12}} \overset{\mathcal{O}(N_c)}{=} \Sigma^{(1)}_{\tilde{t}_2 \tilde{t}_1}. \tag{4.16d}$$

The operator $\widetilde{\operatorname{Re}}$ takes the real part of the loop integrals but leaves complex couplings unaffected. In our calculation, the squark self-energies are momentum independent and so we do not specify any momentum at which the self-energies are to be evaluated. It should be noted that the renormalisation condition for the off-diagonal stop mass terms only in our calculation of N_c contributions implies that the whole renormalised self-energy vanishes (because we chose $\delta Z_{\tilde{q}_{ij}} = \delta \bar{Z}_{\tilde{q}_{ij}} = 0$); in a setting where the squark self-energies are momentum-dependent, an unphysical MOM scheme is often used instead, see Refs. [48, 50, 68, 168, 169].
In this scheme, the A_t counterterm is a dependent quantity:

$$\begin{aligned}\delta^{(1)} A_t = \frac{1}{m_t} \Big[U_{\tilde{t}_{11}} U^*_{\tilde{t}_{12}} \left(\delta^{(1)} m^2_{\tilde{t}_1} - \delta^{(1)} m^2_{\tilde{t}_2} \right) + U_{\tilde{t}_{21}} U^*_{\tilde{t}_{12}} \delta^{(1)} m^2_{\tilde{t}_{12}} + U_{\tilde{t}_{11}} U^*_{\tilde{t}_{22}} \delta^{(1)} m^2_{\tilde{t}_{21}} \Big] \\ - \frac{X_t\, \delta^{(1)} m_t}{m_t} + \frac{\delta^{(1)} \mu^*}{t_\beta} - \frac{\mu^* \delta^{(1)} t_\beta}{t_\beta^2}.\end{aligned} \tag{4.17}$$

(ii) $\overline{\text{DR}}$ scheme. In this scheme, we use A_t to formulate a renormalisation condition instead of $m^2_{\tilde{t}_{12}}$. Now, all the input counterterms are defined in the $\overline{\text{DR}}$ scheme:

$$m^2_{\tilde{t}_1},\ m^2_{\tilde{t}_2},\ m^2_{\tilde{b}_n}, \text{ and } A_t \text{ are renormalised in the } \overline{\text{DR}} \text{ scheme.} \tag{4.18}$$

The $\overline{\text{DR}}$ counterterms for the masses are obtained by simply discarding the finite parts of the OS counterterms. The $\overline{\text{DR}}$ expression for $\delta^{(1)} A_t$ is derived in Sect. 4.1.3.

Finally, the $m^2_{\tilde{t}_{12}}$ counterterm is a dependent quantity now:

$$\delta^{(1)} m^2_{\tilde{t}_{12}} = \frac{1}{|U_{\tilde{t}_{11}}|^2 - |U_{\tilde{t}_{12}}|^2} \Big[U_{\tilde{t}_{11}} U^*_{\tilde{t}_{21}} \left(\delta^{(1)} m^2_{\tilde{t}_1} - \delta^{(1)} m^2_{\tilde{t}_2} \right) + U_{\tilde{t}_{11}} U^*_{\tilde{t}_{22}} \left(m_t \, \delta^{(1)} X^*_t + X^*_t \, \delta^{(1)} m_t \right) - U_{\tilde{t}_{12}} U^*_{\tilde{t}_{21}} \left(m_t \, \delta^{(1)} X_t + X_t \, \delta^{(1)} m_t \right) \Big]. \tag{4.19}$$

(iii) Mixed scheme. The input counterterms are the same as in the $\overline{\text{DR}}$ scheme, but now

$$m^2_{\tilde{t}_1}, \, m^2_{\tilde{t}_2}, \text{ and } m^2_{\tilde{b}_n} \text{ are renormalised on-shell. } A_t \text{ is renormalised } \overline{\text{DR}}. \tag{4.20}$$

$\delta^{(1)} m^2_{\tilde{t}_{12}}$ is calculated by the same expression as in the $\overline{\text{DR}}$ scheme. In this scheme, just as in the $\overline{\text{DR}}$ scheme, μ, t_β, and both A_t and A_b are $\overline{\text{DR}}$ quantities. Consequently, X_t and X_b are $\overline{\text{DR}}$ quantities as well.

Scheme-independent relations. In all three schemes, the counterterms for the sbottom masses $m^2_{\tilde{b}_f}$ and $m^2_{\tilde{b}_{12}}$ are dependent quantities and as such they have to be expressed in terms of the input counterterms. To find the expression for the remaining sbottom mass counterterm, we make use of a relation between the LL entries (see Eq. (4.2)) of the stop and sbottom mass matrix. Both entries contain the SUSY-breaking parameter $M^2_{\tilde{q}_3}$, yielding

$$\begin{aligned} M^2_{\tilde{q}_3} &= \left(\mathbf{M}^2_{\tilde{t}} \right)_{LL} - m^2_t - M^2_Z c_{2\beta} \left(\frac{1}{2} - \frac{2}{3} s^2_{\text{w}} \right) \\ &= \left(\mathbf{M}^2_{\tilde{b}} \right)_{LL} - m^2_b + M^2_Z c_{2\beta} \left(\frac{1}{2} - \frac{1}{3} s^2_{\text{w}} \right) \end{aligned} \tag{4.21a}$$

$$\Leftrightarrow \left(\mathbf{M}^2_{\tilde{b}} \right)_{LL} = \left(\mathbf{M}^2_{\tilde{t}} \right)_{LL} - m^2_t + m^2_b - M^2_W c_{2\beta}. \tag{4.21b}$$

In order to simplify the notation, we introduce the auxiliary renormalisation constant

$$\begin{aligned} \delta^{(1)} \left(\mathbf{M}^2_{\tilde{b}} \right)_{LL} = {} & |U_{\tilde{t}_{11}}|^2 \delta^{(1)} m^2_{\tilde{t}_1} + |U_{\tilde{t}_{12}}|^2 \delta^{(1)} m^2_{\tilde{t}_2} - 2 \, \text{Re} \left\{ U_{\tilde{t}_{22}} U^*_{\tilde{t}_{12}} \delta^{(1)} m^2_{\tilde{t}_{12}} \right\} \\ & - 2 m_t \delta^{(1)} m_t + 2 m_b \delta^{(1)} m_b - c_{2\beta} \delta^{(1)} M^2_W + 4 M^2_W s_\beta c^3_\beta \delta^{(1)} t_\beta. \end{aligned} \tag{4.22}$$

This constant allows us to write the dependent sbottom mass counterterm as

$$\delta^{(1)} m^2_{\tilde{b}_f} = \frac{1}{|U_{\tilde{b}_{1f}}|^2}\Big[|U_{\tilde{b}_{1n}}|^2 \delta^{(1)} m^2_{\tilde{b}_n} + (n-f)\Big(2\ \mathrm{Re}\left\{U_{\tilde{b}_{11}} U^*_{\tilde{b}_{12}}\left(m_b\, \delta^{(1)} X_b^* + X_b^*\, \delta^{(1)} m_b\right)\right\} + \left(|U_{\tilde{b}_{11}}|^2 - |U_{\tilde{b}_{12}}|^2\right) \delta^{(1)}\left(\mathbf{M}^2_{\tilde{b}}\right)_{LL}\Big)\Big]. \tag{4.23}$$

Lastly, the counterterm for $m^2_{\tilde{b}_{12}}$ reads

$$\delta^{(1)} m^2_{\tilde{b}_{12}} = \frac{1}{|U_{\tilde{b}_{11}}|^2 - |U_{\tilde{b}_{12}}|^2}\Big[U_{\tilde{b}_{11}} U^*_{\tilde{b}_{21}}\left(\delta^{(1)} m^2_{\tilde{b}_1} - \delta^{(1)} m^2_{\tilde{b}_2}\right) + U_{\tilde{b}_{11}} U^*_{\tilde{b}_{22}}\left(m_b\, \delta^{(1)} X_b^* + X_b^*\, \delta^{(1)} m_b\right) - U_{\tilde{b}_{12}} U^*_{\tilde{b}_{21}}\left(m_b\, \delta^{(1)} X_b + X_b\, \delta^{(1)} m_b\right)\Big]. \tag{4.24}$$

Renormalisation in the massless case

To extract all terms of order $\mathcal{O}\left((\alpha_{\mathrm{em}} + \alpha_q)^2 N_c^2\right)$ in the Higgs boson mass prediction at the two-loop level, the first and second generation of quarks and squarks need to be taken into account as well. These generations contribute even if their quarks are assumed to be massless. As there are also two-loop Higgs self-energies with both a third generation squark in one loop and a first/second generation squark in the other, those contributions cannot simply be obtained by taking the results for the third generation and applying the massless limit. Instead, the whole calculation has to be done anew. To this end, we assume both the first and second generation of quarks to be massless and again a diagonal CKM matrix.

As for the third generation of squarks, seven independent real parameters appear in the squark mass matrices of each of the first two generations. In the massless limit, however, the trilinear counterterms $\delta^{(1)} A_q$ and correspondingly the off-diagonal mass counterterms $\delta^{(1)} m^2_{\tilde{q}_{12}}$ do not contribute in the sub-loop renormalisation of the Higgs self-energies. This leaves us with three independent parameters in each generation. If we assume generation g to be massless, these are $M^2_{\tilde{q}_g}$, $M^2_{\tilde{u}_g}$, and $M^2_{\tilde{d}_g}$. As before, we fix these parameters by imposing renormalisation conditions on the diagonal squark self-energies. When working with the massive third generation, we used both the stop and one of the sbottom masses as independent input parameters. The remaining sbottom mass was then fixed by virtue of the $SU(2)$ symmetry of the SUSY breaking parameter $M^2_{\tilde{q}_3}$. For the massless first two generations, this procedure needs to be adapted; the squark mass matrices are diagonal in the massless limit and so the corresponding rotation matrices $U_{\tilde{q}}$ are either purely diagonal or purely off-diagonal.

One of the mass eigenstates thus corresponds to the left-handed gauge eigenstate $\tilde{q}_L$, the other one to the right-handed gauge eigenstate $\tilde{q}_R$. The $SU(2)$ symmetry fixes the mass of the left-handed down-type squark in terms of the left-handed up-type squark, and its mass counterterm cannot be chosen independently. This issue becomes clear when looking at Eq. (4.23); this expression for the dependent mass counterterm $\delta^{(1)} m^2_{\tilde{b}_f}$ is undefined if $U_{\tilde{b}_{1f}} = 0$. This can be circumvented by removing the freedom of choice as for which mass is treated independently. We demonstrate the procedure for the second generation and an on-shell renormalisation of the input mass (the first generation and $\overline{\text{DR}}$ renormalisation are treated in analogous fashion). The scalar charm quark mass counterterms are

$$\delta^{(1)} m^2_{\tilde{c}_i} = \text{Re}\, \Sigma^{(1)}_{\tilde{c}_i \tilde{c}_i} = \Sigma^{(1)}_{\tilde{c}_i \tilde{c}_i}, \quad i \in \{1,2\}. \tag{4.25}$$

We cannot freely choose which of the two scalar strange quark masses is used as input. Instead, we fix our choice by the form of $U_{\tilde{s}}$ in order to avoid divergent and thus meaningless expressions:

$U_{\tilde{s}}$ is diagonal. This means that $U_{\tilde{s}_{12}} = U_{\tilde{s}_{21}} = 0$ and the second generation analogue of Eq. (4.23) is only meaningful if $f = 1, n = 2$ is chosen. We arrive at

$$\delta^{(1)} m^2_{\tilde{s}_1} = \delta^{(1)} \left(\mathbf{M}^2_{\tilde{s}} \right)_{LL}, \tag{4.26a}$$

$$\delta^{(1)} m^2_{\tilde{s}_2} = \Sigma^{(1)}_{\tilde{s}_2 \tilde{s}_2}. \tag{4.26b}$$

$U_{\tilde{s}}$ is purely off-diagonal. This means that $U_{\tilde{s}_{11}} = U_{\tilde{s}_{22}} = 0$ and the second generation analogue of Eq. (4.23) is only meaningful if $f = 2, n = 1$ is chosen. We arrive at

$$\delta^{(1)} m^2_{\tilde{s}_1} = \Sigma^{(1)}_{\tilde{s}_1 \tilde{s}_1}, \tag{4.27a}$$

$$\delta^{(1)} m^2_{\tilde{s}_2} = \delta^{(1)} \left(\mathbf{M}^2_{\tilde{s}} \right)_{LL}. \tag{4.27b}$$

We can combine both cases in the formulae

$$\delta^{(1)} m^2_{\tilde{s}_1} = |U_{\tilde{s}_{12}}|^2 \Sigma^{(1)}_{\tilde{s}_1 \tilde{s}_1} + |U_{\tilde{s}_{11}}|^2 \delta^{(1)} \left(\mathbf{M}^2_{\tilde{s}} \right)_{LL}, \tag{4.28a}$$

$$\delta^{(1)} m^2_{\tilde{s}_2} = |U_{\tilde{s}_{11}}|^2 \Sigma^{(1)}_{\tilde{s}_2 \tilde{s}_2} + |U_{\tilde{s}_{12}}|^2 \delta^{(1)} \left(\mathbf{M}^2_{\tilde{s}} \right)_{LL}. \tag{4.28b}$$

$\delta^{(1)} \left(\mathbf{M}^2_{\tilde{s}} \right)_{LL}$ is obtained from Eq. (4.22) by replacing the third generation labels by second generation labels.

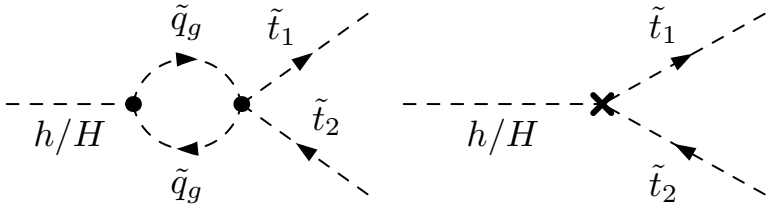

Loop diagram Counterterm diagram

Figure 4.2: The diagrams relevant for the determination of $\delta^{(1)}\mu^{\overline{\text{DR}}}$ and $\delta^{(1)}A_t^{\overline{\text{DR}}}$. In the loop diagram, both stops and sbottoms appear, resulting in eight loop diagrams in total, g is a flavour index. The first and second squark generations do not contribute since their Yukawa couplings are assumed to vanish. $\delta^{(1)}A_b$ is determined from diagrams with two outgoing sbottom squarks.

4.1.3 $\overline{\text{DR}}$ renormalisation of μ and A_q

For a full renormalisation of the squark sector, the counterterms $\delta^{(1)}\mu$, $\delta^{(1)}A_t$, and $\delta^{(1)}A_b$ need to be fixed. The higgsino mass parameter μ is typically defined via the chargino-neutralino sector (see e.g. Ref. [50]). As that sector is otherwise irrelevant to our calculation, we choose a $\overline{\text{DR}}$ renormalisation for μ. As can be seen in Ref. [50], the OS expression for the μ counterterm in a CCN scheme involves elements of both chargino rotation matrices, which transform the gauge eigenstates into mass eigenstates. Taking the divergent part of the OS counterterm yields an expression which is still rather complicated as the rotation matrix elements do not easily cancel out algebraically.

As the higgsino mass parameter enters the $h\tilde{t}\tilde{t}^*$ vertex, an expression for its counterterm can also be obtained from the renormalisation of this vertex. This approach naturally leads to an expression for $\delta^{(1)}A_t$ as well and avoids the need to deal with the chargino rotation matrices. Therefore, we calculate the amplitudes $h \to \tilde{t}_1\tilde{t}_2^*$ and $H \to \tilde{t}_1\tilde{t}_2^*$ at the one-loop level and determine $\delta^{(1)}\mu^{\overline{\text{DR}}}$ and $\delta^{(1)}A_t^{\overline{\text{DR}}}$ from requiring both amplitudes to be finite. The relevant loop and counterterm diagrams are shown in Fig. 4.2.

For both amplitudes we have eight loop diagrams each. The counterterm diagram, apart from $\delta^{(1)}\mu$ and $\delta^{(1)}A_t$, involves the counterterms $\delta^{(1)}M_Z^2$, $\delta^{(1)}M_W^2$, $\delta^{(1)}s_\text{w}$, $\delta^{(1)}Z_e$, $\delta^{(1)}t_\beta$, the Higgs field counterterms $\delta^{(1)}Z_{\mathcal{H}_1}$ and $\delta^{(1)}Z_{\mathcal{H}_2}$, as well as quark mass and squark field counterterms. The quark mass counterterms vanish and the squark field counterterms are finite at $\mathcal{O}(N_c)$, as we have explained in Sect. 4.1.2. The squarks appear as external particles in Fig. 4.2 and so their field counterterms will

not drop out in the full amplitude. Here, we want to determine the counterterms of μ and A_t in a $\overline{\text{DR}}$ scheme, so the finite parts of the squark field counterterms do not matter. The definition of the remaining counterterms is postponed to Sect. 4.2 and we assume them to be known for the current analysis.
As both amplitudes $\hat{\Gamma}^{(1)}_{h\tilde{t}_1\tilde{t}_2^*}$ and $\hat{\Gamma}^{(1)}_{H\tilde{t}_1\tilde{t}_2^*}$ involve both counterterms $\delta^{(1)}\mu$ and $\delta^{(1)}A_t$, we have to solve a linear system of equations. It is instructive to consider the Higgs-stop-stop vertex

$$\begin{aligned}\mathcal{L}_{\phi\tilde{t}\tilde{t}} = -\frac{em_t}{2s_\text{w}M_W s_\beta}\Big[&2m_t\phi_2(\tilde{t}_L^*\tilde{t}_L + \tilde{t}_R^*\tilde{t}_R) + (A_t^*\phi_2 - \mu\phi_1)\tilde{t}_L^*\tilde{t}_R \\ &+ (A_t\phi_2 - \mu^*\phi_1)\tilde{t}_R^*\tilde{t}_L + \mathcal{O}(eM_Z)\Big].\end{aligned} \tag{4.29}$$

We can see that $\phi_1 = c_\alpha H - s_\alpha h$ couples to stop squarks via μ and $\phi_2 = c_\alpha h + s_\alpha H$ couples to the stops via A_t (and m_t). Therefore, we find the two linear combinations:

$$c_\alpha\hat{\Gamma}^{(1)}_{H\tilde{t}_1\tilde{t}_2^*} - s_\alpha\hat{\Gamma}^{(1)}_{h\tilde{t}_1\tilde{t}_2^*}: \quad \delta^{(1)}A_t \text{ drops out}, \tag{4.30a}$$
$$c_\alpha\hat{\Gamma}^{(1)}_{h\tilde{t}_1\tilde{t}_2^*} + s_\alpha\hat{\Gamma}^{(1)}_{H\tilde{t}_1\tilde{t}_2^*}: \quad \delta^{(1)}\mu \text{ drops out}. \tag{4.30b}$$

Now the first expression is used to determine $\delta^{(1)}\mu$ and the second one for $\delta^{(1)}A_t$. The same procedure works for $\delta^{(1)}A_b$ as well:

$$c_\alpha\hat{\Gamma}^{(1)}_{H\tilde{b}_1\tilde{b}_2^*} - s_\alpha\hat{\Gamma}^{(1)}_{h\tilde{b}_1\tilde{b}_2^*}: \quad \delta^{(1)}\mu \text{ drops out}, \tag{4.31a}$$
$$c_\alpha\hat{\Gamma}^{(1)}_{h\tilde{b}_1\tilde{b}_2^*} + s_\alpha\hat{\Gamma}^{(1)}_{H\tilde{b}_1\tilde{b}_2^*}: \quad \delta^{(1)}A_b \text{ drops out}. \tag{4.31b}$$

This follows from

$$\begin{aligned}\mathcal{L}_{\phi\tilde{b}\tilde{b}} = -\frac{em_b}{2s_\text{w}M_W c_\beta}\Big[&2m_b\phi_1(\tilde{b}_L^*\tilde{b}_L + \tilde{b}_R^*\tilde{b}_R) + (A_b^*\phi_1 - \mu\phi_2)\tilde{b}_L^*\tilde{b}_R \\ &+ (A_b\phi_1 - \mu^*\phi_2)\tilde{b}_R^*\tilde{b}_L + \mathcal{O}(eM_Z)\Big].\end{aligned} \tag{4.32}$$

We arrive at

$$\frac{\delta^{(1)}\mu^\text{DR}}{\mu} = \frac{\alpha_\text{em}N_c}{16\pi M_W^2 s_\text{w}^2}\left(\frac{m_t^2}{s_\beta^2} + \frac{m_b^2}{c_\beta^2}\right)\frac{1}{\varepsilon}, \tag{4.33a}$$
$$\frac{\delta^{(1)}A_t^\text{DR}}{A_t} = \frac{\alpha_\text{em}N_c}{8\pi M_W^2 s_\text{w}^2}\frac{m_t^2}{s_\beta^2}\frac{1}{\varepsilon}, \tag{4.33b}$$
$$\frac{\delta^{(1)}A_b^\text{DR}}{A_b} = \frac{\alpha_\text{em}N_c}{8\pi M_W^2 s_\text{w}^2}\frac{m_b^2}{c_\beta^2}\frac{1}{\varepsilon}. \tag{4.33c}$$

The corresponding $\overline{\text{DR}}$ expressions are obtained by the replacement

$$\frac{1}{\varepsilon} \to \frac{\left(4\pi e^{-\gamma_E}\right)^{\varepsilon}}{\varepsilon} = \frac{1}{\varepsilon} + \log(4\pi) - \gamma_E + \frac{\varepsilon}{2}[\log(4\pi) - \gamma_E]^2 + \mathcal{O}\left(\varepsilon^2\right), \tag{4.34}$$

see also Sect. 2.3.2.

4.2 The Higgs and gauge sector of the MSSM

In this section, we fix the notation for the Higgs and gauge sector in the MSSM, making use of Ref. [67]. We discuss the relevant parameters of this sector and give the renormalisation transformations for the parameters and fields. From these, we derive the resulting expressions for the renormalised tadpole and self-energy diagrams up to two-loop order. We explain the renormalisation of each independent parameter, usually in form of a renormalisation condition and a formula for the counterterm. The renormalisation of $\tan(\beta)$ is discussed in Sect. 4.3.

4.2.1 Tree-level

The MSSM Higgs Lagrangian contains, inter alia, the following terms [67]:

$$\begin{aligned}\mathcal{L}_{\text{Higgs}} \supset\ & -(m_1^2 + |\mu|^2)\mathcal{H}_1^\dagger \mathcal{H}_1 - (m_2^2 + |\mu|^2)\mathcal{H}_2^\dagger \mathcal{H}_2 + \left(m_{12}^2 \mathcal{H}_1 \cdot \mathcal{H}_2 + \text{h.c.}\right) \\ & - \tfrac{1}{8}(g^2 + g'^2)(\mathcal{H}_1^\dagger \mathcal{H}_1 - \mathcal{H}_2^\dagger \mathcal{H}_2) - \tfrac{1}{2} g'^2 \left|\mathcal{H}_1^\dagger \mathcal{H}_2\right|^2.\end{aligned} \tag{4.35}$$

In the first line, we used the SU(2) product $a \cdot b = a_1 b_2 - a_2 b_1$, where a and b are SU(2) doublets. Furthermore, the gauge couplings g and g', and the potentially complex higgsino mass parameter μ appear. The parameters m_1^2, m_2^2, and m_{12}^2, of which the latter is possibly complex, break supersymmetry softly. The phase of m_{12}^2 can be removed by a Peccei-Quinn transformation [170–172]. From this point on, we will treat m_{12}^2 as a real parameter.
We write the Higgs doublets in terms of component fields:

$$\mathcal{H}_1 = \begin{pmatrix} v_1 + \frac{1}{\sqrt{2}}(\phi_1 - \mathrm{i}\chi_1) \\ -\phi_1^- \end{pmatrix}, \tag{4.36a}$$

$$\mathcal{H}_2 = e^{\mathrm{i}\xi} \begin{pmatrix} \phi_2^+ \\ v_2 + \frac{1}{\sqrt{2}}(\phi_2 + \mathrm{i}\chi_2) \end{pmatrix}, \tag{4.36b}$$

where v_1 and v_2 are the vacuum expectation values of the Higgs doublets, and ξ is a phase between the doublets. The doublets have have hypercharges $Y_{\mathcal{H}_1} = -1$ and

$Y_{\mathcal{H}_2} = +1$ [173]. They couple to down- and up-type (s)fermions, respectively.
In terms of the component fields, the linear and quadratic terms of the Higgs Lagrangian are

$$\begin{aligned}\mathcal{L}_{\text{Higgs}}^{\text{lin.+bil.}} &= T_{\phi_1}\,\phi_1 + T_{\phi_2}\,\phi_2 + T_{\chi_1}\,\chi_1 + T_{\chi_2}\,\chi_2 \\ &\quad + \tfrac{1}{2}(\partial_\mu\phi_i)(\partial^\mu\phi_i) + \tfrac{1}{2}(\partial_\mu\chi_i)(\partial^\mu\chi_i) + (\partial_\mu\phi_i^+)(\partial^\mu\phi_i^-) \\ &\quad - \tfrac{1}{2}\begin{pmatrix}\phi_1 & \phi_2 & \chi_1 & \chi_2\end{pmatrix}\begin{pmatrix}\mathbf{M}^2_{\phi\phi} & \mathbf{M}^2_{\phi\chi} \\ \mathbf{M}^2_{\chi\phi} & \mathbf{M}^2_{\chi\chi}\end{pmatrix}\begin{pmatrix}\phi_1 \\ \phi_2 \\ \chi_1 \\ \chi_2\end{pmatrix} \\ &\quad - \begin{pmatrix}\phi_1^+ & \phi_2^+\end{pmatrix}\mathbf{M}^2_{\phi^-\phi^+}\begin{pmatrix}\phi_1^- \\ \phi_2^-\end{pmatrix}.\end{aligned} \tag{4.37}$$

The mass (sub-)matrices, whose entries are given in Ref. [67], fulfil the following relations:

$$\left(\mathbf{M}^2_{\phi\phi}\right)^{\mathrm{T}} = \mathbf{M}^2_{\phi\phi}, \tag{4.38a}$$
$$\left(\mathbf{M}^2_{\phi\chi}\right)^{\mathrm{T}} = \mathbf{M}^2_{\chi\phi} = -\mathbf{M}^2_{\phi\chi}, \tag{4.38b}$$
$$\left(\mathbf{M}^2_{\chi\chi}\right)^{\mathrm{T}} = \mathbf{M}^2_{\chi\chi}, \tag{4.38c}$$
$$\left(\mathbf{M}^2_{\phi^-\phi^+}\right)^{\dagger} = \mathbf{M}^2_{\phi^-\phi^+}. \tag{4.38d}$$

In the Higgs-gauge sector, we now have eight independent real parameters: g, g', v_1, v_2, m_1^2, m_2^2, m_{12}^2, and ξ. It should be noted that we do not consider μ to be part of the Higgs-gauge but rather the chargino-neutralino sector; we have explained its renormalisation in Sect. 4.1.3. This set of parameters is, however, not the most convenient to work with. To obtain input parameters which can be linked to physical observables more easily, we replace the gauge couplings and VEVs by the elementary charge e, the gauge boson masses M_Z and M_W, and the VEV ratio $\tan(\beta) = t_\beta$:

$$e = g c_{\mathrm{w}} = g' s_{\mathrm{w}}, \tag{4.39a}$$
$$M_Z^2 = \tfrac{1}{2}(g^2 + g'^2)(v_1^2 + v_2^2), \tag{4.39b}$$
$$M_W^2 = \tfrac{1}{2}g'^2(v_1^2 + v_2^2) = M_Z^2 c_{\mathrm{w}}^2, \tag{4.39c}$$
$$t_\beta = \frac{v_2}{v_1}. \tag{4.39d}$$

c_{w} and s_{w} are the cosine and sine of the weak-mixing angle θ_{w}, respectively.

With these definitions, the mass matrices introduced in Eq. (4.37) fulfil

$$\operatorname{Tr}\mathbf{M}^2_{\phi\phi} = \operatorname{Tr}\mathbf{M}^2_{\chi\chi} + M_Z^2, \tag{4.40a}$$

$$\operatorname{Tr}\mathbf{M}^2_{\phi^-\phi^+} = \operatorname{Tr}\mathbf{M}^2_{\chi\chi} + M_W^2. \tag{4.40b}$$

To replace the four remaining (unphysical) input parameters, we first rotate the Higgs component fields into their mass eigenstates:

$$\begin{pmatrix} h \\ H \\ A \\ G \end{pmatrix} = \begin{pmatrix} -s_\alpha & c_\alpha & 0 & 0 \\ c_\alpha & s_\alpha & 0 & 0 \\ 0 & 0 & -s_{\beta_\mathrm{n}} & c_{\beta_\mathrm{n}} \\ 0 & 0 & c_{\beta_\mathrm{n}} & s_{\beta_\mathrm{n}} \end{pmatrix} \begin{pmatrix} \phi_1 \\ \phi_2 \\ \chi_1 \\ \chi_2 \end{pmatrix}, \tag{4.41a}$$

$$\begin{pmatrix} H^\pm \\ G^\pm \end{pmatrix} = \begin{pmatrix} -s_{\beta_\mathrm{c}} & c_{\beta_\mathrm{c}} \\ c_{\beta_\mathrm{c}} & s_{\beta_\mathrm{c}} \end{pmatrix} \begin{pmatrix} \phi_1^\pm \\ \phi_2^\pm \end{pmatrix}, \tag{4.41b}$$

where $c_x = \cos(x)$ and $s_x = \sin(x)$ for $x \in \{\alpha, \beta_\mathrm{n}, \beta_\mathrm{c}\}$. We use the same notation for all linear combinations of these angles. We call the $\{\phi_1,\phi_2,\chi_1,\chi_2\}$-basis the gauge eigenstates and the $\{h, H, A, G\}$-basis the tree-level mass eigenstates; we use the same terms for the charged sector. Expressed in terms of mass eigenstates, the linear and quadratic terms of the Higgs Lagrangian read

$$\begin{aligned} \mathcal{L}^{\text{lin.+bil.}}_{\text{Higgs}} = {} & T_h\, h + T_H\, H + T_A\, A + T_G\, G \\ & + \tfrac{1}{2}(\partial_\mu h)(\partial^\mu h) + \tfrac{1}{2}(\partial_\mu H)(\partial^\mu H) + \tfrac{1}{2}(\partial_\mu A)(\partial^\mu A) \\ & + \tfrac{1}{2}(\partial_\mu G)(\partial^\mu G) + (\partial_\mu H^+)(\partial^\mu H^-) + (\partial_\mu G^+)(\partial^\mu G^-) \\ & - \tfrac{1}{2}\begin{pmatrix} h & H & A & G \end{pmatrix} \begin{pmatrix} m_h^2 & m_{hH}^2 & m_{hA}^2 & m_{hG}^2 \\ m_{hH}^2 & m_H^2 & m_{HA}^2 & m_{HG}^2 \\ m_{hA}^2 & m_{HA}^2 & m_A^2 & m_{AG}^2 \\ m_{hG}^2 & m_{HG}^2 & m_{AG}^2 & m_G^2 \end{pmatrix} \begin{pmatrix} h \\ H \\ A \\ G \end{pmatrix} \\ & - \begin{pmatrix} H^+ & G^+ \end{pmatrix} \begin{pmatrix} m_{H^\pm}^2 & m_{H^-G^+}^2 \\ m_{G^-H^+}^2 & m_{G^\pm}^2 \end{pmatrix} \begin{pmatrix} H^- \\ G^- \end{pmatrix}. \end{aligned} \tag{4.42}$$

It is important to note that we use a different convention for labelling the off-diagonal entries of the charged Higgs boson mass matrix than Ref. [67], which leads to differences also in the respective counterterms. Instead, our charged counterterms agree with the expressions given in Ref. [50].

To complete our choice of physical input parameters, we choose the tadpole coefficients T_h, T_H and T_A, as well as one of the masses $m_A^2/m_{H^\pm}^2$. If all MSSM parameters are real, we refer to the model as the rMSSM. In this case, the $\mathcal{CP}$-odd scalar A does

not mix with the $\mathcal{CP}$-even scalars h and H, and we use m_A^2 as an input parameter. In the cMSSM, the MSSM with complex parameters, A mixes with the $\mathcal{CP}$-even states through loop corrections, and the $\mathcal{CP}$ eigenstate is not a mass eigenstate anymore. Instead, we use the charged mass $m_{H^\pm}^2$ as input in this case.
To sum up, in the Higgs-gauge sector, we use the input parameters

$$e, M_Z^2, M_W^2, m_A^2/m_{H^\pm}^2, T_h, T_H, T_A, t_\beta. \tag{4.43}$$

The remaining mass parameters and T_G can be expressed in terms of these input parameters and the mixing angles α, β_n and β_c. These relations are needed to derive counterterm expressions and can be found in Ref. [67]. As stated above, we use a different convention for the off-diagonal charged mass counterterms; our $m_{H^-G^+}^2$ is denoted by $m_{G^-H^+}^2$ in Ref. [67] and vice versa.
The trace of a matrix is invariant under a unitary transformation, so Eqs. (4.38) can be rewritten by the masses defined in Eq. (4.42):

$$m_h^2 + m_H^2 = m_A^2 + m_G^2 + M_Z^2, \tag{4.44a}$$
$$m_{H^\pm}^2 + m_{G^\pm}^2 = m_A^2 + m_G^2 + M_W^2. \tag{4.44b}$$

These relations hold before and after applying the minimisation conditions for the Higgs potential.
At tree-level, m_G^2 and $m_{G^\pm}^2$ vanish and we get the familiar relations

$$m_h^2 + m_H^2 = m_A^2 + M_Z^2, \tag{4.45a}$$
$$m_{H^\pm}^2 = m_A^2 + M_W^2. \tag{4.45b}$$

The $\mathcal{CP}$-even tree-level masses are given by

$$m_{h/H}^2 = \tfrac{1}{2}\left(m_A^2 + M_Z^2 \mp \sqrt{(m_A^2 + M_Z^2)^2 - 4m_A^2 M_Z^2 c_{2\beta}^2}\right), \tag{4.46}$$

where $m_h^2 \leq m_H^2$. The tadpoles, the phase ξ, the off-diagonal mass terms, and the m_G^2 and $m_{G^\pm}^2$ entries of the mass matrices vanish at tree-level. The would-be Goldstone bosons can nevertheless obtain a mass from the gauge-symmetry breaking gauge-fixing procedure, see below. The mixing angles at the minimum are

$$\beta_\mathrm{n} = \beta_\mathrm{c} = \beta, \quad 0 < \beta < \tfrac{\pi}{2}, \tag{4.47}$$

and

$$\alpha = \arctan\left[\frac{-(m_A^2 + M_Z^2)s_\beta c_\beta}{M_Z^2 c_\beta^2 + m_A^2 s_\beta^2 - m_h^2}\right], \quad -\tfrac{\pi}{2} < \alpha < 0. \tag{4.48}$$

The bilinear MSSM Lagrangian for electroweak gauge bosons is identical to its SM counterpart. It reads

$$\begin{aligned}\mathcal{L}^{\text{bil.}}_{\text{gauge}} = & -\tfrac{1}{2}\left(\partial_\mu A_\nu \partial^\mu A^\nu - \partial_\mu A_\nu \partial^\nu A^\mu\right) \\ & -\tfrac{1}{2}\left(\partial_\mu Z_\nu \partial^\mu Z^\nu - \partial_\mu Z_\nu \partial^\nu Z^\mu\right) + \tfrac{1}{2}M_Z^2 Z_\mu Z^\mu \\ & -\left(\partial_\mu W_\nu^+ \partial^\mu W^{-\nu} - \partial_\mu W_\nu^+ \partial^\nu W^{-\mu}\right) + M_W^2 W_\mu^+ W^{-\mu}.\end{aligned} \tag{4.49}$$

There are also mixing terms between gauge and Higgs bosons:

$$\mathcal{L}^{\text{bil.}}_{\text{Higgs-gauge}} = M_Z(c_\beta\chi_1 + s_\beta\chi_2)\partial^\mu Z_\mu + \left(\mathrm{i}M_W(c_\beta\phi_1^+ + s_\beta\phi_2^+)\partial^\mu W_\mu^- + \text{h.c.}\right). \tag{4.50}$$

In the 't Hooft-gauge, these mixing terms are exactly cancelled by the gauge-fixing terms at tree-level as explained below. At higher orders, they generate counterterms which renormalise the scalar-vector self-energies.

In a perturbative calculation, we need to introduce gauge-fixing terms to our Lagrangian. These terms break gauge invariance explicitly but they are needed to invert the photon two-point function, which yields the photon propagator. In the most general formulation, the MSSM gauge-fixing terms have nine independent bare gauge parameters. With our choice of gauge parameter renormalisation, the gauge-fixing Lagrangian does not generate counterterms and it takes the convenient form of the 't Hooft-gauge with three independent gauge parameters:

$$\mathcal{L}_{\text{gf}} = -\tfrac{1}{2}\mathscr{F}_\gamma^2 - \tfrac{1}{2}\mathscr{F}_Z^2 - \mathscr{F}_-\mathscr{F}_+, \tag{4.51a}$$

$$\mathscr{F}_\gamma = \xi_\gamma^{-1/2}\left(\partial^\mu A_\mu\right), \tag{4.51b}$$

$$\mathscr{F}_Z = \xi_Z^{-1/2}\left(\partial^\mu Z_\mu + \xi_Z M_Z G\right), \tag{4.51c}$$

$$\mathscr{F}_- = \xi_W^{-1/2}\left(\partial^\mu W_\mu^- - \mathrm{i}\xi_W M_W G^-\right), \tag{4.51d}$$

$$\mathscr{F}_+ = \xi_W^{-1/2}\left(\partial^\mu W_\mu^+ + \mathrm{i}\xi_W M_W G^+\right). \tag{4.51e}$$

These terms cancel the mixing terms in Eq. (4.50) and they give the masses $\sqrt{\xi_Z}M_Z$ and $\sqrt{\xi_W}M_W$ to the would-be Goldstone bosons G and $G^\pm$, respectively. Furthermore, the gauge-fixing terms contribute to the longitudinal part of the vector-boson propagators. The non-renormalisation of the gauge-fixing part means that the would-be Goldstone boson masses are not shifted via loop contributions. In this regard, they are different from the m_G^2 and $m_{G^\pm}^2$ entries of the mass matrices ap-

pearing in Eq. (4.42), which vanish at tree-level but generate counterterms.

The renormalisation transformations

All parameters are renormalised via

$$p \to p + \delta p = p + \delta^{(1)} p + \delta^{(2)} p. \tag{4.52}$$

This means in particular that $t_\beta \to t_\beta + \delta t_\beta$, which is also done in e.g. Refs. [49, 50], but not in Refs. [55, 67]. It should be noted that the mixing angles α, β_n and β_c are not renormalised. Only after the renormalisation transformation we set $\beta_\mathrm{n} = \beta_\mathrm{c} = \beta$. For the elementary charge, we write $e \to e + \delta e \equiv (1 + \delta Z_e)e$. All mass parameters in Eq. (4.42) are also renormalised in the form of Eq. (4.52). Since only the parameters given in Eq. (4.43) are independent in the Higgs and gauge sector, most mass counterterms will be dependent quantities.
We renormalise the fields by

$$\mathcal{H}_i \to \sqrt{1 + \delta Z_{\mathcal{H}_i}}\, \mathcal{H}_i, \tag{4.53a}$$

$$\begin{pmatrix} h \\ H \\ A \\ G \end{pmatrix} \to \begin{pmatrix} \sqrt{1+\delta Z_{hh}} & \frac{1}{2}\delta Z_{hH} & 0 & 0 \\ \frac{1}{2}\delta Z_{hH} & \sqrt{1+\delta Z_{HH}} & 0 & 0 \\ 0 & 0 & \sqrt{1+\delta Z_{AA}} & \frac{1}{2}\delta Z_{AG} \\ 0 & 0 & \frac{1}{2}\delta Z_{AG} & \sqrt{1+\delta Z_{GG}} \end{pmatrix} \begin{pmatrix} h \\ H \\ A \\ G \end{pmatrix}, \tag{4.53b}$$

$$\begin{pmatrix} H^- \\ G^- \end{pmatrix} \to \begin{pmatrix} \sqrt{1+\delta Z_{H^-H^+}} & \frac{1}{2}\delta Z_{H^-G^+} \\ \frac{1}{2}\delta Z_{G^-H^+} & \sqrt{1+\delta Z_{G^-G^+}} \end{pmatrix} \begin{pmatrix} H^- \\ G^- \end{pmatrix}, \tag{4.53c}$$

$$\begin{pmatrix} H^+ \\ G^+ \end{pmatrix} \to \begin{pmatrix} \sqrt{1+\delta Z_{H^-H^+}} & \frac{1}{2}\delta Z_{G^-H^+} \\ \frac{1}{2}\delta Z_{H^-G^+} & \sqrt{1+\delta Z_{G^-G^+}} \end{pmatrix} \begin{pmatrix} H^+ \\ G^+ \end{pmatrix}, \tag{4.53d}$$

$$\begin{pmatrix} A_\mu \\ Z_\mu \end{pmatrix} \to \begin{pmatrix} \sqrt{1+\delta Z_{\gamma\gamma}} & \frac{1}{2}\delta Z_{\gamma Z} \\ \frac{1}{2}\delta Z_{Z\gamma} & \sqrt{1+\delta Z_{ZZ}} \end{pmatrix} \begin{pmatrix} A_\mu \\ Z_\mu \end{pmatrix}, \tag{4.53e}$$

$$W_\mu^\pm \to \sqrt{1 + \delta Z_{WW}}\, W_\mu^\pm, \tag{4.53f}$$

where $\delta Z = \delta^{(1)} Z + \delta^{(2)} Z$ as for the parameter renormalisation. All scalar field renormalisation constants are fixed by $\delta Z_{\mathcal{H}_1}$ and $\delta Z_{\mathcal{H}_2}$. As the Higgs Lagrangian is $\mathcal{CP}$ conserving at tree-level, this means in particular that the mixing field renormalisation constants between the $\mathcal{CP}$-even and $\mathcal{CP}$-odd fields vanish at all orders. The counterterms for the masses in Eq. (4.42) are determined by the counterterms for our input parameters. All relations between the one- and two-loop counterterms are collected in App. A.

Applying the renormalisation transformation to Eqs. (4.44), we find the relations

$$\delta^{(n)} m_h^2 + \delta^{(n)} m_H^2 = \delta^{(n)} m_A^2 + \delta^{(n)} m_G^2 + \delta^{(n)} M_Z^2, \tag{4.54a}$$

$$\delta^{(n)} m_{H^\pm}^2 + \delta^{(n)} m_{G^\pm}^2 = \delta^{(n)} m_A^2 + \delta^{(n)} m_G^2 + \delta^{(n)} M_W^2, \tag{4.54b}$$

which hold to all orders. In the present work, the counterterms $\delta^{(n)} m_h^2$, $\delta^{(n)} m_H^2$, $\delta^{(n)} m_{G^\pm}^2$ and $\delta^{(n)} m_G^2$ are always dependent quantities while the gauge boson mass counterterms, $\delta^{(n)} M_Z^2$ and $\delta^{(n)} M_W^2$, are always defined in an on-shell scheme. Depending on the scenario, either $\delta^{(n)} m_A^2$ or $\delta^{(n)} m_{H^\pm}^2$ is defined on-shell as well, while the other one becomes a dependent counterterm.

4.2.2 Renormalisation at the one-loop level

Renormalised tadpoles and self-energies

The one-loop one-point vertex functions are renormalised by the tadpole counterterms:

$$\hat{\Gamma}_h^{(1)} = \Gamma_h^{(1)} + \delta^{(1)} T_h, \tag{4.55a}$$

$$\hat{\Gamma}_H^{(1)} = \Gamma_H^{(1)} + \delta^{(1)} T_H, \tag{4.55b}$$

$$\hat{\Gamma}_A^{(1)} = \Gamma_A^{(1)} + \delta^{(1)} T_A, \tag{4.55c}$$

$$\hat{\Gamma}_G^{(1)} = \Gamma_G^{(1)} + \delta^{(1)} T_G. \tag{4.55d}$$

The neutral $\mathcal{CP}$-even self-energies are

$$\hat{\Sigma}_{hh}^{(1)}(p^2) = \Sigma_{hh}^{(1)}(p^2) + \delta^{(1)} Z_{hh}(p^2 - m_h^2) - \delta^{(1)} m_h^2, \tag{4.56a}$$

$$\hat{\Sigma}_{hH}^{(1)}(p^2) = \Sigma_{hH}^{(1)}(p^2) + \delta^{(1)} Z_{hH}\left(p^2 - \frac{m_h^2 + m_H^2}{2}\right) - \delta^{(1)} m_{hH}^2, \tag{4.56b}$$

$$\hat{\Sigma}_{HH}^{(1)}(p^2) = \Sigma_{HH}^{(1)}(p^2) + \delta^{(1)} Z_{HH}(p^2 - m_H^2) - \delta^{(1)} m_H^2, \tag{4.56c}$$

while the $\mathcal{CP}$-odd self-energies read

$$\hat{\Sigma}_{AA}^{(1)}(p^2) = \Sigma_{AA}^{(1)}(p^2) + \delta^{(1)} Z_{AA}(p^2 - m_A^2) - \delta^{(1)} m_A^2, \tag{4.57a}$$

$$\hat{\Sigma}_{AG}^{(1)}(p^2) = \Sigma_{AG}^{(1)}(p^2) + \delta^{(1)} Z_{AG}\left(p^2 - \frac{m_A^2}{2}\right) - \delta^{(1)} m_{AG}^2, \tag{4.57b}$$

$$\hat{\Sigma}_{GG}^{(1)}(p^2) = \Sigma_{GG}^{(1)}(p^2) + \delta^{(1)} Z_{GG}\, p^2 - \delta^{(1)} m_G^2. \tag{4.57c}$$

In the case of $\mathcal{CP}$ violation, the self-energies

$$\hat{\Sigma}^{(1)}_{hA}(p^2) = \Sigma^{(1)}_{hA}(p^2) - \delta^{(1)} m^2_{hA}, \tag{4.58a}$$
$$\hat{\Sigma}^{(1)}_{hG}(p^2) = \Sigma^{(1)}_{hG}(p^2) - \delta^{(1)} m^2_{hG}, \tag{4.58b}$$
$$\hat{\Sigma}^{(1)}_{HA}(p^2) = \Sigma^{(1)}_{HA}(p^2) - \delta^{(1)} m^2_{HA}, \tag{4.58c}$$
$$\hat{\Sigma}^{(1)}_{HG}(p^2) = \Sigma^{(1)}_{HG}(p^2) - \delta^{(1)} m^2_{HG} \tag{4.58d}$$

do not vanish. The neutral self-energies are symmetric such that for instance $\hat{\Sigma}^{(1)}_{Hh} = \hat{\Sigma}^{(1)}_{hH}$.
The charged Higgs self-energies are

$$\hat{\Sigma}^{(1)}_{H^-H^+}(p^2) = \Sigma^{(1)}_{H^-H^+}(p^2) + \delta^{(1)} Z_{H^-H^+} \left(p^2 - m^2_{H^\pm}\right) - \delta^{(1)} m^2_{H^\pm}, \tag{4.59a}$$
$$\hat{\Sigma}^{(1)}_{H^-G^+}(p^2) = \Sigma^{(1)}_{H^-G^+}(p^2) + \delta^{(1)} Z_{H^-G^+} \left(p^2 - \frac{m^2_{H^\pm}}{2}\right) - \delta^{(1)} m^2_{H^-G^+}, \tag{4.59b}$$
$$\hat{\Sigma}^{(1)}_{G^-H^+}(p^2) = \Sigma^{(1)}_{G^-H^+}(p^2) + \delta^{(1)} Z_{G^-H^+} \left(p^2 - \frac{m^2_{H^\pm}}{2}\right) - \delta^{(1)} m^2_{G^-H^+}, \tag{4.59c}$$
$$\hat{\Sigma}^{(1)}_{G^-G^+}(p^2) = \Sigma^{(1)}_{G^-G^+}(p^2) + \delta^{(1)} Z_{G^-G^+}\, p^2 - \delta^{(1)} m^2_{G^\pm}. \tag{4.59d}$$

They are symmetric in the sense

$$\hat{\Sigma}^{(1)}_{G^-H^+} = \hat{\Sigma}^{(1)}_{H^+G^-} \tag{4.60}$$

but in general

$$\left(\hat{\Sigma}^{(1)}_{G^-H^+}(p^2)\right)^* \neq \hat{\Sigma}^{(1)}_{H^-G^+}(p^2). \tag{4.61}$$

Instead, we have

$$\left(\hat{\Sigma}^{(1)}_{G^-H^+}(p^2)\right)^* = \widetilde{\mathrm{Co}}\ \hat{\Sigma}^{(1)}_{H^-G^+}(p^2), \tag{4.62}$$

where $\widetilde{\mathrm{Co}}$ takes the complex conjugate of loop integrals only and leaves complex couplings unaffected. Loop integrals are complex quantities for sufficiently large external momenta and so the $\widetilde{\mathrm{Co}}$ must not be left out.
Vector boson self-energies are Lorentz tensors of rank two. We decompose them into a transverse and into a longitudinal component

$$\Sigma^{\mu\nu}(p) = \left(-g^{\mu\nu} + \frac{p^\mu p^\nu}{p^2}\right) \Sigma^T(p^2) - \frac{p^\mu p^\nu}{p^2} \Sigma^L(p^2), \tag{4.63}$$

using the same convention as in Ref. [174].

The renormalised transverse parts of the gauge boson self-energies are

$$\hat{\Sigma}^{T,(1)}_{\gamma\gamma}(p^2) = \Sigma^{T,(1)}_{\gamma\gamma}(p^2) + \delta^{(1)} Z_{\gamma\gamma}\, p^2, \tag{4.64a}$$

$$\begin{aligned}\hat{\Sigma}^{T,(1)}_{\gamma Z}(p^2) &= \Sigma^{T,(1)}_{\gamma Z}(p^2) + \tfrac{1}{2}\delta^{(1)} Z_{\gamma Z}\, p^2 + \tfrac{1}{2}\delta^{(1)} Z_{Z\gamma}(p^2 - M_Z^2) \\ &= \hat{\Sigma}^{T,(1)}_{Z\gamma}(p^2),\end{aligned} \tag{4.64b}$$

$$\hat{\Sigma}^{T,(1)}_{ZZ}(p^2) = \Sigma^{T,(1)}_{ZZ}(p^2) + \delta^{(1)} Z_{ZZ}(p^2 - M_Z^2) - \delta^{(1)} M_Z^2, \tag{4.64c}$$

$$\begin{aligned}\hat{\Sigma}^{T,(1)}_{W^-W^+}(p^2) &= \Sigma^{T,(1)}_{W^-W^+}(p^2) + \delta^{(1)} Z_{WW}(p^2 - M_W^2) - \delta^{(1)} M_W^2 \\ &= \hat{\Sigma}^{T,(1)}_{W^+W^-}(p^2).\end{aligned} \tag{4.64d}$$

The transverse parts of vector self-energies are important already at the one-loop level, as they are used to determine the mass and field counterterms of the gauge bosons. The longitudinal vector boson self-energies enter a Higgs boson mass prediction at the three-loop order and higher, and will not be discussed here.
For a two-loop calculation, we also need self-energies which mix scalars and vectors. Their Lorentz decomposition reads

$$\Sigma^{\mu}_{SV}(p) = p^{\mu}\Sigma^{L}_{SV}(p^2), \tag{4.65a}$$

$$\Sigma^{\mu}_{VS}(p) = p^{\mu}\Sigma^{L}_{VS}(p^2), \tag{4.65b}$$

where $\Sigma^{\mu}_{SV}(p)$ denotes a self-energy with incoming vector $V^\dagger$ and outgoing scalar S, and $\Sigma^{\mu}_{VS}(p)$ denotes a self-energy with incoming scalar $S^\dagger$ and outgoing vector V. We have four neutral scalar-vector self-energies

$$\begin{aligned}\hat{\Sigma}^{L,(1)}_{A\gamma}(p^2) &= \Sigma^{L,(1)}_{A\gamma}(p^2) \\ &= -\hat{\Sigma}^{L,(1)}_{\gamma A}(p^2) \overset{\mathcal{O}(N_c)}{=} 0,\end{aligned} \tag{4.66a}$$

$$\begin{aligned}\hat{\Sigma}^{L,(1)}_{AZ}(p^2) &= \Sigma^{L,(1)}_{AZ}(p^2) - \mathrm{i}M_Z\left(\tfrac{1}{2}\delta^{(1)} Z_{AG} + c_\beta^2 \delta^{(1)} t_\beta\right) \\ &= -\hat{\Sigma}^{L,(1)}_{ZA}(p^2),\end{aligned} \tag{4.66b}$$

$$\begin{aligned}\hat{\Sigma}^{L,(1)}_{G\gamma}(p^2) &= \Sigma^{L,(1)}_{G\gamma}(p^2) - \frac{\mathrm{i}M_Z}{2}\delta^{(1)} Z_{Z\gamma} \\ &= -\hat{\Sigma}^{L,(1)}_{\gamma G}(p^2) \overset{\mathcal{O}(N_c)}{=} 0,\end{aligned} \tag{4.66c}$$

$$\begin{aligned}\hat{\Sigma}^{L,(1)}_{GZ}(p^2) &= \Sigma^{L,(1)}_{GZ}(p^2) - \frac{\mathrm{i}M_Z}{2}\left(\frac{\delta^{(1)} M_Z^2}{M_Z^2} + \delta^{(1)} Z_{ZZ} + \delta^{(1)} Z_{GG}\right) \\ &= -\hat{\Sigma}^{L,(1)}_{ZG}(p^2).\end{aligned} \tag{4.66d}$$

The charged self-energies are

$$\begin{aligned}\hat{\Sigma}^{L,(1)}_{H^-W^+}(p^2) &= \Sigma^{L,(1)}_{H^-W^+}(p^2) + M_W\left(\tfrac{1}{2}\delta^{(1)}Z_{H^-G^+} + c_\beta^2\delta^{(1)}t_\beta\right) \\ &= -\hat{\Sigma}^{L,(1)}_{W^+H^-}(p^2),\end{aligned} \tag{4.67a}$$

$$\begin{aligned}\hat{\Sigma}^{L,(1)}_{W^-H^+}(p^2) &= \Sigma^{L,(1)}_{W^-H^+}(p^2) + M_W\left(\tfrac{1}{2}\delta^{(1)}Z_{G^-H^+} + c_\beta^2\delta^{(1)}t_\beta\right) \\ &= -\hat{\Sigma}^{L,(1)}_{H^+W^-}(p^2).\end{aligned} \tag{4.67b}$$

$$\begin{aligned}\hat{\Sigma}^{L,(1)}_{G^-W^+}(p^2) &= \Sigma^{L,(1)}_{G^-W^+}(p^2) + \frac{M_W}{2}\left(\frac{\delta^{(1)}M_W^2}{M_W^2} + \delta^{(1)}Z_{WW} + \delta^{(1)}Z_{G^-G^+}\right) \\ &= -\hat{\Sigma}^{L,(1)}_{W^+G^-}(p^2),\end{aligned} \tag{4.67c}$$

$$\begin{aligned}\hat{\Sigma}^{L,(1)}_{W^-G^+}(p^2) &= \Sigma^{L,(1)}_{W^-G^+}(p^2) + \frac{M_W}{2}\left(\frac{\delta^{(1)}M_W^2}{M_W^2} + \delta^{(1)}Z_{WW} + \delta^{(1)}Z_{G^-G^+}\right) \\ &= -\hat{\Sigma}^{L,(1)}_{G^+W^-}(p^2).\end{aligned} \tag{4.67d}$$

Again, conjugated diagrams are related via

$$\left(\hat{\Sigma}^{L,(1)}_{W^-H^+}(p^2)\right)^* = \widetilde{\mathrm{Co}}\ \hat{\Sigma}^{L,(1)}_{H^-W^+}(p^2). \tag{4.68}$$

Not all of the self-energies presented in this section are actually needed for our calculation. We have numerically shown the finiteness of all given one-loop self-energies as a crosscheck and provide the derived expressions for the sake of completeness and for future reference.

One-loop renormalisation conditions and counterterms

In this section, we will discuss the one-loop renormalisation of all parameters and fields relevant for our $\mathcal{O}\left((\alpha_{\mathrm{em}}+\alpha_q)^2N_c^2\right)$ calculation. While some of these counterterms only matter for the two-loop part of our work, most are relevant already for a one-loop prediction.
The tadpole counterterms are chosen such that the renormalised one-point vertex functions vanish:

$$\hat{\Gamma}_i^{(1)} \stackrel{!}{=} 0, \quad i \in \{h,H,A\}, \tag{4.69a}$$

$$\Rightarrow \delta^{(1)}T_i = -\Gamma_i^{(1)}. \tag{4.69b}$$

Due to the relation

$$T_G = -\tan(\beta-\beta_n)T_A, \tag{4.70}$$

the counterterm $\delta^{(1)}T_G$ vanishes:

$$\delta^{(1)}T_G = 0. \tag{4.71}$$

Since the unrenormalised vertex function $\Gamma_G^{(1)}$ also vanishes, all renormalised Higgs one-point vertex functions can be set to zero simultaneously. This ensures that our VEVs receive no shifts from loop corrections [146, 175].
We use the input masses M_Z^2, M_W^2, and m_A^2 (in the rMSSM) or $m_{H^\pm}^2$ (in the cMSSM). They are determined by expanding the pole equation

$$\mathcal{M}_i^2 - m_i^2 + \hat{\Sigma}_{ii}^{\text{eff}}(\mathcal{M}_i^2) = 0, \tag{4.72}$$

where $\mathcal{M}_i^2 = M_i^2 - \mathrm{i}M_i\Gamma_i$ is the complex pole of the propagator (matrix) and $\hat{\Sigma}_{ii}^{\text{eff}}$ is the effective self-energy, see also Sect. 3.2.2. For the determination of one-loop counterterms from this equation, mixing effects do not matter. Expanding the pole equation to one-loop order and taking the real part leads to

$$M_i^2 - m_i^2 + \operatorname{Re}\hat{\Sigma}_{ii}^{(1)}(M_i^2) \stackrel{!}{=} 0. \tag{4.73}$$

In an OS scheme, $M_i^2 = m_i^2$, and we find

$$\begin{aligned}
\delta^{(1)}M_Z^2 &= \operatorname{Re}\Sigma_{ZZ}^{T,(1)}(M_Z^2), && && \text{(4.74a)}\\
\delta^{(1)}M_W^2 &= \operatorname{Re}\Sigma_{W^-W^+}^{T,(1)}(M_W^2), && && \text{(4.74b)}\\
\delta^{(1)}m_A^2 &= \operatorname{Re}\Sigma_{AA}^{(1)}(m_A^2) && \text{(in the rMSSM)}, && \text{(4.74c)}\\
\delta^{(1)}m_{H^\pm}^2 &= \operatorname{Re}\Sigma_{H^-H^+}^{(1)}(m_{H^\pm}^2) && \text{(in the cMSSM)}. && \text{(4.74d)}
\end{aligned}$$

Taking the one-loop version of Eq. (4.54b), we get

$$\delta^{(1)}m_{H^\pm}^2 + \delta^{(1)}m_{G^\pm}^2 = \delta^{(1)}m_A^2 + \delta^{(1)}m_G^2 + \delta^{(1)}M_W^2. \tag{4.75}$$

The neutral and charged would-be Goldstone boson mass counterterms are identical at the one-loop level, see App. A. The dependent mass counterterm is therefore given by

$$\begin{aligned}
\delta^{(1)}m_{H^\pm}^2 &= \delta^{(1)}m_A^2 + \delta^{(1)}M_W^2 && \text{(in the rMSSM)}, && \text{(4.76a)}\\
\delta^{(1)}m_A^2 &= \delta^{(1)}m_{H^\pm}^2 - \delta^{(1)}M_W^2 && \text{(in the cMSSM)}. && \text{(4.76b)}
\end{aligned}$$

For the field renormalisation constants, different approaches are used in the Higgs and the gauge sector, respectively. In the Higgs sector, we renormalise the fields

in a $\overline{\text{DR}}$ scheme. It is most convenient to determine the doublet field counterterms from the $\mathcal{CP}$-even, diagonal self-energies at vanishing mixing angle α:

$$\delta^{(1)} Z^{\text{DR}}_{\mathcal{H}_1} = -\left[\partial \Sigma^{(1)}_{HH}\Big|_{\alpha=0}\right]_{\text{Div}}, \tag{4.77a}$$

$$\delta^{(1)} Z^{\text{DR}}_{\mathcal{H}_2} = -\left[\partial \Sigma^{(1)}_{hh}\Big|_{\alpha=0}\right]_{\text{Div}}, \tag{4.77b}$$

where the 'Div operator' performs a series expansion in ε and keeps only the part proportional to the divergence ε^{-1}. The $\overline{\text{DR}}$ version is then obtained from the simple replacement

$$\frac{1}{\varepsilon} \to \frac{\left(4\pi e^{-\gamma_E}\right)^{\varepsilon}}{\varepsilon}, \tag{4.78}$$

see also Sect. 2.3.2. As mentioned above, all Higgs field renormalisation constants are fixed by this choice for the doublet field counterterms.
In the gauge sector, the field counterterms are determined from on-shell conditions. The off-diagonal counterterms $\delta Z_{Z\gamma}$ and $\delta Z_{\gamma Z}$ are chosen such that the mixing self-energy $\hat{\Sigma}^T_{\gamma Z}$ vanishes at the two on-shell momenta $p^2 = 0$ and $p^2 = M_Z^2$:

$$\hat{\Sigma}^{T,(1)}_{\gamma Z}(0) \stackrel{!}{=} 0, \tag{4.79a}$$

$$\Rightarrow \delta^{(1)} Z_{Z\gamma} = \frac{2}{M_Z^2} \Sigma^{T,(1)}_{\gamma Z}(0) \stackrel{\mathcal{O}(N_c)}{=} 0, \tag{4.79b}$$

and

$$\hat{\Sigma}^{T,(1)}_{\gamma Z}(M_Z^2) \stackrel{!}{=} 0, \tag{4.80a}$$

$$\Rightarrow \delta^{(1)} Z_{\gamma Z} = -\frac{2}{M_Z^2} \Sigma^{T,(1)}_{\gamma Z}(M_Z^2). \tag{4.80b}$$

The diagonal field counterterms, on the other hand, are used to set the propagators' residues to unity. The diagonal propagators are just the inverse of the left-hand side of the pole equation above, shown exemplary for the Z boson:

$$\begin{aligned} \mathrm{i}\Delta^{T,(1)}_{ZZ}(p^2) &= \frac{\mathrm{i}}{p^2 - m_Z^2 + \hat{\Sigma}^{T,(1)}_{ZZ}(p^2)} \\ &= \frac{\mathrm{i}}{p^2 - m_Z^2 + \left[\hat{\Sigma}^{T,(1)}_{ZZ}(\mathcal{M}_Z^2) + (p^2 - \mathcal{M}_Z^2)\partial\hat{\Sigma}^{T,(1)}_{ZZ}(\mathcal{M}_Z^2) + \cdots\right]} \\ &\simeq \frac{\mathrm{i}}{\left(p^2 - \mathcal{M}_Z^2\right)\left[1 + \partial\hat{\Sigma}^{T,(1)}_{ZZ}(\mathcal{M}_Z^2)\right]}. \end{aligned} \tag{4.81}$$

Requiring the residues to be unity and expanding to one-loop order, we arrive at

$$\partial\hat{\Sigma}^{T,(1)}_{ZZ}(M_Z^2) \stackrel{!}{=} 0, \tag{4.82a}$$

$$\Rightarrow \delta^{(1)} Z_{ZZ} = -\partial\Sigma^{T,(1)}_{ZZ}(M_Z^2). \tag{4.82b}$$

For the W boson, we analogously find

$$\delta^{(1)} Z_{WW} = -\partial\Sigma^{T,(1)}_{W^-W^+}(M_W^2). \tag{4.83}$$

For the photon, the situation presents itself a bit differently; no mass parameter in the Lagrangian is associated with the photon and so there is also no counterterm to be generated from the renormalisation transformation. This poses no problem, however, as the transverse part of the photon self-energy, at one-loop order, vanishes at zero momentum due to a Slavnov-Taylor identity [175], and so the propagator pole is not shifted away from zero by loop corrections:

$$\Sigma^{T,(1)}_{\gamma\gamma}(0) = 0. \tag{4.84}$$

Because of Eq. (4.64a), this also means

$$\hat{\Sigma}^{T,(1)}_{\gamma\gamma}(0) = 0. \tag{4.85}$$

We expand the self-energy in the propagator around the physical pole:

$$\begin{aligned} \mathrm{i}\Delta^{T,(1)}_{\gamma\gamma}(p^2) &= \frac{\mathrm{i}}{p^2 + \hat{\Sigma}^{T,(1)}_{\gamma\gamma}(p^2)} \\ &\simeq \frac{\mathrm{i}}{p^2\left[1 + \partial\hat{\Sigma}^{T,(1)}_{\gamma\gamma}(0)\right]}. \end{aligned} \tag{4.86}$$

The OS renormalisation condition for the photon propagator corresponds to setting its residue to unity, which means we require

$$\partial\hat{\Sigma}^{T,(1)}_{\gamma\gamma}(0) \stackrel{!}{=} 0, \tag{4.87a}$$

$$\Rightarrow \delta^{(1)} Z_{\gamma\gamma} = -\partial\Sigma^{T,(1)}_{\gamma\gamma}(0). \tag{4.87b}$$

We define the one-loop vacuum polarisation by

$$\Pi^{(1)}_{\gamma\gamma}(p^2) \equiv \frac{\Sigma^{T,(1)}_{\gamma\gamma}(p^2)}{p^2} \quad \text{for } p^2 \neq 0, \tag{4.88a}$$

$$\Pi^{(1)}_{\gamma\gamma}(0) \equiv \partial\Sigma^{T,(1)}_{\gamma\gamma}(0), \tag{4.88b}$$

so

$$\delta^{(1)} Z_{\gamma\gamma} = -\Pi^{(1)}_{\gamma\gamma}(0). \tag{4.89}$$

When evaluating the vacuum polarisation $\Pi^{(1)}_{\gamma\gamma}$ at zero momentum, we can no longer treat the first two generations of quarks as massless since this would lead to infrared divergences. Instead, we take into account the contributions from the five light quarks to the running of the fine-structure constant α_{em}. As a consequence of the conceptual issues related to quark confinement, the light quark masses are not known with sufficient accuracy to use them as input parameters in a perturbative approach. Their contributions are determined from hadronic e^+e^-–annihilation data by using a dispersion relation together with the optical theorem [176].
We start by first splitting the contributions from quarks and squarks to the vacuum polarisation into parts stemming from light and heavy particles:

$$\Pi^{(1)}_{\gamma\gamma}(0) = \Pi^{(1),\text{light}}_{\gamma\gamma}(0) + \Pi^{(1),\text{heavy}}_{\gamma\gamma}(0). \tag{4.90}$$

This is always possible, as the photon interaction is fully diagonal in flavour space. The light part includes contributions from the five light quarks whereas the heavy part contains the squark and top contributions; the heavy part can be calculated perturbatively. In accordance with Refs. [177, 178], we rewrite the light part of the vacuum polarisation as

$$\begin{aligned} \Pi^{(1),\text{light}}_{\gamma\gamma}(0) &= \Pi^{(1),\text{light}}_{\gamma\gamma}(0) - \operatorname{Re}\Pi^{(1),\text{light}}_{\gamma\gamma}(M_Z^2) + \operatorname{Re}\Pi^{(1),\text{light}}_{\gamma\gamma}(M_Z^2) \\ &\equiv \Delta\alpha_{\text{em}}(M_Z^2) + \operatorname{Re}\Pi^{(1),\text{light}}_{\gamma\gamma}(M_Z^2), \end{aligned} \tag{4.91}$$

where we defined

$$\begin{aligned} \Delta\alpha_{\text{em}}(M_Z^2) &= \Pi^{(1),\text{light}}_{\gamma\gamma}(0) - \operatorname{Re}\Pi^{(1),\text{light}}_{\gamma\gamma}(M_Z^2) \\ &= \Delta\alpha_{\text{lep}}(M_Z^2) + \Delta\alpha^{(5)}_{\text{had}}(M_Z^2). \end{aligned} \tag{4.92}$$

The numerical values we use for $\Delta\alpha_{\text{lep}}(M_Z^2)$ and $\Delta\alpha^{(5)}_{\text{had}}(M_Z^2)$ are given in Eq. (7.2). $\Delta\alpha_{\text{lep}}(M_Z^2)$ is calculated perturbatively, and $\Delta\alpha^{(5)}_{\text{had}}(M_Z^2)$ is extracted from experimental input via dispersion relations. As the leptonic contributions to the running of the fine-structure constant are sizeable, we include them in our definition of $\Delta\alpha_{\text{em}}(M_Z^2)$ although they are not of $\mathcal{O}(N_c)$.
With this, our expression for the photon field counterterm is modified to

$$\delta^{(1)} Z_{\gamma\gamma} = -\Pi^{(1),\text{heavy}}_{\gamma\gamma}(0) - \operatorname{Re}\Pi^{(1),\text{light}}_{\gamma\gamma}(M_Z^2) - \Delta\alpha_{\text{em}}(M_Z^2). \tag{4.93}$$

In the second term, we can now safely set the quark masses of the first two generations to zero without having to worry about infrared divergences.
The elementary charge is renormalised such that all corrections to the $ee\gamma$-vertex (and, by charge universality, to any $ff\gamma$-vertex) vanish for external on-shell particles in the Thomson limit. With this renormalisation condition, we get the relation

$$Z_e \left(\sqrt{Z_{\gamma\gamma}} - \frac{s_\mathrm{w} + \delta s_\mathrm{w}}{c_\mathrm{w} + \delta c_\mathrm{w}} \frac{\delta Z_{Z\gamma}}{2} \right) = 1, \tag{4.94}$$

which holds to all orders [164,179–181]. Expanding up to one-loop order, we see that the elementary charge counterterm is fully determined by gauge field counterterms:

$$\delta^{(1)} Z_e \equiv \frac{\delta^{(1)} e}{e} = \frac{1}{2} \left(\frac{s_\mathrm{w}}{c_\mathrm{w}} \delta^{(1)} Z_{Z\gamma} - \delta^{(1)} Z_{\gamma\gamma} \right). \tag{4.95}$$

The sign difference with respect to Refs. [164,180] stems from a different convention in the SU(2) term of the gauge-covariant derivative, which is often found between the SM and the MSSM. While Eq. (4.94) corresponds to the common MSSM choice, the "SM convention" is obtained by exchanging the minus sign with a plus sign.
The weak mixing angle is not an independent parameter but fixed by the electroweak vector boson mass counterterms via the relation

$$c_\mathrm{w}^2 = \frac{M_W^2}{M_Z^2}, \quad s_\mathrm{w}^2 = 1 - c_\mathrm{w}^2, \tag{4.96a}$$

$$\Rightarrow \delta^{(1)} s_\mathrm{w} = \frac{1}{2} \frac{c_\mathrm{w}^2}{s_\mathrm{w}} \left(\frac{\delta^{(1)} M_Z^2}{M_Z^2} - \frac{\delta^{(1)} M_W^2}{M_W^2} \right). \tag{4.96b}$$

Lastly, we introduce the auxiliary renormalisation constants related to the ubiquitous factor $e/(s_\mathrm{w} M_W)$:

$$\delta^{(1)} Z_\mathrm{w} \equiv \delta^{(1)} Z_e - \frac{\delta^{(1)} M_W^2}{2 M_W^2} - \frac{\delta^{(1)} s_\mathrm{w}}{s_\mathrm{w}}. \tag{4.97}$$

The only parameter we have not renormalised at the one-loop level so far is t_β. Its renormalisation is discussed in Sect. 4.3.

4.2.3 Renormalisation at the two-loop level

Renormalised one-point functions and self-energies

At the two-loop level, the renormalised one-point vertex functions read

$$\hat{\Gamma}_h^{(2)} = \Gamma_h^{(2)} + \delta^{(2)} T_h + \tfrac{1}{2}\delta^{(1)} Z_{hh} \delta^{(1)} T_h + \tfrac{1}{2}\delta^{(1)} Z_{hH} \delta^{(1)} T_H, \tag{4.98a}$$

$$\hat{\Gamma}_H^{(2)} = \Gamma_H^{(2)} + \delta^{(2)} T_H + \tfrac{1}{2}\delta^{(1)} Z_{HH} \delta^{(1)} T_H + \tfrac{1}{2}\delta^{(1)} Z_{hH} \delta^{(1)} T_h, \tag{4.98b}$$

$$\hat{\Gamma}_A^{(2)} = \Gamma_A^{(2)} + \delta^{(2)} T_A + \tfrac{1}{2}\delta^{(1)} Z_{AA} \delta^{(1)} T_A + \tfrac{1}{2}\delta^{(1)} Z_{AG} \delta^{(1)} T_G, \tag{4.98c}$$

$$\hat{\Gamma}_G^{(2)} = \Gamma_G^{(2)} + \delta^{(2)} T_G + \tfrac{1}{2}\delta^{(1)} Z_{GG} \delta^{(1)} T_G + \tfrac{1}{2}\delta^{(1)} Z_{AG} \delta^{(1)} T_A. \tag{4.98d}$$

The renormalised $\mathcal{CP}$-even two-loop self-energies read

$$\begin{aligned}\hat{\Sigma}_{hh}^{(2)}(p^2) = {} & \Sigma_{hh}^{(2)}(p^2) + \delta^{(2)} Z_{hh}(p^2 - m_h^2) - \delta^{(2)} m_h^2 \\ & + \tfrac{1}{4}\left(\delta^{(1)} Z_{hH}\right)^2 (p^2 - m_H^2) - \delta^{(1)} Z_{hh} \delta^{(1)} m_h^2 - \delta^{(1)} Z_{hH} \delta^{(1)} m_{hH}^2,\end{aligned} \tag{4.99a}$$

$$\begin{aligned}\hat{\Sigma}_{hH}^{(2)}(p^2) = {} & \Sigma_{hH}^{(2)}(p^2) + \delta^{(2)} Z_{hH}\left(p^2 - \frac{m_h^2 + m_H^2}{2}\right) - \delta^{(2)} m_{hH}^2 \\ & + \tfrac{1}{4}\delta^{(1)} Z_{hH} \delta^{(1)} Z_{hh}(p^2 - m_h^2) + \tfrac{1}{4}\delta^{(1)} Z_{hH} \delta^{(1)} Z_{HH}(p^2 - m_H^2) \\ & - \delta^{(1)} Z_{hH} \frac{\delta^{(1)} m_h^2 + \delta^{(1)} m_H^2}{2} - \frac{\delta^{(1)} Z_{hh} + \delta^{(1)} Z_{HH}}{2} \delta^{(1)} m_{hH}^2,\end{aligned} \tag{4.99b}$$

$$\begin{aligned}\hat{\Sigma}_{HH}^{(2)}(p^2) = {} & \Sigma_{HH}^{(2)}(p^2) + \delta^{(2)} Z_{HH}(p^2 - m_H^2) - \delta^{(2)} m_H^2 \\ & + \tfrac{1}{4}\left(\delta^{(1)} Z_{hH}\right)^2 (p^2 - m_h^2) - \delta^{(1)} Z_{HH} \delta^{(1)} m_H^2 - \delta^{(1)} Z_{hH} \delta^{(1)} m_{hH}^2.\end{aligned} \tag{4.99c}$$

Similarly, the $\mathcal{CP}$-odd self-energies are

$$\begin{aligned}\hat{\Sigma}_{AA}^{(2)}(p^2) = {} & \Sigma_{AA}^{(2)}(p^2) + \delta^{(2)} Z_{AA}(p^2 - m_A^2) - \delta^{(2)} m_A^2 \\ & + \tfrac{1}{4}\left(\delta^{(1)} Z_{AG}\right)^2 p^2 - \delta^{(1)} Z_{AA} \delta^{(1)} m_A^2 - \delta^{(1)} Z_{AG} \delta^{(1)} m_{AG}^2,\end{aligned} \tag{4.100a}$$

$$\begin{aligned}\hat{\Sigma}_{AG}^{(2)}(p^2) = {} & \Sigma_{AG}^{(2)}(p^2) + \delta^{(2)} Z_{AG}\left(p^2 - \frac{m_A^2}{2}\right) - \delta^{(2)} m_{AG}^2 \\ & + \tfrac{1}{4}\delta^{(1)} Z_{AG} \delta^{(1)} Z_{AA}(p^2 - m_A^2) + \tfrac{1}{4}\delta^{(1)} Z_{AG} \delta^{(1)} Z_{GG}\, p^2 \\ & - \delta^{(1)} Z_{AG} \frac{\delta^{(1)} m_A^2 + \delta^{(1)} m_G^2}{2} - \frac{\delta^{(1)} Z_{AA} + \delta^{(1)} Z_{GG}}{2} \delta^{(1)} m_{AG}^2,\end{aligned} \tag{4.100b}$$

$$\begin{aligned}\hat{\Sigma}_{GG}^{(2)}(p^2) = {} & \Sigma_{GG}^{(2)}(p^2) + \delta^{(2)} Z_{GG}\, p^2 - \delta^{(2)} m_G^2 \\ & + \tfrac{1}{4}\left(\delta^{(1)} Z_{AG}\right)^2 (p^2 - m_A^2) - \delta^{(1)} Z_{GG} \delta^{(1)} m_G^2 - \delta^{(1)} Z_{AG} \delta^{(1)} m_{AG}^2.\end{aligned} \tag{4.100c}$$

Finally, the $\mathcal{CP}$-mixing self-energies read

$$\begin{aligned}\hat{\Sigma}^{(2)}_{hA}(p^2) &= \Sigma^{(2)}_{hA}(p^2) - \delta^{(2)} m^2_{hA} \\ &\quad - \frac{\delta^{(1)} Z_{hh} + \delta^{(1)} Z_{AA}}{2} \delta^{(1)} m^2_{hA} - \tfrac{1}{2} Z_{hH} m^2_{HA} - \tfrac{1}{2} Z_{AG} m^2_{hG},\end{aligned} \tag{4.101a}$$

$$\begin{aligned}\hat{\Sigma}^{(2)}_{hG}(p^2) &= \Sigma^{(2)}_{hG}(p^2) - \delta^{(2)} m^2_{hG} \\ &\quad - \frac{\delta^{(1)} Z_{hh} + \delta^{(1)} Z_{GG}}{2} \delta^{(1)} m^2_{hG} - \tfrac{1}{2} Z_{hH} m^2_{HG} - \tfrac{1}{2} Z_{AG} m^2_{hA},\end{aligned} \tag{4.101b}$$

$$\begin{aligned}\hat{\Sigma}^{(2)}_{HA}(p^2) &= \Sigma^{(2)}_{HA}(p^2) - \delta^{(2)} m^2_{HA} \\ &\quad - \frac{\delta^{(1)} Z_{HH} + \delta^{(1)} Z_{AA}}{2} \delta^{(1)} m^2_{HA} - \tfrac{1}{2} Z_{hH} m^2_{hA} - \tfrac{1}{2} Z_{AG} m^2_{HG},\end{aligned} \tag{4.101c}$$

$$\begin{aligned}\hat{\Sigma}^{(2)}_{HG}(p^2) &= \Sigma^{(2)}_{HG}(p^2) - \delta^{(2)} m^2_{HG} \\ &\quad - \frac{\delta^{(1)} Z_{HH} + \delta^{(1)} Z_{GG}}{2} \delta^{(1)} m^2_{HG} - \tfrac{1}{2} Z_{hH} m^2_{hG} - \tfrac{1}{2} Z_{AG} m^2_{HA}.\end{aligned} \tag{4.101d}$$

The renormalised charged self-energies are

$$\begin{aligned}\hat{\Sigma}^{(2)}_{H^-H^+}(p^2) &= \Sigma^{(2)}_{H^-H^+}(p^2) + \delta^{(2)} Z_{H^-H^+}(p^2 - m^2_{H^\pm}) - \delta^{(2)} m^2_{H^\pm} \\ &\quad + \frac{\delta^{(1)} Z_{H^-G^+} \delta^{(1)} Z_{G^-H^+}}{4} p^2 - \delta^{(1)} Z_{H^-H^+} \delta^{(1)} m^2_{H^\pm} \\ &\quad - \tfrac{1}{2} \delta^{(1)} Z_{H^-G^+} \delta^{(1)} m^2_{G^-H^+} - \tfrac{1}{2} \delta^{(1)} Z_{G^-H^+} \delta^{(1)} m^2_{H^-G^+},\end{aligned} \tag{4.102a}$$

$$\begin{aligned}\hat{\Sigma}^{(2)}_{H^-G^+}(p^2) &= \Sigma^{(2)}_{H^-G^+}(p^2) + \delta^{(2)} Z_{H^-G^+} \left(p^2 - \frac{m^2_{H^\pm}}{2}\right) - \delta^{(2)} m^2_{H^-G^+} \\ &\quad + \tfrac{1}{4} \delta^{(1)} Z_{H^-G^+} \delta^{(1)} Z_{H^-H^+}(p^2 - m^2_{H^\pm}) \\ &\quad + \tfrac{1}{4} \delta^{(1)} Z_{H^-G^+} \delta^{(1)} Z_{G^-G^+} p^2 \\ &\quad - \delta^{(1)} Z_{H^-G^+} \frac{\delta^{(1)} m^2_{H^\pm} + \delta^{(1)} m^2_{G^\pm}}{2} \\ &\quad - \frac{\delta^{(1)} Z_{H^-H^+} + \delta^{(1)} Z_{G^-G^+}}{2} \delta^{(1)} m^2_{H^-G^+},\end{aligned} \tag{4.102b}$$

$$\begin{aligned}\hat{\Sigma}^{(2)}_{G^-H^+}(p^2) &= \Sigma^{(2)}_{G^-H^+}(p^2) + \delta^{(2)} Z_{G^-H^+} \left(p^2 - \frac{m^2_{H^\pm}}{2}\right) - \delta^{(2)} m^2_{G^-H^+} \\ &\quad + \tfrac{1}{4} \delta^{(1)} Z_{G^-H^+} \delta^{(1)} Z_{H^-H^+}(p^2 - m^2_{H^\pm}) \\ &\quad + \tfrac{1}{4} \delta^{(1)} Z_{G^-H^+} \delta^{(1)} Z_{G^-G^+} p^2 \\ &\quad - \delta^{(1)} Z_{G^-H^+} \frac{\delta^{(1)} m^2_{H^\pm} + \delta^{(1)} m^2_{G^\pm}}{2} \\ &\quad - \frac{\delta^{(1)} Z_{H^-H^+} + \delta^{(1)} Z_{G^-G^+}}{2} \delta^{(1)} m^2_{G^-H^+},\end{aligned} \tag{4.102c}$$

$$\begin{aligned}\hat{\Sigma}^{(2)}_{G^-G^+}(p^2) = \Sigma^{(2)}_{G^-G^+}(p^2) &+ \delta^{(2)} Z_{G^-G^+}\, p^2 - \delta^{(2)} m^2_{G^\pm} \\ &+ \frac{\delta^{(1)} Z_{H^-G^+} \delta^{(1)} Z_{G^-H^+}}{4}(p^2 - m^2_{H^\pm}) - \delta^{(1)} Z_{G^-G^+} \delta^{(1)} m^2_{G^\pm} \\ &- \tfrac{1}{2}\delta^{(1)} Z_{H^-G^+} \delta^{(1)} m^2_{G^-H^+} - \tfrac{1}{2}\delta^{(1)} Z_{G^-H^+} \delta^{(1)} m^2_{H^-G^+}.\end{aligned} \tag{4.102d}$$

The renormalised transverse parts of the two-loop gauge boson self-energies are

$$\hat{\Sigma}^{T,(2)}_{\gamma\gamma}(p^2) = \Sigma^{T,(2)}_{\gamma\gamma}(p^2) + \delta^{(2)} Z_{\gamma\gamma}\, p^2 + \tfrac{1}{4}\left(\delta^{(1)} Z_{Z\gamma}\right)^2 (p^2 - M_Z^2), \tag{4.103a}$$

$$\begin{aligned}\hat{\Sigma}^{T,(2)}_{\gamma Z}(p^2) &= \Sigma^{T,(2)}_{\gamma Z}(p^2) + \tfrac{1}{2}\left(\delta^{(2)} Z_{\gamma Z} + \tfrac{1}{2}\delta^{(1)} Z_{\gamma Z} \delta^{(1)} Z_{\gamma\gamma}\right) p^2 \\ &\quad + \tfrac{1}{2}\left(\delta^{(2)} Z_{Z\gamma} + \tfrac{1}{2}\delta^{(1)} Z_{Z\gamma} \delta^{(1)} Z_{ZZ}\right)(p^2 - M_Z^2) \\ &\quad - \tfrac{1}{2}\delta^{(1)} Z_{Z\gamma} \delta^{(1)} M_Z^2 \\ &= \hat{\Sigma}^{T,(2)}_{Z\gamma}(p^2),\end{aligned} \tag{4.103b}$$

$$\begin{aligned}\hat{\Sigma}^{T,(2)}_{ZZ}(p^2) &= \Sigma^{T,(2)}_{ZZ}(p^2) + \delta^{(2)} Z_{ZZ}(p^2 - M_Z^2) - \delta^{(2)} M_Z^2 \\ &\quad + \tfrac{1}{4}\left(\delta^{(1)} Z_{\gamma Z}\right)^2 p^2 - \delta^{(1)} Z_{ZZ} \delta^{(1)} M_Z^2,\end{aligned} \tag{4.103c}$$

$$\begin{aligned}\hat{\Sigma}^{T,(2)}_{W^-W^+}(p^2) &= \Sigma^{T,(2)}_{W^-W^+}(p^2) + \delta^{(2)} Z_{WW}(p^2 - M_W^2) - \delta^{(2)} M_W^2 \\ &\quad - \delta^{(1)} Z_{WW} \delta^{(1)} M_W^2 \\ &= \hat{\Sigma}^{T,(2)}_{W^+W^-}(p^2).\end{aligned} \tag{4.103d}$$

At the two-loop level, the renormalised transverse part of the photon self-energy receives a non-vanishing contribution at $p^2 = 0$ from the mixing with the Z boson. Another non-vanishing contribution stems from the sub-loop part of the unrenormalised self-energy. To demonstrate this, we write the unrenormalised self-energy as

$$\Sigma^{T,(2)}_{\gamma\gamma}(p^2) = \widetilde{\Sigma}^{T,(2)}_{\gamma\gamma}(p^2) + \delta^{(1)} Z_{\gamma\gamma} \Sigma^{T,(1)}_{\gamma\gamma}(p^2) + \delta^{(1)} Z_{Z\gamma} \Sigma^{T,(1)}_{\gamma Z}(p^2), \tag{4.104}$$

where $\widetilde{\Sigma}^{T,(2)}_{\gamma\gamma}(p^2)$ does not contain any field renormalisation constants. While the second term on the right-hand side vanishes at zero momentum due to a Slavnov-Taylor identity, the third term will usually give a non-vanishing contribution.[5] The third term of Eq. (4.103a) and the third term of Eq. (4.104) will drop out once the effective two-loop self-energy, which we define below, is considered.

The renormalised two-loop self-energy vanishes at zero momentum if an on-shell renormalisation is chosen for $\delta^{(1)} Z_{Z\gamma}$. In our calculation, the on-shell condition leads to $\delta Z_{Z\gamma} = 0$.

[5] For the set of contributions considered in this thesis, $\Sigma^{T,(1)}_{\gamma Z}(0) = 0$.

The two-loop Higgs-vector mixing self-energies

$$\begin{aligned}
\hat{\Sigma}^{L,(2)}_{AZ}(p^2) &= \Sigma^{L,(2)}_{AZ}(p^2) - \mathrm{i}M_Z\Big(c_\beta^2\delta^{(2)}t_\beta - c_\beta^3 s_\beta(\delta^{(1)}t_\beta)^2 \\
&\quad + \tfrac{1}{2}\delta^{(2)}Z_{AG} + \tfrac{1}{2}c_\beta^2\delta^{(1)}t_\beta\delta^{(1)}Z_{AA}\Big) \\
&\quad - \frac{\mathrm{i}M_Z}{2}\left(c_\beta^2\delta^{(1)}t_\beta + \tfrac{1}{2}\delta^{(1)}Z_{AG}\right)\left(\frac{\delta^{(1)}M_Z^2}{M_Z^2} + \delta^{(1)}Z_{ZZ}\right) \\
&= -\hat{\Sigma}^{L,(2)}_{ZA}(p^2),
\end{aligned} \tag{4.105a}$$

$$\begin{aligned}
\hat{\Sigma}^{L,(2)}_{H^-W^+}(p^2) &= \Sigma^{L,(2)}_{H^-W^+}(p^2) + M_W\Big(c_\beta^2\delta^{(2)}t_\beta - c_\beta^3 s_\beta(\delta^{(1)}t_\beta)^2 \\
&\quad + \tfrac{1}{2}\delta^{(2)}Z_{H^-G^+} + \tfrac{1}{2}c_\beta^2\delta^{(1)}t_\beta\delta^{(1)}Z_{H^-H^+}\Big) \\
&\quad + \frac{M_W}{2}\left(c_\beta^2\delta^{(1)}t_\beta + \tfrac{1}{2}\delta^{(1)}Z_{H^-G^+}\right)\left(\frac{\delta^{(1)}M_W^2}{M_W^2} + \delta^{(1)}Z_{WW}\right) \\
&= -\hat{\Sigma}^{L,(2)}_{W^+H^-}(p^2)
\end{aligned} \tag{4.105b}$$

are used in some schemes to determine the two-loop counterterm for t_β, see Sect. 4.3.

Two-loop renormalisation conditions and counterterms

Similarly to the one-loop level, we choose the tadpole counterterms such that the one-point vertex functions vanish:

$$\hat{\Gamma}^{(2)}_i \stackrel{!}{=} 0, \quad i \in \{h,H,A\}, \tag{4.106a}$$

$$\Rightarrow \delta^{(2)}T_h = -\Gamma^{(2)}_h - \tfrac{1}{2}\delta^{(1)}Z_{hh}\delta^{(1)}T_h - \tfrac{1}{2}\delta^{(1)}Z_{hH}\delta^{(1)}T_H, \tag{4.106b}$$

$$\delta^{(2)}T_H = -\Gamma^{(2)}_H - \tfrac{1}{2}\delta^{(1)}Z_{HH}\delta^{(1)}T_H - \tfrac{1}{2}\delta^{(1)}Z_{hH}\delta^{(1)}T_h, \tag{4.106c}$$

$$\delta^{(2)}T_A = -\Gamma^{(2)}_A - \tfrac{1}{2}\delta^{(1)}Z_{AA}\delta^{(1)}T_A - \tfrac{1}{2}\delta^{(1)}Z_{AG}\delta^{(1)}T_G. \tag{4.106d}$$

The field renormalisation constants which appear explicitly on the right-hand side cancel with the ones from the sub-loop renormalisation of the $\Gamma^{(2)}_i$. As a consequence, the two-loop tadpole counterterms are independent of any field renormalisation.
From Eq. (4.70), we obtain the dependent $\delta^{(2)}T_G$ counterterm:

$$\delta^{(2)}T_G = -c_\beta^2\delta^{(1)}t_\beta\delta^{(1)}T_A. \tag{4.107}$$

Using this counterterm, the remaining one-point vertex function $\hat{\Gamma}^{(2)}_G$ vanishes as well.
The masses of the electroweak vector bosons and the Higgs bosons are renormalised in an OS scheme as before. At the two-loop level, however, mixing effects have to

be taken into account. We do this using the effective self-energy, that we defined in Sect. 3.2.2. The following effective self-energies enter in our results:

$$\hat{\Sigma}^{T,(2),\text{eff}}_{\gamma\gamma}(p^2) = \hat{\Sigma}^{T,(2)}_{\gamma\gamma}(p^2) - \frac{\left(\hat{\Sigma}^{T,(1)}_{\gamma Z}(p^2)\right)^2}{p^2 - M_Z^2}, \tag{4.108a}$$

$$\hat{\Sigma}^{T,(2),\text{eff}}_{ZZ}(p^2) = \hat{\Sigma}^{T,(2)}_{ZZ}(p^2) - \frac{\left(\hat{\Sigma}^{T,(1)}_{\gamma Z}(p^2)\right)^2}{p^2}, \tag{4.108b}$$

$$\hat{\Sigma}^{T,(2),\text{eff}}_{W^-W^+}(p^2) = \hat{\Sigma}^{T,(2)}_{W^-W^+}(p^2), \tag{4.108c}$$

$$\hat{\Sigma}^{(2),\text{eff}}_{AA}(p^2) = \hat{\Sigma}^{(2)}_{AA}(p^2) - \frac{\left(\hat{\Sigma}^{(1)}_{AG}(p^2)\right)^2}{p^2 - \xi_Z M_Z^2} + \xi_Z p^2 \frac{\hat{\Sigma}^{L,(1)}_{AZ}(p^2)\hat{\Sigma}^{L,(1)}_{ZA}(p^2)}{p^2 - \xi_Z M_Z^2}, \tag{4.108d}$$

$$\begin{aligned}\hat{\Sigma}^{(2),\text{eff}}_{H^-H^+}(p^2) = \hat{\Sigma}^{(2)}_{H^-H^+}(p^2) &- \frac{\hat{\Sigma}^{(1)}_{H^-G^+}(p^2)\hat{\Sigma}^{(1)}_{G^-H^+}(p^2)}{p^2 - \xi_W M_W^2} \\ &+ \xi_W p^2 \frac{\hat{\Sigma}^{L,(1)}_{H^-W^+}(p^2)\hat{\Sigma}^{L,(1)}_{W^-H^+}(p^2)}{p^2 - \xi_W M_W^2}.\end{aligned} \tag{4.108e}$$

It should be noted that these expressions have already been expanded up to the two-loop level. The effective Higgs self-energies depend explicitly on the gauge parameters ξ_Z and ξ_W. This dependence vanishes once we go on-shell:

$$\hat{\Sigma}^{(2),\text{eff}}_{AA}(m_A^2) = \hat{\Sigma}^{(2)}_{AA}(m_A^2) - \frac{\left(\hat{\Sigma}^{(1)}_{AG}(m_A^2)\right)^2}{m_A^2}, \tag{4.109a}$$

$$\hat{\Sigma}^{(2),\text{eff}}_{H^-H^+}(m^2_{H^\pm}) = \hat{\Sigma}^{(2)}_{H^-H^+}(m^2_{H^\pm}) - \frac{\hat{\Sigma}^{(1)}_{H^-G^+}(m^2_{H^\pm})\hat{\Sigma}^{(1)}_{G^-H^+}(m^2_{H^\pm})}{m^2_{H^\pm}}. \tag{4.109b}$$

Here, we have used the on-shell Slavnov-Taylor identities given in Eqs. (B.4). To determine the two-loop mass counterterms, we expand the pole equation (3.41) up to the two-loop order; this is shown exemplary in App. C. We arrive at

$$\begin{aligned}\delta^{(2)}M_Z^2 = {} & \operatorname{Re}\Sigma^{T,(2)}_{ZZ}(M_Z^2) - \operatorname{Re}\{\delta^{(1)}Z_{ZZ}\}\delta^{(1)}M_Z^2 + \tfrac{1}{4}\operatorname{Re}\{(\delta^{(1)}Z_{\gamma Z})^2\}M_Z^2 \\ & + \operatorname{Im}\{\hat{\Sigma}^{T,(1)}_{ZZ}(M_Z^2)\}\operatorname{Im}\{\partial\hat{\Sigma}^{T,(1)}_{ZZ}(M_Z^2)\} + \frac{\left(\operatorname{Im}\hat{\Sigma}^{T,(1)}_{\gamma Z}(M_Z^2)\right)^2}{M_Z^2},\end{aligned} \tag{4.110a}$$

$$\begin{aligned}\delta^{(2)}M_W^2 = {} & \operatorname{Re}\Sigma^{T,(2)}_{W^-W^+}(M_W^2) - \operatorname{Re}\{\delta^{(1)}Z_{WW}\}\delta^{(1)}M_W^2 \\ & + \operatorname{Im}\{\hat{\Sigma}^{T,(1)}_{W^-W^+}(M_W^2)\}\operatorname{Im}\{\partial\hat{\Sigma}^{T,(1)}_{W^-W^+}(M_W^2)\},\end{aligned} \tag{4.110b}$$

$$\begin{aligned}\delta^{(2)}m_A^2 = {} & \operatorname{Re}\Sigma^{(2)}_{AA}(m_A^2) - \delta^{(1)}Z_{AA}\delta^{(1)}m_A^2 - \delta^{(1)}Z_{AG}\delta^{(1)}m^2_{AG} \\ & + \tfrac{1}{4}(\delta^{(1)}Z_{AG})^2 m_A^2 + \operatorname{Im}\{\hat{\Sigma}^{(1)}_{AA}(m_A^2)\}\operatorname{Im}\{\partial\hat{\Sigma}^{(1)}_{AA}(m_A^2)\} \\ & - \operatorname{Re}\frac{\left(\hat{\Sigma}^{(1)}_{AG}(m_A^2)\right)^2}{m_A^2} \quad \text{(in the rMSSM)},\end{aligned} \tag{4.110c}$$

$$\begin{aligned}\delta^{(2)}m^2_{H^\pm} = {} & \operatorname{Re}\Sigma^{(2)}_{H^-H^+}(m^2_{H^\pm}) - \delta^{(1)}Z_{H^-H^+}\delta^{(1)}m^2_{H^\pm} - \tfrac{1}{2}\delta^{(1)}Z_{H^-G^+}\delta^{(1)}m^2_{G^-H^+} \\ & - \tfrac{1}{2}\delta^{(1)}Z_{G^-H^+}\delta^{(1)}m^2_{H^-G^+} + \tfrac{1}{4}\delta^{(1)}Z_{H^-G^+}\delta^{(1)}Z_{G^-H^+}m^2_{H^\pm} \\ & + \operatorname{Im}\{\hat{\Sigma}^{(1)}_{H^-H^+}(m^2_{H^\pm})\}\operatorname{Im}\{\partial\hat{\Sigma}^{(1)}_{H^-H^+}(m^2_{H^\pm})\} \\ & - \operatorname{Re}\frac{\hat{\Sigma}^{(1)}_{H^-G^+}(m^2_{H^\pm})\hat{\Sigma}^{(1)}_{G^-H^+}(m^2_{H^\pm})}{m^2_{H^\pm}} \quad \text{(in the cMSSM)}.\end{aligned} \tag{4.110d}$$

The last terms in the expressions for the Z, A and $H^\pm$ mass counterterm stem from the mixing contribution in the effective self-energy. As indicated, we use two different input parameters for the rMSSM and the cMSSM also at the two-loop level. In all mass counterterms, the diagonal one-loop field renormalisation constants drop out. To get a relation between the Higgs boson mass counterterms, we take the two-loop version of Eq. (4.54b):

$$\delta^{(2)}m^2_{H^\pm} + \delta^{(2)}m^2_{G^\pm} = \delta^{(2)}m^2_A + \delta^{(2)}m^2_G + \delta^{(2)}M^2_W. \tag{4.111}$$

At the two-loop level, the neutral and charged would-be Goldstone boson mass counterterms do not agree with each other anymore. Instead, they fulfil

$$\delta^{(2)}m^2_{G^\pm} - \delta^{(2)}m^2_G = c^4_\beta M^2_W\left(\delta^{(1)}t_\beta\right)^2, \tag{4.112}$$

see App. A. From there,

$$\delta^{(2)}m^2_{H^\pm} - \delta^{(2)}m^2_A - \delta^{(2)}M^2_W + c^4_\beta M^2_W\left(\delta^{(1)}t_\beta\right)^2 = 0 \tag{4.113}$$

follows directly. All previous Feynman-diagrammatic two-loop calculations for the Higgs boson mass did not require the $(\delta^{(1)}t_\beta)^2$ term as they were focusing on QCD corrections [51, 52, 56, 68] or on pure Yukawa corrections [74–77]. In both of these cases, the $(\delta^{(1)}t_\beta)^2$ term does not contribute, and it is to our best knowledge also not mentioned in the literature. In our calculation, however, this term is needed in order to render all scalar two-loop self-energies finite.
Depending on the scenario, the dependent mass counterterm is given by

$$\delta^{(2)}m^2_{H^\pm} = \delta^{(2)}m^2_A + \delta^{(2)}M^2_W - c^4_\beta M^2_W\left(\delta^{(1)}t_\beta\right)^2 \quad \text{(in the rMSSM)}, \tag{4.114a}$$

$$\delta^{(2)}m^2_A = \delta^{(2)}m^2_{H^\pm} - \delta^{(2)}M^2_W + c^4_\beta M^2_W\left(\delta^{(1)}t_\beta\right)^2 \quad \text{(in the cMSSM)}. \tag{4.114b}$$

The two-loop Higgs field counterterms are defined in a $\overline{\text{DR}}$ scheme again. First, we

define the DR counterterms via

$$\delta^{(2)} Z^{\mathrm{DR}}_{\mathcal{H}_1} = -\left[\partial\Sigma^{(2)}_{HH}\Big|_{\alpha=0}\right]_{\mathrm{Div}}, \tag{4.115a}$$

$$\delta^{(2)} Z^{\mathrm{DR}}_{\mathcal{H}_2} = -\left[\partial\Sigma^{(2)}_{hh}\Big|_{\alpha=0}\right]_{\mathrm{Div}}, \tag{4.115b}$$

where α denotes the $\mathcal{CP}$-even Higgs mixing angle. We obtain the $\overline{\mathrm{DR}}$ versions via the procedure explained in Sect. 2.3.2.

The two-loop weak-mixing angle counterterm is already determined by the counterterms of the electroweak gauge boson masses:

$$\delta^{(2)} s_{\mathrm{w}} = \frac{c_{\mathrm{w}}^2}{2 s_{\mathrm{w}}}\left[\frac{\delta^{(2)} M_Z^2}{M_Z^2} - \frac{\delta^{(2)} M_W^2}{M_W^2} - \left(\frac{\delta^{(1)} M_Z^2}{M_Z^2}\right)^2 + \frac{\delta^{(1)} M_W^2}{M_W^2}\frac{\delta^{(1)} M_Z^2}{M_Z^2} - \left(\frac{\delta^{(1)} s_{\mathrm{w}}}{c_{\mathrm{w}}}\right)^2\right]. \tag{4.116}$$

As at the one-loop level, we again fix the elementary charge via the electromagnetic vertices in the Thomson limit. This means that Eq. (4.94) holds again. Expanding this relation up to two-loop order, we get

$$\delta^{(2)} Z_e = -\frac{1}{2}\delta^{(2)} Z_{\gamma\gamma} + \frac{s_{\mathrm{w}}}{2c_{\mathrm{w}}}\delta^{(2)} Z_{Z\gamma} + \left(\delta^{(1)} Z_e\right)^2 + \frac{1}{8}\left(\delta^{(1)} Z_{\gamma\gamma}\right)^2 + \frac{1}{2c_{\mathrm{w}}^3}\delta^{(1)} Z_{Z\gamma}\,\delta^{(1)} s_{\mathrm{w}}, \tag{4.117}$$

in agreement with Ref. [182].

The off-diagonal field renormalisation constants are chosen such that the renormalised mixing self-energies vanish on-shell:

$$\begin{aligned} &\hat{\Sigma}^{T,(2)}_{\gamma Z}(0) \stackrel{!}{=} 0 \\ \Rightarrow\ &\delta^{(2)} Z_{Z\gamma} = \frac{2}{M_Z^2}\Sigma^{T,(2)}_{\gamma Z}(0) - \frac{1}{2}\delta^{(1)} Z_{Z\gamma}\delta^{(1)} Z_{ZZ} - \delta^{(1)} Z_{Z\gamma}\frac{\delta^{(1)} M_Z^2}{M_Z^2}, \end{aligned} \tag{4.118a}$$

$$\begin{aligned} &\hat{\Sigma}^{T,(2)}_{\gamma Z}(M_Z^2) \stackrel{!}{=} 0 \\ \Rightarrow\ &\delta^{(2)} Z_{\gamma Z} = -\frac{2}{M_Z^2}\Sigma^{T,(1)}_{\gamma Z}(M_Z^2) - \frac{1}{2}\delta^{(1)} Z_{\gamma Z}\delta^{(1)} Z_{\gamma\gamma} + \delta^{(1)} Z_{Z\gamma}\frac{\delta^{(1)} M_Z^2}{M_Z^2}. \end{aligned} \tag{4.118b}$$

The renormalisation constant $\delta^{(2)} Z_{\gamma Z}$ is not needed in our calculation but was included for the sake of completeness. The unrenormalised transverse part of the γZ self-energy vanishes at zero momentum also at the two-loop order. This implies

$$\delta^{(2)} Z_{Z\gamma} \stackrel{\mathcal{O}\left(N_c^2\right)}{=} 0. \tag{4.119}$$

The diagonal photon field counterterm, on the other hand, is again used to set the

propagator's residue to unity. The derivation proceeds in analogous fashion to the one-loop case. With the effective self-energy defined in Eq. (4.108), the two-loop propagator reads

$$\begin{aligned} \mathrm{i}\Delta_{\gamma\gamma}^{T,(2)}(p^2) &= \frac{\mathrm{i}}{p^2 + \hat{\Sigma}_{\gamma\gamma}^{T,(1)}(p^2) + \hat{\Sigma}_{\gamma\gamma}^{T,(2),\mathrm{eff}}(p^2)} \\ &= \frac{\mathrm{i}}{p^2 + \hat{\Sigma}_{\gamma\gamma}^{T,(1)}(p^2) + \hat{\Sigma}_{\gamma\gamma}^{T,(2)}(p^2) - \left(\hat{\Sigma}_{\gamma Z}^{T,(1)}(p^2)\right)^2/(p^2 - M_Z^2)}. \end{aligned} \tag{4.120}$$

In the vicinity of the pole, using Eqs. (4.79a), (4.85), and (4.87a), the propagator reads

$$\mathrm{i}\Delta_{\gamma\gamma}^{T,(2)}(p^2) \simeq \frac{\mathrm{i}}{p^2 + \hat{\Sigma}_{\gamma\gamma}^{T,(2)}(0) + p^2 \partial\hat{\Sigma}_{\gamma\gamma}^{T,(2)}(0)} \tag{4.121}$$

The transverse part of the unrenormalised $\gamma\gamma$ two-loop self-energy vanishes on-shell

$$\Sigma_{\gamma\gamma}^{T,(2)}(0) \overset{\mathcal{O}\left(N_c^2\right)}{=} 0 \tag{4.122}$$

and so, with Eq. (4.79b)

$$\hat{\Sigma}_{\gamma\gamma}^{T,(2)}(0) \overset{\mathcal{O}\left(N_c^2\right)}{=} 0. \tag{4.123}$$

We can thus impose a renormalisation condition on the derivative of the self-energy to fix the residue of the propagator:

$$\partial\hat{\Sigma}_{\gamma\gamma}^{T,(2)}(0) = 0, \tag{4.124a}$$

$$\Rightarrow \delta^{(2)} Z_{\gamma\gamma} = -\partial\Sigma_{\gamma\gamma}^{T,(2)}(0) - \frac{1}{4}\left(\delta^{(1)} Z_{Z\gamma}\right)^2. \tag{4.124b}$$

We also give a two-loop version of the auxiliary counterterm δZ_{w}:

$$\begin{aligned} \delta^{(2)} Z_{\mathrm{w}} \equiv{}& \frac{1}{2}\left(\delta^{(1)} Z_{\mathrm{w}}\right)^2 + \delta^{(2)} Z_e - \frac{1}{2}\left(\delta^{(1)} Z_e\right)^2 - \frac{\delta^{(2)} M_W^2}{2M_W^2} + \left(\frac{\delta^{(1)} M_W^2}{2M_W^2}\right)^2 \\ &- \frac{\delta^{(2)} s_{\mathrm{w}}}{s_{\mathrm{w}}} + \frac{1}{2}\left(\frac{\delta^{(1)} s_{\mathrm{w}}}{s_{\mathrm{w}}}\right)^2. \end{aligned} \tag{4.125}$$

4.3 Renormalisation of $\tan(\beta)$

In this section, we discuss the renormalisation of the MSSM parameter t_β. Both the precise definition and the numerical value of this parameter have a large impact on the prediction of MSSM observables, in particular the mass of the SM-like Higgs boson [183]. t_β appears in the calculation of the $\mathcal{CP}$-even Higgs boson masses already at the tree-level. Thus, for a prediction at two-loop order, expressions for the t_β counterterms at two-loop order are required.

In this section, we will discuss three renormalisation schemes for t_β: The Dabelstein-Chankowski-Pokorski-Rosiek scheme (DCPR), the $\overline{\text{DR}}$ scheme, and an OS definition via the decay $A \to \tau^-\tau^+$. Of these, the two latter will be important for our two-loop Higgs boson mass prediction at $\mathcal{O}\Big((\alpha_{\text{em}} + \alpha_q)^2 N_c^2\Big)$. We include a brief discussion of the DCPR scheme at the one-loop level as well to illustrate some interesting concepts in the t_β renormalisation.

The $\overline{\text{DR}}$ choice is popular since t_β has no natural physical observable to which it is related, and a minimal renormalisation often simplifies a calculation, cf. Refs. [55,67, 74,75,183–185]. Furthermore, the $\overline{\text{DR}}$ definition is process-independent and provides numerically stable results in the sense of renormalisation scale dependence [183]. It does, however, lead to a gauge-dependent definition of t_β in an R_ξ gauge at the two-loop level.

As an alternative, we investigate an OS definition of t_β in terms of the decay width $\Gamma(A \to \tau^-\tau^+)$.[6] We choose this particular decay width as it has a relatively clean signature and, in the region of larger t_β involves a sizeable coupling to the leptons [185]. As a renormalisation condition, we require the square of the amplitude $A \to \tau^-\tau^+$ to not receive any higher-order corrections and from this determine an OS t_β counterterm. This definition is gauge-independent, numerically stable and, of course, process-dependent [183, 184].

Before we discuss the different renormalisation schemes, we introduce the one- and two-loop counterterms for s_β and c_β:

$$\delta^{(1)} s_\beta = c_\beta^3 \delta^{(1)} t_\beta, \tag{4.126a}$$

$$\delta^{(1)} c_\beta = -s_\beta c_\beta^2 \delta^{(1)} t_\beta, \tag{4.126b}$$

$$\delta^{(2)} s_\beta = c_\beta^3 \delta^{(2)} t_\beta - \tfrac{3}{2} c_\beta^4 s_\beta \Big(\delta^{(1)} t_\beta\Big)^2, \tag{4.126c}$$

$$\delta^{(2)} c_\beta = -s_\beta c_\beta^2 \delta^{(2)} t_\beta - \frac{1}{2} c_\beta^3 \Big(c_\beta^2 - 2 s_\beta^2\Big) \Big(\delta^{(1)} t_\beta\Big)^2. \tag{4.126d}$$

[6] In a $\mathcal{CP}$-violating scenario, one would use $\Gamma(H^- \to \tau^- \bar{\nu}_\tau)$ instead.

4.3.1 The DCPR scheme

The renormalisation of t_β is closely tied to the renormalisation of the vacuum expectation values and the Higgs fields. We write the renormalisation transformation for the VEVs in two equivalent ways:

$$\begin{aligned} v_i &\to v_i + \delta v_i \\ &= Z_{\mathcal{H}_i}(v_i + \delta \bar{v}_i). \end{aligned} \tag{4.127}$$

At the one-loop level, the t_β counterterm reads

$$\delta^{(1)} t_\beta = t_\beta \Big(\frac{\delta^{(1)} \bar{v}_2}{v_2} - \frac{\delta^{(1)} \bar{v}_1}{v_1} + \frac{1}{2} \big[\delta^{(1)} Z_{\mathcal{H}_2} - \delta^{(1)} Z_{\mathcal{H}_1} \big] \Big). \tag{4.128}$$

The one-loop relation

$$\left[\frac{\delta^{(1)} \bar{v}_1}{v_1} \right]_{\text{Div}} = \left[\frac{\delta^{(1)} \bar{v}_2}{v_2} \right]_{\text{Div}} \tag{4.129}$$

was noted in Refs. [23, 24]. In the DCPR scheme, the choice

$$\frac{\delta^{(1)} \bar{v}_1^{\text{DCPR}}}{v_1} = \frac{\delta^{(1)} \bar{v}_2^{\text{DCPR}}}{v_2} \tag{4.130}$$

leads to

$$\delta^{(1)} t_\beta^{\text{DCPR}} = \frac{t_\beta}{2} \Big(\delta^{(1)} Z_{\mathcal{H}_2}^{\text{DCPR}} - \delta^{(1)} Z_{\mathcal{H}_1}^{\text{DCPR}} \Big). \tag{4.131}$$

The field counterterms for the mass eigenstates then read

$$\delta^{(1)} Z_{AG}^{\text{DCPR}} = 2 c_\beta^2 \delta^{(1)} t_\beta^{\text{DCPR}}, \tag{4.132a}$$

$$\delta^{(1)} Z_{H^- G^+}^{\text{DCPR}} = 2 c_\beta^2 \delta^{(1)} t_\beta^{\text{DCPR}}. \tag{4.132b}$$

This relation allows us to rewrite the scalar-vector mixing self-energies

$$\hat{\Sigma}_{AZ}^{L,(1)}(p^2) = \Sigma_{AZ}^{L,(1)}(p^2) - 2\mathrm{i} M_Z c_\beta^2 \delta^{(1)} t_\beta^{\text{DCPR}}, \tag{4.133a}$$

$$\hat{\Sigma}_{H^- W^+}^{L,(1)}(p^2) = \Sigma_{H^- W^+}^{L,(1)}(p^2) + 2 M_W c_\beta^2 \delta^{(1)} t_\beta^{\text{DCPR}}, \tag{4.133b}$$

which we introduced in Eqs. (4.66b) and (4.67a). The on-shell renormalisation conditions are

$$\operatorname{Im} \hat{\Sigma}_{AZ}^{L,(1)}(m_A^2) \stackrel{!}{=} 0, \tag{4.134a}$$

$$\Rightarrow \delta^{(1)} t_\beta^{\text{DCPR}} = \frac{1}{2 M_Z c_\beta^2} \operatorname{Im} \Sigma_{AZ}^{L,(1)}(m_A^2) \tag{4.134b}$$

in the rMSSM [183–185] and

$$\operatorname{Re}\hat{\Sigma}^{L,(1)}_{H^-W^+}(m^2_{H^\pm}) \stackrel{!}{=} 0, \tag{4.135a}$$

$$\Rightarrow \delta^{(1)}t_\beta^{\mathrm{DCPR}} = -\frac{1}{2M_W c_\beta^2}\operatorname{Re}\Sigma^{L,(1)}_{H^-W^+}(m^2_{H^\pm}) \tag{4.135b}$$

in the cMSSM [186]. With the on-shell Slavnov-Taylor identities given in App. B, this also implies

$$\operatorname{Re}\hat{\Sigma}^{(1)}_{AG}(m^2_A) = 0 \quad \text{in the rMSSM}, \tag{4.136a}$$

$$\operatorname{Re}\hat{\Sigma}^{(1)}_{H^-G^+}(m^2_{H^\pm}) = 0 \quad \text{in the cMSSM}. \tag{4.136b}$$

The DCPR definition of t_β simplifies our calculation where mixing effects have to be taken into account, but it comes at a cost: We can no longer define both Higgs field counterterms in the simple $\overline{\mathrm{DR}}$ scheme.[7] In the DCPR scheme, the renormalisation condition (4.130) for the VEV counterterms replaces the renormalisation condition for one of the Higgs fields.
Furthermore, a DCPR counterterm for t_β leads to less numerically stable results than a $\overline{\mathrm{DR}}$ scheme definition in some regions of the parameter space [187]. As we also prefer the handiness of the $\overline{\mathrm{DR}}$ field counterterms over the simple DCPR definition of t_β, we will not make use of the DCPR scheme in this thesis. Instead, we use the $\overline{\mathrm{DR}}$ scheme and a different OS scheme, which we discuss now.

4.3.2 $\overline{\mathrm{DR}}$ renormalisation via the AZ transition

If t_β is renormalised in the $\overline{\mathrm{DR}}$-scheme, its counterterm consists of divergent terms only. Taking the divergent part of Eq. (4.128) and using the one-loop relation in Eq. (4.129), we find

$$\delta^{(1)}t_\beta^{\overline{\mathrm{DR}}} = \frac{t_\beta}{2}\Big(\delta^{(1)}Z^{\overline{\mathrm{DR}}}_{\mathcal{H}_2} - \delta^{(1)}Z^{\overline{\mathrm{DR}}}_{\mathcal{H}_1}\Big). \tag{4.137}$$

This relation is often used to determine $\delta^{(1)}t_\beta^{\overline{\mathrm{DR}}}$ in schemes with $\overline{\mathrm{DR}}$ field renormalisation. [161]. At the two-loop level, Eq. (4.129) does not hold in general, and another approach has to be taken.
In this thesis, we determine the t_β counterterm by demanding the finiteness of the

[7] For the definition of the $\delta^{(1)}Z_{\mathcal{H}_i}$ in the DCPR scheme, see Ref. [23].

AZ mixing self-energy:

$$\left[\hat{\Sigma}^{L,(1)}_{AZ}\right]_{\text{Div}} = 0, \tag{4.138a}$$

$$\Rightarrow \delta^{(1)} t_\beta^{\text{DR}} = \frac{1}{\mathrm{i} c_\beta^2 M_Z}\left[\Sigma^{L,(1)}_{AZ}\right]_{\text{Div}} - \frac{\delta^{(1)} Z_{AG}^{\text{DR}}}{2c_\beta^2}. \tag{4.138b}$$

The $\overline{\text{DR}}$ term is then obtained as we explained in Sect. 2.3.2 and agrees with the expression given in Eq. (4.137). This prescription allows us to determine a counterterm for t_β without having to consider the renormalisation of the VEVs.
The $\overline{\text{DR}}$ renormalisation via AZ transitions can easily be extended to the two-loop level:

$$\left[\hat{\Sigma}^{L,(2)}_{AZ}\right]_{\text{Div}} = 0, \tag{4.139a}$$

$$\begin{aligned}\Rightarrow \delta^{(2)} t_\beta^{\text{DR}} = {} & \frac{1}{\mathrm{i} c_\beta^2 M_Z}\left[\Sigma^{L,(2)}_{AZ}\right]_{\text{Div}} - \frac{\delta^{(2)} Z_{AG}^{\text{DR}}}{2c_\beta^2} \\ & + c_\beta s_\beta \left(\delta^{(1)} t_\beta^{\text{DR}}\right)^2 - \tfrac{1}{2}\delta^{(1)} t_\beta^{\text{DR}} \delta^{(1)} Z_{AA}^{\text{DR}} \\ & - \frac{1}{2}\left(\delta^{(1)} t_\beta^{\text{DR}} + \frac{\delta^{(1)} Z_{AG}^{\text{DR}}}{2c_\beta^2}\right)\left[\frac{\delta^{(1)} M_Z^2}{M_Z^2} + \delta^{(1)} Z_{ZZ}\right]_{\text{Div}}.\end{aligned} \tag{4.139b}$$

The $\overline{\text{DR}}$ version is obtained as described in Sect. 2.3.2.
Of course, we could also use the $H^- W^+$ self-energy to determine an expression for δt_β. Since, in this chapter, we are only interested in extracting divergences to define t_β in a minimal subtraction scheme, the charged self-energies would yield the same result. We checked the finiteness of the charged self-energy as a validation.

4.3.3 OS renormalisation via the decay $A \to \tau^- \tau^+$

Several different on-shell definitions of t_β can be found in the literature. We have already illustrated the DCPR scheme at the one-loop level and we pointed out its weaknesses. In this section, we present an OS scheme which is defined via the Higgs decay process $A \to \tau^- \tau^+$ [183–185].
This approach yields a gauge-independent definition of t_β due to its direct relation to an observable (the partial decay width $\Gamma(A \to \tau^- \tau^+)$). Furthermore, this method provides a numerically stable prediction due to the smallness of loop corrections to the decay [184].
This definition, however, comes with its own drawbacks as well. First of all, it is process- and flavour-dependent and as such it is somewhat inconvenient; any decay into fermions or even an entirely different observable could be used to define t_β

instead. Secondly, if such a decay were observed and the corresponding partial decay width were measured, the extraction of an experimental value for t_β would require the calculation of the respective three-point vertex to the desired order. Beyond the one-loop level, this can become quite tedious [183, 184].
The second issue does not concern us, however, as no such decay has been observed up to now, and no experimental value for t_β needs to be extracted. Furthermore, for the contributions that are of interest to us, no virtual corrections to the three-point vertex exist.
For our on-shell definition of t_β, we impose the renormalisation condition that the decay width $\Gamma(A \to \tau^-\tau^+)$ receives no quantum corrections. This is equivalent to demanding that the absolute value of the physical three-point amplitude $\Gamma^{\text{ph}}_{A\tau\tau}$ receives no loop corrections. We will also work in a $\mathcal{CP}$-conserving scenario, in which the $\mathcal{CP}$-odd Higgs boson mixes with both the neutral would-be Goldstone boson G and the longitudinal part of the Z boson (and nothing else).
Our starting point is the physical vertex amplitude

$$\hat{\Gamma}^{\text{ph}}_{A\tau\tau} = \sqrt{\hat{Z}_A}\Big(\hat{\Gamma}_{A\tau\tau} + \hat{Z}_{AG}\hat{\Gamma}_{G\tau\tau} + AZ \text{ mixing}\Big). \tag{4.140}$$

It takes into account mixing effects with unphysical states as well as the correct normalisation of the $\mathcal{S}$-matrix by including finite wave-function normalisation factors. The contribution from the unphysical states is gauge-dependent for each term separately, but in the sum the dependence drops out. We have shown this explicitly at the one-loop level utilising the Slavnov-Taylor identities presented in App. B. From now on, we work in the Landau gauge $\xi_Z = 0$ exclusively:[8]

$$\hat{\Gamma}^{\text{ph}}_{A\tau\tau} = \sqrt{\hat{Z}_A}\Big(\hat{\Gamma}_{A\tau\tau} + \hat{Z}_{AG}\hat{\Gamma}_{G\tau\tau}\Big)\Big|_{\xi_Z=0}. \tag{4.141}$$

Comparing this with the notation used in Refs. [163, 188], some remarks have to be made. In this paper, the mixing of tree-level mass eigenstates into loop-corrected mass eigenstates is discussed. In the case of $\mathcal{CP}$ violation, the three tree-level eigenstates h, H, and A mix into three loop-corrected eigenstates h_1, h_2, and h_3. We only consider the case of $\mathcal{CP}$ conservation here, so no mixing between the $\mathcal{CP}$-even and the $\mathcal{CP}$-odd states takes place. There is, however, still mixing between the $\mathcal{CP}$-odd states A and G, which is only well-defined when taking into account contributions from the longitudinal degrees of the Z vector boson as well. To this end, we employ the formalism established in Ref. [163].

[8] Due to gauge independence we can of course work in any arbitrary R_ξ gauge; the Landau gauge is the most convenient for the following discussion as it sets the AZ mixing to 0.

Therein, the diagonal and off-diagonal wave function normalisation factors are defined as

$$\hat{Z}_A = \left[1 + \partial\hat{\Sigma}_{AA}(p^2) - \frac{\partial}{\partial p^2}\frac{\left(\hat{\Sigma}_{AG}(p^2)\right)^2}{p^2 - \xi_Z M_Z^2 + \hat{\Sigma}_{GG}(p^2)}\right]^{-1}\Bigg|_{p^2=\mathcal{M}_A^2}, \tag{4.142a}$$

$$\hat{Z}_{AG} = -\frac{\hat{\Sigma}_{AG}(\mathcal{M}_A^2)}{\mathcal{M}_A^2 - \xi_Z M_Z^2 + \hat{\Sigma}_{GG}(\mathcal{M}_A^2)}. \tag{4.142b}$$

We can see that, in the case of on-shell renormalisation,[9] $\hat{Z}_A = 1$ and $\hat{Z}_{AG} = 0$.
Now we only need expressions for the 'bare' vertex functions in Eq. (4.141). We derive them from the Lagrangian

$$\mathcal{L}_{\chi\tau\tau+Z\tau\tau} = \frac{\mathrm{i}em_\tau}{2s_\mathrm{w}M_W c_\beta}\overline{\tau}\gamma_5\tau\left(s_{\beta_\mathrm{n}}A - c_{\beta_\mathrm{n}}G\right) - \frac{e}{s_\mathrm{w}c_\mathrm{w}}\overline{\tau}\gamma^\mu\left[g_L^\tau P_L - g_R^\tau P_R\right]\tau Z_\mu, \tag{4.143}$$

which contains all interactions of bosons with τ leptons relevant to us, via a renormalisation transformation. We have introduced the abbreviations $g_L^\tau = T_{3L}^\tau(1 - 4T_{3L}^\tau Q_\tau s_\mathrm{w}^2)$ and $g_R^\tau = 4(T_{3L}^\tau)^2 Q_\tau s_\mathrm{w}^2$.
As a renormalisation condition, we require the absolute square of the physical amplitude to not receive any higher order corrections:

$$\begin{aligned}\left|\hat{\Gamma}_{A\tau\tau}^\mathrm{ph}\right|^2 &= \left|\Gamma_{A\tau\tau}^{(0)} + \hat{\Gamma}_{A\tau\tau}^{\mathrm{ph},(1)} + \hat{\Gamma}_{A\tau\tau}^{\mathrm{ph},(2)} + \cdots\right|^2 \\ &= \left|\Gamma_{A\tau\tau}^{(0)}\right|^2\left(1 + 2\,\mathrm{Re}\,\tilde{\Gamma}_{A\tau\tau}^{\mathrm{ph},(1)} + 2\,\mathrm{Re}\,\tilde{\Gamma}_{A\tau\tau}^{\mathrm{ph},(2)} + \left|\tilde{\Gamma}_{A\tau\tau}^{\mathrm{ph},(1)}\right|^2 + \cdots\right) \\ &\overset{!}{=} \left|\Gamma_{A\tau\tau}^{(0)}\right|^2,\end{aligned} \tag{4.144}$$

where we defined $\tilde{\Gamma}_{A\tau\tau}^{\mathrm{ph},(\mathrm{i})}$ via

$$\hat{\Gamma}_{A\tau\tau}^{\mathrm{ph},(\mathrm{i})} \equiv \tilde{\Gamma}_{A\tau\tau}^{\mathrm{ph},(\mathrm{i})}\Gamma_{A\tau\tau}^{(0)}. \tag{4.145}$$

From this, we obtain both the one-loop and the two-loop renormalisation condition

$$\mathrm{Re}\,\tilde{\Gamma}_{A\tau\tau}^{\mathrm{ph},(1)} = 0, \tag{4.146a}$$

$$\mathrm{Re}\,\tilde{\Gamma}_{A\tau\tau}^{\mathrm{ph},(2)} = -\frac{1}{2}\,\mathrm{Im}^2\,\tilde{\Gamma}_{A\tau\tau}^{\mathrm{ph},(1)}. \tag{4.146b}$$

[9] Proper on-shell renormalisation sets diagonal field counterterms such that the corresponding propagator has unit residue and the off-diagonal field counterterms such that mixing contributions vanish on the mass-shell.

One-loop order

Expanding Eq. (4.141) to the one-loop order, we obtain

$$\hat{\Gamma}^{\mathrm{ph},(1)}_{A\tau\tau} = \hat{\Gamma}^{(1)}_{A\tau\tau} - \frac{1}{2}\partial\hat{\Sigma}^{(1)}_{AA}(m_A^2)\Gamma^{(0)}_{A\tau\tau} - \frac{\hat{\Sigma}^{(1)}_{AG}(m_A^2)}{m_A^2}\Gamma^{(0)}_{G\tau\tau}. \tag{4.147}$$

The first term is the renormalised one-loop vertex, which in our case is just the vertex counterterm, as no loop contributions exist at $\mathcal{O}(N_c)$. We obtain the counterterm by applying the renormalisation transformation presented in Sect. 4.2.1 to the tree-level vertex:

$$\hat{\Gamma}^{(1)}_{A\tau\tau} \overset{\mathcal{O}(N_c)}{=} \delta^{(1)}\Gamma_{A\tau\tau} \overset{\mathcal{O}(N_c)}{=} \Big(-\frac{\delta^{(1)}c_\beta}{c_\beta} + \delta^{(1)}Z_{\mathrm{w}} + \frac{1}{2}\delta^{(1)}Z_{AA} - \frac{1}{2t_\beta}\delta^{(1)}Z_{AG}\Big)\Gamma^{(0)}_{A\tau\tau}. \tag{4.148}$$

The $G\tau\tau$ tree-level vertex is simply

$$\Gamma^{(0)}_{G\tau\tau} = -\frac{1}{t_\beta}\Gamma^{(0)}_{A\tau\tau}. \tag{4.149}$$

All field renormalisation constants drop out in the physical amplitude, as one would expect. This allows us to define $\delta^{(1)}t_\beta$ independently of the renormalisation conditions for the fields. The t_β counterterm appears in both the vertex counterterm (through $\delta^{(1)}c_\beta$) and the renormalised AG self-energy (through the mass counterterm $\delta^{(1)}m^2_{AG}$).
Solving Eq. (4.146a) for $\delta^{(1)}t_\beta$ leads to

$$\frac{\delta^{(1)}t_\beta^{\mathrm{OS}}}{t_\beta} = -\delta^{(1)}Z_{\mathrm{w}} + \frac{1}{2}\operatorname{Re}\partial\Sigma^{(1)}_{AA}(m_A^2) - \frac{\operatorname{Re}\Sigma^{(1)}_{AG}(m_A^2) - \delta^{(1)}m^2_{AG}}{t_\beta m_A^2}\Big|_{\delta^{(1)}t_\beta=0}. \tag{4.150}$$

The last term can be rewritten by noting

$$\begin{aligned}\operatorname{Re}\Sigma^{(1)}_{AG}(m_A^2) - \delta^{(1)}m^2_{AG}\Big|_{\delta^{(1)}t_\beta=0} &= \operatorname{Re}\Sigma^{(1)}_{AG}(m_A^2) - \delta^{(1)}m^2_{AG} - \delta^{(1)}t_\beta c_\beta^2 m_A^2 \\ &= -\frac{m_A^2}{M_Z}\operatorname{Im}\Sigma^{L,(1)}_{AZ}(m_A^2),\end{aligned} \tag{4.151}$$

where we used Eq. (B.2a) from the first to the second line. With this, we can write

$$\frac{\delta^{(1)}t_\beta^{\mathrm{OS}}}{t_\beta} = -\delta^{(1)}Z_{\mathrm{w}} + \frac{1}{2}\operatorname{Re}\partial\Sigma^{(1)}_{AA}(m_A^2) + \frac{1}{t_\beta}\frac{\operatorname{Im}\Sigma^{L,(1)}_{AZ}(m_A^2)}{M_Z}. \tag{4.152}$$

Two-loop order

The physical two-loop vertex is obtained by expanding Eq. (4.141) up to the two-loop order:

$$\begin{aligned}
\hat{\Gamma}^{\mathrm{ph},(2)}_{A\tau\tau} = \hat{\Gamma}^{(2)}_{A\tau\tau} &- \frac{1}{2}\partial\hat{\Sigma}^{(1)}_{AA}(m_A^2)\hat{\Gamma}^{(1)}_{A\tau\tau} - \frac{\hat{\Sigma}^{(1)}_{AG}(m_A^2)}{m_A^2}\hat{\Gamma}^{(1)}_{G\tau\tau} \\
&- \frac{1}{2}\left[\partial\hat{\Sigma}^{(2)}_{AA}(m_A^2) - \frac{3}{4}\Big(\partial\hat{\Sigma}^{(1)}_{AA}(m_A^2)\Big)^2 - \frac{\partial}{\partial p^2}\frac{\Big(\hat{\Sigma}^{(1)}_{AG}(p^2)\Big)^2}{p^2}\Big|_{p^2=m_A^2}\right]\Gamma^{(0)}_{A\tau\tau} \\
&- \left[\frac{\hat{\Sigma}^{(2)}_{AG}(m_A^2)}{m_A^2} - \frac{\hat{\Sigma}^{(1)}_{AG}(m_A^2)\hat{\Sigma}^{(1)}_{GG}(m_A^2)}{m_A^4} - \frac{1}{2}\partial\hat{\Sigma}^{(1)}_{AA}(m_A^2)\frac{\hat{\Sigma}^{(1)}_{AG}(m_A^2)}{m_A^2}\right]\Gamma^{(0)}_{G\tau\tau} \\
&+ \frac{\mathrm{i}}{2}\,\mathrm{Im}\,\hat{\Sigma}^{(1)}_{AA}(m_A^2)\partial^2\hat{\Sigma}^{(1)}_{AA}(m_A^2)\Gamma^{(0)}_{A\tau\tau} \\
&+ \frac{\mathrm{i}\,\mathrm{Im}\,\hat{\Sigma}^{(1)}_{AA}(m_A^2)}{m_A^2}\left[\partial\hat{\Sigma}^{(1)}_{AG}(m_A^2) - \frac{\hat{\Sigma}^{(1)}_{AG}(m_A^2)}{m_A^2}\right]\Gamma^{(0)}_{G\tau\tau}.
\end{aligned} \tag{4.153}$$

The terms in the last line appear because we defined the wave function normalisation constants at the complex rather than at the real pole. When taking the real part of the physical amplitude, the last line will produce products of imaginary parts. As the real part of the two-loop vertex and the imaginary part of the one-loop vertex appear in the two-loop renormalisation condition, we give their explicit expressions here:

$$\begin{aligned}
\mathrm{Re}\,\hat{\Gamma}^{\mathrm{ph},(2)}_{A\tau\tau} = \hat{\Gamma}^{(2)}_{A\tau\tau} &- \frac{1}{2}\,\mathrm{Re}\,\partial\hat{\Sigma}^{(1)}_{AA}(m_A^2)\hat{\Gamma}^{(1)}_{A\tau\tau} - \frac{\mathrm{Re}\,\hat{\Sigma}^{(1)}_{AG}(m_A^2)}{m_A^2}\hat{\Gamma}^{(1)}_{G\tau\tau} \\
&- \frac{1}{2}\,\mathrm{Re}\left\{\partial\hat{\Sigma}^{(2)}_{AA}(m_A^2) - \frac{3}{4}\Big(\partial\hat{\Sigma}^{(1)}_{AA}(m_A^2)\Big)^2 - \frac{\partial}{\partial p^2}\frac{\Big(\hat{\Sigma}^{(1)}_{AG}(p^2)\Big)^2}{p^2}\Big|_{p^2=m_A^2}\right\}\Gamma^{(0)}_{A\tau\tau} \\
&- \mathrm{Re}\left\{\frac{\hat{\Sigma}^{(2)}_{AG}(m_A^2)}{m_A^2} - \frac{\hat{\Sigma}^{(1)}_{AG}(m_A^2)\hat{\Sigma}^{(1)}_{GG}(m_A^2)}{m_A^4} - \frac{\partial\hat{\Sigma}^{(1)}_{AA}(m_A^2)}{2}\frac{\hat{\Sigma}^{(1)}_{AG}(m_A^2)}{m_A^2}\right\}\Gamma^{(0)}_{G\tau\tau} \\
&- \frac{1}{2}\,\mathrm{Im}\,\hat{\Sigma}^{(1)}_{AA}(m_A^2)\,\mathrm{Im}\,\partial^2\hat{\Sigma}^{(1)}_{AA}(m_A^2)\Gamma^{(0)}_{A\tau\tau} \\
&- \frac{\mathrm{Im}\,\hat{\Sigma}^{(1)}_{AA}(m_A^2)}{m_A^2}\left[\mathrm{Im}\,\partial\hat{\Sigma}^{(1)}_{AG}(m_A^2) - \frac{\mathrm{Im}\,\hat{\Sigma}^{(1)}_{AG}(m_A^2)}{m_A^2}\right]\Gamma^{(0)}_{G\tau\tau},
\end{aligned} \tag{4.154a}$$

$$\mathrm{Im}\,\hat{\Gamma}^{\mathrm{ph},(1)}_{A\tau\tau} = -\frac{1}{2}\partial\,\mathrm{Im}\,\hat{\Sigma}^{(1)}_{AA}(m_A^2)\Gamma^{(0)}_{A\tau\tau} - \frac{\mathrm{Im}\,\hat{\Sigma}^{(1)}_{AG}(m_A^2)}{m_A^2}\Gamma^{(0)}_{G\tau\tau}. \tag{4.154b}$$

In our calculation, the two-loop vertex again just contains the counterterm

$$\begin{aligned}\hat{\Gamma}^{(2)}_{A\tau\tau} \overset{\mathcal{O}\left(N_c^2\right)}{=} \delta^{(2)}\Gamma_{A\tau\tau} \overset{\mathcal{O}\left(N_c^2\right)}{=} \Bigg[&- \frac{\delta^{(2)}c_\beta}{c_\beta} + \left(\frac{\delta^{(1)}c_\beta}{c_\beta}\right)^2 + \delta^{(2)}Z_{\mathrm{w}} - \delta^{(1)}Z_{\mathrm{w}}\frac{\delta^{(1)}c_\beta}{c_\beta} \\ &+ \frac{1}{2}\delta^{(2)}Z_{AA} - \frac{1}{8}\Big(\delta^{(1)}Z_{AA}\Big)^2 + \frac{1}{2}\delta^{(1)}Z_{AA}\left(\delta^{(1)}Z_{\mathrm{w}} - \frac{\delta^{(1)}c_\beta}{c_\beta}\right) \\ &- \frac{1}{2t_\beta}\delta^{(2)}Z_{AG} - \frac{1}{2t_\beta}\delta^{(1)}Z_{AG}\left(\delta^{(1)}Z_{\mathrm{w}} - \frac{\delta^{(1)}c_\beta}{c_\beta}\right)\Bigg]\Gamma^{(0)}_{A\tau\tau}.\end{aligned} \tag{4.155}$$

At the two-loop level, also the one-loop $G\tau\tau$ vertex appears:

$$\hat{\Gamma}^{(1)}_{G\tau\tau} \overset{\mathcal{O}(N_c)}{=} \delta^{(1)}\Gamma_{G\tau\tau} \overset{\mathcal{O}(N_c)}{=} \left(-\frac{\delta^{(1)}c_\beta}{c_\beta} + \delta^{(1)}Z_{\mathrm{w}} + \frac{1}{2}\delta^{(1)}Z_{GG} - \frac{t_\beta}{2}\delta^{(1)}Z_{AG}\right)\Gamma^{(0)}_{G\tau\tau}. \tag{4.156}$$

Before we give an explicit expression for the two-loop t_β counterterm, we introduce the symbol

$$\tilde{\Sigma}^{(2)}(p^2) = \Sigma^{(2)}(p^2)\Big|_{\delta^{(1)}Z=0}, \tag{4.157}$$

which denotes an unrenormalised two-loop self-energy where the one-loop field counterterms in the sub-loop diagrams have been set to 0. This means in particular

$$\Sigma^{(2)}_{AA} = \tilde{\Sigma}^{(2)}_{AA} + \delta^{(1)}Z_{AA}\Sigma^{(1)}_{AA} + \delta^{(1)}Z_{AG}\Sigma^{(1)}_{AG}, \tag{4.158a}$$

$$\Sigma^{(2)}_{AG} = \tilde{\Sigma}^{(2)}_{AG} + \tfrac{1}{2}\Big(\delta^{(1)}Z_{AA} + \delta^{(1)}Z_{GG}\Big)\Sigma^{(1)}_{AG} + \tfrac{1}{2}\delta^{(1)}Z_{AG}\Big(\Sigma^{(1)}_{AA} + \Sigma^{(1)}_{GG}\Big). \tag{4.158b}$$

We now insert Eqs. (4.154) into Eq. (4.146b) and solve for $\delta^{(2)}t_\beta$. As in the one-loop case, the t_β counterterm appears as a contribution to $\delta^{(2)}c_\beta$ in the vertex counterterm and to the mass counterterm $\delta^{(2)}m^2_{AG}$ in the renormalised two-loop AG self-energy.

Putting everything together, we obtain

$$
\begin{aligned}
\frac{\delta^{(2)} t_\beta^{\overline{\text{DR}}}}{t_\beta} = & -\frac{1}{2} c_\beta^2 \left(c_\beta^2 - 2 s_\beta^2\right) \left(\delta^{(1)} t_\beta\right)^2 - \left(\frac{\delta^{(1)} c_\beta}{c_\beta}\right)^2 - \delta^{(2)} Z_{\text{w}} + \delta^{(1)} Z_{\text{w}} \frac{\delta^{(1)} c_\beta}{c_\beta} \\
& + \frac{1}{2} \operatorname{Re} \partial \Sigma_{AA}^{(1)}(m_A^2) \left(- \frac{\delta^{(1)} c_\beta}{c_\beta} + \delta^{(1)} Z_{\text{w}} \right) \\
& - \frac{\operatorname{Re} \Sigma_{AG}^{(1)}(m_A^2) - \delta^{(1)} m_{AG}^2}{t_\beta m_A^2} \left(- \frac{\delta^{(1)} c_\beta}{c_\beta} + \delta^{(1)} Z_{\text{w}} \right) \\
& + \frac{1}{2} \operatorname{Re} \left\{ \partial \tilde{\Sigma}_{AA}^{(2)}(m_A^2) - \frac{3}{4} \left(\partial \Sigma_{AA}^{(1)}(m_A^2)\right)^2 \right. \\
& \left. - \frac{2 \left(\Sigma_{AG}^{(1)}(m_A^2) - \delta^{(1)} m_{AG}^2\right) \partial \Sigma_{AG}^{(1)}(m_A^2)}{m_A^2} + \frac{\left(\Sigma_{AG}^{(1)}(m_A^2) - \delta^{(1)} m_{AG}^2\right)^2}{m_A^4} \right\} \\
& - \operatorname{Re} \left\{ \frac{\tilde{\Sigma}_{AG}^{(2)}(m_A^2) - \delta^{(2)} m_{AG}^2}{t_\beta m_A^2} \Big|_{\delta^{(2)} t_\beta = 0} - \frac{\partial \Sigma_{AA}^{(1)}(m_A^2)}{2} \frac{\Sigma_{AG}^{(1)}(m_A^2) - \delta^{(1)} m_{AG}^2}{t_\beta m_A^2} \right. \\
& \left. - \frac{\left(\Sigma_{AG}^{(1)}(m_A^2) - \delta^{(1)} m_{AG}^2\right) \left(\Sigma_{GG}^{(1)}(m_A^2) - \delta^{(1)} m_G^2\right)}{t_\beta m_A^4} \right\} \\
& + \frac{1}{2} \operatorname{Im} \Sigma_{AA}^{(1)}(m_A^2) \operatorname{Im} \partial^2 \Sigma_{AA}^{(1)}(m_A^2) \\
& - \frac{\operatorname{Im} \Sigma_{AA}^{(1)}(m_A^2)}{t_\beta m_A^2} \left[\operatorname{Im} \partial \Sigma_{AG}^{(1)}(m_A^2) - \frac{\operatorname{Im} \Sigma_{AG}^{(1)}(m_A^2)}{m_A^2} \right] \\
& - \frac{1}{2} \operatorname{Im}^2 \left\{ \frac{1}{2} \partial \Sigma_{AA}^{(1)}(m_A^2) - \frac{\Sigma_{AG}^{(1)}(m_A^2)}{t_\beta m_A^2} \right\} \\
& - \frac{1}{2} \delta^{(1)} Z_{AG} \frac{\operatorname{Re} \Sigma_{AA}^{(1)}(m_A^2) - \delta^{(1)} m_A^2}{t_\beta m_A^2}.
\end{aligned}
\tag{4.159}
$$

Again, any field renormalisation constant drops out in the final expression for the two-loop t_β counterterm. In order to assure this feature, however, we have to make use of the fact that m_A^2 has been defined as an on-shell quantity, as can be seen from the last term. In a $\mathcal{CP}$-violating scenario, we would thus have to use the decay of a charged Higgs boson into τ and ν_τ together with a charged on-shell mass.

5 Calculation of electroweak $\mathcal{O}\left(N_c^2\right)$ terms to the Higgs boson masses

In this thesis, we calculate for the first time the complete two-loop corrections of $\mathcal{O}\left((\alpha_{\text{em}}+\alpha_q)^2 N_c^2\right)$ to the Higgs boson masses in the MSSM. The setup of our calculation is general enough to allow for both real and complex input parameters.[10] We refer to these scenarios as the rMSSM and the cMSSM, respectively. The masses of the $\mathcal{CP}$-even Higgs bosons h and H obtain contributions from particle mixing at the two-loop order and beyond in both scenarios. The presence of non-vanishing phases in the cMSSM gives rise to non-vanishing $\mathcal{CP}$-violating self-energies and thus leads to mixing with the $\mathcal{CP}$-odd Higgs boson A. Hence, we have a 2×2 propagator matrix in the rMSSM and a 3×3 matrix in the cMSSM. In most scenarios, the difference between the tree-level masses m_H^2 and m_A^2 is rather small, leading potentially to large mixing effects in the cMSSM, see Sect. 3.2.4.

We start this chapter by giving an overview of the current status of Higgs mass predictions in the MSSM, focussing especially on the fixed-order approach for determining the Higgs masses. Next, we discuss the two-loop Feynman diagrams calculated in this work. We analyse their structure in terms of coupling constants, colour factors and loop integrals. Subsequently, we motivate why QCD corrections, terms of $\mathcal{O}(N_c)$ and other known corrections are not taken into account, leading to the considered class of $\mathcal{O}\left((\alpha_{\text{em}}+\alpha_q)^2 N_c^2\right)$ contributions. We continue by giving an overview over the different codes and packages used to obtain algebraic expressions for the relevant one- and two-loop self-energies.

After renormalisation, the self-energies become finite quantities and can be used to make a prediction for the Higgs masses in the MSSM. The divergent, finite and $\mathcal{O}(\varepsilon)$ parts of the loop integrals appearing in our calculation can be evaluated analytically in the most general setting. We will show that the choice of an on-shell renormalisation scheme at two-loop order leads to the cancellation of the $\mathcal{O}(\varepsilon)$ parts of loop integrals and thus simplifies the analytical structure of the finite result.

[10] So far, we have calculated the on-shell t_β counterterms from the $A\to\tau^-\tau^+$ decay for a scenario with $\mathcal{CP}$-symmetry conservation. The definition of an on-shell t_β in a $\mathcal{CP}$-violating scenario via the decay $H^+\to\tau^+\nu_\tau$ is straightforward.

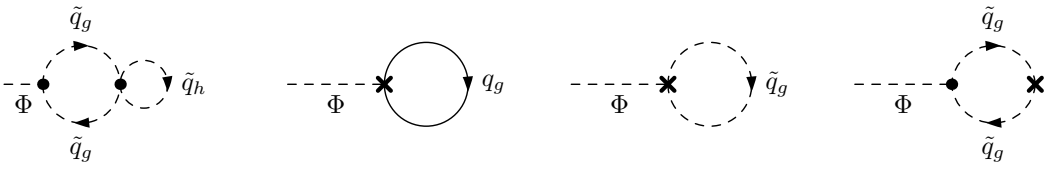

Figure 5.1: Topologies of the two-loop tadpole diagrams. $\Phi = h, H, A, G$; g and h are flavour indices. The cross denotes the insertion of a one-loop counterterm. Counterterm topologies which have not been listed vanish for the considered class of contributions.

We present the leading one-loop contributions in an algebraic form in Ch. 6. The combined one- and two-loop results are investigated numerically for several different scenarios in Ch. 7.

5.1 Current status of the MSSM Higgs boson mass prediction

Already in the mid-1990s the full one-loop corrections to the Higgs boson mass have been available, albeit in the MSSM with real parameters (rMSSM) and no flavour mixing [20–25]. One-loop results for the complex MSSM can be found in Refs. [57–67]. Two-loop corrections to the neutral Higgs masses, in the limit of vanishing external momentum and vanishing electroweak gauge couplings, followed in subsequent years [26–40]. Only a decade later, the corresponding two-loop calculations were done for the mass of the charged Higgs boson [41, 42]. The effective-potential method allowed for the incorporation of electroweak two-loop effects into the predictions for the Higgs boson masses in the MSSM, still in the limit of vanishing external momentum, in 2002 [43, 44].
In 2004, using a Feynman-diagrammatic (FD) approach, the full two-loop contributions involving all diagrams in which $\alpha_s \equiv g_s^2/(4\pi)$, $\alpha_t \equiv h_t^2/(4\pi)$, $\alpha_b \equiv h_b^2/(4\pi)$, or $\alpha_\tau \equiv h_\tau^2/(4\pi)$ appear have been calculated [45].[11] For these diagrams, the full dependence on the external momentum p^2 was kept, as well as a non-vanishing fine-structure constant $\alpha_{\text{em}} \equiv e^2/(4\pi)$. Those numerical results, however, do not include contributions from the first or second generation of fermions, or generation mixing. Furthermore, the results of Ref. [45] were obtained in a pure $\overline{\text{DR}}$ scheme, which greatly simplifies the renormalisation process.

[11] g_s is the strong gauge coupling, and h_t, h_b and h_τ are third generation Yukawa couplings.

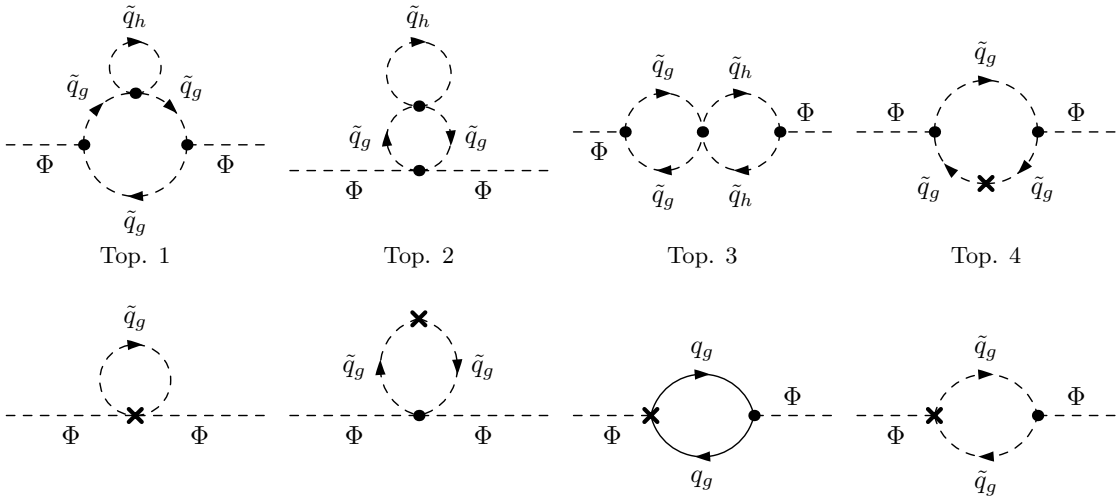

Figure 5.2: Topologies of the neutral two-loop self-energy diagrams. $\Phi = h, H, A, G$; g and h are flavour indices. The cross denotes the insertion of a one-loop counterterm. Counterterm topologies which have not been listed vanish for the considered class of contributions.

In 2014, the leading two-loop contributions of $\mathcal{O}(\alpha_t\alpha_s)$ including the contributions from a non-vanishing external momentum were calculated in a mixed OS-$\overline{\text{DR}}$ scheme in Ref. [51]. A few months later and in an independent calculation, Ref. [52] also incorporated the subleading $\mathcal{O}(\alpha_{\text{em}}\alpha_s)$ contributions, working both in a mixed and in a pure $\overline{\text{DR}}$ scheme. In 2018, Ref. [56] included all QCD contributions, giving results of $\mathcal{O}\left(\alpha_q\alpha_s\right)$ and $\mathcal{O}(\alpha_{\text{em}}\alpha_s)$, where α_q denotes a product of any two Yukawa couplings. In Ref. [56], a mixed OS-$\overline{\text{DR}}$ scheme was used and complex parameters were taken into account. The leading Yukawa corrections of $\mathcal{O}\left((\alpha_t + \alpha_b)^2\right)$ are given in Refs. [74–77] for the case of general complex parameters and vanishing external momentum.

We go beyond the previously obtained results by fully taking into account electroweak and Yukawa two-loop contributions for non-vanishing external momenta in a mixed OS-$\overline{\text{DR}}$ scheme within the considered class of contributions. In our calculation, we allow for the general case of complex parameters in the MSSM, and we take into account flavour- and generation-mixing Feynman diagrams. Since we still use a unit CKM matrix, our calculation is not as general as it could be with regard to flavour. We focus on the contributions of $\mathcal{O}\left((\alpha_{\text{em}} + \alpha_q)^2 N_c^2\right)$. This avoids the need to calculate diagrams with internal leptons, Higgs and gauge bosons as well as their respective supersymmetric partners.

The relevant tadpole diagrams are shown in Fig. 5.1, while the neutral and charged self-energies consist of the diagrams shown in Figs. 5.2 and 5.3, respectively. The

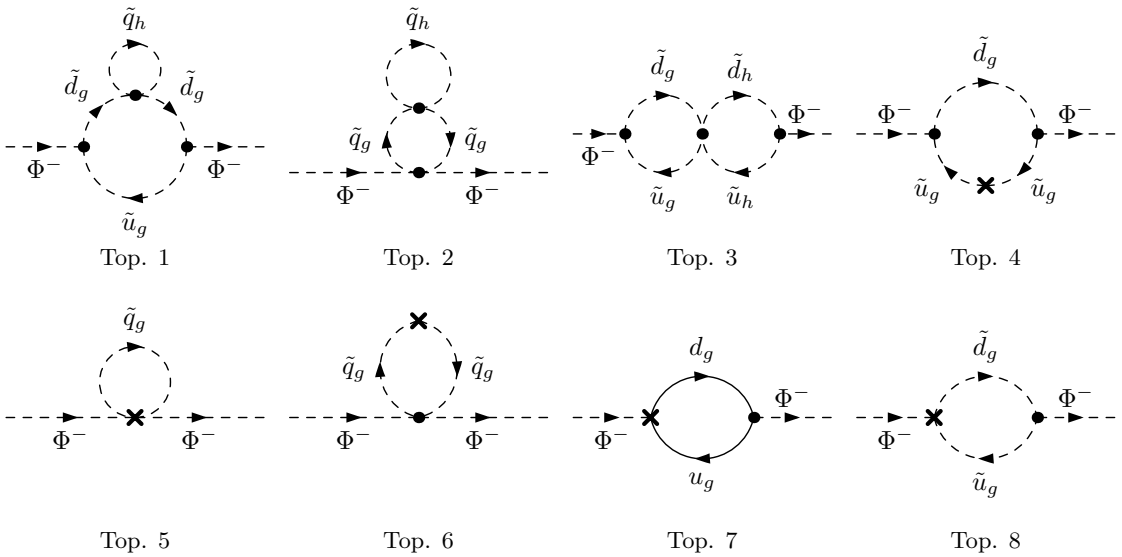

Figure 5.3: Topologies of the charged two-loop self-energy diagrams. $\Phi^- = H^-, G^-$; g and h are flavour indices. The cross denotes the insertion of a one-loop counterterm. Counterterm topologies which have not been listed vanish for the considered class of contributions.

calculated two-loop vector boson self-energies and scalar-vector mixing self-energies have the same topological structure. All of these topologies lead to diagrams which can be written as products of one-loop integrals.

5.2 The structure of the self-energies

When discussing two-loop self-energies, we distinguish between so-called "genuine" diagrams with two independent loop momenta, see e.g. topologies 1–3 in Fig. 5.2, and "sub-loop" diagrams with a one-loop counterterm insertion, see e.g. topologies 4–8 in Fig. 5.2.

All genuine two-loop diagrams have two loop momenta that are integrated over. In our case, no internal propagator depends on both loop momenta, and our two-loop diagrams decompose into mere products of one-loop integrals. The sub-loop diagrams have a very similar form as they are products of a one-loop integral and a one-loop counterterm.

The genuine diagrams all contain a four-squark interaction vertex. To better understand their overall structure in terms of colour factors and coupling constants, we investigate the vacuum diagram shown in Fig. 5.4. All genuine tadpole and neutral self-energy diagrams can be obtained from this diagram by simply adding external legs to the vacuum bubble. As such, all genuine diagrams will have the same colour

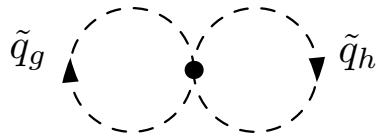

Figure 5.4: The basic two-loop vacuum diagram $V_{\tilde{q}_g\tilde{q}_h}$ with the four-squark vertex. Here, g and h are flavour indices.

structure as the vacuum diagram.
The colours of the internal squark propagators in Fig. 5.4 can have all possible values, and hence they need to be summed over; we label them by the indices a and b. Keeping the colour sum explicit, the vacuum bubble has the structure

$$V_{\tilde{q}_g\tilde{q}_h} = \sum_{a,b=1}^{N_c} \Big[\alpha_s \frac{1}{2}\Big(\delta_{ab}\delta_{ab} - \frac{1}{N_c}\delta_{aa}\delta_{bb}\Big)S_{gh} + \alpha_s \frac{1}{2}\Big(\delta_{aa}\delta_{bb} - \frac{1}{N_c}\delta_{ab}\delta_{ab}\Big)S'_{gh} + \alpha_{\rm em}\delta_{ab}G_{gh} + \alpha_{\rm em}G'_{gh} + \alpha_q\delta_{ab}Y_{gh} + \alpha_q Y'_{gh}\Big], \tag{5.1}$$

where the coefficients S_{gh}, S'_{gh}, G_{gh}, G'_{gh}, Y_{gh}, and Y'_{gh} contain entries of the squark-mixing matrices and other numerical factors, but no couplings constants or colour factors. After performing the colour sums, we find

$$V_{\tilde{q}_g\tilde{q}_h} = \alpha_s N_c C_F S'_{gh} + \alpha_{\rm em}(N_c G_{gh} + N_c^2 G'_{gh}) + \alpha_q(N_c Y_{gh} + N_c^2 Y'_{gh}), \tag{5.2}$$

where we introduced the Casimir operator C_F of the fundamental representation,

$$C_F = \frac{N_c^2 - 1}{2N_c}. \tag{5.3}$$

Depending on which squark flavours appear in the loops, the coefficients have the following properties:

- If the squarks have the same flavour, $g = h$:
  $S_{gg} = S'_{gg}$, $G_{gg} = G'_{gg}$ and $Y_{gg} = Y'_{gg}$. All coefficients are non-vanishing.

- If the squarks have different flavours but are of the same generation:

$S'_{gh} = 0$, $G_{gh} \neq G'_{gh}$, and $Y'_{gh} = 0$.

- If the squarks stem from different generations but are of the same type: $S'_{gh} = 0$, $G_{gh} = 0$ and $Y_{gh} = 0$.
- If the squarks stem from different generations and are of a different type: $S'_{gh} = 0$, $G_{gh} = 0$, and $Y_{gh} = Y'_{gh} = 0$.

These relations are read off the four-squark-vertex Feynman rules, see e.g. Ref. [173]. The contributions parameterised by S_{gh}, G_{gh} and Y_{gh} are irrelevant to us as they do not produce terms of $\mathcal{O}\left(N_c^2\right)$. The term with the coefficient S'_{gh} is proportional to $N_c C_F$, and hence formally contains a factor N_c^2, as one sees from Eq. (5.3). Other genuine two-loop diagrams, like the one shown in Fig. 5.5, also contribute at $\mathcal{O}(\alpha_s N_c C_F)$. This diagram does not decompose into a simple product of one-loop integrals. Since the complete two-loop QCD contributions have already been calculated in Refs. [51, 52, 56, 68], we set

$$\alpha_s \equiv 0 \tag{5.4}$$

in the diagrams that are evaluated in this thesis. We give estimates for the size of the left-out QCD corrections in the scenarios discussed in Ch. 7.
With this restriction, all diagrams appearing in our calculation contain only quarks and squarks as internal particles. We are interested in the $\mathcal{O}\left(N_c^2\right)$ parts of these two-loop diagrams, i.e. the contributions parameterised by the coefficients G'_{gh} and Y'_{gh}. The genuine two-loop self-energy diagrams in Fig. 5.2 are obtained from the vacuum bubble Fig. 5.4 by adding two cubic Higgs-squark-squark vertices or a single quartic Higgs-Higgs-squark-squark vertex; the self-energies are hence of $\mathcal{O}\left((\alpha_{\text{em}} + \alpha_q)^2 N_c^2\right)$.

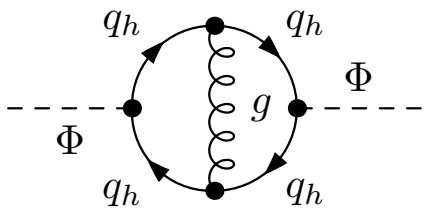

Figure 5.5: This two-loop diagram is proportional to $\alpha_s N_c C_F$. h is a flavour index.

We treat the first and second generation quarks as massless. This leaves us with the three non-vanishing couplings

$$\alpha_{\text{em}}, \alpha_t, \alpha_b. \tag{5.5}$$

These are sufficient to describe any four-squark vertex, as well as any Higgs-quark or Higgs-squark vertex. The coupling structure of the one- and two-loop corrections to the Higgs boson pole masses is then typically of the form

$$\begin{aligned}\Delta^{(1)} M^2_{h/H} \sim \mathcal{O}\Big(& N_c\alpha_t(m_t+\mu+A_t)^2 + N_c\alpha_b(m_b+\mu+A_b)^2 \\ & + N_c\alpha_{\text{em}}\Big[m_t(m_t+\mu+A_t) + m_b(m_b+\mu+A_b) + M_Z^2\Big]\Big),\end{aligned} \tag{5.6a}$$

$$\begin{aligned}\Delta^{(2)} M^2_{h/H} \sim \mathcal{O}\Big(& N_c^2\alpha_t^2(m_t+\mu+A_t)^2 + N_c^2\alpha_b^2(m_b+\mu+A_b)^2 \\ & + N_c^2\alpha_{\text{em}}\Big[\sqrt{\alpha_t}(m_t+\mu+A_t) + \sqrt{\alpha_b}(m_b+\mu+A_b)\Big]^2 \\ & + N_c^2\alpha_{\text{em}}^2\Big[m_t(m_t+\mu+A_t) + m_b(m_b+\mu+A_b) + M_Z^2\Big]\Big),\end{aligned} \tag{5.6b}$$

where the plus signs in the parentheses and brackets are used to indicate possible combinations but do not imply that the terms always occur in this exact form. We have derived these expressions by considering the two-loop self-energy diagrams of the first and third topology shown in Fig. 5.2.

While the one-loop result was already fully known, for the two-loop contribution only the $\mathcal{O}\left(\alpha_t^2\right)$ and $\mathcal{O}\left(\alpha_b^2\right)$ part (first line of Eq. (5.6b)) had so far been evaluated. The second and third line of Eq. (5.6b) vanish in the gaugeless limit and are calculated for the first time in the present work.

We stress again that two-loop terms of $\mathcal{O}(N_c)$ are not included in our calculation. Two-loop diagrams with one internal squark and an additional internal Higgs boson are also of this order and therefore would have to be included in a full discussion of $\mathcal{O}(N_c)$ contributions.

5.3 Algebraic calculation of the two-loop self-energies

In this section we describe the technical tools which we used for our calculation and outline the procedure step by step. Every part of the calculation, from the generation of the required Feynman diagrams up to the numerical evaluation, is performed within the computer algebra program Wolfram Mathematica. We use mostly pre-existing tools and packages and we created our own packages where necessary. Our calculational setup closely follows the one presented in Ref. [76].

Generating the amplitudes. We turn the one- and two-loop diagrams presented in Sect. 5.2 into a mathematical form with the MATHEMATICA package FEYNARTS 3.11 [189, 190]. We treat the tadpoles and self-energies such that they do not contain topologies with tadpole sub-diagrams by setting the flag `ExcludeTopologies` → `Internal`. These excluded topologies exactly cancel each other for schemes employing an OS definition for the tadpole counterterms, which is the prescription that we use exclusively in this thesis.
We use the FEYNARTS model files `MSSMCT.mod` [50] and `Nc.mod`. The former includes the information on MSSM particles and the generation of one-loop counterterms while the latter allows us to keep the number of (s)quark colours as a symbol. In this way we can easily use this parameter for extracting the $\mathcal{O}\left(N_c^2\right)$ contributions.
The numbers of generated diagrams per two-loop self-energy are displayed in Table 5.1. For the case of a single (s)quark generation, 4080 genuine two-loop diagrams and 1242 sub-loop diagrams have been calculated, amounting to a total of 5322 diagrams. When taking into account all three generations of matter, we have 36720 genuine and 3726 sub-loop diagrams, for a combined total number of 40446 diagrams at the particle level.

Preparing the amplitudes for tensor reduction. The sub-loop diagrams have a simple one-loop topology and hence they can be reduced using by the package FORMCALC 9.9 [191, 192]. The genuine two-loop diagrams, on the other hand, are reduced with TWOCALC [174, 193]. Before they can be reduced, the genuine diagrams have to be adapted to the conventions used in TWOCALC. The sub-loop diagrams can also be reduced using the one-loop version of TWOCALC, which is called ONECALC [174, 193], but this requires a prior modification of the amplitudes as well.
These conversions are done by the packages `SimpSubstFA3.m` for the genuine two-loop diagrams and `OneSimpSubstFA3.m` for the sub-loop diagrams. As we can eval-

no. of gen.	top.	Φ	$\Phi\Phi$	$\Phi^-\Phi^+$	$A\gamma$	AZ	H^-W^+	$\gamma\gamma$	γZ
1	genuine	32	224	112	96	192	80	64	128
	sub-loop	14	64	38	32	52	26	28	44
3	genuine	288	2016	1008	864	1728	720	576	1152
	sub-loop	42	192	114	96	156	78	84	132

Table 5.1: The number of genuine and sub-loop diagrams for each tadpole and self-energy, and for the case of both one and three generations of matter. $\Phi \in \{h, H, A, G\}$; $\Phi^\pm \in \{H^\pm, G^\pm\}$. The numbers for ZZ and W^-W^+ are identical to the ones of the neutral and charged scalar self-energies, respectively. The numbers for $G\gamma$ coincide with the ones for $A\gamma$, etc.

uate the sub-loop diagrams using either OneCalc or FormCalc, we will subsequently compare the results as a cross check. The conversion packages, together with OneCalc and TwoCalc, are included in FeynHiggs [30,67,88,90,128,129, 194–196], a Fortran code which, i.a., calculates the masses of MSSM Higgs bosons. While FormCalc automatically evaluates the colour sums even for a general symbol N_c, OneCalc and TwoCalc do not. We developed the package `ColorSimp.m` to evaluate colour sums symbolically also at the two-loop level. This package and its usage are documented in App. E. After the evaluation of the colour sums and the subsequent conversion with `SimpleSubst`, both the sub-loop and the genuine two-loop amplitudes are ready to be evaluated using OneCalc and TwoCalc.

The tensor reduction. As already mentioned, the two-loop diagrams with counterterm insertions are reduced using both FormCalc and OneCalc. The genuine two-loop diagrams have two independent loop momenta and are therefore evaluated with TwoCalc.
For both OneCalc and TwoCalc, we set the flags `DimReduction` → `True` and `Dimension` → `$D`. Afterwards, we invoke the package `Simple.m` to further reduce scalar integrals. At this step, all self-energies are expressed in terms of A_0, B_0 and B_0' integrals, which are defined in App. D. FormCalc further reduces the B_0' integral in terms of A_0 and B_0; we give the reduction formula in Sect. D.2.2.
The FormCalc and the OneCalc results fully agree, as they should. It should be noted that the loop integrals appearing in FormCalc and OneCalc use different conventions for the arguments of the loop integrals. In our work, we write the mass arguments of loop integrals as squared masses, i.e. they have mass dimension two.

Simplification of the self-energies. Before renormalisation, we simplify the self-energies to obtain more compact expressions. In the genuine two-loop diagrams, the coupling α_s appears, which we set to 0 for the considered contributions as explained above. Furthermore, we discard terms of $\mathcal{O}(N_c)$ and $\mathcal{O}\left(N_c^0\right)$. Subsequently, we apply the operation `USfSimplify` from the package `USfSimplify.m` to combine products of squark mixing matrices into a single expression. This facilitates the usage of relations which rely on the unitarity of said mixing matrices.
The sub-loop diagrams are mere products of one-loop diagrams and one-loop counterterms, and they are, therefore, never proportional to α_s. We set the counterterms for the quark masses, quark fields and squark fields to zero. This can be done as quark counterterms obtain no $\mathcal{O}(N_c)$ contribution, and the squark field counterterms drop out, see Sect. 4.1.2.

Determination of counterterms. Now that we have obtained explicit algebraic expressions for the two-loop tadpoles and self-energies, we determine the one- and two-loop counterterms as described in Ch. 4. For each sector, different choices for the renormalisation are possible:

- Quark-squark sector: Six different renormalisation schemes are possible, see Sect. 4.1. An overview is given in Table 5.2.
- Higgs-gauge sector: We choose m_A^2 as input parameter in the rMSSM and $m_{H^\pm}^2$ as input parameter in the cMSSM, see Sect. 4.2.
- $\tan(\beta)$: t_β can be renormalised in the $\overline{\text{DR}}$ or in an OS scheme, see Sect. 4.3. The latter choice requires additional electroweak two-loop counterterms, all of which are given in Sect. 4.2.

Expansion of the renormalised self-energies. We combine the unrenormalised two-loop self-energies, which consist of the genuine two-loop diagrams as well as the sub-loop renormalisation diagrams, and the counterterms as per the expressions found throughout Sect. 4.2.3. This yields the renormalised self-energies, which are finite. We expand the renormalised self-energies in ε using the package `ExpandDel.m`, see Ref. [76]. Any one-loop integral is thereby written as

$$L = L^{\text{div}}\frac{1}{\varepsilon} + L^{\text{fin}} + L^{\varepsilon}\varepsilon + \mathcal{O}\left(\varepsilon^2\right), \tag{5.7}$$

where L is either an A_0, a B_0, or a B_0' loop function. Similarly, we expand the one-loop counterterms as

$$\delta^{(1)}c = \delta^{(1)}c^{\text{div}}\frac{1}{\varepsilon} + \delta^{(1)}c^{\text{fin}} + \delta^{(1)}c^{\varepsilon}\varepsilon + \mathcal{O}\left(\varepsilon^2\right), \tag{5.8}$$

scheme	$m_{\tilde{t}_1}^2$	$m_{\tilde{t}_2}^2$	$m_{\tilde{t}_{12}}^2$	$m_{\tilde{b}_1}^2$	$m_{\tilde{b}_2}^2$	$m_{\tilde{b}_{12}}^2$	A_t	A_b
`OS[1]`	OS	OS	OS	OS	dep.	dep.	dep.	$\overline{\text{DR}}$
`OS[2]`	OS	OS	OS	dep.	OS	dep.	dep.	$\overline{\text{DR}}$
`DR[1]`	$\overline{\text{DR}}$	$\overline{\text{DR}}$	dep.	$\overline{\text{DR}}$	dep.	dep.	$\overline{\text{DR}}$	$\overline{\text{DR}}$
`DR[2]`	$\overline{\text{DR}}$	$\overline{\text{DR}}$	dep.	dep.	$\overline{\text{DR}}$	dep.	$\overline{\text{DR}}$	$\overline{\text{DR}}$
`MIX[1]`	OS	OS	dep.	OS	dep.	dep.	$\overline{\text{DR}}$	$\overline{\text{DR}}$
`MIX[2]`	OS	OS	dep.	dep.	OS	dep.	$\overline{\text{DR}}$	$\overline{\text{DR}}$

Table 5.2: An overview of the different renormalisation schemes used for the quark-squark sector. In each scheme, five parameters are used as input, corresponding to the free parameters in the third-generation squark mixing matrices. The formulae for the dependent parameters are given in Sect. 4.1.2.

where c is a parameter or field. One-loop counterterms appear in the sub-loop part of the unrenormalised two-loop self-energies as well as in the two-loop counterterms. Keeping the expansion coefficients of one-loop integrals and counterterms as symbols speeds up the expansion in ε significantly. The coefficients can later be evaluated numerically.
We expand the two-loop self-energy up to $\mathcal{O}\left(\varepsilon^0\right)$:

$$\Sigma^{(2)} = \Sigma^{(2),\text{ddiv}} \frac{1}{\varepsilon^2} + \Sigma^{(2),\text{div}} \frac{1}{\varepsilon} + \Sigma^{(2),\text{fin}} + \mathcal{O}(\varepsilon). \tag{5.9}$$

The one-loop integrals and counterterms enter the self-energy coefficients via

$$\Sigma^{(2),\text{ddiv}} \supset L^{\text{div}}, \delta^{(1)} c^{\text{div}}, \tag{5.10a}$$
$$\Sigma^{(2),\text{div}} \supset L^{\text{div}}, \delta^{(1)} c^{\text{div}}, L^{\text{fin}}, \delta^{(1)} c^{\text{fin}}, \tag{5.10b}$$
$$\Sigma^{(2),\text{fin}} \supset L^{\text{div}}, \delta^{(1)} c^{\text{div}}, L^{\text{fin}}, \delta^{(1)} c^{\text{fin}}, L^{\varepsilon}, \delta^{(1)} c^{\varepsilon}. \tag{5.10c}$$

The renormalised self-energies are UV-finite, so

$$\hat{\Sigma}^{(2),\text{ddiv}} = 0, \tag{5.11a}$$
$$\hat{\Sigma}^{(2),\text{div}} = 0. \tag{5.11b}$$

We have numerically checked the finiteness of all renormalised two-loop tadpoles, the neutral and charged two-loop Higgs self-energies, and the scalar-vector mixing two-loop self-energies $A\gamma$, AZ, $G\gamma$ and H^-W^+.
If all parameters which need to be renormalised at the two-loop level are defined in an OS scheme, the $\mathcal{O}(\varepsilon)$ parts L^{ε} and $\delta^{(1)} c^{\varepsilon}$ will drop out in the determination of $\hat{\Sigma}^{(2),\text{fin}}$. We will analyse this observation in the following section.

5.4 The cancellation of $\mathcal{O}(\varepsilon)$ parts of one-loop integrals and counterterms

To understand how the $\mathcal{O}(\varepsilon)$ parts of loop integrals and counterterms cancel in a renormalised self-energy, we have to study the structure of the unrenormalised two-loop self-energies first. It is important to note that the findings of this section do not necessarily apply to arbitrary two-loop fixed-order calculations; we only consider two-loop self-energies which have the handy property that they fully decompose into products of one-loop integrals and counterterms. In a more general calculation, a two-loop self-energy will not be of this form.

When trying to cast self-energy diagrams into an analytic form, keeping the one-loop integrals as symbols, there is always some freedom involved in the choice of the resulting expression. This is due to reduction formulae relating different loop integrals to one another, for example

$$B_0(0, m^2, m^2) = (1 - \varepsilon)\frac{A_0(m^2)}{m^2}. \tag{5.12}$$

Inserting Eq. (5.7) into Eq. (5.12) allows us to relate the coefficients of A_0 and B_0 in the expansion with respect to ε to each other:

$$B_0^{\text{div}}(0, m^2, m^2) = \frac{A_0^{\text{div}}(m^2)}{m^2}, \tag{5.13a}$$

$$B_0^{\text{fin}}(0, m^2, m^2) = \frac{A_0^{\text{fin}}(m^2) - A_0^{\text{div}}(m^2)}{m^2}, \tag{5.13b}$$

$$B_0^{\varepsilon}(0, m^2, m^2) = \frac{A_0^{\varepsilon}(m^2) - A_0^{\text{fin}}(m^2)}{m^2}. \tag{5.13c}$$

We can also invert these relations:

$$A_0^{\text{div}}(m^2) = m^2 B_0^{\text{div}}(0, m^2, m^2), \tag{5.14a}$$

$$A_0^{\text{fin}}(m^2) = m^2 \left(B_0^{\text{fin}}(0, m^2, m^2) + B_0^{\text{div}}(0, m^2, m^2)\right), \tag{5.14b}$$

$$A_0^{\varepsilon}(m^2) = m^2 \left(B_0^{\varepsilon}(0, m^2, m^2) + B_0^{\text{fin}}(0, m^2, m^2) + B_0^{\text{div}}(0, m^2, m^2)\right). \tag{5.14c}$$

We can see that if a cancellation of $\mathcal{O}(\varepsilon)$ parts of loop integrals occurs for a particular choice of the base integrals, it will also occur for the other possible choices.
As mentioned before, all two-loop diagrams appearing in our calculation are products of one-loop integrals and counterterms. This allows us to cast the unrenormalised two-loop self-energy in the following still quite general form:

$$\Sigma^{(2)} = \sum_i L_i M_i + \sum_j N_j \delta c_j. \tag{5.15}$$

Here, the L_i, M_i, and N_j are one-loop integrals. The δc_j are one-loop counterterms. The first term contains all genuine diagrams, the second one the diagrams with sub-loop renormalisation. In the following, we leave the summation over i and j implicit.
To see how the aforementioned cancellation takes place, we first expand the functions

and counterterms according to Eqs. (5.7) and (5.8):

$$\begin{aligned}\Sigma^{(2)} = &\frac{L_i^{\text{div}} M_i^{\text{div}} + N_j^{\text{div}} \delta c_j^{\text{div}}}{\varepsilon^2} + \frac{L_i^{\text{div}} M_i^{\text{fin}} + L_i^{\text{fin}} M_i^{\text{div}} + N_j^{\text{div}} \delta c_j^{\text{fin}} + N_j^{\text{fin}} \delta c_j^{\text{div}}}{\varepsilon} \\ &+ L_i^{\text{div}} M_i^{\varepsilon} + L_i^{\text{fin}} M_i^{\text{fin}} + L_i^{\varepsilon} M_i^{\text{div}} + N_j^{\text{div}} \delta c_j^{\varepsilon} + N_j^{\text{fin}} \delta c_j^{\text{fin}} + N_j^{\varepsilon} \delta c_j^{\text{div}} \\ &+ \mathcal{O}(\varepsilon).\end{aligned} \tag{5.16}$$

For the next step, we derive a relation between the genuine contributions and the contributions involving sub-loop renormalisation. Every genuine two-loop diagram comes with a number of sub-loop renormalisation diagrams that are associated with it. The sum of a genuine diagram and its sub-loop renormalisation diagrams is free from non-local divergences, i.e. terms of the form $\log\left(p^2\right)\varepsilon^{-1}$. These terms have to cancel after the process of sub-loop renormalisation in a renormalisable theory [197]. We obtain the sub-loop renormalisation diagrams by shrinking one of the loops of the genuine two-loop diagram to a single point and inserting a one-loop counterterm at this point. Let us demonstrate this for the squark topologies in Fig. 5.2: Topology 1 leads to the sub-loop renormalisation topology 4 when shrinking the upper loop, and to topology 5 when shrinking the lower one. Topology 2 will similarly lead to the sub-loop renormalisation topologies 5 and 6; topology 3 leads to two diagrams of topology 8. We see that two genuine diagrams of a different topology can lead to the same sub-loop renormalisation diagram. Therefore, the following relations are understood to hold only when all genuine and all sub-loop renormalisation diagrams are taken into account.

To derive the required relations, as an example, let us first consider a simple two-loop "test" self-energy

$$\Sigma^{(2)}_{\text{test}} = A_0 B_0 + A_0 \delta c_B + B_0 \delta c_A. \tag{5.17}$$

The first term corresponds to a genuine diagram (like topology 2 in Fig. 5.2, but without any couplings), and the second and third term stem from sub-loop renormalisation diagrams. The divergent parts of the counterterms are given by the divergence of the loop which was shrunk but with an additional minus sign:

$$\delta c_A^{\text{div}} = -A_0^{\text{div}}, \tag{5.18a}$$

$$\delta c_B^{\text{div}} = -B_0^{\text{div}}. \tag{5.18b}$$

This implies the relations

$$A_0^{\text{div}}\delta c_B^{\text{div}} + B_0^{\text{div}}\delta c_A^{\text{div}} = -2A_0^{\text{div}}B_0^{\text{div}}, \tag{5.19a}$$

$$A_0^{\text{fin}}\delta c_B^{\text{div}} + B_0^{\text{fin}}\delta c_A^{\text{div}} = -A_0^{\text{fin}}B_0^{\text{div}} - B_0^{\text{fin}}A_0^{\text{div}}, \tag{5.19b}$$

$$A_0^{\varepsilon}\delta c_B^{\text{div}} + B_0^{\varepsilon}\delta c_A^{\text{div}} = -A_0^{\varepsilon}B_0^{\text{div}} - B_0^{\varepsilon}A_0^{\text{div}}. \tag{5.19c}$$

This derivation can be straightforwardly extended to other products of one-loop integrals. Consequently, in the notation of Eq. (5.15), this means

$$N_j^{\text{div}}\delta c_j^{\text{div}} = -2L_i^{\text{div}}M_i^{\text{div}}, \tag{5.20a}$$

$$N_j^{\text{fin}}\delta c_j^{\text{div}} = -L_i^{\text{fin}}M_i^{\text{div}} - L_i^{\text{div}}M_i^{\text{fin}}, \tag{5.20b}$$

$$N_j^{\varepsilon}\delta c_j^{\text{div}} = -L_i^{\varepsilon}M_i^{\text{div}} - L_i^{\text{div}}M_i^{\varepsilon}, \tag{5.20c}$$

where now all sub-loop renormalisation diagrams are included on the left-hand side and all genuine diagrams contribute to the right-hand side. These relations hold independently of the renormalisation scheme as only the divergent (and therefore scheme-independent) parts of the one-loop counterterms appear. Inserting all three relations into the expression for the unrenormalised self-energy leaves us with

$$\Sigma^{(2)} = -\frac{L_i^{\text{div}}M_i^{\text{div}}}{\varepsilon^2} + \frac{N_j^{\text{div}}\delta c_j^{\text{fin}}}{\varepsilon} + L_i^{\text{fin}}M_i^{\text{fin}} + N_j^{\text{div}}\delta c_j^{\varepsilon} + N_j^{\text{fin}}\delta c_j^{\text{fin}} + \mathcal{O}(\varepsilon). \tag{5.21}$$

We have numerically verified that, in our calculation, the $\mathcal{O}\left(\varepsilon^{-1}\right)$ part is indeed only generated by the finite part of the one-loop counterterms. Similarly, all $\mathcal{O}(\varepsilon)$ parts of loop integrals in the final result stem from the one-loop counterterms. It becomes clear that some, if not all, two-loop counterterms have to include finite pieces in order to cancel the δc_j^{ε}-terms in the renormalised self-energy, as subtracting only the divergences—as is done in a $\overline{\text{DR}}$ scheme—will leave the finite part unaltered. In a pure $\overline{\text{DR}}$ scheme, however, all $\mathcal{O}(\varepsilon)$ parts cancel after the sub-loop renormalisation already.

We demonstrate these findings with the example of the two-loop AA self-energy and show under which circumstances the $\mathcal{O}(\varepsilon)$ part of the one-loop counterterm $\delta^{(1)}M_W^2$ cancels after renormalisation. To simplify the analysis, we restrict ourselves to a $\overline{\text{DR}}$ renormalisation of t_β, which in this case is needed only up to the one-loop order.

The renormalised two-loop AA self-energy is given in Eq. (4.100a). Genuine two-loop counterterms as well as products of one-loop counterterms appear. The counterterm products can be neglected in our discussion as $\delta^{(1)}M_W^2$ plays no role at the one-loop level if t_β is renormalised in a $\overline{\text{DR}}$ scheme. The W mass counterterm appears,

however, in the sub-loop renormalisation part of $\Sigma^{(2)}_{AA}$ in a product with one-loop integrals. Therefore, it plays a role in the determination of the two-loop counterterms. The relevant terms in the renormalised self-energy are

$$\begin{aligned}\hat{\Sigma}^{(2)}_{AA}(p^2) &= \Sigma^{(2)}_{AA}(p^2) + \delta^{(2)}Z_{AA}(p^2 - m_A^2) - \delta^{(2)}m_A^2 + \text{terms without } \delta^{(1)}M_W^2 \\ &= N^{\text{div}}(p^2)(\delta^{(1)}M_W^2)^\varepsilon + \delta^{(2)}Z_{AA}(p^2 - m_A^2) - \delta^{(2)}m_A^2 \\ &\quad + \text{terms without } (\delta^{(1)}M_W^2)^\varepsilon.\end{aligned} \tag{5.22}$$

As before, $N^{\text{div}}(p^2)$ is the divergent part of the loop integrals which are multiplied with $\delta^{(1)}M_W^2$ in the sub-loop renormalisation diagrams. It has to be a polynomial of degree one in p^2, so we can write $N^{\text{div}}(p^2) = \nu_1 p^2 + \nu_0$.
When defining the mass m_A^2 in an OS scheme, it contains the $\mathcal{O}(\varepsilon)$ part of $\delta^{(1)}M_W^2$ as well, since

$$\begin{aligned}\delta^{(2)}m_A^2 &= \operatorname{Re}\Sigma^{(2)}_{AA}(m_A^2) + \text{terms without } \delta^{(1)}M_W^2 \\ &= \underbrace{N^{\text{div}}(m_A^2)}_{=\nu_1 m_A^2 + \nu_0}(\delta^{(1)}M_W^2)^\varepsilon + \text{terms without } (\delta^{(1)}M_W^2)^\varepsilon.\end{aligned} \tag{5.23}$$

Inserting this back into the renormalised self-energy, we arrive at

$$\begin{aligned}\hat{\Sigma}^{(2)}_{AA}(p^2) = &\underbrace{\left(N^{\text{div}}(p^2) - N^{\text{div}}(m_A^2)\right)}_{=\nu_1(p^2 - m_A^2)}(\delta^{(1)}M_W^2)^\varepsilon + \delta^{(2)}Z_{AA}(p^2 - m_A^2) \\ &+ \text{terms without } (\delta^{(1)}M_W^2)^\varepsilon.\end{aligned} \tag{5.24}$$

We can see that the on-shell self-energy $\hat{\Sigma}^{(2)}_{AA}(m_A^2)$ is free from $(\delta^{(1)}M_W^2)^\varepsilon$. To obtain this property also for off-shell momenta, we need to use an on-shell renormalisation for the field counterterm $\delta^{(2)}Z_{AA}$ as well:

$$\begin{aligned}\delta^{(2)}Z_{AA} &= -\partial\Sigma^{(2)}_{AA}(m_A^2) + \text{terms without } \delta^{(1)}M_W^2 \\ &= -\underbrace{\frac{\partial N^{\text{div}}(p^2)}{\partial p^2}}_{=\nu_1}(\delta^{(1)}M_W^2)^\varepsilon + \text{terms without } (\delta^{(1)}M_W^2)^\varepsilon.\end{aligned} \tag{5.25}$$

With $\delta^{(2)}m_A^2$ and $\delta^{(2)}Z_{AA}$ defined in an on-shell scheme, we find

$$\begin{aligned}\hat{\Sigma}^{(2)}_{AA}(p^2) &\overset{\text{OS}}{=} \nu_1(p^2 - m_A^2)(\delta^{(1)}M_W^2)^\varepsilon - \nu_1(\delta^{(1)}M_W^2)^\varepsilon(p^2 - m_A^2) \\ &\quad + \text{terms without } (\delta^{(1)}M_W^2)^\varepsilon \\ &= \text{terms without } (\delta^{(1)}M_W^2)^\varepsilon.\end{aligned} \tag{5.26}$$

The same logic applies to all other one-loop counterterms as well. Thus, in a full OS renormalisation, all $\mathcal{O}(\varepsilon)$ parts of loop integrals will drop out for arbitrary momenta. Alternatively, we could have used a full $\overline{\text{DR}}$ renormalisation for all one- and two-loop counterterms. In this case, Eq. (5.21) takes the form

$$\Sigma^{(2)} \overset{\overline{\text{DR}}}{=} -\frac{L_i^{\text{div}} M_i^{\text{div}}}{\varepsilon^2} + L_i^{\text{fin}} M_i^{\text{fin}} + \mathcal{O}(\varepsilon). \tag{5.27}$$

The two-loop counterterms will remove the $\mathcal{O}\left(\varepsilon^2\right)$ divergence, and the renormalised self-energy reads

$$\hat{\Sigma}^{(2)} \overset{\overline{\text{DR}}}{=} L_i^{\text{fin}} M_i^{\text{fin}} + \mathcal{O}(\varepsilon). \tag{5.28}$$

Again, the renormalised self-energy is free from $\mathcal{O}(\varepsilon)$ terms of loop integrals and counterterms.

It becomes clear that, in our two-loop calculation, the $\mathcal{O}(\varepsilon)$ parts of loop integrals and counterterms contribute only in a mixed renormalisation scheme where at least one one-loop counterterm is defined in an on-shell scheme and at least one two-loop counterterm is defined in a minimal subtraction scheme. To demonstrate this, let us assume that we need two counterterms δc_1 and δc_2 to renormalise the two-loop self-energy. δc_1 is only needed at the one-loop level and defined in the OS scheme, δc_2 is needed at the one- and two-loop level and defined in the $\overline{\text{DR}}$ scheme. Then

$$\Sigma^{(2)} \overset{\text{MIX}}{=} -\frac{L_i^{\text{div}} M_i^{\text{div}}}{\varepsilon^2} + \frac{N_1^{\text{div}} \delta c_1^{\text{fin}}}{\varepsilon} + L_i^{\text{fin}} M_i^{\text{fin}} + N_1^{\text{div}} \delta c_1^{\varepsilon} + N_1^{\text{fin}} \delta c_1^{\text{fin}} + \mathcal{O}(\varepsilon). \tag{5.29}$$

The $\overline{\text{DR}}$ δc_2 counterterm will then only remove the divergences and we find

$$\hat{\Sigma}^{(2)} \overset{\text{MIX}}{=} L_i^{\text{fin}} M_i^{\text{fin}} + N_1^{\text{div}} \delta c_1^{\varepsilon} + N_1^{\text{fin}} \delta c_1^{\text{fin}} + \mathcal{O}(\varepsilon). \tag{5.30}$$

In schemes where the $\mathcal{O}(\varepsilon)$ terms of the counterterms cancel out, it is possible to do the renormalisation in one scheme and then do a finite reparameterisation into a different scheme. This is not possible if, in one of the two schemes, the $\mathcal{O}(\varepsilon)$ parts of the counterterms contribute.

This was already noted in Ref. [55]. They compared two calculations, both of which employed a mixed renormalisation scheme [51, 52]. In Ref. [52], the mixed scheme is implemented by starting in a pure $\overline{\text{DR}}$ scheme and subsequently reparameterising the top quark mass and the stop squark masses into an OS scheme. This approach leads to a complete cancellation of $\mathcal{O}(\varepsilon)$ terms even in a mixed scheme. The disagreement between the two calculations was therefore traced back to a different implementation of the $\overline{\text{DR}}$ scheme at the two-loop level.

6 Algebraic expressions for the leading $\mathcal{O}(N_c)$ one-loop terms

In this chapter, we give explicit expressions for the leading one-loop contributions to the Higgs boson self-energies in the complex MSSM. While these contributions, as all one-loop results, have been known for some time already [20–25], they served as a cross check for our calculational setup, which we explained in Ch. 5. We verified our computation of the full third-generation Yukawa terms of $\mathcal{O}\big(\alpha_q N_c\big)$ via cross-checking with FeynHiggs [30, 67, 88, 90, 128, 129, 194–196]. The numerical results presented in Ch. 7 include the full electroweak one-loop self-energies of $\mathcal{O}\big((\alpha_{\text{em}} + \alpha_q)N_c\big)$.

At first, we worked in the gaugeless limit, which we explain in Sect. 6.1, and only included top quarks and stop squarks as internal particles. The resulting expressions are the dominant one-loop contributions to the Higgs boson masses in the MSSM, which are proportional to m_t^4. This approach is useful only when restricting ourselves to the MSSM with real parameters and the calculation of neutral self-energies. For a prediction of the mass of the charged Higgs boson, diagrams with internal bottom quarks and sbottom squarks need to be included as well.

In the presence of complex parameters, we define the charged Higgs mass as an on-shell quantity and use it as an input parameter, as we have explained in Sect. 4.2. In this case, we have to include internal bottom quarks and sbottom squarks in the self-energies even if we are only interested in the prediction for the neutral Higgs boson masses. To extract the leading one-loop m_t^4 contributions, we work in the limit $m_b \to 0$ as well as the aforementioned gaugeless limit. The results presented in this chapter are cast in a form that is valid in both the rMSSM and the cMSSM. The algebraic expressions for the renormalised neutral one-loop self-energies are given in Sect. 6.2. We calculate the difference between the $\mathcal{CP}$-odd and the charged Higgs boson self-energy in Sect. 6.3.

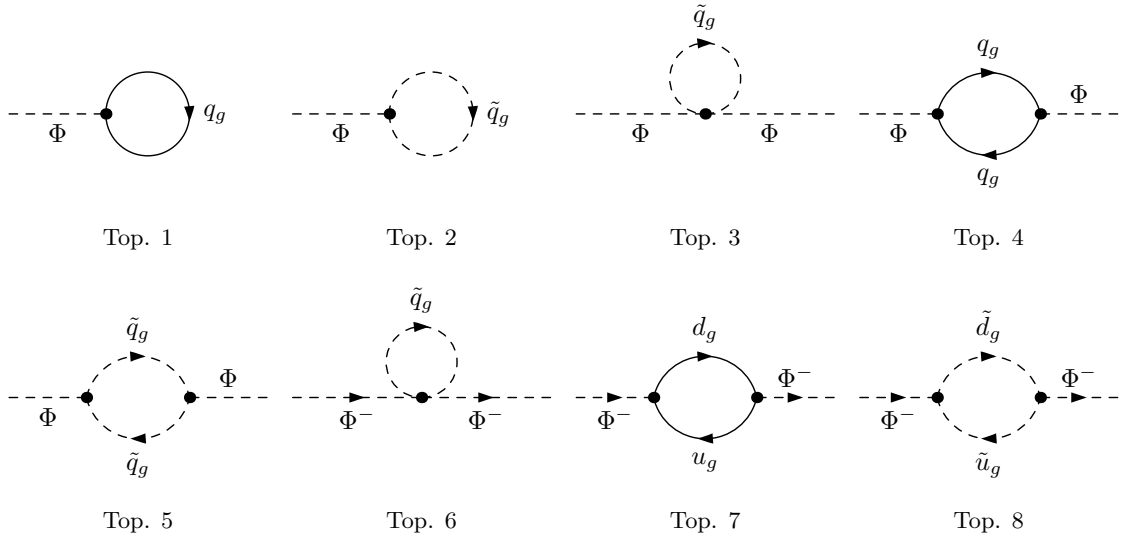

Figure 6.1: Topologies of the one-loop tadpole and self-energy diagrams. $\Phi = h, H, A, G$; $\Phi^- = H^-, G^-$; g is a flavour index.

6.1 The gaugeless limit and further approximations

To extract the leading corrections proportional to m_t^4, we employ the so-called "gaugeless limit" to the tadpole and self-energy diagrams shown in Fig. 6.1; we set the electric charge e (or, equivalently, the fine-structure constant α_{em}) to zero. This leads to a number of simplifications: at tree level, the mass of the lightest $\mathcal{CP}$-even Higgs boson h vanishes exactly, and the heavier H, A, and $H^\pm$ bosons are mass-degenerate. The Higgs mixing angle α and the angle β that is obtained from the VEV ratio are related by

$$\beta - \alpha \overset{\text{gl.}}{=} \frac{\pi}{2}. \tag{6.1}$$

Whenever we put a "gl." on top of an equal sign, the equation will hold in the gaugeless limit but not necessarily in a more complete calculation. While not technically part of the gaugeless limit, we also employ the limit $m_b \to 0$ when writing the symbol "gl.".

In this limit, the Z and W bosons become massless. In order to apply the gaugeless limit in a consistent way, we have to rewrite the electroweak vector boson masses in terms of the electric charge and the vacuum expectation values v_1 and v_2 as follows:

$$M_Z^2 = \frac{e^2}{2 s_{\text{w}}^2 c_{\text{w}}^2}(v_1^2 + v_2^2), \tag{6.2a}$$

$$M_W^2 = \frac{e^2}{2 s_{\text{w}}^2}(v_1^2 + v_2^2). \tag{6.2b}$$

In this form, the limit $e \to 0$ can easily be taken. The VEVs can be replaced by Fermi's constant by virtue of

$$v_1^2 + v_2^2 = \frac{1}{2\sqrt{2}G_F}. \tag{6.3}$$

Additionally, all self-energies are evaluated at a vanishing external momentum p^2. To allow for an on-shell renormalisation, we therefore set the degenerate masses $m^2_{H^\pm} = m^2_H = m^2_A$ to zero as well. In this limit, all Higgs bosons are massless at the tree-level, and no counterterms are needed for $\tan(\beta)$ and the Higgs fields. The mass counterterms for the electroweak gauge bosons vanish in the gaugeless limit due to their proportionality to the fine-structure constant. Thus, only the counterterms for m^2_A, $m^2_{H^\pm}$, and the tadpoles are needed.
As mentioned above, a final approximation needs to be made in order to get the leading m_t^4 terms; one has to set the mass of the bottom quark m_b to zero (and also neglect the first and second generation quark masses as well as the lepton masses). In this limit, in combination with the gaugeless limit, all diagrams with (s)bottom (s)quarks in the loop do not contribute to the neutral Higgs self-energies. In the charged self-energies, however, a dependence on the left-handed SUSY breaking mass $M^2_{\tilde{q}_3}$ remains. In the gaugeless limit, $M^2_{\tilde{q}_3}$ is related to the stop masses through the identity

$$M^2_{\tilde{q}_3} \overset{\text{gl.}}{=} c^2_{\tilde{t}} m^2_{\tilde{t}_1} + s^2_{\tilde{t}} m^2_{\tilde{t}_2} - m^2_t. \tag{6.4}$$

6.2 The leading one-loop contributions to the neutral Higgs-boson self-energies

In this section, we give the leading expressions for all neutral Higgs-boson self-energies in the interaction eigenbasis. Our formulae hold for the case of real parameters as well as for a scenario with complex parameters. For the rMSSM and the cMSSM, we use different renormalisation schemes: In the rMSSM, we renormalise the $\mathcal{CP}$-odd Higgs boson mass in an on-shell scheme and hence $\hat{\Sigma}^{(1)}_{AA}(0)$ vanishes in any such scenario. In the cMSSM, however, the charged Higgs mass is renormalised on-shell and $\hat{\Sigma}^{(1)}_{AA}(0) \neq 0$.

$$\delta^{(1)} m^2_A \overset{\text{gl.}}{=} \Sigma^{(1)}_{AA}(0) \qquad \text{(in the rMSSM)}, \tag{6.5a}$$

$$\delta^{(1)} m^2_{H^\pm} \overset{\text{gl.}}{=} \Sigma^{(1)}_{H^- H^+}(0) \quad \text{(in the cMSSM)}. \tag{6.5b}$$

Since $\delta^{(1)} M_W^2$ vanishes in the gaugeless limit, we also have

$$\delta^{(1)} m^2_{H^\pm} \overset{\text{gl.}}{=} \Sigma^{(1)}_{AA}(0) \qquad \text{(in the rMSSM)}, \tag{6.6a}$$

$$\delta^{(1)} m^2_{A} \overset{\text{gl.}}{=} \Sigma^{(1)}_{H^- H^+}(0) \quad \text{(in the cMSSM)}. \tag{6.6b}$$

This means

$$\hat{\Sigma}^{(1)}_{AA}(0) \overset{\text{gl.}}{=} 0 \quad \text{(in the rMSSM)}, \tag{6.7a}$$

$$\hat{\Sigma}^{(1)}_{H^- H^+}(0) \overset{\text{gl.}}{=} 0 \quad \text{(in the cMSSM)}, \tag{6.7b}$$

and

$$\hat{\Sigma}^{(1)}_{H^- H^+}(0) \overset{\text{gl.}}{=} \Sigma^{(1)}_{H^- H^+}(0) - \Sigma^{(1)}_{AA}(0) \equiv -\Delta^{(1)} m^2_{H^\pm} \quad \text{(in the rMSSM)}, \tag{6.8a}$$

$$\hat{\Sigma}^{(1)}_{AA}(0) \overset{\text{gl.}}{=} \Sigma^{(1)}_{AA}(0) - \Sigma^{(1)}_{H^- H^+}(0) = +\Delta^{(1)} m^2_{H^\pm} \quad \text{(in the cMSSM)}, \tag{6.8b}$$

where we introduced the abbreviation $\Delta^{(1)} m^2_{H^\pm}$ from Ref. [41].
We determine the tadpole counterterms as explained in Sect. 4.2. To obtain expressions which are valid in both the rMSSM and the cMSSM, we write the $\mathcal{CP}$-odd mass counterterm as

$$\delta^{(1)} m^2_A \overset{\text{gl.}}{=} \Sigma^{(1)}_{AA}(0) - \hat{\Sigma}^{(1)}_{AA}(0). \tag{6.9}$$

For the remainder of this section, we keep $\hat{\Sigma}^{(1)}_{AA}(0)$ as a symbol. $\hat{\Sigma}^{(1)}_{AA}(0)$ vanishes in the rMSSM, while in the cMSSM it is given by $\Delta^{(1)} m^2_{H^\pm}$. We calculate $\Delta^{(1)} m^2_{H^\pm}$ in Sect. 6.3. To further simplify our results, we give the neutral self-energies in the interaction eigenbasis instead of the tree-level mass eigenbasis. The self-energies in the different bases are related by

$$\hat{\Sigma}^{(1)}_{hh} = c_\alpha^2 \hat{\Sigma}^{(1)}_{\phi_2\phi_2} + s_\alpha^2 \hat{\Sigma}^{(1)}_{\phi_1\phi_1} - s_{2\alpha} \hat{\Sigma}^{(1)}_{\phi_1\phi_2}, \tag{6.10a}$$

$$\hat{\Sigma}^{(1)}_{hH} = c_{2\alpha} \hat{\Sigma}^{(1)}_{\phi_1\phi_2} - s_\alpha c_\alpha (\hat{\Sigma}^{(1)}_{\phi_1\phi_1} - \hat{\Sigma}^{(1)}_{\phi_2\phi_2}), \tag{6.10b}$$

$$\hat{\Sigma}^{(1)}_{HH} = c_\alpha^2 \hat{\Sigma}^{(1)}_{\phi_1\phi_1} + s_\alpha^2 \hat{\Sigma}^{(1)}_{\phi_2\phi_2} + s_{2\alpha} \hat{\Sigma}^{(1)}_{\phi_1\phi_2}, \tag{6.10c}$$

$$\hat{\Sigma}^{(1)}_{AA} = c_\beta^2 \hat{\Sigma}^{(1)}_{\chi_2\chi_2} + s_\beta^2 \hat{\Sigma}^{(1)}_{\chi_1\chi_1} - s_{2\beta} \hat{\Sigma}^{(1)}_{\chi_1\chi_2}, \tag{6.10d}$$

$$\hat{\Sigma}^{(1)}_{AG} = c_{2\beta} \hat{\Sigma}^{(1)}_{\chi_1\chi_2} - s_\beta c_\beta (\hat{\Sigma}^{(1)}_{\chi_1\chi_1} - \hat{\Sigma}^{(1)}_{\chi_2\chi_2}), \tag{6.10e}$$

$$\hat{\Sigma}^{(1)}_{GG} = c_\beta^2 \hat{\Sigma}^{(1)}_{\chi_1\chi_1} + s_\beta^2 \hat{\Sigma}^{(1)}_{\chi_2\chi_2} + s_{2\beta} \hat{\Sigma}^{(1)}_{\chi_1\chi_2}, \tag{6.10f}$$

$$\hat{\Sigma}^{(1)}_{hA} = c_\alpha c_\beta \hat{\Sigma}^{(1)}_{\phi_2\chi_2} + s_\alpha s_\beta \hat{\Sigma}^{(1)}_{\phi_1\chi_1} - s_\alpha c_\beta \hat{\Sigma}^{(1)}_{\phi_1\chi_2} - c_\alpha s_\beta \hat{\Sigma}^{(1)}_{\phi_2\chi_1}, \tag{6.10g}$$

$$\hat{\Sigma}^{(1)}_{hG} = c_\alpha c_\beta \hat{\Sigma}^{(1)}_{\phi_2\chi_1} - s_\alpha s_\beta \hat{\Sigma}^{(1)}_{\phi_1\chi_2} - s_\alpha c_\beta \hat{\Sigma}^{(1)}_{\phi_1\chi_1} + c_\alpha s_\beta \hat{\Sigma}^{(1)}_{\phi_2\chi_2}, \tag{6.10h}$$

$$\hat{\Sigma}^{(1)}_{HA} = c_\alpha c_\beta \hat{\Sigma}^{(1)}_{\phi_1\chi_2} - s_\alpha s_\beta \hat{\Sigma}^{(1)}_{\phi_2\chi_1} + s_\alpha c_\beta \hat{\Sigma}^{(1)}_{\phi_2\chi_2} - c_\alpha s_\beta \hat{\Sigma}^{(1)}_{\phi_1\chi_1}, \tag{6.10i}$$

$$\hat{\Sigma}^{(1)}_{HG} = c_\alpha c_\beta \hat{\Sigma}^{(1)}_{\phi_1\chi_1} + s_\alpha s_\beta \hat{\Sigma}^{(1)}_{\phi_2\chi_2} + s_\alpha c_\beta \hat{\Sigma}^{(1)}_{\phi_2\chi_1} + c_\alpha s_\beta \hat{\Sigma}^{(1)}_{\phi_1\chi_2}, \tag{6.10j}$$

where we again used the shorthand notations $s_x = \sin x$ and $c_x = \cos x$.
After consistently employing the gaugeless limit and setting the bottom mass to zero, the leading m_t^4 contributions to the renormalised $\mathcal{CP}$-even Higgs boson self-energies are found to be

$$\hat{\Sigma}^{(1)}_{\phi_1\phi_1}(0) \overset{\text{gl.}}{=} -\frac{N_c G_F m_t^4}{2\sqrt{2}\pi^2 s_\beta^2}\left[\frac{\mathrm{Re}\{\mu^2 X_t^2\}}{(m^2_{\tilde{t}_1}-m^2_{\tilde{t}_2})^2} g(m^2_{\tilde{t}_1}, m^2_{\tilde{t}_2})\right] + s_\beta^2 \hat{\Sigma}^{(1)}_{AA}, \tag{6.11a}$$

$$\begin{aligned}\hat{\Sigma}^{(1)}_{\phi_1\phi_2}(0) \overset{\text{gl.}}{=} &-\frac{N_c G_F m_t^4}{2\sqrt{2}\pi^2 s_\beta^2}\left[-\frac{\mathrm{Re}\{\mu X_t\}}{m^2_{\tilde{t}_1}-m^2_{\tilde{t}_2}}\log\left(\frac{m^2_{\tilde{t}_1}}{m^2_{\tilde{t}_2}}\right) - \frac{\mathrm{Re}\{\mu X_t^2 A_t^*\}}{(m^2_{\tilde{t}_1}-m^2_{\tilde{t}_2})^2} g(m^2_{\tilde{t}_1}, m^2_{\tilde{t}_2})\right] \\ &- s_\beta c_\beta \hat{\Sigma}^{(1)}_{AA},\end{aligned} \tag{6.11b}$$

$$\begin{aligned}\hat{\Sigma}^{(1)}_{\phi_2\phi_2}(0) \overset{\text{gl.}}{=} &-\frac{N_c G_F m_t^4}{2\sqrt{2}\pi^2 s_\beta^2}\left[\log\left(\frac{m^2_{\tilde{t}_1} m^2_{\tilde{t}_2}}{m_t^4}\right) + \frac{2\,\mathrm{Re}\{X_t A_t^*\}}{m^2_{\tilde{t}_1}-m^2_{\tilde{t}_2}}\log\frac{m^2_{\tilde{t}_1}}{m^2_{\tilde{t}_2}}\right. \\ &\left. + \frac{\mathrm{Re}\{X_t^2 A_t^{*2}\}}{(m^2_{\tilde{t}_1}-m^2_{\tilde{t}_2})^2} g(m^2_{\tilde{t}_1}, m^2_{\tilde{t}_2})\right] + c_\beta^2 \hat{\Sigma}^{(1)}_{AA},\end{aligned} \tag{6.11c}$$

where we used the definition

$$g(m^2_{\tilde{t}_1}, m^2_{\tilde{t}_2}) \equiv 2 - \frac{m^2_{\tilde{t}_1}+m^2_{\tilde{t}_2}}{m^2_{\tilde{t}_1}-m^2_{\tilde{t}_2}}\log\frac{m^2_{\tilde{t}_1}}{m^2_{\tilde{t}_2}}. \tag{6.12}$$

These expression generalise the ones found in Ref. [30] to the case of complex parameters.[12] The same self-energies have been calculated in Ref. [198] also in the case of complex parameters and an on-shell renormalisation of the charged Higgs mass. The results of Ref. [198] are expressed using the abbreviations $\mathcal{C}_{112-122}$ and $\mathcal{C}_{12L}$. We find full agreement making use of the identities

$$\begin{aligned}\mathcal{C}_{112-122} &\equiv C_0(0,0,0,m^2_{\tilde{t}_1}, m^2_{\tilde{t}_1}, m^2_{\tilde{t}_2}) - C_0(0,0,0,m^2_{\tilde{t}_1}, m^2_{\tilde{t}_2}, m^2_{\tilde{t}_2}) \\ &= -\frac{g(m^2_{\tilde{t}_1}, m^2_{\tilde{t}_2})}{m^2_{\tilde{t}_1}-m^2_{\tilde{t}_2}},\end{aligned} \tag{6.13a}$$

$$\begin{aligned}\mathcal{C}_{12L} &\equiv C_0(0,0,0,m^2_{\tilde{t}_1}, m^2_{\tilde{t}_2}, M^2_{\tilde{q}_3}) \\ &= -\frac{1}{2}\left[\frac{M^2_{\tilde{q}_3}}{(M^2_{\tilde{q}_3}-m^2_{\tilde{t}_1})(M^2_{\tilde{q}_3}-m^2_{\tilde{t}_2})}\log\left(\frac{M^4_{\tilde{q}_3}}{m^2_{\tilde{t}_1} m^2_{\tilde{t}_2}}\right)\right. \\ &\qquad \left. - \frac{m^2_{\tilde{t}_1}(M^2_{\tilde{q}_3}-m^2_{\tilde{t}_2}) + m^2_{\tilde{t}_2}(M^2_{\tilde{q}_3}-m^2_{\tilde{t}_1})}{(M^2_{\tilde{q}_3}-m^2_{\tilde{t}_1})(M^2_{\tilde{q}_3}-m^2_{\tilde{t}_2})(m^2_{\tilde{t}_1}-m^2_{\tilde{t}_2})}\log\left(\frac{m^2_{\tilde{t}_1}}{m^2_{\tilde{t}_2}}\right)\right].\end{aligned} \tag{6.13b}$$

We define the three-point integral C_0 in Eqs. (D.1).

[12] In Ref. [28], an overall minus sign is missing in the self-energies, as has been verified by the authors.

At tree-level, the MSSM Higgs sector is $\mathcal{CP}$ conserving also in the presence of complex parameters. The self-energies which mix $\mathcal{CP}$-even and $\mathcal{CP}$-odd states and hence violate $\mathcal{CP}$ symmetry, arise at the one-loop level due to non-zero imaginary parts of the parameters:

$$\hat{\Sigma}^{(1)}_{\phi_1\chi_1}(0) \overset{\text{gl.}}{=} -\frac{N_c G_F m_t^4}{4\sqrt{2}\pi^2 s_\beta^2}\left[\frac{\operatorname{Im}\{\mu^2 X_t^2\}}{(m^2_{\tilde{t}_1}-m^2_{\tilde{t}_2})^2} g(m^2_{\tilde{t}_1}, m^2_{\tilde{t}_2})\right], \tag{6.14a}$$

$$\hat{\Sigma}^{(1)}_{\phi_2\chi_2}(0) \overset{\text{gl.}}{=} -\frac{N_c G_F m_t^4}{4\sqrt{2}\pi^2 s_\beta^2}\left[\frac{2\operatorname{Im}\{X_t A_t^*\}}{m^2_{\tilde{t}_1}-m^2_{\tilde{t}_2}} \log\frac{m^2_{\tilde{t}_1}}{m^2_{\tilde{t}_2}} + \frac{\operatorname{Im}\{X_t^2 A_t^{*2}\}}{(m^2_{\tilde{t}_1}-m^2_{\tilde{t}_2})^2} g(m^2_{\tilde{t}_1}, m^2_{\tilde{t}_2})\right], \tag{6.14b}$$

$$\begin{aligned}\hat{\Sigma}^{(1)}_{\phi_1\chi_2}(0) &\overset{\text{gl.}}{=} -\frac{N_c G_F m_t^4}{4\sqrt{2}\pi^2 s_\beta^2}\left[-\frac{\operatorname{Im}\{\mu X_t^2 A_t^*\}}{(m^2_{\tilde{t}_1}-m^2_{\tilde{t}_2})^2} g(m^2_{\tilde{t}_1}, m^2_{\tilde{t}_2})\right.\\ &\quad\left.+\frac{|X_t|^2\operatorname{Im}\{\mu X_t\}}{(m^2_{\tilde{t}_1}-m^2_{\tilde{t}_2})^2} g(m^2_{\tilde{t}_1}, m^2_{\tilde{t}_2})\right] \qquad (6.14c)\\ &\overset{\text{gl.}}{=} -t_\beta^{-1}\hat{\Sigma}^{(1)}_{\phi_1\chi_1}(0)\end{aligned}$$

$$\begin{aligned}\hat{\Sigma}^{(1)}_{\phi_2\chi_1}(0) &\overset{\text{gl.}}{=} -\frac{N_c G_F m_t^4}{4\sqrt{2}\pi^2 s_\beta^2}\left[-\frac{2\operatorname{Im}\{\mu X_t\}}{m^2_{\tilde{t}_1}-m^2_{\tilde{t}_2}} \log\frac{m^2_{\tilde{t}_1}}{m^2_{\tilde{t}_2}} - \frac{\operatorname{Im}\{\mu X_t^2 A_t^*\}}{(m^2_{\tilde{t}_1}-m^2_{\tilde{t}_2})^2} g(m^2_{\tilde{t}_1}, m^2_{\tilde{t}_2})\right.\\ &\quad\left.-\frac{|X_t|^2\operatorname{Im}\{\mu X_t\}}{(m^2_{\tilde{t}_1}-m^2_{\tilde{t}_2})^2} g(m^2_{\tilde{t}_1}, m^2_{\tilde{t}_2})\right] \qquad (6.14d)\\ &\overset{\text{gl.}}{=} -t_\beta\hat{\Sigma}^{(1)}_{\phi_2\chi_2}(0).\end{aligned}$$

All $\mathcal{CP}$-odd self-energies are proportional to $\hat{\Sigma}^{(1)}_{AA}$:

$$\hat{\Sigma}^{(1)}_{\chi_1\chi_1}(0) \overset{\text{gl.}}{=} s_\beta^2\hat{\Sigma}^{(1)}_{AA}(0), \tag{6.15a}$$

$$\hat{\Sigma}^{(1)}_{\chi_1\chi_2}(0) \overset{\text{gl.}}{=} -s_\beta c_\beta\hat{\Sigma}^{(1)}_{AA}(0), \tag{6.15b}$$

$$\hat{\Sigma}^{(1)}_{\chi_2\chi_2}(0) \overset{\text{gl.}}{=} c_\beta^2\hat{\Sigma}^{(1)}_{AA}(0). \tag{6.15c}$$

Inserting Eqs. (6.14) and (6.15) into Eqs. (6.10), we see that the self-energies with external would-be Goldstone bosons vanish:

$$\hat{\Sigma}^{(1)}_{AG}(0) \overset{\text{gl.}}{=} 0, \tag{6.16a}$$

$$\hat{\Sigma}^{(1)}_{GG}(0) \overset{\text{gl.}}{=} 0, \tag{6.16b}$$

$$\hat{\Sigma}^{(1)}_{hG}(0) \overset{\text{gl.}}{=} 0, \tag{6.16c}$$

$$\hat{\Sigma}^{(1)}_{HG}(0) \overset{\text{gl.}}{=} 0. \tag{6.16d}$$

This behaviour is to be expected as all self-energies are evaluated at vanishing external momentum, for which self-energies with external Goldstone bosons vanish due

to a Slavnov-Taylor identity [57, 199].
Inserting Eqs. (6.11) into Eqs. (6.10) and keeping only the leading logarithmic terms $\sim \log\left(m_{\tilde{t}_1}^2 m_{\tilde{t}_2}^2/m_t^4\right)$, we find

$$\hat{\Sigma}_{hh}^{(1)}(0) \overset{\text{gl.}}{\approx} -\frac{N_c G_F m_t^4}{2\sqrt{2}\pi^2 s_\beta^2} \log\left(\frac{m_{\tilde{t}_1}^2 m_{\tilde{t}_2}^2}{m_t^4}\right) c_\alpha^2, \tag{6.17a}$$

$$\hat{\Sigma}_{hH}^{(1)}(0) \overset{\text{gl.}}{\approx} -\frac{N_c G_F m_t^4}{2\sqrt{2}\pi^2 s_\beta^2} \log\left(\frac{m_{\tilde{t}_1}^2 m_{\tilde{t}_2}^2}{m_t^4}\right) s_\alpha c_\alpha, \tag{6.17b}$$

$$\hat{\Sigma}_{HH}^{(1)}(0) \overset{\text{gl.}}{\approx} -\frac{N_c G_F m_t^4}{2\sqrt{2}\pi^2 s_\beta^2} \log\left(\frac{m_{\tilde{t}_1}^2 m_{\tilde{t}_2}^2}{m_t^4}\right) s_\alpha^2. \tag{6.17c}$$

6.3 The difference between the $\mathcal{CP}$-odd and the charged self-energy in the cMSSM

We close this chapter by calculating the leading contributions to

$$\Delta^{(1)} m_{H^\pm}^2 = \Sigma_{AA}^{(1)}(0) - \Sigma_{H^- H^+}^{(1)}(0), \tag{6.18}$$

which we first introduced in Sect. 6.2. We will work in the most general scenario, allowing for complex model parameters. This quantity is the one-loop correction to the charged Higgs mass in the rMSSM [41], hence the symbol. In the cMSSM, it agrees with the renormalised $\mathcal{CP}$-odd self-energy $\hat{\Sigma}_{AA}^{(1)}(0)$, which appears in the renormalised self-energies of Sect. 6.2. For its calculation, we need the unrenormalised self-energy of the $\mathcal{CP}$-odd Higgs boson and the charged Higgs boson.
Allowing for complex parameters, the unrenormalised self-energy of the $\mathcal{CP}$-odd Higgs boson is

$$\begin{aligned}\Sigma_{AA}^{(1)}(0) \overset{\text{gl.}}{=} & -\frac{N_c G_F m_t^4}{2\sqrt{2}\pi^2 s_\beta^4}\left(\frac{\text{Im}\{\mu X_t\}}{m_{\tilde{t}_1}^2 - m_{\tilde{t}_2}^2}\right)^2 g(m_{\tilde{t}_1}^2, m_{\tilde{t}_2}^2) \\ & -\frac{N_c G_F m_t^2}{4\sqrt{2}\pi^2 t_\beta^2}\left[2A_0(m_t^2) - A_0(m_{\tilde{t}_1}^2) - A_0(m_{\tilde{t}_2}^2) - |Y_t|^2 B_0(0, m_{\tilde{t}_1}^2, m_{\tilde{t}_2}^2)\right],\end{aligned} \tag{6.19}$$

where we introduced the abbreviation

$$Y_t \equiv A_t + \mu^* \tan(\beta). \tag{6.20}$$

The self-energy of the charged Higgs boson is given by

$$\begin{aligned}\Sigma^{(1)}_{H^-H^+}(0) \overset{\text{gl.}}{=} & -\frac{N_c G_F m_t^2}{4\sqrt{2}\pi^2 t_\beta^2}\Big[2A_0(m_t^2) - A_0(M_{\tilde{q}_3}^2) - s_{\tilde{t}}^2 A_0(m_{\tilde{t}_1}^2) - c_{\tilde{t}}^2 A_0(m_{\tilde{t}_2}^2) \\ & - |c_{\tilde{t}} m_t - e^{-\mathrm{i}\phi_{\tilde{t}}} s_{\tilde{t}} Y_t|^2 B_0(0, m_{\tilde{t}_1}^2, M_{\tilde{q}_3}^2) \\ & - |e^{\mathrm{i}\phi_{\tilde{t}}} s_{\tilde{t}} m_t + c_{\tilde{t}} Y_t|^2 B_0(0, m_{\tilde{t}_2}^2, M_{\tilde{q}_3}^2)\Big].\end{aligned} \tag{6.21}$$

The soft SUSY-breaking mass $M_{\tilde{q}_3}^2$ was introduced in Eqs. (4.3). The expressions for the self-energies in Eqs. (6.19) and (6.21) generalise the ones given in Ref. [41] to the case of complex parameters. We use a different sign convention in the unitary transformation introduced in Eq. (4.5), leading to an additional minus sign in all $s_{\tilde{t}}$ terms in comparison with Ref. [41].
Combining the results above yields

$$\begin{aligned}\Delta^{(1)} m_{H^\pm}^2 \overset{\text{gl.}}{=} & -\frac{N_c G_F m_t^4}{2\sqrt{2}\pi^2 s_\beta^4}\left(\frac{\mathrm{Im}\{\mu X_t\}}{m_{\tilde{t}_1}^2 - m_{\tilde{t}_2}^2}\right)^2 g(m_{\tilde{t}_1}^2, m_{\tilde{t}_2}^2) + \frac{N_c G_F m_t^2}{4\sqrt{2}\pi^2 t_\beta^2} \\ & \times \Bigg[M_{\tilde{q}_3}^2\left(1 + \frac{|c_{\tilde{t}} m_t - e^{-\mathrm{i}\phi_{\tilde{t}}} s_{\tilde{t}} Y_t|^2}{M_{\tilde{q}_3}^2 - m_{\tilde{t}_1}^2} + \frac{|e^{\mathrm{i}\phi_{\tilde{t}}} s_{\tilde{t}} m_t + c_{\tilde{t}} Y_t|^2}{M_{\tilde{q}_3}^2 - m_{\tilde{t}_2}^2}\right)\log\left(\frac{M_{\tilde{q}_3}^2}{m_{\tilde{t}_1}^2}\right) \\ & + m_{\tilde{t}_2}^2\left(-s_{\tilde{t}}^2 + \frac{|Y_t|^2}{m_{\tilde{t}_1}^2 - m_{\tilde{t}_2}^2} - \frac{|e^{\mathrm{i}\phi_{\tilde{t}}} s_{\tilde{t}} m_t + c_{\tilde{t}} Y_t|^2}{M_{\tilde{q}_3}^2 - m_{\tilde{t}_2}^2}\right)\log\left(\frac{m_{\tilde{t}_2}^2}{m_{\tilde{t}_1}^2}\right)\Bigg].\end{aligned} \tag{6.22}$$

We can further eliminate the stop mixing angle $\theta_{\tilde{t}}$ and the phase $\phi_{\tilde{t}}$ by using Eqs. (4.9). This leaves us with

$$\begin{aligned}\Delta^{(1)} m_{H^\pm}^2 \overset{\text{gl.}}{=} & -\frac{N_c G_F m_t^4}{2\sqrt{2}\pi^2 s_\beta^4}\Bigg[\left(\frac{\mathrm{Im}\{\mu X_t\}}{m_{\tilde{t}_1}^2 - m_{\tilde{t}_2}^2}\right)^2 g(m_{\tilde{t}_1}^2, m_{\tilde{t}_2}^2) \\ & + \frac{|\mu|^2}{4}\Bigg(\frac{M_{\tilde{q}_3}^2}{(M_{\tilde{q}_3}^2 - m_{\tilde{t}_1}^2)(M_{\tilde{q}_3}^2 - m_{\tilde{t}_2}^2)}\log\left(\frac{M_{\tilde{q}_3}^4}{m_{\tilde{t}_1}^2 m_{\tilde{t}_2}^2}\right) \\ & + \frac{m_{\tilde{t}_1}^2}{(m_{\tilde{t}_1}^2 - m_{\tilde{t}_2}^2)(m_{\tilde{t}_1}^2 - M_{\tilde{q}_3}^2)}\log\left(\frac{m_{\tilde{t}_1}^2}{m_{\tilde{t}_2}^2}\right) \\ & + \frac{m_{\tilde{t}_2}^2}{(m_{\tilde{t}_2}^2 - m_{\tilde{t}_1}^2)(m_{\tilde{t}_2}^2 - M_{\tilde{q}_3}^2)}\log\left(\frac{m_{\tilde{t}_2}^2}{m_{\tilde{t}_1}^2}\right)\Bigg)\Bigg] \\ = & \frac{N_c G_F m_t^4}{2\sqrt{2}\pi^2 s_\beta^4}\left[\frac{\mathrm{Im}^2\{\mu X_t\}}{m_{\tilde{t}_1}^2 - m_{\tilde{t}_2}^2}\mathcal{C}_{112-122} + \frac{|\mu|^2}{2}\mathcal{C}_{12L}\right].\end{aligned} \tag{6.23}$$

This result generalises the one given in Ref. [41] to the case of complex parameters and fully agrees with the one found in Ref. [198].

7 Numerical analysis of the full electroweak $\mathcal{O}\left(N_c^2\right)$ two-loop results

In this chapter, we present the numerical results of our two-loop prediction for the MSSM Higgs boson masses. Our main emphasis lies on the size of our newly calculated contributions relative to the experimental uncertainty of the Higgs boson mass at $M_h = 125.25 \pm 0.17$ GeV [7]. In the discussed scenarios, it will therefore not be our goal to include all known one-loop [20–25, 57–67] and two-loop contributions [26–40, 43, 45, 51, 52, 56, 68, 74–77] to the MSSM Higgs boson mass and to perform a resummation of large logarithms [31, 32, 81–127]. Instead, we take into account all one-loop contributions of $\mathcal{O}(N_c)$ and the full two-loop contributions of $\mathcal{O}\left(N_c^2\right)$. As we explained in the previous chapters, we neglect the quark masses of the first and second generation. Since they do not belong to the class of $\mathcal{O}\left(N_c^2\right)$ contributions, we note that we also do not include the numerically sizeable two-loop QCD corrections that have been calculated previously [51, 52, 56, 68].

The couplings relevant to us are α_{em}, α_t, and α_b. We go beyond Refs. [74–77] in including the dependence on the external momentum also for the Yukawa terms of $\mathcal{O}\left(N_c^2\right)$.

The MSSM in its most general R-parity conserving form—with complex parameters and taking into account all possible mixing contributions between the sfermions—has 124 input parameters compared to the 19 parameters in the SM [173, 200]. Despite having worked out the renormalisation for the most general case of complex parameters in Ch. 4, we restrict ourselves to $\mathcal{CP}$-conserving scenarios in the following analyses. As we have explained in Sect. 4.1, we also assume flavour diagonal squark mass matrices and a unit CKM matrix. This already greatly reduces the number of MSSM parameters entering our calculation.

In the Higgs-gauge sector, the most important parameters for a Higgs boson mass prediction are the mass of the $\mathcal{CP}$-odd Higgs boson, m_A, and the VEV ratio t_β. They fully determine the tree-level masses of the $\mathcal{CP}$-even Higgs bosons, see Eq. (4.46). Starting from the one-loop level, parameters from the squark sector also enter the mass prediction through self-energy diagrams containing squarks in the loops. These

parameters appear in the squark mass matrices given in Eqs. (4.3); we have the squark mass parameters $M_{\tilde{q}_g}$, $M_{\tilde{u}_g}$, and $M_{\tilde{d}_g}$ for each generation g, the trilinear couplings A_t and A_b,[13] and the higgsino mass parameters μ. All of these parameters have a non-vanishing mass dimension and, with the exception of μ, break supersymmetry softly. The trilinear couplings and μ determine the off-diagonal elements of the squark mass matrices and are hence responsible for the strength of the squark mass mixing. In our analysis, we typically set these parameters to one single common value, the SUSY scale M_S.
We investigate the calculated corrections for five different MSSM scenarios:

- The dependence of the light Higgs boson mass M_h on the SUSY scale M_S for $t_\beta = 15$ and $A_q = 0$.
- The dependence of the light Higgs boson mass M_h on the SUSY scale M_S for $t_\beta = 15$ and $A_q = -2M_S$.
- The dependence of the light Higgs boson mass M_h on the trilinear coupling A_q for $t_\beta = 15$ and $M_S = 1.5$ TeV.
- The dependence of the heavy Higgs boson mass M_H on the SUSY scale M_S for $t_\beta = 7$, $m_A = 750$ GeV, and $A_q = +2M_S$.
- The dependence of the $\mathcal{CP}$-even Higgs boson masses on the trilinear coupling A_q in the M_h^{125} scenario [133] for $t_\beta = 5$ and $m_A = 90$ GeV.

In order to estimate the size of the individual corrections contributing to the $\mathcal{O}\left(N_c^2\right)$ prediction, we perform calculations for different values of the coupling constants in each scenario. For the full prediction, we use the parameter values given below. Additionally, we make predictions for sufficiently small values for the electric charge and the bottom mass, the former allowing us to take the gaugeless limit (see Sect. 6.1) numerically. By appropriately adding and subtracting the different predictions, we can then separate the Yukawa contributions from the gauge contributions. The limit of vanishing bottom mass allows us to separate the dominant top contributions from the smaller bottom and the top-bottom-mixing contributions. The details are given in App. F.
Our scenarios respect the $\mathcal{CP}$ symmetry and hence only the $\mathcal{CP}$-even Higgs bosons h and H mix with each other. We therefore use an on-shell definition for the mass of the $\mathcal{CP}$-odd Higgs boson A. Furthermore, we use the on-shell renormalisation for

[13] The trilinear couplings A_u, A_c, A_d, and A_s do not appear in our calculation since we set the corresponding quark masses to zero.

t_β which we explained in detail in Sect. 4.3.3. For the quark-squark sector we choose a mixed on-shell-$\overline{\text{DR}}$ renormalisation; in the first four scenarios, we use the `MIX[2]` scheme while for the fifth we use the scheme `MIX[1]`, see Table 5.2.
The squared Higgs boson masses are calculated at the two-loop order according to the procedure explained in Sect. 3.2.3. For us, this means

$$\begin{aligned} M_h^2 &= m_h^2 - \operatorname{Re}\hat{\Sigma}^{(1)}_{hh}(m_h^2) - \operatorname{Re}\hat{\Sigma}^{(2)}_{hh}(m_h^2) \\ &\quad + \operatorname{Re}\left\{\hat{\Sigma}^{(1)}_{hh}(m_h^2)\partial\hat{\Sigma}^{(1)}_{hh}(m_h^2)\right\} - \operatorname{Re}\frac{\left(\hat{\Sigma}^{(1)}_{hH}(m_h^2)\right)^2}{m_H^2 - m_h^2}, \end{aligned} \tag{7.1a}$$

$$\begin{aligned} M_H^2 &= m_H^2 - \operatorname{Re}\hat{\Sigma}^{(1)}_{HH}(m_H^2) - \operatorname{Re}\hat{\Sigma}^{(2)}_{HH}(m_H^2) \\ &\quad + \operatorname{Re}\left\{\hat{\Sigma}^{(1)}_{HH}(m_H^2)\partial\hat{\Sigma}^{(1)}_{HH}(m_H^2)\right\} + \operatorname{Re}\frac{\left(\hat{\Sigma}^{(1)}_{hH}(m_H^2)\right)^2}{m_H^2 - m_h^2}. \end{aligned} \tag{7.1b}$$

It is important to note that the fixed-order approach via self-energies gives corrections to the squared Higgs boson masses since the mass parameters appearing in the Lagrangian are of mass dimension two, see Eq. (4.42). In order to be able to compare our results with the experimental value for the Higgs boson mass, which is of mass dimension one, we have to take the square root of the above expressions. This will naturally mix different contributions and orders of perturbation theory. For a full analysis, we therefore calculate:

- The Higgs boson mass, M_{h_i}. It contains the full tree-level as well as one-loop and two-loop contributions of order $\mathcal{O}(N_c)$ and $\mathcal{O}\left(N_c^2\right)$, respectively. It is obtained by simply taking the square root of the squared Higgs boson mass, see Eqs. (F.3). This calculation gives an estimate of the overall value of the Higgs boson mass (where, as explained above, numerically sizeable contributions that are not of $\mathcal{O}(N_c)$ or $\mathcal{O}\left(N_c^2\right)$ have not been incorporated).

- Two-loop contributions of $\mathcal{O}\left(N_c^2\right)$ to the squared Higgs boson mass, $\Delta^{(2)}M_{h_i}^2$. They are obtained by adding and subtracting different Higgs boson mass squares appropriately, see Eqs. (F.4). These calculations allow us to study the logarithmic dependence of the Higgs boson masses on e.g. the SUSY scale M_S without mixing contributions from different sectors of the theory and without mixing different orders of perturbation theory.

- Two-loop contributions of $\mathcal{O}\left(N_c^2\right)$ to the Higgs boson mass, $\Delta^{(2)}M_{h_i}$. They are calculated by subtracting different predictions for the Higgs boson mass, see Eqs. (F.5). These calculations allow us to compare the size of our newly calculated contributions to the experimental uncertainty of the observed Higgs

boson mass. This will mix contributions from different sectors as well as different orders of perturbation theory.

For our parameters, unless explicitly stated otherwise, we use the following values:

$$\begin{aligned}
\alpha_{\text{em}}^{-1} &= 137.035999084 \text{ [201]}, & \alpha_s &= 0, \\
\Delta\alpha_{\text{lep}}(M_Z^2) &= 0.031497687 \text{ [202]}, & \Delta\alpha_{\text{had}}^{(5)}(M_Z^2) &= 0.02766 \text{ [201]}, \\
M_Z &= 91.1876 \text{ GeV [201]}, & M_W &= 80.379 \text{ GeV [201]}, \\
m_u &= 0, & m_c &= 0, \\
m_t &= M_t = 172.76 \text{ GeV [201]}, & m_d &= 0, \\
m_s &= 0, & m_b &= 4.18 \text{ GeV [201]}, \\
t_\beta &= t_\beta^{\text{OS}} = 15, & m_A &= M_A = M_S, \\
M_{\tilde{q}_g}^2 &= M_S^2, & M_{\tilde{u}_g}^2 &= M_S^2, \\
M_{\tilde{d}_g}^2 &= M_S^2, & \mu &= M_S, \\
A_t &= A_q, & A_b &= A_q.
\end{aligned} \tag{7.2}$$

The trilinear couplings of the first and second generation do not need to be specified since only the product $m_q A_q$ enters the calculation, and the associated quark masses vanish in our approximation. The given top-quark mass is defined as the pole mass. We can estimate the size of the leading QCD corrections by comparing the one-loop predictions for the Higgs boson mass where we either use for m_t the value given above or the $\overline{\text{MS}}$ value at the scale M_t. The two masses are related by [32, 203]

$$m_t^{\overline{\text{MS}}}(M_t) = \frac{M_t}{1 + \frac{4}{3\pi}\alpha_s^{\overline{\text{MS}}}(M_t)}. \tag{7.3}$$

Using $\alpha_s^{\overline{\text{MS}}}(M_t) = 0.1079$ [204, 205], we find $m_t^{\overline{\text{MS}}}(M_t) \approx 165.2$ GeV.
All plots in the following analyses have been created using the pole mass value M_t as an input to our calculation. In the first three scenarios, we have also performed predictions at the one-loop level where we used the $\overline{\text{MS}}$ mass instead. The difference between a one-loop prediction using M_t and a one-loop prediction using $m_t^{\overline{\text{MS}}}(M_t)$ is formally of the two-loop order. While we have not included the predictions with the $\overline{\text{MS}}$ mass in the plots, we could estimate the size of the two-loop QCD corrections that have been omitted in our work by comparing the different predictions.

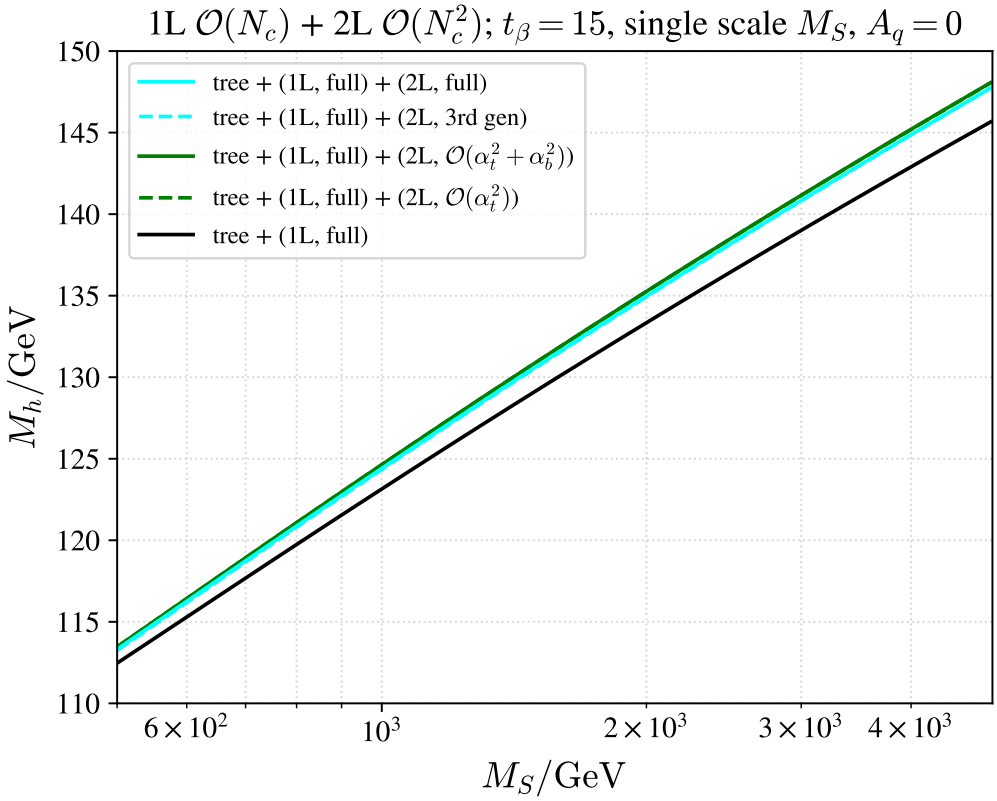

Figure 7.1: The dependence of the Higgs boson mass M_h on the SUSY scale M_S for $A_q = 0$. The solid cyan curve includes the tree-level prediction as well as the one-loop contributions of $\mathcal{O}(N_c)$ and the two-loop contributions of $\mathcal{O}\left(N_c^2\right)$. The dashed cyan curve takes into account only the third generation of quarks and squarks at the two-loop level. The green curves include only the $\mathcal{O}\left(N_c^2\right)$ Yukawa contributions at the two-loop level. The black curve shows the prediction of the Higgs boson mass at the one-loop order.

7.1 Scenario 1: The dependence of M_h on the scale M_S for $A_q = 0$

For our first scenario, we investigate how the mass of the light $\mathcal{CP}$-even Higgs boson, h, depends on the SUSY scale M_S. We set the VEV ratio $t_\beta = 15$ and we assume the third generation trilinear couplings, A_t and A_b, to vanish. The remaining soft SUSY-breaking parameters, the squark masses and μ, are set to the same value M_S. Furthermore, we set the $\mathcal{CP}$-odd mass m_A to M_S as well.

In Fig. 7.1, we give predictions for light $\mathcal{CP}$-even mass M_h at the one-loop (black curve) and two-loop level (cyan and green curves). The different two-loop predictions yield very similar predictions and, hence, not all curves are clearly visible in the plot. The solid cyan curve is obtained by including all two-loop contributions of $\mathcal{O}\left(N_c^2\right)$. For $M_S = 500$ GeV, the full two-loop contribution shifts the Higgs boson mass by

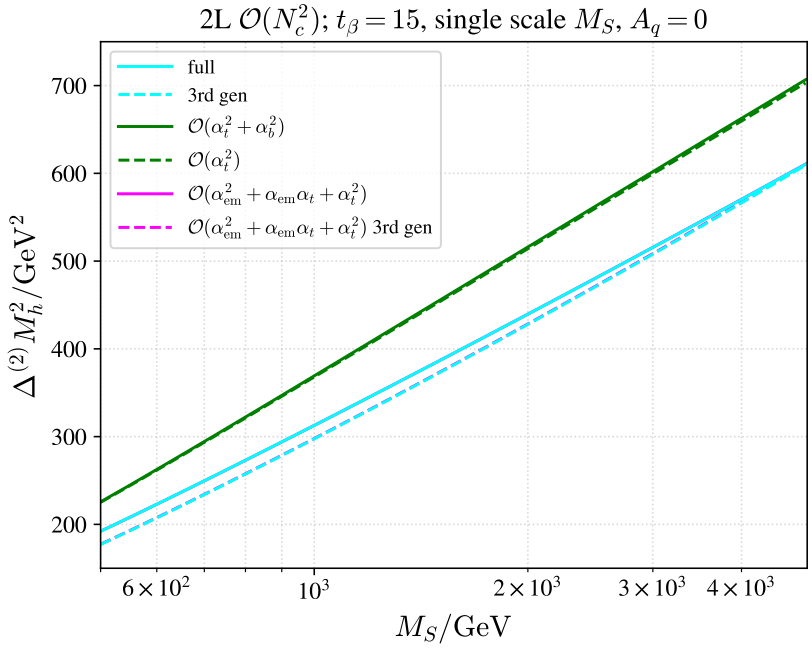

(a)

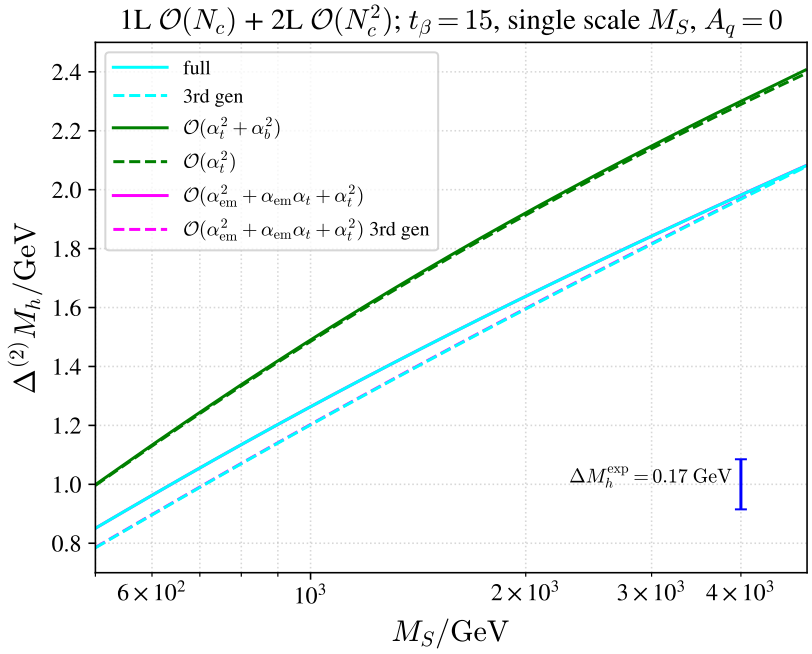

(b)

Figure 7.2: The leading two-loop contributions to the light Higgs boson mass M_h for $A_q = 0$. The solid cyan curve includes all two-loop contributions at $\mathcal{O}\left(N_c^2\right)$, the dashed cyan curve uses only contributions from the third generation. The green curves give the two-loop Yukawa contributions at $\mathcal{O}\left(N_c^2\right)$. The magenta curves do not contain contributions proportional to the bottom Yukawa coupling. In both plots, they lie under the cyan curves. The upper plot shows the contributions in terms of the squared Higgs boson mass, the lower plot in terms of the Higgs boson mass. In blue, we give the experimental uncertainty for the Higgs boson mass.

approximately 1 GeV while for $M_S = 5$ TeV the shift amounts to about 2 GeV. We stress again, that these results do not include any QCD corrections, which would lower the Higgs boson mass by 3–7.5 GeV in the current scenario. The size of the omitted QCD corrections was estimated by making a second one-loop prediction using $m_t = m_t^{\overline{\text{MS}}}(M_t)$ instead of the pole mass M_t, which was used in the creation of all plots in this chapter. We explain the determination of $m_t^{\overline{\text{MS}}}(M_t)$ below Eq. (7.2). In Fig. 7.2, we show the leading two-loop contributions in our first scenario. The pure Yukawa corrections, shown in green, are dominated by the top and stop contributions of $\mathcal{O}\left(\alpha_t^2\right)$. The bottom and sbottom contributions are negligible in this scenario. The cyan curves contain the full electroweak two-loop contributions of $\mathcal{O}\left(N_c^2\right)$. We also made a prediction in the limit $m_b \to 0$, which is supposed to be shown in magenta. Due to the aforementioned smallness of the $\mathcal{O}\left(\alpha_b^2\right)$ terms, the magenta curves are not distinguisable from the cyan ones and hence lie behind them.
The green curves represent the contributions of our calculation that were already known. The cyan curves additionally contain pure gauge ($\mathcal{O}\left(\alpha_{\text{em}}^2\right)$) and mixed gauge-Yukawa ($\mathcal{O}\left(\alpha_{\text{em}}\alpha_q\right)$) contributions, that were calculated for the first time in this thesis. Independently of the value chosen for M_S, these terms lower the $\mathcal{O}\left(N_c^2\right)$ two-loop corrections by approximately 15% of the pure Yukawa contributions (Fig. 7.2a). This reduction is even larger when regarding only the contributions of the third generation of quarks and squarks (the dashed cyan curve).
A similar relative size between the new contributions and the known Yukawa terms can be seen in Fig. 7.2b. From it we can infer that our additional contributions lead to a shift of the Higgs boson mass of 0.15 GeV for smaller values of M_S and more than 0.3 GeV for larger values. Again, this shift is even larger under exclusion of the first and second generation of squarks. In any case, the new contributions shift the mass of the light Higgs boson by an amount that is larger than the current experimental uncertainty.

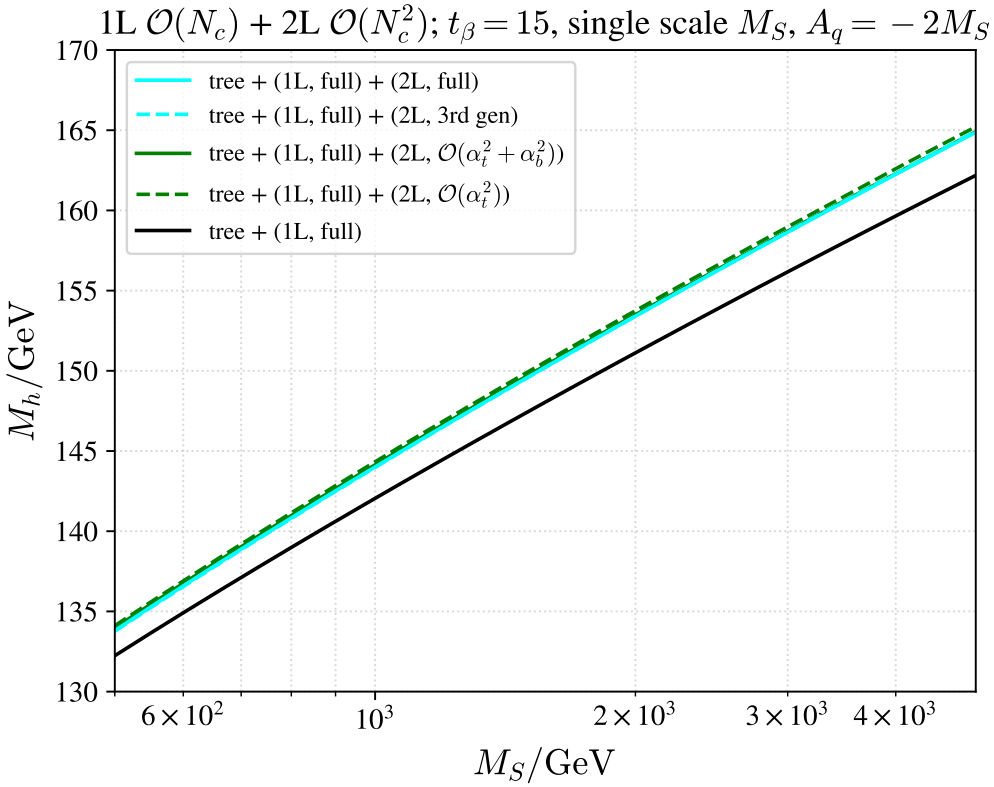

Figure 7.3: The dependence of the Higgs boson mass M_h on the SUSY scale M_S for $A_q = -2M_S$. The solid cyan curve includes the tree-level prediction as well as the one-loop contributions of $\mathcal{O}(N_c)$ and the two-loop contributions of $\mathcal{O}\left(N_c^2\right)$. The dashed cyan curve takes into account only the third generation of quarks and squarks at the two-loop level. The green curves include only the $\mathcal{O}\left(N_c^2\right)$ Yukawa contributions at the two-loop level. The black curve shows the prediction of the Higgs boson mass at the one-loop order.

7.2 Scenario 2: The dependence of M_h on the scale M_S for $A_q = -2M_S$

The second scenario uses the same parameters as the first one, the only difference is that the trilinear couplings are now set to $A_q = -2M_S$. The value of the stop-mixing parameter X_t is therefore close to the one for which the maximal value of M_h is obtained [133].

The light Higgs boson mass M_h now ranges between approximately 135 GeV and 165 GeV (Fig. 7.3) at the two-loop level and it is therefore considerably larger than the experimentally observed value. The cyan curves (full electroweak contributions) and the green curves (Yukawa terms only) are very similar in this plot and hence not all are clearly visible.

We emphasise again that we work only with part of the available two-loop contri-

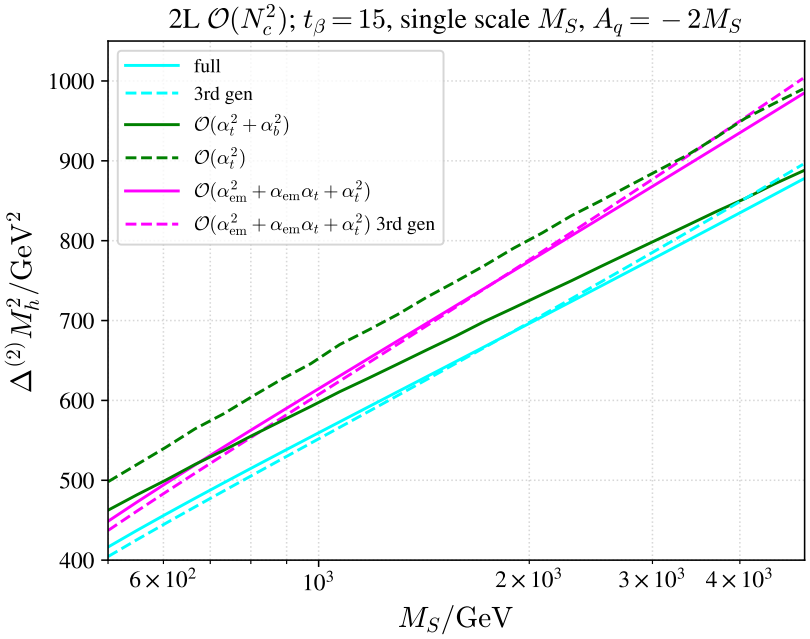

(a)

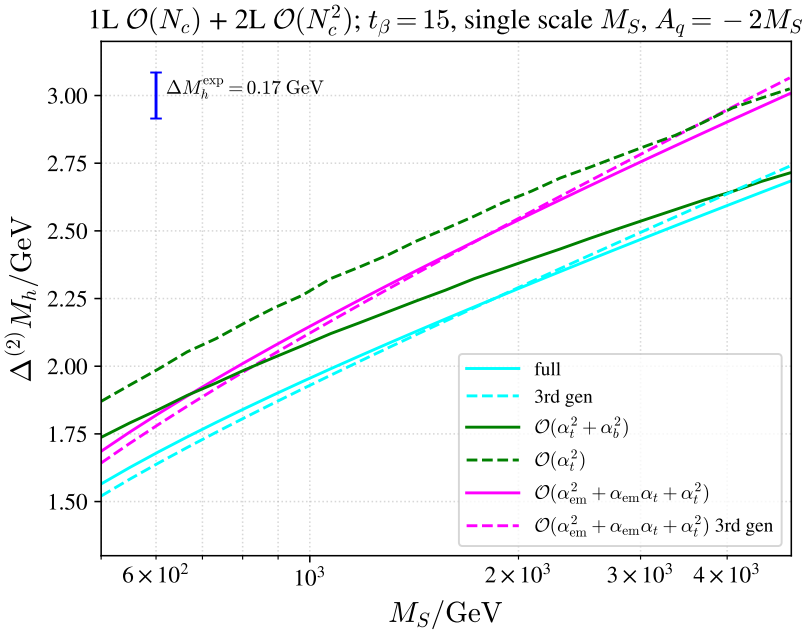

(b)

Figure 7.4: The leading two-loop contributions to the light Higgs boson mass M_h for $A_q = -2M_S$. The solid cyan curve includes all two-loop contributions at $\mathcal{O}\left(N_c^2\right)$, the dashed cyan curve uses only contributions from the third generation. The green curves give the two-loop Yukawa contributions at $\mathcal{O}\left(N_c^2\right)$. The magenta curves do not contain contributions proportional to the bottom Yukawa coupling. The upper plot shows the contributions in terms of the squared Higgs boson mass, the lower plot in terms of the Higgs boson mass. In blue, we give the experimental uncertainty for the Higgs boson mass.

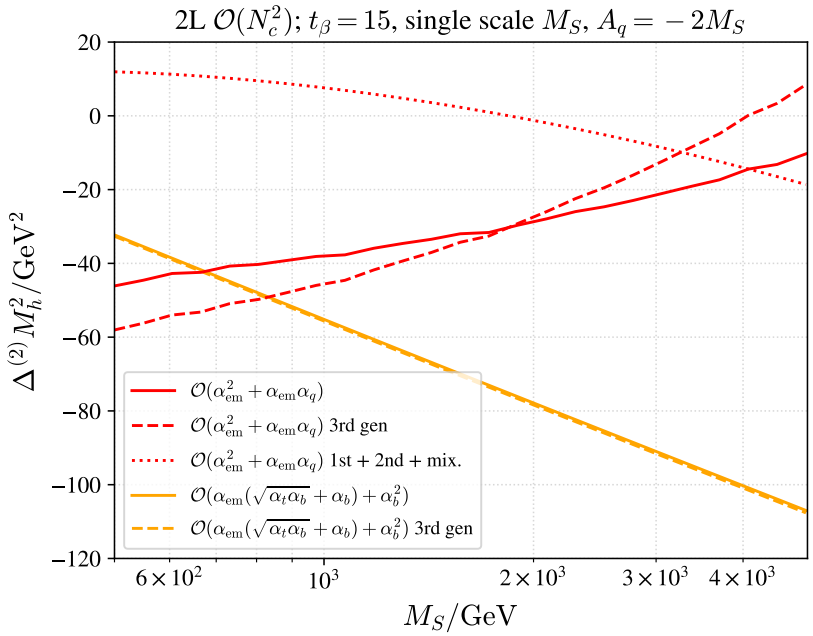

(a)

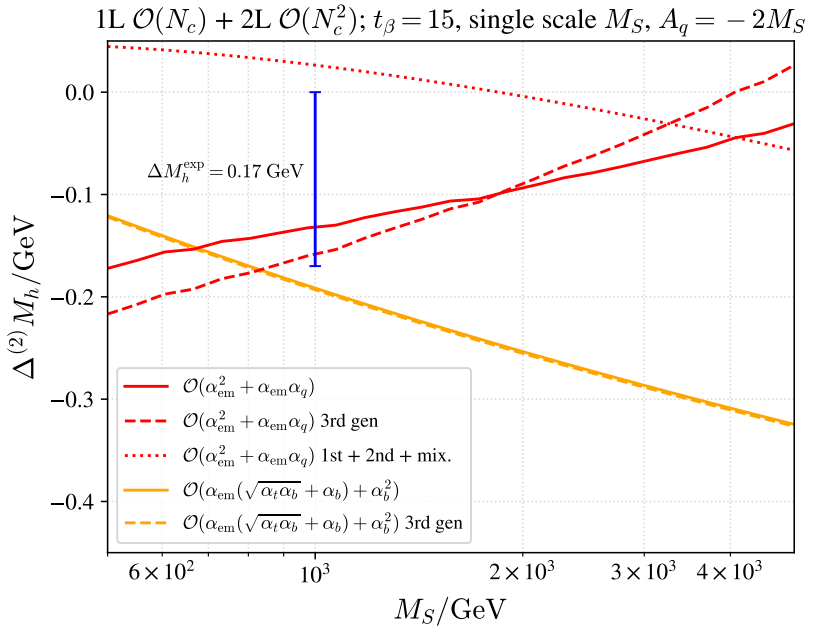

(b)

Figure 7.5: The subleading two-loop contributions to the light Higgs boson mass M_h for $A_q = -2M_S$. The red curves correspond to the contributions depending on the fine-structure constant α_{em}. The orange curves give the contributions which vanish in the limit $m_b \to 0$. The upper plot shows the contributions in terms of the squared Higgs boson mass, the lower plot in terms of the Higgs boson mass. In blue, we give the experimental uncertainty for the Higgs boson mass.

butions, as was explained before. The QCD contributions are expected to lower the Higgs boson mass by 5.5–9.5 GeV, as we have estimated by making two predictions at the one-loop level, using $m_t = m_t^{\overline{\rm MS}}(M_t)$ and $m_t = M_t$, respectively. All plots of this scenario were made using $m_t = M_t$. Our main focus, however, is again to estimate the size of our newly obtained corrections.

We have isolated the leading two-loop corrections in Fig. 7.4. Regarding the pure Yukawa corrections (green curves), we see that the bottom and sbottom contributions now make up a considerable part of the full Yukawa contribution. The full two-loop correction (solid cyan curve) is again dominated by the Yukawa terms; the combined gauge and the mixed gauge-Yukawa contributions make up between 1% for high M_S and 10% for low M_S of the full two-loop correction (Fig. 7.4a). This corresponds to a shift of 0.03–0.17 GeV for the Higgs boson mass prediction, as one can see in Fig. 7.4b. The bottom and sbottom contributions, on the other hand, give a shift of 0.12–0.32 GeV.

In Fig. 7.5, we give the subleading contributions to our Higgs mass prediction in the second scenario. They have been obtained by appropriate subtraction of the curves from Fig. 7.4. From Fig. 7.5a, we see that a cancellation takes place between the contributions from the quarks and squarks of the third generation (dashed red curve) and the combined first, second, and generation-mixing contributions (dotted red curve). Nevertheless, our newly obtained corrections (solid red curve) are comparable to the experimental uncertainty for not too large values of M_S, see Fig. 7.5b.

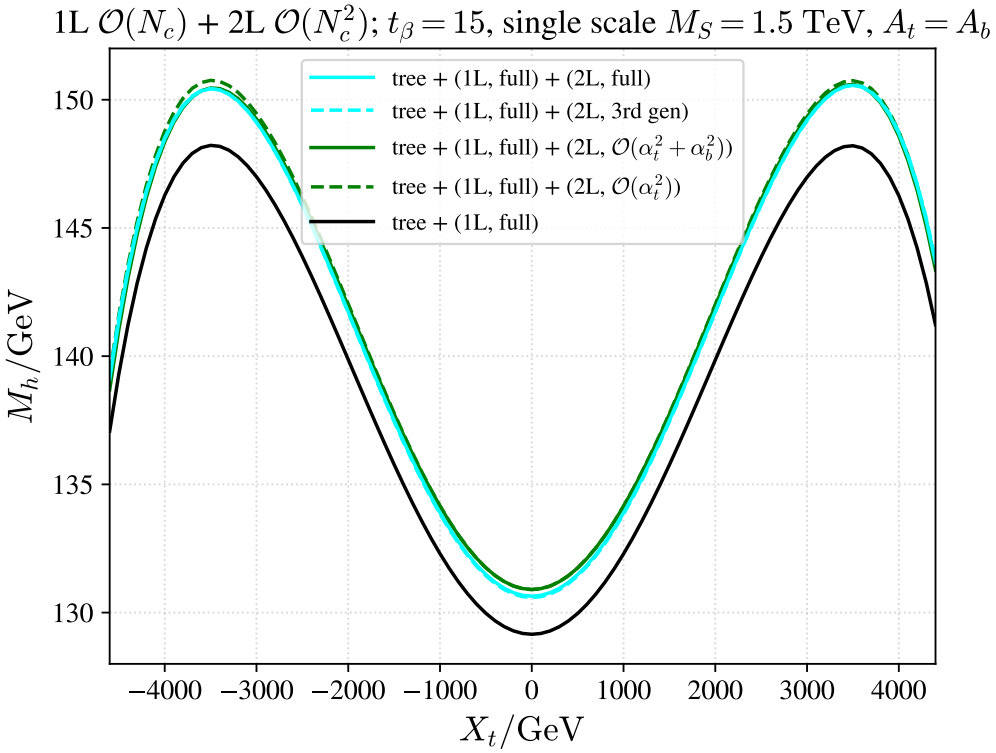

Figure 7.6: The dependence of the Higgs boson mass M_h on the trilinear coupling A_q. We plot the mass against the stop-mixing parameter $X_t = A_t - \mu/t_\beta$. The solid cyan curve includes the tree-level prediction as well as the one-loop contributions of $\mathcal{O}(N_c)$ and the two-loop contributions of $\mathcal{O}\left(N_c^2\right)$. The dashed cyan curve takes into account only the third generation of quarks and squarks at the two-loop level. The green curves include only the $\mathcal{O}\left(N_c^2\right)$ Yukawa contributions at the two-loop level. The black curve shows the prediction of the Higgs boson mass at the one-loop order.

7.3 Scenario 3: The dependence of M_h on the trilinear coupling A_q

In our third scenario, we analyse how our prediction for the mass of the light $\mathcal{CP}$-even Higgs boson depends on the trilinear couplings A_t and A_b. To this end, we will assume a single value for the trilinear couplings and set $A_t = A_q = A_b$. All other SUSY-breaking parameters, the higgsino mass parameter μ, and the mass of the $\mathcal{CP}$-odd Higgs boson m_A are set to the fixed value $M_S = 1.5$ TeV. Plots for this scenario are shown as a function of the stop-mixing parameter $X_t = A_t - \mu/t_\beta = A_q - \mu/t_\beta$. In Fig. 7.6, we show how our two-loop prediction for the Higgs boson pole mass M_h depends on A_q. As expected, the dependence on the parameter X_t is dominated by the well-known quartic dependence of the one-loop correction to the lightest $\mathcal{CP}$-even Higgs boson mass. This shape appears because, in the limit $M_S \gg m_t$, the

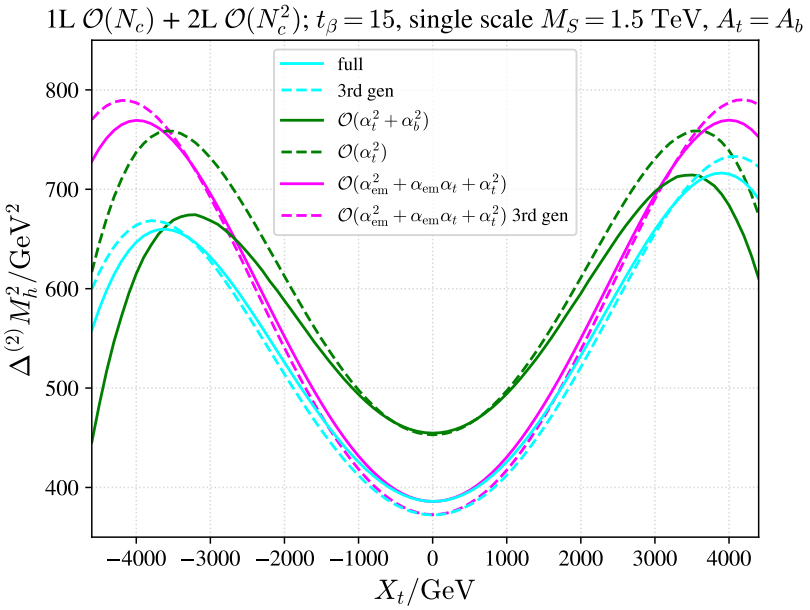

(a)

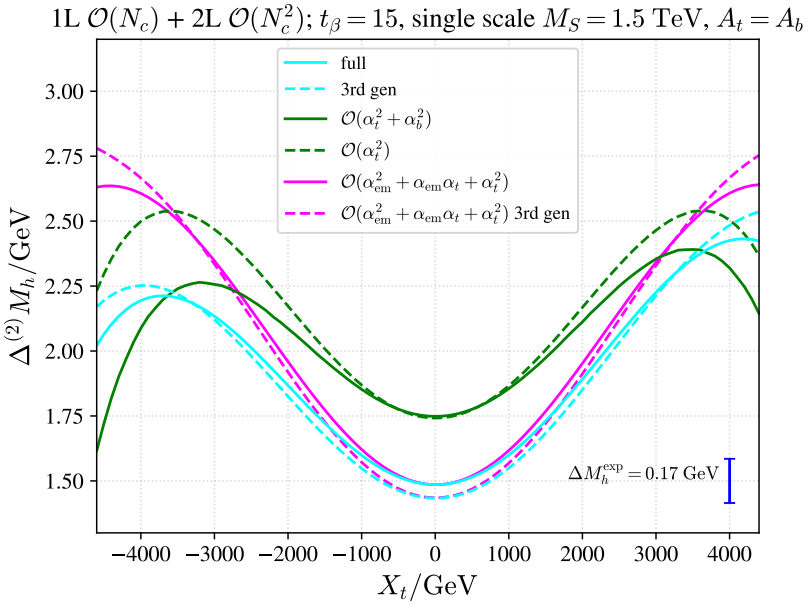

(b)

Figure 7.7: The leading two-loop contributions to the light Higgs boson mass M_h. We plot the corrections against the stop-mixing parameter $X_t = A_t - \mu/t_\beta$. The solid cyan curve includes all two-loop contributions at $\mathcal{O}\left(N_c^2\right)$, the dashed cyan curve uses only contributions from the third generation. The green curves give the two-loop Yukawa contributions at $\mathcal{O}\left(N_c^2\right)$. The magenta curves do not contain contributions proportional to the bottom Yukawa coupling. The upper plot shows the contributions in terms of the squared Higgs boson mass, the lower plot in terms of the Higgs boson mass. In blue, we give the experimental uncertainty for the Higgs boson mass.

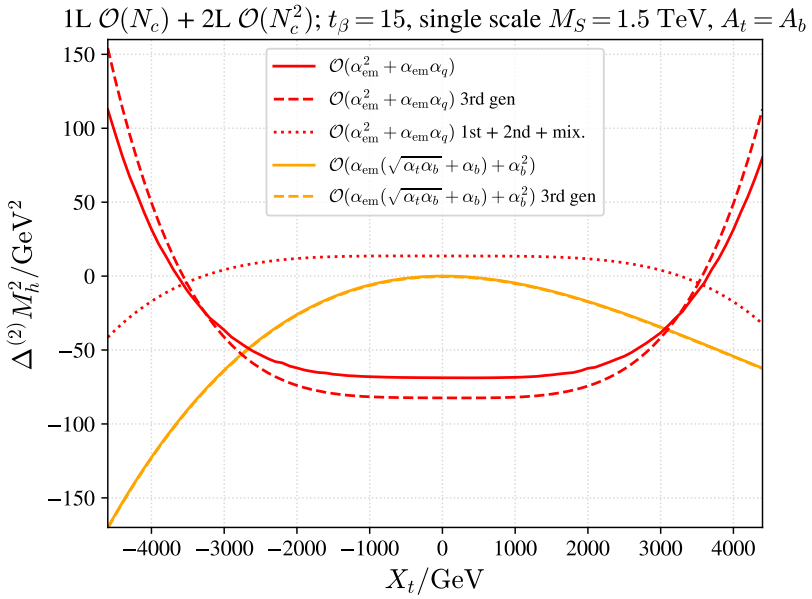

(a)

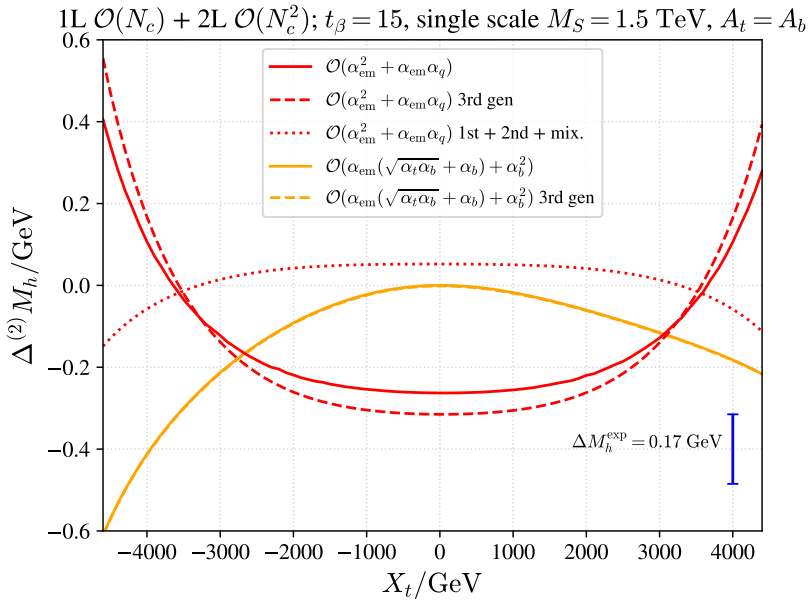

(b)

Figure 7.8: The subleading two-loop contributions to the light Higgs boson mass M_h. We plot the corrections against the stop-mixing parameter $X_t = A_t - \mu/t_\beta$. The red curves give the contributions depending on the fine-structure constant $\alpha_{\rm em}$. The orange curves give the contributions which vanish in the limit $m_b \to 0$. The upper plot shows the contributions in terms of the squared Higgs boson mass, the lower plot in terms of the Higgs boson mass. In blue, we give the experimental uncertainty for the Higgs boson mass.

dominant $\mathcal{O}(\alpha_t)$ contributions are [32, 140]

$$\Delta^{(1)} M_h^2 \overset{\mathcal{O}(\alpha_t)}{\approx} \frac{3m_t^4}{4\pi^2 v^2}\left(\log\frac{M_S^2}{m_t^2} + \frac{X_t^2}{M_S^2} - \frac{X_t^4}{12M_S^4}\right). \tag{7.4}$$

At $X_t = 0$, the stop-mixing matrix (see Eqs. (4.3)) is diagonal and the Higgs boson mass takes a minimal value of $M_h \approx 131$ GeV under inclusion of all electroweak two-loop contributions (solid cyan curve). In the same prediction, the mass becomes maximal with $M_h \approx 150$ GeV at $X_t \approx \pm\sqrt{6}M_S \approx \pm 3.7$ TeV. We estimate the leading two-loop QCD corrections to lower the overall value of the Higgs boson mass by 5–8 GeV in this scenario. This estimate was obtained by comparing two one-loop predictions, using $m_t = m_t^{\overline{\text{MS}}}(M_t)$ and $m_t = M_t$, respectively.

In Fig. 7.7, we show the dominant contributions in the third scenario. Here, we can see that the two-loop corrections shift the Higgs boson mass by 1.4–2.8 GeV (Fig. 7.7b), depending on the contributions chosen. Again, the Yukawa contributions make up the largest part of the two-loop contributions. The pure top contributions of $\mathcal{O}\left(\alpha_t^2\right)$ (dashed green curve) are very symmetric with respect to their dependence on X_t. When including also the bottom contributions (solid green curve), which are symmetric with respect to $X_b = A_b - \mu t_\beta$, the curve loses its X_t symmetry; for negative values of X_t, the pure bottom corrections are larger than for positive values of the same $|X_t|$ (see also Fig. 7.8). The bottom contributions lower the prediction by roughly 10%, as we can see from comparing the magenta curves with the cyan ones, or the dashed green one with the solid green curve in Fig. 7.7a.

The additional inclusion of gauge contributions (cyan curves) leaves the maximal value for the corrections largely unaffected (solid cyan vs. solid green). They, however, shift the position of the maximum to larger values of $|X_t| \approx 4$ TeV. The minimum remains at $X_t \approx 0$, but the gauge contributions lower it by around 0.25 GeV in comparison to the pure Yukawa corrections.

In Fig. 7.8, we show the subleading contributions in our third scenario. We can clearly see the aforementioned, strong asymmetry of the bottom corrections with respect to X_t. The corrections proportional to the gauge couplings are dominated by contributions from the third generation squarks, see Fig. 7.8a. In the whole range of $|X_t| < 2$ TeV, the gauge corrections lower the Higgs boson mass by more than 0.2 GeV and hence exceed the experimental uncertainty (Fig. 7.8b). In the same range, the gauge corrections which stem from the first and second generation squarks and generation mixing increase the Higgs boson mass by ~ 0.05 GeV.

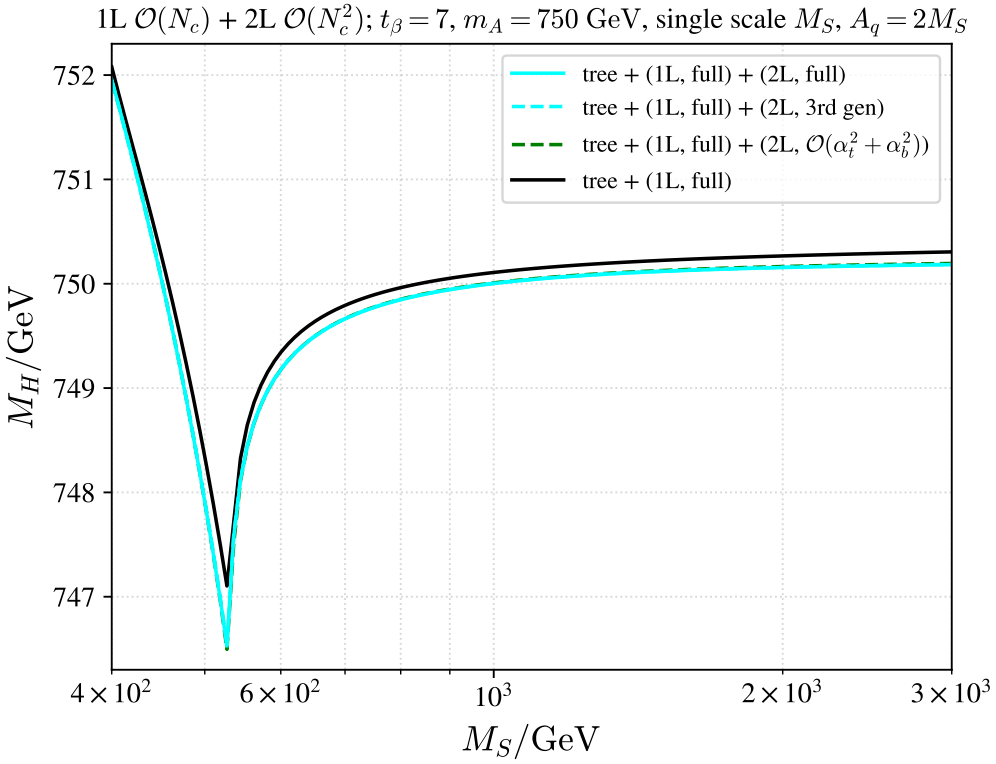

Figure 7.9: The dependence of the Higgs boson mass M_H on the SUSY scale M_S. The solid cyan curve includes the tree-level prediction as well as the one-loop contributions of $\mathcal{O}(N_c)$ and the two-loop contributions of $\mathcal{O}\left(N_c^2\right)$. The dashed cyan curve takes into account only the third generation of quarks and squarks at the two-loop level. The green curve includes only the $\mathcal{O}\left(N_c^2\right)$ Yukawa contributions at the two-loop level. The black curve shows the prediction of the Higgs boson mass at the one-loop order.

7.4 Scenario 4: The dependence of M_H on the SUSY scale M_S

In this scenario, we investigate how our newly calculated contributions affect the prediction for the mass of the heavy $\mathcal{CP}$-even MSSM Higgs boson H. These results are included for completeness; for a heavy $\mathcal{CP}$-even Higgs boson, the relative effects of the loop contributions are quite small, and it is not expected that the new two-loop contributions are numerically significant in this case.

We set $t_\beta = 7$, and for the mass of the $\mathcal{CP}$-odd Higgs boson we choose $m_A = 750$ GeV. We set the remaining SUSY-breaking parameters and the higgsino mass parameter to the common value M_S; for the trilinear couplings, in particular, we make the choice $A_q = +2M_S$. Within this framework, we vary M_S between 400 GeV and 3 TeV.

In Fig. 7.9, we show our prediction for the heavy Higgs boson mass M_H. The most

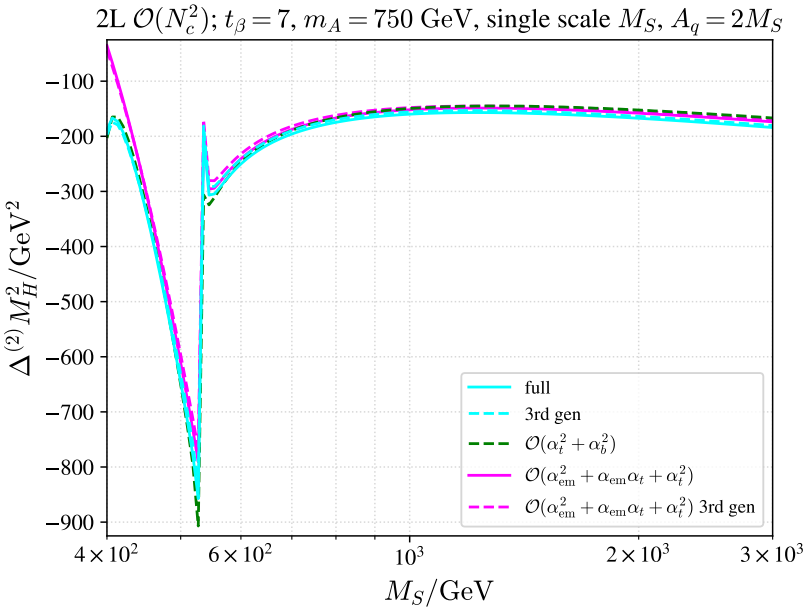

(a)

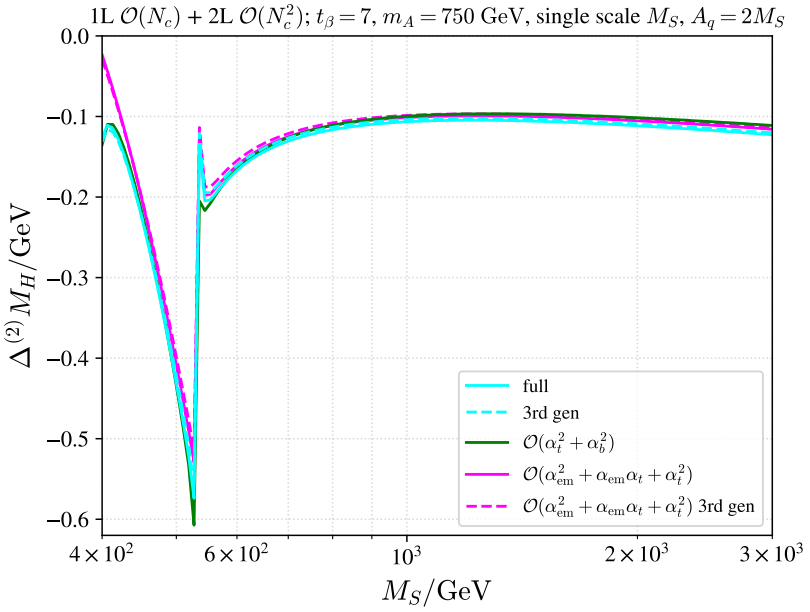

(b)

Figure 7.10: The leading two-loop contributions to the heavy Higgs boson mass M_H. The solid cyan curve includes all two-loop contributions at $\mathcal{O}\left(N_c^2\right)$, the dashed cyan curve uses only contributions from the third generation. The green curve gives the two-loop Yukawa contributions at $\mathcal{O}\left(N_c^2\right)$. The magenta curves do not contain contributions proportional to the bottom Yukawa coupling. The upper plot shows the contributions in terms of the squared Higgs boson mass, the lower plot in terms of the Higgs boson mass.

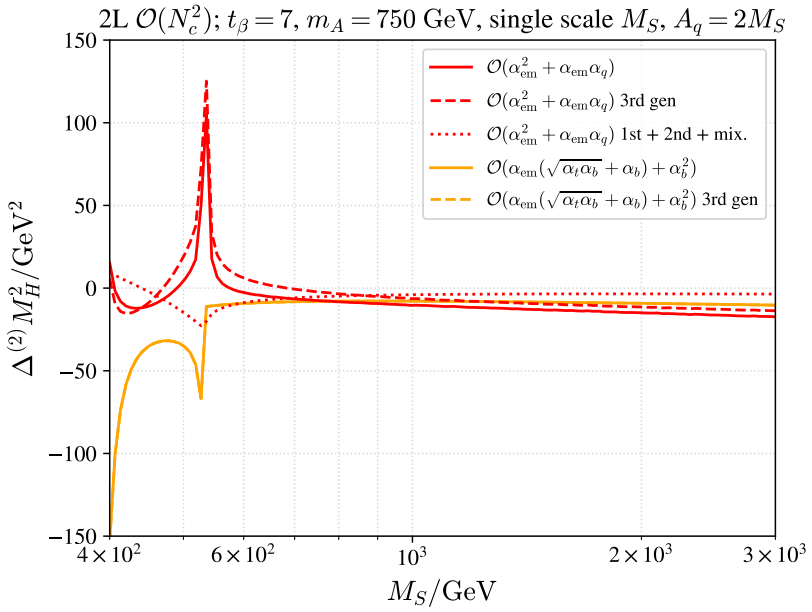

(a)

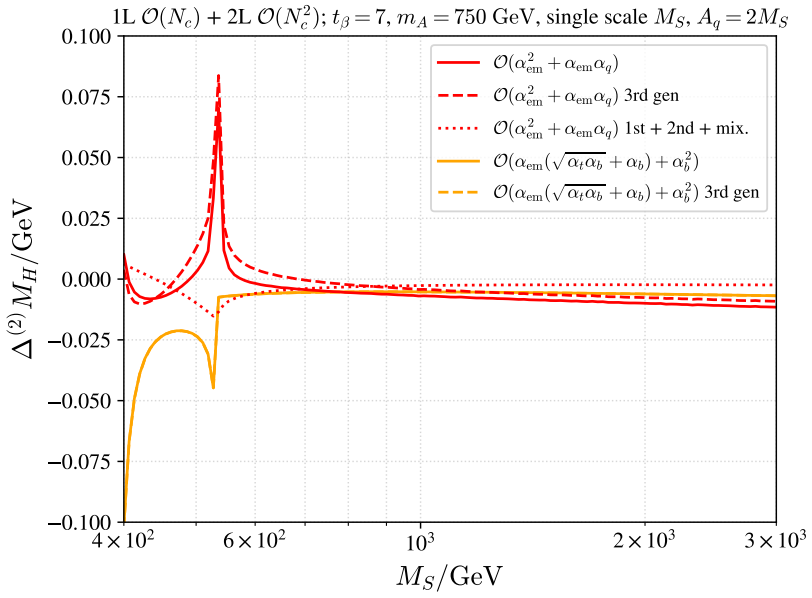

(b)

Figure 7.11: The subleading two-loop contributions to the heavy Higgs boson mass M_H. The red curves correspond to the contributions depending on the fine-structure constant $\alpha_{\rm em}$. The orange curves give the contributions which vanish in the limit $m_b \to 0$. The upper plot shows the contributions in terms of the squared Higgs boson mass, the lower plot in terms of the Higgs boson mass.

striking feature is a kink at $M_S \approx 530$ GeV, which is present in all the curves. These kinks are a result of Feynman diagrams like the "Top. 5" diagram shown in Fig. 6.1 with two internal light stop squark mass eigenstates $\tilde{t}_1$, that enter our prediction for the Higgs boson mass. At $M_S \approx 530$ GeV, the light stop squark $\tilde{t}_1$ has a mass of $m_{\tilde{t}_1} \approx 375$ GeV. Since we evaluate the self-energy at the tree-level value $p^2 = m_H^2 \approx 750$ GeV, this is the threshold value for M_S beyond which the internal stop squarks become to heavy to go on-shell. At this threshold, the derivative of the self-energy with respect to the squark mass is singular.[14] A precise prediction for the threshold region would require a dedicated analysis, for instance an expansion around the threshold, taking into account finite width effects of the internal stop squark.

In this scenario, the tree-level value of the heavy $\mathcal{CP}$-even Higgs boson is $m_H \approx 750.4$ GeV. The one-loop $\mathcal{O}(N_c)$ corrections lower the prediction by 0.1–0.3 GeV in the range $M_S = 1$–3 TeV (black curve in Fig. 7.9). For the same values of M_S, the full $\mathcal{O}\left(N_c^2\right)$ two-loop prediction yields a mass which is reduced by an additional 0.1 GeV (cyan vs. black curve in Fig. 7.9, cyan curve in Fig. 7.10b). We compare the relative size of our corrections against the already known Yukawa contribution in Fig. 7.10a; the green curve includes only the top and bottom Yukawa contributions while the cyan curves take into account the gauge contributions as well. The inclusion of gauge and gauge-Yukawa-mixing contributions further lowers the predicted Higgs boson mass, but only by $\approx 10\%$ of the two-loop Yukawa terms.

In Fig. 7.11, we further split up the gauge corrections (red curves) into the contributions originating from the third generation of squarks and the parts which are obtained from additionally including the first and second generation, and generation mixing. Like in the previous scenarios, the third generation contributions are responsible for the bulk of the gauge corrections (see Fig. 7.11a). This demonstrates that the $\mathcal{O}\left(\alpha_{\text{em}}\alpha_q\right)$ terms dominate the $\mathcal{O}\left(\alpha_{\text{em}}^2\right)$ terms. The gauge and gauge-Yukawa-mixing corrections lower the Higgs boson mass prediction by approximately 0.01 GeV for $M_S > 1$ TeV (see Fig. 7.11b).

[14] For a more detailed analysis of this feature, cf. Ref. [206].

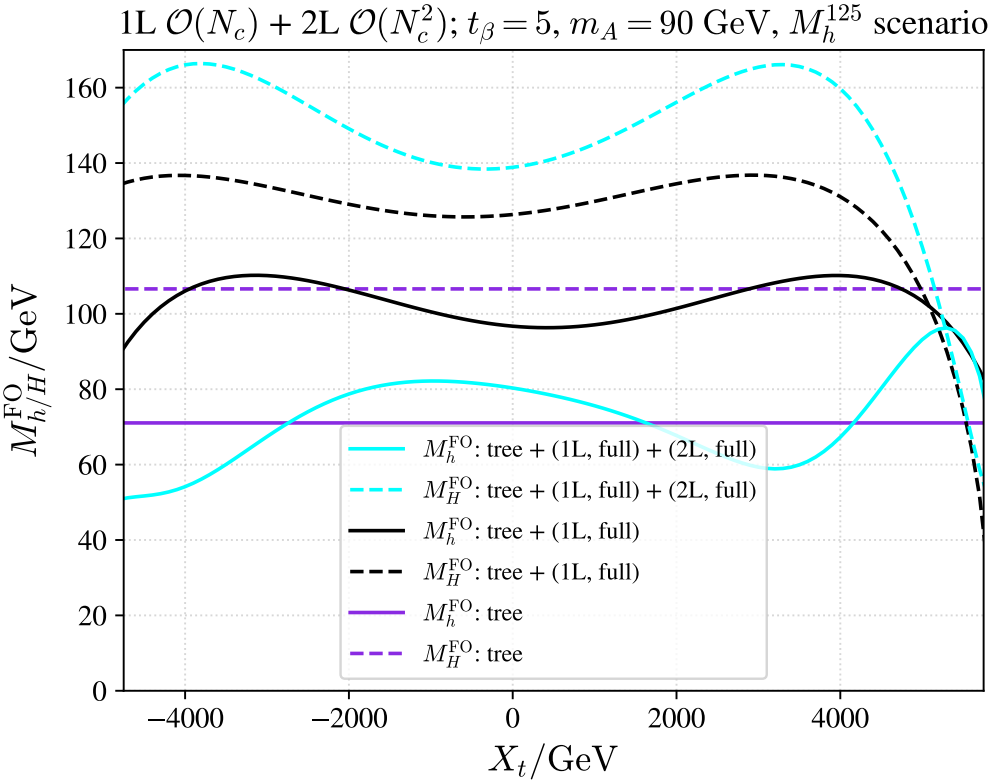

Figure 7.12: The dependence of the $\mathcal{CP}$-even Higgs boson masses, M_h and M_H, on the trilinear coupling A_q. We plot the masses against the stop-mixing parameter $X_t = A_t - \mu/t_\beta$. The cyan curves include the tree-level prediction as well as the one-loop contributions of $\mathcal{O}(N_c)$ and the two-loop contributions of $\mathcal{O}\left(N_c^2\right)$. The black curves show the prediction the Higgs boson masses omitting the two-loop contributions. The purple lines indicate the tree-level predictions. All curves have been generated by including all three generations of matter in a strict fixed-order approach (see Eqs. (7.1)).

7.5 Scenario 5: The Higgs boson masses in the M_h^{125} scenario with strong mixing

In the four scenarios discussed so far, we have exclusively used the fixed-order method (see Sect. 3.2.3) to predict the MSSM Higgs boson masses. This allowed us to cleanly separate the different contributions entering the prediction and, hence, we could compare the size of our newly calculated gauge and gauge-Yukawa-mixing terms of $\mathcal{O}\left((\alpha_{\mathrm{em}}^2 + \alpha_{\mathrm{em}}\alpha_q)N_c^2\right)$ against the already known pure Yukawa terms of $\mathcal{O}\left((\alpha_t^2 + \alpha_b^2)N_c^2\right)$. Such an approach yields a reliable prediction only when the difference between the tree-level masses m_h and m_H is sufficiently large (for a more detailed discussion, we refer the reader to Sect. 3.2.4). Until now, the tree-level mass split was sizeable enough for the fixed-order method to work.

In this fifth scenario, we now want to investigate a case where we can no longer

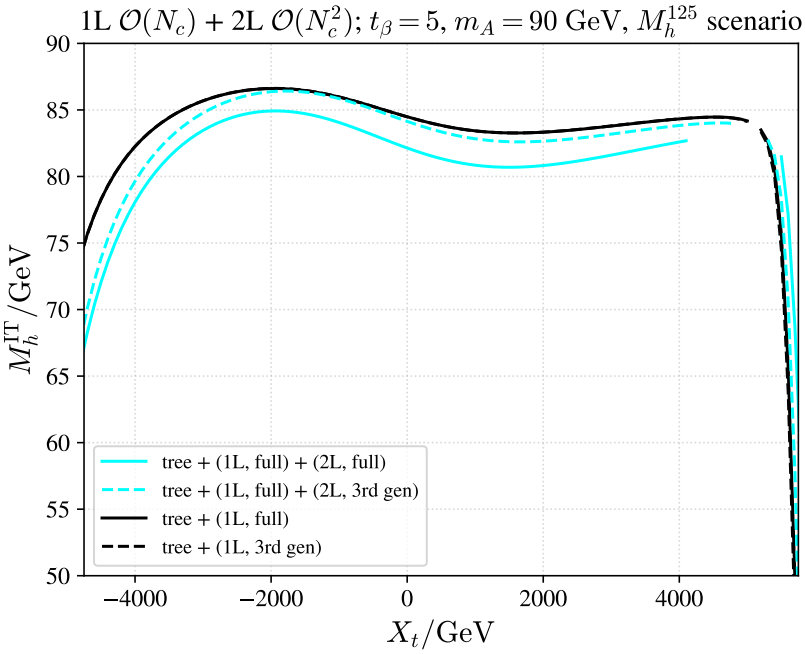

(a)

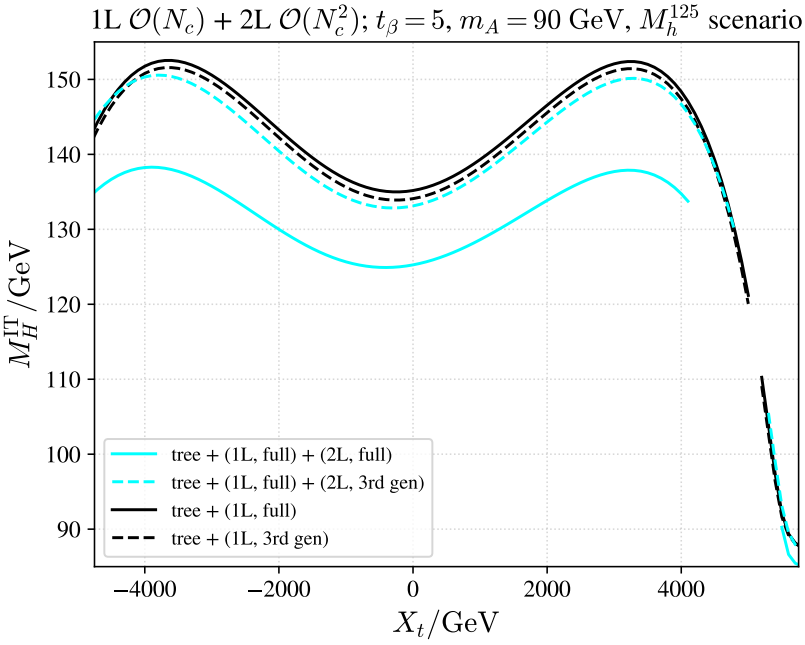

(b)

Figure 7.13: The dependence of the $\mathcal{CP}$-even Higgs boson masses, M_h and M_H, on A_q. The pole masses have been determined using a fixed-point iteration. We plot them against the stop-mixing parameter $X_t = A_t - \mu/t_\beta$. The cyan curves include the tree-level prediction as well as the one-loop contributions of $\mathcal{O}(N_c)$ and the two-loop contributions of $\mathcal{O}\left(N_c^2\right)$. The black curves show the prediction of the Higgs boson masses omitting the two-loop contributions. The solid curves have been generated by including all three generations of matter. The dashed curves include only contributions from the third generation.

predict the Higgs boson masses in a strict perturbative approach. Our scenario of choice is a slightly modified version of the "M_h^{125} scenario" as it has been defined in Ref. [133]. For the Standard Model parameters, we use their values given in Eqs. (7.2). For the MSSM parameters, we set

$$\begin{aligned} t_\beta &= 5, & m_A &= 90 \text{ GeV}, \\ M_{\tilde{q}_1}^2 &= M_{\tilde{u}_1}^2 = M_{\tilde{d}_1}^2 = (2 \text{ TeV})^2, & M_{\tilde{q}_2}^2 &= M_{\tilde{u}_2}^2 = M_{\tilde{d}_2}^2 = (2 \text{ TeV})^2, \\ M_{\tilde{q}_3}^2 &= M_{\tilde{u}_3}^2 = M_{\tilde{d}_3}^2 = (1.5 \text{ TeV})^2, & \mu &= 1 \text{ TeV}, \\ A_t &= A_q, & A_b &= A_q. \end{aligned} \tag{7.5}$$

The "M_h^{125} scenario" was designed such that with the theoretical prediction at that time one got a Higgs boson mass that was compatible with the experimental value within the theoretical uncertainties over a wide range of m_A and t_β. In this original version, the stop-mixing parameter X_t is fixed and hence determines the trilinear coupling A_q.

We pursue a different approach; we impose values for t_β and m_A, allowing us to investigate the dependence of the Higgs boson masses on the trilinear coupling A_q. We emphasise that a scenario with two light $\mathcal{CP}$-even states and a similarly light $\mathcal{CP}$-odd state is excluded by experimental measurements and searches. This scenario is, nevertheless, useful to showcase some interesting features of our newly calculated contributions. These features will be present in a similar manner for the mixing between the nearly mass-degenerate two heavy neutral Higgs bosons H and A in a $\mathcal{CP}$-violating scenario.

For our choice of parameters, the $\mathcal{CP}$-even tree-level masses are $m_h \approx 71$ GeV and $m_H \approx 107$ GeV, shown by the purple lines in Fig. 7.12. The difference between these tree-level values is small enough for large resonance effects to spoil the perturbative ansatz, as we can see from the loop-corrected masses (black and cyan curves in Fig. 7.12). The one-loop corrections shift M_h by up to 40 GeV, M_H is increased by up to 30 GeV. The two-loop corrections, on the other hand, lower M_h by more than 50 GeV around $X_t \approx 3$ TeV; the two-loop prediction for M_H is more than 30 GeV larger than the one-loop result for the same value of X_t. In this scenario, the perturbative series is no longer well-behaved if the pole masses are determined by a strict fixed-order approach. We therefore make use of the fixed-point iteration procedure, which we explained in Sect. 3.2.4, to reliably determine the pole masses. This also allows us to incorporate the momentum dependence of the $\mathcal{O}\left((\alpha_t^2 + \alpha_b^2)N_c^2\right)$ Yukawa terms, which has not been available before.

The results of the fixed-point iteration are shown in Fig. 7.13. The plots contain

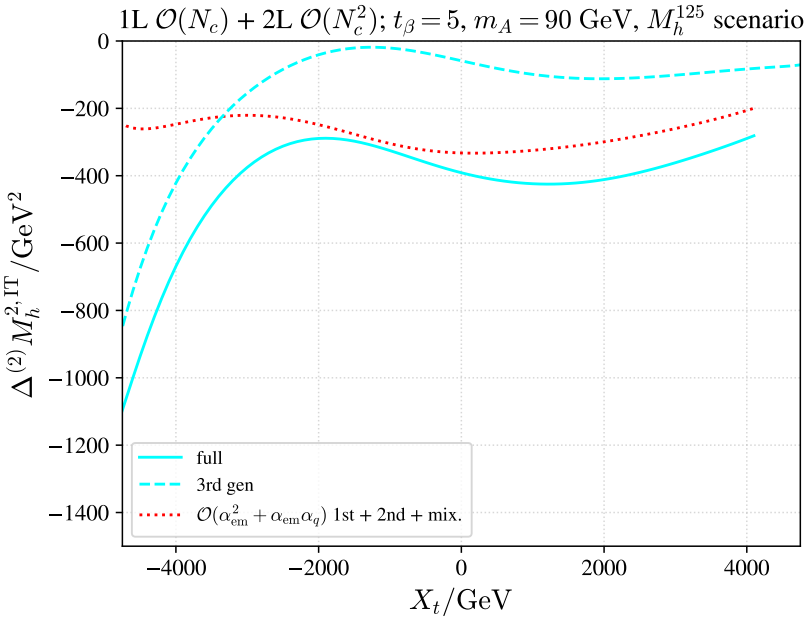

(a)

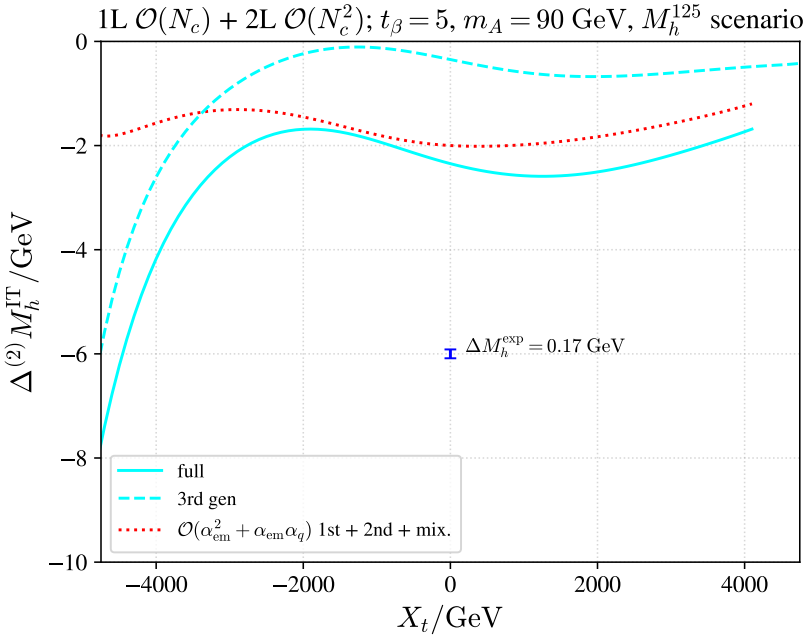

(b)

Figure 7.14: The two-loop contributions to the light Higgs boson mass M_h. The solid cyan curve includes all two-loop contributions at $\mathcal{O}\left(N_c^2\right)$, the dashed cyan curve uses only contributions from the third generation. The red curve gives the contributions that stem from the inclusion of the first and second generation of squarks as well as generation mixing. These contributions vanish in the gaugeless limit. The upper plot shows the contributions in terms of the squared Higgs boson mass, the lower plot in terms of the Higgs boson mass. In blue, we give the experimental uncertainty for the Higgs boson mass.

gaps in the region $X_t > 4$ TeV because, for these parameter points, the fixed-point iteration did not converge within the desired relative precision (10^{-5}) after a designated number of steps (~ 1000) .
In both cases, the two-loop predictions are much closer to the one-loop results than they were in Fig. 7.12. In contrast to the fixed-order method, for which the hierarchy between the tree-level mass eigenstates h and H got inverted at around $X_t \approx 5$ TeV, we now also have a clear separation between the masses. With the iterated procedure, the lighter mass M_h is always lower than 90 GeV (Fig. 7.13a) while the heavier mass exceeds 120 GeV for $X_t < 4$ TeV (Fig. 7.13b).
The most astonishing feature of the iterated results is the large difference between the two-loop predictions which include either all (s)quarks (solid cyan) or only the third generation (dashed cyan). For the light mass M_h (for which the two-loop contributions are shown in Fig. 7.14b), the inclusion of the first and second generation as well as generation mixing lowers the Higgs mass prediction by around 2 GeV across the whole considered range of X_t. The effect of these contributions exceeds the experimental uncertainty by one order of magnitude and is also responsible for the bulk of the two-loop corrections for $X_t > -3$ TeV. In Fig. 7.14a we can see that they are two to three times larger than the contributions which stem from the third generation alone (dotted red curve vs dashed cyan curve).
In this scenario, we have have showcased that a strict fixed-order method can lead to unreliable predictions for pole masses if the states that mix with each other have sufficiently similar tree-level masses. A fixed-point iteration, which determines the exact location of the propagator pole, remedies the issues of the fixed-order approach at the cost of mixing different loop orders and contributions. In our case, the inclusion of gauge and gauge-Yukawa-mixing contributions, which we calculated for the first time in this thesis, leads to a large shift of the Higgs boson masses in such a scenario. We stress again, however, that a scenario with two light $\mathcal{CP}$-even Higgs bosons is excluded by experimental observations while similar mixing scenarios can appear between the heavy $\mathcal{CP}$-even H and $\mathcal{CP}$-odd A bosons if $\mathcal{CP}$-violating phases are non-zero.

8 Conclusions and outlook

Despite the undisputed success of the Standard Model of Particle Physics, its many phenomenological and theoretical shortcomings have sparked the search for more advanced models in an attempt to remedy these issues. Since many years, one of the most promising candidates for a Standard Model extension is the MSSM, which combines the SM with a softly broken supersymmetry. While so far no superpartners have been discovered, the MSSM remains well-motivated since it addresses many of the shortcomings of the SM.

The probably most striking feature of the MSSM is that it relates the masses of the various Higgs bosons to other parameters. Therefore, the Higgs boson masses can be predicted from the model. Different approaches have been pursued in order to obtain such predictions with sufficient accuracy, one of which is a perturbative pole mass calculation in terms of self-energy Feynman diagrams. So far, all one-loop contributions, the leading two-loop terms, and some three-loop parts have been determined for the MSSM Higgs boson masses. In this thesis, we focused on so-far undetermined two-loop terms of $\mathcal{O}\Big((\alpha_{\text{em}} + \alpha_q)^2 N_c^2\Big)$, which are expected to constitute the dominant part of those two-loop electroweak corrections that had not been known up to now. From this class of contributions, only the pure Yukawa subpart of $\mathcal{O}\Big(\alpha_q^2 N_c^2\Big)$ was known so far, albeit in the limit of vanishing external momentum only.

The inclusion of pure gauge and gauge-Yukawa-mixing contributions required us to generalise a relation between two-loop mass counterterms of Higgs, would-be Goldstone, and gauge bosons in order to obtain a finite result for the neutral Higgs boson self-energies in a $\mathcal{CP}$-violating scenario. If $\mathcal{CP}$ symmetry holds, the prediction for the masses of the charged bosons is finite only if the more general relation is considered. To our best knowledge, this new relation had not been known in the literature up to now; the additional terms do not contribute at the order of perturbation theory analysed in the existing literature and, therefore, were not taken into account. Additionally, we generalised the modified two-loop relation to an expression that holds in all orders of perturbation theory (Eq. (4.54b)).

In our calculation, we employed a mixed OS-$\overline{\text{DR}}$ renormalisation scheme at the

two-loop level. In Sect. 5.4, we studied how the choice of renormalisation scheme has an influence on which parts of one-loop integrals enter the final prediction for the Higgs boson mass. We concluded that, in a fixed-order prediction with on-shell self-energies, both a full OS renormalisation and a full $\overline{\text{DR}}$ renormalisation lead to a total cancellation of $\mathcal{O}(\varepsilon)$ parts of the loop integrals. In case a mixed renormalisation scheme is used, all two-loop parameter counterterms need to be defined in a momentum-subtraction scheme for this cancellation to take place. We stress that the dependence of a pole mass prediction on $\mathcal{O}(\varepsilon)$ terms of loop integrals is a spurious one in the sense that these terms always drop out in relations between physical observables. Furthermore, a scheme involving uncancelled $\mathcal{O}(\varepsilon)$ contributions cannot be translated into a different scheme via the usual kind of reparameterisation.
As we opted for a mixed renormalisation scheme, we required an OS definition at the one- and two-loop level for the VEV ratio parameter t_β.[15] We have performed the OS renormalisation via the decay $A \to \tau^-\tau^+$ by requiring the absolute square of the associated physical amplitude to not receive any higher order corrections. If this decay were to be observed, a numerical value for t_β^{OS} could be extracted from its measurement. We checked that our definition of the one-loop (Eq. (4.150)) and the two-loop (Eq. (4.159)) counterterm does not depend on the choice of the field renormalisations. As expected, this definition of t_β leads to a total cancellation of the $\mathcal{O}(\varepsilon)$ terms of loop integrals in the Higgs boson pole mass prediction at the two-loop order.
In Ch. 7, we have made predictions for the neutral MSSM Higgs boson masses in five different, $\mathcal{CP}$-conserving scenarios including our newly calculated contributions. We have compared their size against the already known pure Yukawa contributions of $\mathcal{O}\left(N_c^2\right)$ and also against the experimental uncertainty of the Higgs boson mass measurement. While expectedly smaller than the pure Yukawa contributions (by typically an order of magnitude), the pure gauge and gauge-Yukawa-mixing terms were larger than or at least of a similar size as the experimental uncertainty. Their inclusion in any full MSSM Higgs mass prediction will therefore lower the theoretical uncertainty significantly. In the fifth scenario, we have also showcased the fact that a strict fixed-order treatment becomes insufficient for cases where there is large mixing between particles that are nearly mass-degenerate at lowest order. We showed that only the fixed-point iteration leads to a reliable prediction in this case, but at the cost of mixing different orders of perturbation theory. Depending on the investigated scenario, the appropriate method has to be chosen and the drawbacks of each approach have to be taken into account.

[15] In the literature, this parameter is more commonly defined as a $\overline{\text{DR}}$ quantity.

We want to close this thesis by giving a brief outlook. The renormalisation of the MSSM Higgs-gauge sector that we have carried out in detail at the two-loop level includes full electroweak effects and goes significantly beyond the renormalisation of electroweak two-loop contributions in the MSSM performed elsewhere. The obtained results should hence be useful for any future prediction heading in a similar direction. We expect that the ingredients of the analyses in this thesis can directly be transferred to a more general n-loop order calculation of electroweak $\mathcal{O}(N_c^n)$ terms as well; these contributions will similarly decompose into products of one-loop integrals for the Higgs and vector boson self-energies. It remains to be seen whether the renormalisation of the quark-squark sector, which for the two-loop predictions of the Higgs boson masses carried out in this thesis were needed only at the one-loop order, can as easily be extended to the two-loop case.

Since the renormalisation described in this work was performed allowing for $\mathcal{CP}$-violating phases of MSSM parameters, the study of $\mathcal{CP}$-violating scenarios requires only little additional work. The OS renormalisation of t_β in terms of a charged Higgs boson decay like $H^+ \to \tau^+\nu_\tau$ (instead of $A \to \tau^-\tau^+$) is expected to be straightforward. The relevant Slavnov-Taylor identities involving charged particles are included in App. B alongside the ones for the neutral particles.

Electroweak two-loop contributions of $\mathcal{O}\left(N_c^2\right)$ also appear in extensions of the MSSM, like e.g. the *Next-to-Minimal Supersymmetric Standard Model* (NMSSM). Our results can therefore serve as a building block for similar calculations in extended SUSY models as well.

Going beyond the particular relevance for supersymmetric models, our work has led to new insights about the renormalisation of a specific theory, but also about the application of quantum field theories in general. Most four-dimensional quantum field theories have to be treated with regularisation and renormalisation, and understanding these procedures is of utmost importance. Unstable particles and particle mixing are present in a wide variety of physical models and their proper treatment is paramount in order to provide accurate theory predictions.

Acknowledgements

First and foremost, I want to express my deepest gratitude to Georg Weiglein, who supervised me for the last four and a half years. His in-depth knowledge about quantum field theories, Higgs bosons, and physics in general was a great guide on my journey that ultimately culminated in this work. Georg's never-ending patience allowed me to progress at my own pace and lead to many fascinating discoveries that otherwise might have never been made. Our weekly discussions on both physics and the Bundesliga were as much educating as they were entertaining. I could not have wished for a better supervisor.

I also want to thank Henning Bahl, whose input in the weekly meetings was invaluable. Whenever it felt like I had hit a dead end in one of my approaches, Henning came up with an idea that lead me back on track. His extensive proof-reading of this work in its entirety helped to elevate it to its current form.

Furthermore, I want to thank Geraldine Servant, who is the second assessor of my dissertation. I also thank my DESY mentor Volker Schomerus. Thanks also to Michael Potthoff, Timo Weigand, and Christian Schwanenberger for agreeing to be part of the examination commission of my disputation.

I also want to thank all the amazing people I met and the good friends I made during my time at DESY and in Hamburg. All of you made my time here more enjoyable than I could have ever imagined. Thank you, Áron, Berthold, Finn, Gaia, Georgios, Helen, Ivan, Jan H., Jan S.-E., Laura, Malte, Marius, Melina, Nico, Philipp, Stefan, Stella, Tjaard, and Victor.

Last but not least, I also want to thank my parents Minni and Heinz-Willi. Their emotional, financial and parental support not only during my time in Hamburg but all the time before as well always allowed me to fully focus on my work and my studies. Without you, nothing of this would have been possible.

A One- and two-loop field and parameter counterterms

In this appendix, we give the one- and two-loop expressions for the counterterms of all Higgs boson mass parameters appearing in Eq. (4.42). The counterterms will be expressed as combinations of the one- and two-loop counterterms of the input parameters. The renormalisation of the input parameters is explained in Sects. 4.2.2 and 4.2.3. We also relate the renormalisation constants of the Higgs fields to the Higgs doublet counterterms.

A.1 One-loop counterterms

A.1.1 One-loop mass counterterms

$$\begin{aligned}
\delta^{(1)}m_h^2 = {}& \delta^{(1)}m_A^2 c_{\alpha-\beta}^2 + \delta^{(1)}M_Z^2 s_{\alpha+\beta}^2 \\
& + \delta^{(1)}t_\beta c_\beta^2 \Big(m_A^2 s_{2(\alpha-\beta)} + M_Z^2 s_{2(\alpha+\beta)}\Big) \\
& + \frac{e s_{\alpha-\beta}}{2M_W s_\mathrm{w}} \Big(\delta^{(1)}T_h (1 + c_{\alpha-\beta}^2) + \delta^{(1)}T_H c_{\alpha-\beta} s_{\alpha-\beta}\Big),
\end{aligned} \tag{A.1a}$$

$$\begin{aligned}
\delta^{(1)}m_{hH}^2 = {}& \delta^{(1)}m_A^2 c_{\alpha-\beta} s_{\alpha-\beta} - \delta^{(1)}M_Z^2 c_{\alpha+\beta} s_{\alpha+\beta} \\
& - \delta^{(1)}t_\beta c_\beta^2 \Big(m_A^2 c_{2(\alpha-\beta)} + M_Z^2 c_{2(\alpha+\beta)}\Big) \\
& - \frac{e}{2M_W s_\mathrm{w}} \Big(\delta^{(1)}T_h c_{\alpha-\beta}^3 - \delta^{(1)}T_H s_{\alpha-\beta}^3\Big),
\end{aligned} \tag{A.1b}$$

$$\begin{aligned}
\delta^{(1)}m_H^2 = {}& \delta^{(1)}m_A^2 s_{\alpha-\beta}^2 + \delta^{(1)}M_Z^2 c_{\alpha+\beta}^2 \\
& - \delta^{(1)}t_\beta c_\beta^2 \Big(m_A^2 s_{2(\alpha-\beta)} + M_Z^2 s_{2(\alpha+\beta)}\Big) \\
& - \frac{e c_{\alpha-\beta}}{2M_W s_\mathrm{w}} \Big(\delta^{(1)}T_h c_{\alpha-\beta} s_{\alpha-\beta} + \delta^{(1)}T_H (1 + s_{\alpha-\beta}^2)\Big),
\end{aligned} \tag{A.1c}$$

$$\begin{aligned}
\delta^{(1)}m_{AG}^2 = {}& - \delta^{(1)}t_\beta c_\beta^2 m_A^2 \\
& - \frac{e}{2M_W s_\mathrm{w}} \Big(\delta^{(1)}T_h c_{\alpha-\beta} + \delta^{(1)}T_H s_{\alpha-\beta}\Big),
\end{aligned} \tag{A.1d}$$

$$\delta^{(1)}m_G^2 = \frac{e}{2M_W s_\mathrm{w}} \Big(\delta^{(1)}T_h s_{\alpha-\beta} - \delta^{(1)}T_H c_{\alpha-\beta}\Big), \tag{A.1e}$$

$$\delta^{(1)} m_{hA}^2 = \frac{e s_{\alpha-\beta}}{2 M_W s_\mathrm{w}} \delta^{(1)} T_A, \tag{A.1f}$$

$$\delta^{(1)} m_{HA}^2 = -\frac{e c_{\alpha-\beta}}{2 M_W s_\mathrm{w}} \delta^{(1)} T_A, \tag{A.1g}$$

$$\delta^{(1)} m_{hG}^2 = \frac{e c_{\alpha-\beta}}{2 M_W s_\mathrm{w}} \delta^{(1)} T_A = -\delta^{(1)} m_{HA}^2, \tag{A.1h}$$

$$\delta^{(1)} m_{HG}^2 = \frac{e s_{\alpha-\beta}}{2 M_W s_\mathrm{w}} \delta^{(1)} T_A = \delta^{(1)} m_{hA}^2, \tag{A.1i}$$

$$\begin{aligned} \delta^{(1)} m_{H^- G^+}^2 = & -\delta^{(1)} t_\beta c_\beta^2 m_{H^\pm}^2 \\ & - \frac{e}{2 M_W s_\mathrm{w}} \Big(\delta^{(1)} T_h c_{\alpha-\beta} + \delta^{(1)} T_H s_{\alpha-\beta} - \mathrm{i} \delta^{(1)} T_A \Big), \end{aligned} \tag{A.1j}$$

$$\begin{aligned} \delta^{(1)} m_{G^- H^+}^2 = & -\delta^{(1)} t_\beta c_\beta^2 m_{H^\pm}^2 \\ & - \frac{e}{2 M_W s_\mathrm{w}} \Big(\delta^{(1)} T_h c_{\alpha-\beta} + \delta^{(1)} T_H s_{\alpha-\beta} + \mathrm{i} \delta^{(1)} T_A \Big) \\ = & \Big(\delta^{(1)} m_{H^- G^+}^2 \Big)^*, \end{aligned} \tag{A.1k}$$

$$\delta^{(1)} m_{G^\pm}^2 = \frac{e}{2 M_W s_\mathrm{w}} \Big(\delta^{(1)} T_h s_{\alpha-\beta} - \delta^{(1)} T_H c_{\alpha-\beta} \Big) = \delta^{(1)} m_G^2. \tag{A.1l}$$

A.1.2 One-loop field counterterms

$$\delta^{(1)} Z_{hh} = s_\alpha^2 \delta^{(1)} Z_{\mathcal{H}_1} + c_\alpha^2 \delta^{(1)} Z_{\mathcal{H}_2}, \tag{A.2a}$$

$$\delta^{(1)} Z_{hH} = s_\alpha c_\alpha \Big(\delta^{(1)} Z_{\mathcal{H}_2} - \delta^{(1)} Z_{\mathcal{H}_1} \Big), \tag{A.2b}$$

$$\delta^{(1)} Z_{HH} = c_\alpha^2 \delta^{(1)} Z_{\mathcal{H}_1} + s_\alpha^2 \delta^{(1)} Z_{\mathcal{H}_2}, \tag{A.2c}$$

$$\delta^{(1)} Z_{AA} = s_\beta^2 \delta^{(1)} Z_{\mathcal{H}_1} + c_\beta^2 \delta^{(1)} Z_{\mathcal{H}_2}, \tag{A.2d}$$

$$\delta^{(1)} Z_{AG} = s_\beta c_\beta \Big(\delta^{(1)} Z_{\mathcal{H}_2} - \delta^{(1)} Z_{\mathcal{H}_1} \Big), \tag{A.2e}$$

$$\delta^{(1)} Z_{GG} = c_\beta^2 \delta^{(1)} Z_{\mathcal{H}_1} + s_\beta^2 \delta^{(1)} Z_{\mathcal{H}_2}, \tag{A.2f}$$

$$\delta^{(1)} Z_{H^- H^+} = s_\beta^2 \delta^{(1)} Z_{\mathcal{H}_1} + c_\beta^2 \delta^{(1)} Z_{\mathcal{H}_2}, \tag{A.2g}$$

$$\delta^{(1)} Z_{H^- G^+} = s_\beta c_\beta \Big(\delta^{(1)} Z_{\mathcal{H}_2} - \delta^{(1)} Z_{\mathcal{H}_1} \Big), \tag{A.2h}$$

$$\delta^{(1)} Z_{G^- H^+} = s_\beta c_\beta \Big(\delta^{(1)} Z_{\mathcal{H}_2} - \delta^{(1)} Z_{\mathcal{H}_1} \Big), \tag{A.2i}$$

$$\delta^{(1)} Z_{G^- G^+} = c_\beta^2 \delta^{(1)} Z_{\mathcal{H}_1} + s_\beta^2 \delta^{(1)} Z_{\mathcal{H}_2}. \tag{A.2j}$$

A.1.3 One-loop DR counterterms at $\mathcal{O}(N_c)$

$$\delta^{(1)} Z_{\mathcal{H}_1}^{\mathrm{DR}} = -\frac{\alpha_{\mathrm{em}} N_c}{8\pi M_W^2 s_{\mathrm{w}}^2} \frac{m_b^2}{c_\beta^2} \frac{1}{\varepsilon}, \tag{A.3a}$$

$$\delta^{(1)} Z_{\mathcal{H}_2}^{\mathrm{DR}} = -\frac{\alpha_{\mathrm{em}} N_c}{8\pi M_W^2 s_{\mathrm{w}}^2} \frac{m_t^2}{s_\beta^2} \frac{1}{\varepsilon}, \tag{A.3b}$$

$$\frac{\delta^{(1)} t_\beta^{\mathrm{DR}}}{t_\beta} = -\frac{\alpha_{\mathrm{em}} N_c}{16\pi M_W^2 s_{\mathrm{w}}^2} \Big(\frac{m_t^2}{s_\beta^2} - \frac{m_b^2}{c_\beta^2} \Big) \frac{1}{\varepsilon}, \tag{A.3c}$$

$$\frac{\delta^{(1)} \mu^{\mathrm{DR}}}{\mu} = \frac{\alpha_{\mathrm{em}} N_c}{16\pi M_W^2 s_{\mathrm{w}}^2} \Big(\frac{m_t^2}{s_\beta^2} + \frac{m_b^2}{c_\beta^2} \Big) \frac{1}{\varepsilon}, \tag{A.3d}$$

$$\frac{\delta^{(1)} A_t^{\mathrm{DR}}}{A_t} = \frac{\alpha_{\mathrm{em}} N_c}{8\pi M_W^2 s_{\mathrm{w}}^2} \frac{m_t^2}{s_\beta^2} \frac{1}{\varepsilon}, \tag{A.3e}$$

$$\frac{\delta^{(1)} A_b^{\mathrm{DR}}}{A_b} = \frac{\alpha_{\mathrm{em}} N_c}{8\pi M_W^2 s_{\mathrm{w}}^2} \frac{m_b^2}{c_\beta^2} \frac{1}{\varepsilon}, \tag{A.3f}$$

$$\begin{aligned} \delta^{(1)} X_t^{\mathrm{DR}} &= \delta^{(1)} A_t - \frac{1}{t_\beta} \delta^{(1)} \mu^* + \frac{\mu^*}{t_\beta^2} \delta^{(1)} t_\beta \\ &= \frac{\alpha_{\mathrm{em}} N_c}{8\pi M_W^2 s_{\mathrm{w}}^2} \frac{m_t^2}{s_\beta^2} \frac{X_t}{\varepsilon}, \end{aligned} \tag{A.3g}$$

$$\begin{aligned} \delta^{(1)} X_b^{\mathrm{DR}} &= \delta^{(1)} A_b - t_\beta \delta^{(1)} \mu^* - \mu^* \delta^{(1)} t_\beta \\ &= \frac{\alpha_{\mathrm{em}} N_c}{8\pi M_W^2 s_{\mathrm{w}}^2} \frac{m_b^2}{c_\beta^2} \frac{X_b}{\varepsilon}, \end{aligned} \tag{A.3h}$$

where

$$\varepsilon = \frac{4 - D}{2}. \tag{A.4}$$

The respective $\overline{\mathrm{DR}}$ expressions are obtained by replacing

$$\frac{1}{\varepsilon} \to \frac{\big(4\pi e^{-\gamma_E}\big)^\varepsilon}{\varepsilon} = \frac{1}{\varepsilon} + \log(4\pi) - \gamma_E + \frac{\varepsilon}{2} \big[\log(4\pi) - \gamma_E \big]^2 + \mathcal{O}\big(\varepsilon^2\big). \tag{A.5}$$

For two-loop counterterms, the procedure is more complicated, see Sect. 2.3.2.

A.2 Two-loop counterterms

A.2.1 Two-loop mass counterterms

$$
\begin{aligned}
\delta^{(2)}m_h^2 = {}& \delta^{(2)}m_A^2 c_{\alpha-\beta}^2 + \delta^{(2)}M_Z^2 s_{\alpha+\beta}^2 \\
& + \delta^{(2)}t_\beta c_\beta^2\Big(m_A^2 s_{2(\alpha-\beta)} + M_Z^2 s_{2(\alpha+\beta)}\Big) \\
& + \delta^{(1)}t_\beta c_\beta^2\Big(\delta^{(1)}m_A^2 s_{2(\alpha-\beta)} + \delta^{(1)}M_Z^2 s_{2(\alpha+\beta)}\Big) \\
& + \tfrac{1}{2}\Big(\delta^{(1)}t_\beta\Big)^2 c_\beta^3\Big[m_A^2 s_{\alpha-\beta}(3s_{\alpha-2\beta} - s_\alpha) + 2M_Z^2 c_{2\alpha+3\beta}\Big] \\
& + \frac{e s_{\alpha-\beta}}{2M_W s_\mathrm{w}}\Big[\Big(\delta^{(2)}T_h + \delta^{(1)}Z_\mathrm{w}\delta^{(1)}T_h\Big)(1 + c_{\alpha-\beta}^2) \\
& \qquad + \Big(\delta^{(2)}T_H + \delta^{(1)}Z_\mathrm{w}\delta^{(1)}T_H\Big)c_{\alpha-\beta}s_{\alpha-\beta} \\
& \qquad + \delta^{(1)}t_\beta c_\beta^2\Big(\delta^{(1)}T_h c_{\alpha-\beta} + \delta^{(1)}T_H s_{\alpha-\beta}\Big)s_{\alpha-\beta}\Big],
\end{aligned}
\tag{A.6a}
$$

$$
\begin{aligned}
\delta^{(2)}m_{hH}^2 = {}& \delta^{(2)}m_A^2 c_{\alpha-\beta}s_{\alpha-\beta} - \delta^{(2)}M_Z^2 c_{\alpha+\beta}s_{\alpha+\beta} \\
& - \delta^{(2)}t_\beta c_\beta^2\Big(m_A^2 c_{2(\alpha-\beta)} + M_Z^2 c_{2(\alpha+\beta)}\Big) \\
& - \delta^{(1)}t_\beta c_\beta^2\Big(\delta^{(1)}m_A^2 c_{2(\alpha-\beta)} + \delta^{(1)}M_Z^2 c_{2(\alpha+\beta)}\Big) \\
& - \tfrac{1}{2}\Big(\delta^{(1)}t_\beta\Big)^2 c_\beta^3\Big[m_A^2\frac{c_{\alpha-\beta}(3s_{\alpha-2\beta} - s_\alpha) + s_{\alpha-\beta}(3c_{\alpha-2\beta} - c_\alpha)}{2} \\
& \qquad - 2M_Z^2 s_{2\alpha+3\beta}\Big] \\
& - \frac{e}{2M_W s_\mathrm{w}}\Big[\Big(\delta^{(2)}T_h + \delta^{(1)}Z_\mathrm{w}\delta^{(1)}T_h\Big)c_{\alpha-\beta}^3 \\
& \qquad - \Big(\delta^{(2)}T_H + \delta^{(1)}Z_\mathrm{w}\delta^{(1)}T_H\Big)s_{\alpha-\beta}^3 \\
& \qquad + \delta^{(1)}t_\beta c_\beta^2\Big(\delta^{(1)}T_h c_{\alpha-\beta} + \delta^{(1)}T_H s_{\alpha-\beta}\Big)c_{\alpha-\beta}s_{\alpha-\beta}\Big],
\end{aligned}
\tag{A.6b}
$$

$$
\begin{aligned}
\delta^{(2)}m_H^2 = {}& \delta^{(2)}m_A^2 s_{\alpha-\beta}^2 + \delta^{(2)}M_Z^2 c_{\alpha+\beta}^2 \\
& - \delta^{(2)}t_\beta c_\beta^2\Big(m_A^2 s_{2(\alpha-\beta)} + M_Z^2 s_{2(\alpha+\beta)}\Big) \\
& - \delta^{(1)}t_\beta c_\beta^2\Big(\delta^{(1)}m_A^2 s_{2(\alpha-\beta)} + \delta^{(1)}M_Z^2 s_{2(\alpha+\beta)}\Big) \\
& + \tfrac{1}{2}\Big(\delta^{(1)}t_\beta\Big)^2 c_\beta^3\Big[m_A^2 c_{\alpha-\beta}(3c_{\alpha-2\beta} - c_\alpha) - 2M_Z^2 c_{2\alpha+3\beta}\Big] \\
& - \frac{e c_{\alpha-\beta}}{2M_W s_\mathrm{w}}\Big[\Big(\delta^{(2)}T_h + \delta^{(1)}Z_\mathrm{w}\delta^{(1)}T_h\Big)c_{\alpha-\beta}s_{\alpha-\beta} \\
& \qquad + \Big(\delta^{(2)}T_H + \delta^{(1)}Z_\mathrm{w}\delta^{(1)}T_H\Big)(1 + s_{\alpha-\beta}^2) \\
& \qquad - \delta^{(1)}t_\beta c_\beta^2\Big(\delta^{(1)}T_h c_{\alpha-\beta} + \delta^{(1)}T_H s_{\alpha-\beta}\Big)c_{\alpha-\beta}\Big],
\end{aligned}
\tag{A.6c}
$$

$$\begin{aligned}\delta^{(2)}m^2_{AG} =& -\delta^{(2)}t_\beta c^2_\beta m^2_A - \delta^{(1)}t_\beta c^2_\beta \delta^{(1)} m^2_A + \Big(\delta^{(1)}t_\beta\Big)^2 c^3_\beta s_\beta m^2_A \\ & - \frac{e}{2M_W s_\mathrm{w}}\Big[\Big(\delta^{(2)}T_h + \delta^{(1)}Z_\mathrm{w}\delta^{(1)}T_h\Big)c_{\alpha-\beta} \\ & \qquad + \Big(\delta^{(2)}T_H + \delta^{(1)}Z_\mathrm{w}\delta^{(1)}T_H\Big)s_{\alpha-\beta}\Big],\end{aligned} \tag{A.6d}$$

$$\begin{aligned}\delta^{(2)}m^2_{G} =& \Big(\delta^{(1)}t_\beta\Big)^2 c^4_\beta m^2_A \\ & + \frac{e}{2M_W s_\mathrm{w}}\Big[\Big(\delta^{(2)}T_h + \delta^{(1)}Z_\mathrm{w}\delta^{(1)}T_h\Big)s_{\alpha-\beta} \\ & \qquad - \Big(\delta^{(2)}T_H + \delta^{(1)}Z_\mathrm{w}\delta^{(1)}T_H\Big)c_{\alpha-\beta} \\ & \qquad + \delta^{(1)}t_\beta c^2_\beta\Big(\delta^{(1)}T_h c_{\alpha-\beta} + \delta^{(1)}T_H s_{\alpha-\beta}\Big)\Big],\end{aligned} \tag{A.6e}$$

$$\delta^{(2)}m^2_{hA} = \frac{e s_{\alpha-\beta}}{2M_W s_\mathrm{w}}\Big(\delta^{(2)}T_A + \delta^{(1)}Z_\mathrm{w}\delta^{(1)}T_A\Big), \tag{A.6f}$$

$$\delta^{(2)}m^2_{HA} = -\frac{e c_{\alpha-\beta}}{2M_W s_\mathrm{w}}\Big(\delta^{(2)}T_A + \delta^{(1)}Z_\mathrm{w}\delta^{(1)}T_A\Big), \tag{A.6g}$$

$$\delta^{(2)}m^2_{hG} = \frac{e c_{\alpha-\beta}}{2M_W s_\mathrm{w}}\Big(\delta^{(2)}T_A + \delta^{(1)}Z_\mathrm{w}\delta^{(1)}T_A\Big) = -\delta^{(2)}m^2_{HA}, \tag{A.6h}$$

$$\delta^{(2)}m^2_{HG} = \frac{e s_{\alpha-\beta}}{2M_W s_\mathrm{w}}\Big(\delta^{(2)}T_A + \delta^{(1)}Z_\mathrm{w}\delta^{(1)}T_A\Big) = \delta^{(2)}m^2_{hA}, \tag{A.6i}$$

$$\begin{aligned}\delta^{(2)}m^2_{H^-G^+} =& -\delta^{(2)}t_\beta c^2_\beta m^2_{H^\pm} - \delta^{(1)}t_\beta c^2_\beta \delta^{(1)} m^2_{H^\pm} + \Big(\delta^{(1)}t_\beta\Big)^2 c^3_\beta s_\beta m^2_{H^\pm} \\ & - \frac{e}{2M_W s_\mathrm{w}}\Big[\Big(\delta^{(2)}T_h + \delta^{(1)}Z_\mathrm{w}\delta^{(1)}T_h\Big)c_{\alpha-\beta} \\ & \qquad + \Big(\delta^{(2)}T_H + \delta^{(1)}Z_\mathrm{w}\delta^{(1)}T_H\Big)s_{\alpha-\beta} \\ & \qquad - \mathrm{i}\Big(\delta^{(2)}T_A + \delta^{(1)}Z_\mathrm{w}\delta^{(1)}T_A\Big)\Big],\end{aligned} \tag{A.6j}$$

$$\begin{aligned}\delta^{(2)}m^2_{G^-H^+} =& -\delta^{(2)}t_\beta c^2_\beta m^2_{H^\pm} - \delta^{(1)}t_\beta c^2_\beta \delta^{(1)} m^2_{H^\pm} + \Big(\delta^{(1)}t_\beta\Big)^2 c^3_\beta s_\beta m^2_{H^\pm} \\ & - \frac{e}{2M_W s_\mathrm{w}}\Big[\Big(\delta^{(2)}T_h + \delta^{(1)}Z_\mathrm{w}\delta^{(1)}T_h\Big)c_{\alpha-\beta} \\ & \qquad + \Big(\delta^{(2)}T_H + \delta^{(1)}Z_\mathrm{w}\delta^{(1)}T_H\Big)s_{\alpha-\beta} \\ & \qquad + \mathrm{i}\Big(\delta^{(2)}T_A + \delta^{(1)}Z_\mathrm{w}\delta^{(1)}T_A\Big)\Big] \\ =& \Big(\delta^{(2)}m^2_{H^-G^+}\Big)^*,\end{aligned} \tag{A.6k}$$

$$\begin{aligned}\delta^{(2)}m^2_{G^\pm} =& \Big(\delta^{(1)}t_\beta\Big)^2 c^4_\beta m^2_{H^\pm} \\ & + \frac{e}{2M_W s_\mathrm{w}}\Big[\Big(\delta^{(2)}T_h + \delta^{(1)}Z_\mathrm{w}\delta^{(1)}T_h\Big)s_{\alpha-\beta} \\ & \qquad - \Big(\delta^{(2)}T_H + \delta^{(1)}Z_\mathrm{w}\delta^{(1)}T_H\Big)c_{\alpha-\beta} \\ & \qquad + \delta^{(1)}t_\beta c^2_\beta\Big(\delta^{(1)}T_h c_{\alpha-\beta} + \delta^{(1)}T_H s_{\alpha-\beta}\Big)\Big].\end{aligned} \tag{A.6l}$$

A.2.2 Two-loop field counterterms

$$\delta^{(2)} Z_{hh} = s_\alpha^2 \left(\delta^{(2)} Z_{\mathcal{H}_1} - \frac{1}{4} \left(\delta^{(1)} Z_{\mathcal{H}_1} \right)^2 \right) + c_\alpha^2 \left(\delta^{(2)} Z_{\mathcal{H}_2} - \frac{1}{4} \left(\delta^{(1)} Z_{\mathcal{H}_2} \right)^2 \right) + \frac{1}{4} \left(\delta^{(1)} Z_{hh} \right)^2, \tag{A.7a}$$

$$\delta^{(2)} Z_{hH} = s_\alpha c_\alpha \left[\delta^{(2)} Z_{\mathcal{H}_2} - \frac{1}{4} \left(\delta^{(1)} Z_{\mathcal{H}_2} \right)^2 - \delta^{(2)} Z_{\mathcal{H}_1} + \frac{1}{4} \left(\delta^{(1)} Z_{\mathcal{H}_1} \right)^2 \right], \tag{A.7b}$$

$$\delta^{(2)} Z_{HH} = c_\alpha^2 \left(\delta^{(2)} Z_{\mathcal{H}_1} - \frac{1}{4} \left(\delta^{(1)} Z_{\mathcal{H}_1} \right)^2 \right) + s_\alpha^2 \left(\delta^{(2)} Z_{\mathcal{H}_2} - \frac{1}{4} \left(\delta^{(1)} Z_{\mathcal{H}_2} \right)^2 \right) + \frac{1}{4} \left(\delta^{(1)} Z_{HH} \right)^2, \tag{A.7c}$$

$$\delta^{(2)} Z_{AA} = s_\beta^2 \left(\delta^{(2)} Z_{\mathcal{H}_1} - \frac{1}{4} \left(\delta^{(1)} Z_{\mathcal{H}_1} \right)^2 \right) + c_\beta^2 \left(\delta^{(2)} Z_{\mathcal{H}_2} - \frac{1}{4} \left(\delta^{(1)} Z_{\mathcal{H}_2} \right)^2 \right) + \frac{1}{4} \left(\delta^{(1)} Z_{AA} \right)^2, \tag{A.7d}$$

$$\delta^{(2)} Z_{AG} = s_\beta c_\beta \left[\delta^{(2)} Z_{\mathcal{H}_2} - \frac{1}{4} \left(\delta^{(1)} Z_{\mathcal{H}_2} \right)^2 - \delta^{(2)} Z_{\mathcal{H}_1} + \frac{1}{4} \left(\delta^{(1)} Z_{\mathcal{H}_1} \right)^2 \right], \tag{A.7e}$$

$$\delta^{(2)} Z_{GG} = c_\beta^2 \left(\delta^{(2)} Z_{\mathcal{H}_1} - \frac{1}{4} \left(\delta^{(1)} Z_{\mathcal{H}_1} \right)^2 \right) + s_\beta^2 \left(\delta^{(2)} Z_{\mathcal{H}_2} - \frac{1}{4} \left(\delta^{(1)} Z_{\mathcal{H}_2} \right)^2 \right) + \frac{1}{4} \left(\delta^{(1)} Z_{GG} \right)^2, \tag{A.7f}$$

$$\delta^{(2)} Z_{H^- H^+} = s_\beta^2 \left(\delta^{(2)} Z_{\mathcal{H}_1} - \frac{1}{4} \left(\delta^{(1)} Z_{\mathcal{H}_1} \right)^2 \right) + c_\beta^2 \left(\delta^{(2)} Z_{\mathcal{H}_2} - \frac{1}{4} \left(\delta^{(1)} Z_{\mathcal{H}_2} \right)^2 \right) + \frac{1}{4} \left(\delta^{(1)} Z_{H^- H^+} \right)^2, \tag{A.7g}$$

$$\delta^{(2)} Z_{H^- G^+} = s_\beta c_\beta \left[\delta^{(2)} Z_{\mathcal{H}_2} - \frac{1}{4} \left(\delta^{(1)} Z_{\mathcal{H}_2} \right)^2 - \delta^{(2)} Z_{\mathcal{H}_1} + \frac{1}{4} \left(\delta^{(1)} Z_{\mathcal{H}_1} \right)^2 \right], \tag{A.7h}$$

$$\delta^{(2)} Z_{G^- H^+} = s_\beta c_\beta \left[\delta^{(2)} Z_{\mathcal{H}_2} - \frac{1}{4} \left(\delta^{(1)} Z_{\mathcal{H}_2} \right)^2 - \delta^{(2)} Z_{\mathcal{H}_1} + \frac{1}{4} \left(\delta^{(1)} Z_{\mathcal{H}_1} \right)^2 \right], \tag{A.7i}$$

$$\delta^{(2)} Z_{G^- G^+} = c_\beta^2 \left(\delta^{(2)} Z_{\mathcal{H}_1} - \frac{1}{4} \left(\delta^{(1)} Z_{\mathcal{H}_1} \right)^2 \right) + s_\beta^2 \left(\delta^{(2)} Z_{\mathcal{H}_2} - \frac{1}{4} \left(\delta^{(1)} Z_{\mathcal{H}_2} \right)^2 \right) + \frac{1}{4} \left(\delta^{(1)} Z_{GG} \right)^2. \tag{A.7j}$$

B Slavnov-Taylor identities for scalar-vector mixing

Slavnov-Taylor (ST) identities are the generalisation of the abelian Ward-Takahashi (WT) identities to non-abelian gauge theories. While WT identities follow from gauge symmetry, ST identities are a consequence of the Becchi-Rouet-Stora-Tyutin (BRST) symmetry, which is an extension of gauge symmetry after gauge fixing. For the present discussion, we will not derive ST identities from BRST invariance but simply check relations between the relevant self-energies algebraically or numerically. In Refs. [207,208], MSSM Slavnov-Taylor identities for self-energies in the AGZ and the $H^\pm G^\pm W^\pm$ system are given. As was pointed out in Ref. [185], the identities given in Refs. [207,208] hold only in a linear gauge and on-shell. Refs. [185,198] give ST identities also for off-shell momenta.

In our analysis, we only consider self-energy contributions of $\mathcal{O}(N_c)$ and in a general R_ξ gauge. Therefore, no diagrams with electroweak particles in the loops appear, and the self-energies are gauge-parameter independent.

Our starting point are the equations

$$\Sigma^{(1),\text{notad}}_{AG}(p^2) - \mathrm{i}\frac{p^2}{M_Z}\Sigma^{L,(1),\text{notad}}_{AZ}(p^2) \overset{\mathcal{O}(N_c)}{=} \frac{e}{2s_\text{w}M_W}\Big(\Gamma^{(1)}_h c_{\alpha-\beta} + \Gamma^{(1)}_H s_{\alpha-\beta}\Big), \tag{B.1a}$$

$$\Sigma^{(1),\text{notad}}_{H^-G^+}(p^2) - \frac{p^2}{M_W}\Sigma^{L,(1),\text{notad}}_{H^-W^+}(p^2) \overset{\mathcal{O}(N_c)}{=} \frac{e}{2s_\text{w}M_W}\Big(\Gamma^{(1)}_h c_{\alpha-\beta} + \Gamma^{(1)}_H s_{\alpha-\beta} - \mathrm{i}\Gamma^{(1)}_A\Big), \tag{B.1b}$$

$$\Sigma^{(1),\text{notad}}_{G^-H^+}(p^2) - \frac{p^2}{M_W}\Sigma^{L,(1),\text{notad}}_{W^-H^+}(p^2) \overset{\mathcal{O}(N_c)}{=} \frac{e}{2s_\text{w}M_W}\Big(\Gamma^{(1)}_h c_{\alpha-\beta} + \Gamma^{(1)}_H s_{\alpha-\beta} + \mathrm{i}\Gamma^{(1)}_A\Big), \tag{B.1c}$$

which we have explicitly verified. The superscript 'notad' denotes that we do not include tadpole contributions in the respective self-energy. Instead, the tadpole contributions appear explicitly in the form of unrenormalised one-point functions on the right-hand side of the equations.

Using on-shell definitions for the one-loop tadpole counterterms, $\delta^{(1)}T_i = -\Gamma^{(1)}_i$, we

can write

$$\Sigma^{(1),\text{notad}}_{AG}(p^2) - \mathrm{i}\frac{p^2}{M_Z}\Sigma^{L,(1),\text{notad}}_{AZ}(p^2) \overset{\mathcal{O}(N_c)}{=} \delta^{(1)} m^2_{AG} + \delta^{(1)} t_\beta c^2_\beta m^2_A, \tag{B.2a}$$

$$\Sigma^{(1),\text{notad}}_{H^-G^+}(p^2) - \frac{p^2}{M_W}\Sigma^{L,(1),\text{notad}}_{H^-W^+}(p^2) \overset{\mathcal{O}(N_c)}{=} \delta^{(1)} m^2_{H^-G^+} + \delta^{(1)} t_\beta c^2_\beta m^2_{H^\pm}, \tag{B.2b}$$

$$\Sigma^{(1),\text{notad}}_{G^-H^+}(p^2) - \frac{p^2}{M_W}\Sigma^{L,(1),\text{notad}}_{W^-H^+}(p^2) \overset{\mathcal{O}(N_c)}{=} \delta^{(1)} m^2_{G^-H^+} + \delta^{(1)} t_\beta c^2_\beta m^2_{H^\pm}, \tag{B.2c}$$

where he have used the expressions for the one-loop Higgs mass counterterms, which were introduced in App. A.

For the renormalised self-energies (the definitions are given in Sect. 4.2.2), we arrive at the following off-shell Slavnov-Taylor identities

$$\hat{\Sigma}^{(1)}_{AG}(p^2) - \mathrm{i}\frac{p^2}{M_Z}\hat{\Sigma}^{L,(1)}_{AZ}(p^2) \overset{\mathcal{O}(N_c)}{=} (p^2 - m^2_A)\Big(\tfrac{1}{2}\delta^{(1)} Z_{AG} - \delta^{(1)} t_\beta c^2_\beta\Big), \tag{B.3a}$$

$$\hat{\Sigma}^{(1)}_{H^-G^+}(p^2) - \frac{p^2}{M_W}\hat{\Sigma}^{L,(1)}_{H^-W^+}(p^2) \overset{\mathcal{O}(N_c)}{=} (p^2 - m^2_{H^\pm})\Big(\tfrac{1}{2}\delta^{(1)} Z_{H^-G^+} - \delta^{(1)} t_\beta c^2_\beta\Big), \tag{B.3b}$$

$$\hat{\Sigma}^{(1)}_{G^-H^+}(p^2) - \frac{p^2}{M_W}\hat{\Sigma}^{L,(1)}_{W^-H^+}(p^2) \overset{\mathcal{O}(N_c)}{=} (p^2 - m^2_{H^\pm})\Big(\tfrac{1}{2}\delta^{(1)} Z_{G^-H^+} - \delta^{(1)} t_\beta c^2_\beta\Big), \tag{B.3c}$$

which are in agreement with the ones given in Ref. [185].

The right-hand side of Eqs. (B.3) vanishes in the DCPR and in a $\overline{\text{DR}}$ scheme for any value of p^2, see Sect. 4.3. This is in agreement with Ref. [198], which employs the $\overline{\text{DR}}$ version. As we allow for an on-shell renormalisation of t_β while keeping the field counterterms defined in the minimal $\overline{\text{DR}}$ scheme, the right-hand side will not vanish in general. The on-shell ST identities

$$\hat{\Sigma}^{(1)}_{AG}(m^2_A) - \mathrm{i}\frac{m^2_A}{M_Z}\hat{\Sigma}^{L,(1)}_{AZ}(m^2_A) = 0, \tag{B.4a}$$

$$\hat{\Sigma}^{(1)}_{H^-G^+}(m^2_{H^\pm}) - \frac{m^2_{H^\pm}}{M_W}\hat{\Sigma}^{L,(1)}_{H^-W^+}(m^2_{H^\pm}) = 0, \tag{B.4b}$$

$$\hat{\Sigma}^{(1)}_{G^-H^+}(m^2_{H^\pm}) - \frac{m^2_{H^\pm}}{M_W}\hat{\Sigma}^{L,(1)}_{W^-H^+}(m^2_{H^\pm}) = 0 \tag{B.4c}$$

hold independently of the renormalisation chosen for t_β and the Higgs field counterterms. In a linear gauge, they are also valid when terms of $\mathcal{O}\big(N_c^0\big)$ are taken into account [185, 198].

C Renormalisation of the mass M_W

In the first section of this appendix, we determine the one- and two-loop corrections to the particle pole mass that were given without derivation in Sect. 3.2.3. We also show how to include imaginary parts of self-energies in an on-shell mass counterterm for the case of an unstable particle. As an example, we work with the mass M_W of the W boson. The transverse part of the W boson self-energy does not receive mixing contributions from other particles in the theory, hence $\hat{\Sigma}^{T,\text{eff}}_{WW} = \hat{\Sigma}^{T}_{WW}$. All steps performed in this appendix can easily be extended to the case of a non-trivial effective self-energy for particle masses that are affected by mixing effects.

C.1 Calculating the pole mass M_W

Our starting point is the equation which defines the complex pole

$$\mathcal{M}_W^2 - m_W^2 + \hat{\Sigma}^T_{WW}(\mathcal{M}_W^2) = 0, \tag{C.1}$$

where $\mathcal{M}_W^2 = M_W^2 - \mathrm{i}M_W\Gamma_W$. Taking the real and imaginary parts and expanding the self-energy up to the two-loop order yields

$$M_W^2 - m_W^2 + \operatorname{Re}\hat{\Sigma}^{T,(1)}_{WW}(\mathcal{M}_W^2) + \operatorname{Re}\hat{\Sigma}^{T,(2)}_{WW}(\mathcal{M}_W^2) + \mathcal{O}\Big(k^3\Big) = 0, \tag{C.2a}$$

$$-M_W\Gamma_W + \operatorname{Im}\hat{\Sigma}^{T,(1)}_{WW}(\mathcal{M}_W^2) + \operatorname{Im}\hat{\Sigma}^{T,(2)}_{WW}(\mathcal{M}_W^2) + \mathcal{O}\Big(k^3\Big) = 0, \tag{C.2b}$$

where k counts the loop order. We then expand the one- and two-loop self-energies perturbatively around the real part of the complex pole. For the one- and two-loop self energies, this means

$$\hat{\Sigma}^{T,(1)}_{WW}(\mathcal{M}_W^2) = \hat{\Sigma}^{T,(1)}_{WW}(M_W^2) + \partial\hat{\Sigma}^{T,(1)}_{WW}(M_W^2)\,(-\mathrm{i}M_W\Gamma_W) + \mathcal{O}\Big(k^3\Big), \tag{C.3a}$$

$$\hat{\Sigma}^{T,(2)}_{WW}(\mathcal{M}_W^2) = \hat{\Sigma}^{T,(2)}_{WW}(M_W^2) + \mathcal{O}\Big(k^3\Big). \tag{C.3b}$$

Inserting Eq. (C.2b) into Eq. (C.3a) and taking the real part, we find

$$\operatorname{Re}\hat{\Sigma}^{T,(1)}_{WW}(\mathcal{M}_W^2) = \operatorname{Re}\hat{\Sigma}^{T,(1)}_{WW}(M_W^2) + \operatorname{Im}\hat{\Sigma}^{T,(1)}_{WW}(M_W^2)\operatorname{Im}\partial\hat{\Sigma}^{T,(1)}_{WW}(M_W^2) + \mathcal{O}\Big(k^3\Big). \tag{C.4}$$

Inserting Eqs. (C.3b) and (C.4) into Eq. (C.2a), we arrive at

$$\begin{aligned} M_W^2 - m_W^2 + \operatorname{Re}\hat{\Sigma}_{WW}^{T,(1)}(M_W^2) + \operatorname{Im}\hat{\Sigma}_{WW}^{T,(1)}(M_W^2)\operatorname{Im}\partial\hat{\Sigma}_{WW}^{T,(1)}(M_W^2) \\ + \operatorname{Re}\hat{\Sigma}_{WW}^{T,(2)}(M_W^2) + \mathcal{O}\left(k^3\right) = 0. \end{aligned} \tag{C.5}$$

Lastly, we expand the self-energy around the tree-level mass m_W^2 to obtain

$$\begin{aligned} M_W^2 &= m_W^2 - \operatorname{Re}\hat{\Sigma}_{WW}^{T,(1)}(M_W^2) + \mathcal{O}\left(k^2\right) \\ &= m_W^2 - \operatorname{Re}\hat{\Sigma}_{WW}^{T,(1)}(m_W^2) + \mathcal{O}\left(k^2\right). \end{aligned} \tag{C.6}$$

We insert this expansion into the real part of the self-energy:

$$\operatorname{Re}\hat{\Sigma}_{W}^{T,(1)}(M_W^2) = \operatorname{Re}\hat{\Sigma}_{WW}^{T,(1)}(m_W^2) - \operatorname{Re}\hat{\Sigma}_{WW}^{T,(1)}(m_W^2)\operatorname{Re}\partial\hat{\Sigma}_{WW}^{T,(1)}(m_W^2). \tag{C.7}$$

We can now solve Eq. (C.5) using only tree-level masses in the arguments of the self-energies:

$$\begin{aligned} M_W^2 - m_W^2 + \operatorname{Re}\hat{\Sigma}_{WW}^{T,(1)}(m_W^2) - \operatorname{Re}\hat{\Sigma}_{WW}^{T,(1)}(m_W^2)\operatorname{Re}\partial\hat{\Sigma}_{WW}^{T,(1)}(m_W^2) \\ + \operatorname{Im}\hat{\Sigma}_{WW}^{T,(1)}(m_W^2)\operatorname{Im}\partial\hat{\Sigma}_{WW}^{T,(1)}(m_W^2) + \operatorname{Re}\hat{\Sigma}_{WW}^{T,(2)}(m_W^2) + \mathcal{O}\left(k^3\right) = 0, \end{aligned} \tag{C.8}$$

which is equivalent to

$$\begin{aligned} M_W^2 - m_W^2 + \operatorname{Re}\hat{\Sigma}_{WW}^{T,(1)}(m_W^2) - \operatorname{Re}\left\{\hat{\Sigma}_{WW}^{T,(1)}(m_W^2)\partial\hat{\Sigma}_{WW}^{T,(1)}(m_W^2)\right\} \\ + \operatorname{Re}\hat{\Sigma}_{WW}^{T,(2)}(m_W^2) + \mathcal{O}\left(k^3\right) = 0. \end{aligned} \tag{C.9}$$

We can write the pole mass as

$$M_W^2 = m_W^2 + \Delta^{(1)}M_W^2 + \Delta^{(2)}M_W^2 + \mathcal{O}\left(k^3\right), \tag{C.10}$$

where we introduced the one- and two-loop corrections

$$\Delta^{(1)}M_W^2 = -\operatorname{Re}\hat{\Sigma}_{WW}^{T,(1)}(m_W^2), \tag{C.11a}$$

$$\Delta^{(2)}M_W^2 = -\operatorname{Re}\hat{\Sigma}_{WW}^{T,(2)}(m_W^2) + \operatorname{Re}\left\{\hat{\Sigma}_{WW}^{T,(1)}(m_W^2)\partial\hat{\Sigma}_{WW}^{T,(1)}(m_W^2)\right\}. \tag{C.11b}$$

These expressions are equivalent to the ones given in Sect. 3.2.3 for the case of no mixing.

C.2 The on-shell counterterms

If a mass parameter is defined in an on-shell scheme, its tree-level and loop-corrected value agree: $M_W^2 = m_W^2$. According to C.8, this is equivalent to demanding

$$\operatorname{Re}\hat{\Sigma}^{T,(1)}_{WW}(m_W^2) \stackrel{!}{=} 0, \tag{C.12a}$$

$$\operatorname{Re}\hat{\Sigma}^{T,(2)}_{WW}(m_W^2) \stackrel{!}{=} \operatorname{Re}\left\{\hat{\Sigma}^{T,(1)}_{WW}(m_W^2)\partial\hat{\Sigma}^{T,(1)}_{WW}(m_W^2)\right\}, \tag{C.12b}$$

which are our on-shell renormalisation conditions. Inserting the renormalised self-energies from Eqs. (4.64d) and (4.103d) into Eqs. (C.12), we find

$$\delta^{(1)}M_W^2 = \operatorname{Re}\Sigma^{T,(1)}_{WW}(m_W^2), \tag{C.13a}$$

$$\begin{aligned}\delta^{(2)}M_W^2 &= \operatorname{Re}\Sigma^{T,(2)}_{WW}(m_W^2) - \operatorname{Re}\{\delta^{(1)}Z_{WW}\}\delta^{(1)}M_W^2 \\ &\quad - \operatorname{Re}\left\{\hat{\Sigma}^{T,(1)}_{WW}(m_W^2)\partial\hat{\Sigma}^{T,(1)}_{WW}(m_W^2)\right\} \\ &= \operatorname{Re}\Sigma^{T,(2)}_{WW}(m_W^2) - \operatorname{Re}\{\delta^{(1)}Z_{WW}\}\delta^{(1)}M_W^2 \\ &\quad + \operatorname{Im}\hat{\Sigma}^{T,(1)}_{WW}(m_W^2)\operatorname{Im}\partial\hat{\Sigma}^{T,(1)}_{WW}(m_W^2)\end{aligned} \tag{C.13b}$$

for the mass counterterms. These expressions fully agree with the ones given in Sects. 4.2.2 and 4.2.3.

We can further write the unrenormalised two-loop self-energy as

$$\Sigma^{T,(2)}_{WW}(m_W^2) = \widetilde{\Sigma}^{T,(2)}_{WW}(m_W^2) + \delta^{(1)}Z_{WW}\Sigma^{T,(1)}_{WW}(m_W^2), \tag{C.14}$$

where $\widetilde{\Sigma}^{T,(2)}_{WW}$ does not contain any field counterterms entering through sub-loop renormalisation. With this notation, the two-loop counterterm reads

$$\begin{aligned}\delta^{(2)}M_W^2 &= \operatorname{Re}\widetilde{\Sigma}^{T,(2)}_{WW}(m_W^2) - \operatorname{Im}\{\delta^{(1)}Z_{WW}\}\operatorname{Im}\Sigma^{T,(1)}_{WW}(m_W^2) \\ &\quad - \operatorname{Re}\left\{\hat{\Sigma}^{T,(1)}_{WW}(m_W^2)\partial\hat{\Sigma}^{T,(1)}_{WW}(m_W^2)\right\} \\ &= \operatorname{Re}\widetilde{\Sigma}^{T,(2)}_{WW}(m_W^2) - \operatorname{Im}\{\delta^{(1)}Z_{WW}\}\operatorname{Im}\Sigma^{T,(1)}_{WW}(m_W^2) \\ &\quad + \operatorname{Im}\hat{\Sigma}^{T,(1)}_{WW}(m_W^2)\operatorname{Im}\partial\hat{\Sigma}^{T,(1)}_{WW}(m_W^2) \\ &= \operatorname{Re}\widetilde{\Sigma}^{T,(2)}_{WW}(m_W^2) + \operatorname{Im}\Sigma^{T,(1)}_{WW}(m_W^2)\operatorname{Im}\partial\Sigma^{T,(1)}_{WW}(m_W^2).\end{aligned} \tag{C.15}$$

In the last step, we used

$$\operatorname{Im}\hat{\Sigma}^{T,(1)}_{WW}(m_W^2) = \operatorname{Im}\Sigma^{T,(1)}_{WW}(m_W^2), \tag{C.16a}$$

$$\operatorname{Im}\partial\hat{\Sigma}^{T,(1)}_{WW}(m_W^2) = \operatorname{Im}\partial\Sigma^{T,(1)}_{WW}(m_W^2) + \operatorname{Im}\{\delta^{(1)}Z_{WW}\}. \tag{C.16b}$$

We see that the OS mass counterterm does not depend on the field counterterm.

D One-loop integrals

D.1 Definitions

In this section, we give the definitions used in this thesis of scalar and tensor one-loop integrals as well as their most important derivatives. The scalar integrals are defined as

$$A_0(m^2) = C \int \mathrm{d}^D q \, \frac{1}{q^2 - m^2}, \tag{D.1a}$$

$$B_0(p^2,m_1^2,m_2^2) = C \int \mathrm{d}^D q \, \frac{1}{[q^2 - m_1^2][(q+p)^2 - m_2^2]}, \tag{D.1b}$$

$$\begin{aligned} &C_0(p_1^2,p_2^2,(p_1+p_2)^2,\{m_i^2\}) \\ &\qquad = C \int \mathrm{d}^D q \, \frac{1}{[q^2 - m_1^2][(q+p_1)^2 - m_2^2][(q+p_1+p_2)^2 - m_3^2]}, \end{aligned} \tag{D.1c}$$

where

$$C = \frac{16\pi^2}{i} \frac{\mu_{\mathrm{D}}^{2\varepsilon}}{(2\pi)^D}, \tag{D.2a}$$

$$D = 4 - 2\varepsilon, \tag{D.2b}$$

and μ_{D} denotes the regularisation scale. The C_0 integral is UV-finite and hence does not need to be regularised. When working in D dimensions, the integrals have an $\mathcal{O}(\varepsilon)$ part, which can give a non-vanishing contribution. If these parts contribute or not, depends on the choice of the renormalisation scheme, see Sect. 5.4.
The following symmetry relations are useful:

$$B_0(p^2,m_1^2,m_2^2) = B_0(p^2,m_2^2,m_1^2), \tag{D.3a}$$

$$\begin{aligned} C_0(0,p^2,p^2,m_1^2,m_2^2,m_3^2) &= C_0(0,p^2,p^2,m_2^2,m_1^2,m_3^2) \\ &= C_0(p^2,0,p^2,m_3^2,m_1^2,m_2^2) \\ &= C_0(p^2,0,p^2,m_3^2,m_2^2,m_1^2). \end{aligned} \tag{D.3b}$$

When taking a derivative with respect to the external momentum p^2, we use the notation

$$\partial B_0(p^2,m_1^2,m_2^2) \equiv \frac{\partial}{\partial p^2} B_0(p^2,m_1^2,m_2^2). \tag{D.4}$$

We also define the B_0' function as

$$B_0'(p^2,m_1^2,m_2^2) \equiv \frac{\partial}{\partial m_1^2} B_0(p^2,m_1^2,m_2^2). \tag{D.5}$$

In the following, the symbols ∂B_0 and B_0' always refer to the first and second partial derivative of the B_0 integral, i.e., in the case of identical mass arguments, we take the derivative first and then insert the masses:

$$B_0'(p^2,m^2,m^2) = \frac{\partial}{\partial m_1^2}\, B_0(p^2,m_1^2,m_2^2)\Big|_{m_1^2=m_2^2=m^2}. \tag{D.6}$$

We define two-point tensor integrals and their scalar coefficients by

$$\begin{aligned} B^\mu(p^2,m_1^2,m_2^2) &\equiv C\int \mathrm{d}^D q\, \frac{q^\mu}{[q^2-m_1^2][(q+p)^2-m_2^2]} \\ &\equiv p^\mu B_1(p^2,m_1^2,m_2^2), \end{aligned} \tag{D.7a}$$

$$\begin{aligned} B^{\mu\nu}(p^2,m_1^2,m_2^2) &\equiv C\int \mathrm{d}^D q\, \frac{q^\mu q^\nu}{[q^2-m_1^2][(q+p)^2-m_2^2]} \\ &\equiv g^{\mu\nu} B_{00}(p^2,m_1^2,m_2^2) + p^\mu p^\nu B_{11}(p^2,m_1^2,m_2^2). \end{aligned} \tag{D.7b}$$

The two following three-point tensor integrals often appear in self-energy diagrams as well:

$$\begin{aligned} C^\mu(0,p^2,p^2,m_1^2,m_1^2,m_2^2) &\equiv C\int \mathrm{d}^D q\, \frac{q^\mu}{[q^2-m_1^2]^2[(q+p)^2-m_2^2]} \\ &\equiv p^\mu C_2(0,p^2,p^2,m_1^2,m_1^2,m_2^2), \end{aligned} \tag{D.8a}$$

$$\begin{aligned} C^\mu(p^2,0,p^2,m_1^2,m_2^2,m_2^2) &\equiv C\int \mathrm{d}^D q\, \frac{q^\mu}{[q^2-m_1^2][(q+p)^2-m_2^2]^2} \\ &\equiv p^\mu \left[C_1(p^2,0,p^2,m_1^2,m_2^2,m_2^2) + C_2(p^2,0,p^2,m_1^2,m_2^2,m_2^2)\right]. \end{aligned} \tag{D.8b}$$

As we follow the notation of `FormCalc` and `LoopTools`, two coefficient functions appear in the second integral although the Lorentz decomposition requires only one. In practice, only this sum of C_1 and C_2 appears. The same logic applies for the

tensor integrals of rank two:

$$\begin{aligned} C^{\mu\nu}(0,p^2,p^2,m_1^2,m_1^2,m_2^2) &= C\int \mathrm{d}^D q\, \frac{q^\mu q^\nu}{[q^2-m_1^2]^2[(q+p)^2-m_2^2]} \\ &\equiv g^{\mu\nu} C_{00}(0,p^2,p^2,m_1^2,m_1^2,m_2^2) \\ &\quad + p^\mu p^\nu C_{22}(0,p^2,p^2,m_1^2,m_1^2,m_2^2), \end{aligned} \tag{D.9a}$$

$$\begin{aligned} C^{\mu\nu}(p^2,0,p^2,m_1^2,m_2^2,m_2^2) &= C\int \mathrm{d}^D q\, \frac{q^\mu q^\nu}{[q^2-m_1^2][(q+p)^2-m_2^2]^2} \\ &\equiv g^{\mu\nu} C_{00}(p^2,0,p^2,m_1^2,m_2^2,m_2^2) \\ &\quad + p^\mu p^\nu \left[C_{11}(\ldots)+C_{12}(\ldots)+C_{21}(\ldots)+C_{22}(\ldots)\right]. \end{aligned} \tag{D.9b}$$

The C^μ integrals are UV-finite and require in principle no regularisation. We define them in D dimensions anyway, for the reasons given above. The $C^{\mu\nu}$ integrals are UV-divergent. While not all of the integrals defined above appear in our calculation, the definitions have been included for the sake of completeness.

D.2 Reducing the integrals

In this section, we show that the B_0' integral and the coefficients of tensor integrals can be expressed in terms of the simpler A_0 and B_0 integrals. For these integrals, analytic expression up to $\mathcal{O}(\varepsilon)$ are known for all combinations of the external momentum and the masses. We also give all tensor coefficients relevant for our work as well as some additional relations that were derived over the course of this thesis.

D.2.1 The scalar integrals

The two-point integral B_0 and the three-point integral C_0 can be reduced to simpler functions in some special cases:

$$B_0(0,m_1^2,m_2^2) = \frac{A_0(m_1^2)-A_0(m_2^2)}{m_1^2-m_2^2}, \tag{D.10a}$$

$$C_0(0,p^2,p^2,m_1^2,m_2^2,m_3^2) = \frac{B_0(p^2,m_1^2,m_3^2)-B_0(p^2,m_2^2,m_3^2)}{m_1^2-m_2^2}, \tag{D.10b}$$

$$\begin{aligned} C_0(0,0,0,m_1^2,m_2^2,m_3^2) &= \frac{A_0(m_1^2)}{(m_1^2-m_2^2)(m_1^2-m_3^2)} + \frac{A_0(m_2^2)}{(m_2^2-m_1^2)(m_2^2-m_3^2)} \\ &\quad + \frac{A_0(m_3^2)}{(m_3^2-m_1^2)(m_3^2-m_2^2)}. \end{aligned} \tag{D.10c}$$

In the case of identical masses, the differential quotients turn into derivatives:

$$\begin{aligned} B_0(0,m^2,m^2) &= \frac{\partial A_0(m^2)}{\partial m^2} \\ &= (1-\varepsilon)\frac{A_0(m^2)}{m^2}, \end{aligned} \tag{D.11a}$$

$$\begin{aligned} C_0(0,p^2,p^2,m_1^2,m_1^2,m_2^2) &= \frac{\partial B_0(p^2,m_1^2,m_2^2)}{\partial m_1^2} \\ &= B_0'(p^2,m_1^2,m_2^2). \end{aligned} \tag{D.11b}$$

The expression for the derivative of the A_0 function was obtained by inserting a factor $1 = D^{-1}\frac{\partial q^\mu}{\partial q^\mu}$ into the definition of the A_0 integral. In the next section, we use the same trick to further reduce the B_0' integral in terms of A_0 and B_0 functions.

D.2.2 The B_0' function

To derive an expression for the B_0' integral, we insert a factor $1 = D^{-1}\frac{\partial q^\mu}{\partial q^\mu}$ into the definition of the B_0 integral, and we integrate by parts:

$$B_0(p^2,m_1^2,m_2^2) = -\frac{C}{D}\int \mathrm{d}^D q\, q^\mu \frac{\partial}{\partial q^\mu}\frac{1}{[q^2-m_1^2][(q+p)^2-m_2^2]}. \tag{D.12}$$

After performing the derivative and some algebraic manipulations, we obtain the expression

$$\begin{aligned} B_0(p^2,m_1^2,m_2^2) = D^{-1}\Big[&3B_0(p^2,m_1^2,m_2^2) + B_0(0,m_2^2,m_2^2) + 2m_1^2 B_0'(p^2,m_1^2,m_2^2) \\ &- (p^2-m_1^2-m_2^2)B_0'(p^2,m_2^2,m_1^2)\Big]. \end{aligned} \tag{D.13}$$

The B_0 integral is symmetric in its mass arguments, so the right-hand side has to be invariant under exchange of the masses as well. We find

$$\begin{aligned} B_0(p^2,m_1^2,m_2^2) = D^{-1}\Big[&3B_0(p^2,m_1^2,m_2^2) + B_0(0,m_1^2,m_1^2) + 2m_2^2 B_0'(p^2,m_2^2,m_1^2) \\ &- (p^2-m_1^2-m_2^2)B_0'(p^2,m_1^2,m_2^2)\Big]. \end{aligned} \tag{D.14}$$

Solving the system of equations (D.13) and (D.14) for $B_0'(p^2,m_1^2,m_2^2)$, we obtain

$$\begin{aligned} B_0'(p^2,m_1^2,m_2^2) = \frac{-1}{\lambda(p^2,m_1^2,m_2^2)}\Big[&(p^2-m_1^2+m_2^2)(1-2\varepsilon)B_0(p^2,m_1^2,m_2^2) \\ &- 2(1-\varepsilon)A_0(m_2^2) - \frac{p^2-m_1^2-m_2^2}{m_1^2}(1-\varepsilon)A_0(m_1^2)\Big], \end{aligned} \tag{D.15}$$

where λ is the Källén function $\lambda(a,b,c) = a^2+b^2+c^2-2ab-2ac-2bc$. From Eq. (D.15), a few special cases are readily derived:

$$B_0'(p^2,m^2,m^2) = \frac{(1-2\varepsilon)B_0(p^2,m^2,m^2) - B_0(0,m^2,m^2)}{4m^2-p^2}, \tag{D.16a}$$

$$B_0'(p^2,m^2,0) = \frac{(1-2\varepsilon)B_0(p^2,m^2,0) - B_0(0,m^2,m^2)}{m^2-p^2}, \tag{D.16b}$$

$$B_0'(0,m^2,m^2) = \frac{-\varepsilon}{2m^2}B_0(0,m^2,m^2). \tag{D.16c}$$

As we explained above, for identical mass arguments we take the derivative with respect to the first mass argument before setting the masses equal.
Setting $m_1^2 = 0$ and $m_2^2 = m^2$ in Eq. (D.15), we obtain the relation

$$\begin{aligned} B_0(0,0,0) - (p^2-m^2)B_0'(p^2,0,m^2) = \\ \frac{(p^2+m^2)(1-2\varepsilon)B_0(p^2,m^2,0) - 2(1-\varepsilon)A_0(m^2)}{p^2-m^2}. \end{aligned} \tag{D.17}$$

$B_0(0,0,0)$ and $B_0'(p^2,0,m^2)$ are both IR-divergent while the integrals on the right-hand side are IR-finite.

D.2.3 The tensor coefficients

The two-point tensor coefficients can be reduced in terms of A_0 and B_0 functions:

$$\begin{aligned} B_1(p^2,m_1^2,m_2^2) = \frac{1}{2p^2}\Big[&A_0(m_1^2) - A_0(m_2^2) \\ &- (p^2-m_2^2+m_1^2)B_0(p^2,m_1^2,m_2^2)\Big], \end{aligned} \tag{D.18a}$$

$$\begin{aligned} B_{00}(p^2,m_1^2,m_2^2) = \frac{1}{6-4\varepsilon}\Big[&A_0(m_2^2) + 2m_1^2B_0(p^2,m_1^2,m_2^2) \\ &+ (p^2-m_2^2+m_1^2)B_1(p^2,m_1^2,m_2^2)\Big], \end{aligned} \tag{D.18b}$$

For B_1, the limit $p^2 \to 0$ needs to be taken carefully. We first cast the B_1 integral in the form

$$B_1(p^2, m_1^2, m_2^2) = -\frac{1}{2} B_0(p^2, m_1^2, m_2^2) + \frac{m_2^2 - m_1^2}{2} \frac{B_0(p^2, m_1^2, m_2^2) - B_0(0, m_1^2, m_2^2)}{p^2}. \tag{D.19}$$

By identifying the differential quotient in the second term on the right-hand side, we can now safely send $p^2 \to 0$:

$$B_1(0,m_1^2,m_2^2) = -\frac{1}{2} B_0(0,m_1^2,m_2^2) + \frac{m_2^2 - m_1^2}{2} \partial B_0(0,m_1^2,m_2^2). \tag{D.20}$$

Reduction formulae for ∂B_1 and ∂B_{00} are obtained by differentiating the relations for B_1 and B_{00} with respect to p^2.
The three-point tensor coefficients can be reduced via

$$\begin{aligned} C_2(0,p^2,p^2,m_1^2,m_1^2,m_2^2) = \frac{1}{2p^2}\Big[& B_0(0,m_1^2,m_1^2) - B_0(p^2,m_1^2,m_2^2) \\ & - (p^2 - m_2^2 + m_1^2) C_0(0,p^2,p^2,m_1^2,m_1^2,m_2^2)\Big], \end{aligned} \tag{D.21a}$$

$$\begin{aligned} C_2(p^2,0,p^2,m_1^2,m_2^2,m_2^2) = & - C_0(0,p^2,p^2,m_2^2,m_2^2,m_1^2) - C_1(p^2,0,p^2,m_1^2,m_2^2,m_2^2) \\ & - C_2(0,p^2,p^2,m_2^2,m_2^2,m_1^2), \end{aligned} \tag{D.21b}$$

$$\begin{aligned} C_{00}(0,p^2,p^2,m_1^2,m_1^2,m_2^2) = \frac{1}{6-4\varepsilon}\Big[& 2B_0(p^2,m_1^2,m_2^2) + B_1(p^2,m_1^2,m_2^2) \\ & + 2m_1^2 C_0(0,p^2,p^2,m_1^2,m_1^2,m_2^2) \\ & + (p^2 - m_2^2 + m_1^2) C_2(0,p^2,p^2,m_1^2,m_1^2,m_2^2)\Big], \end{aligned} \tag{D.21c}$$

$$\begin{aligned} C_{00}(p^2,0,p^2,m_1^2,m_2^2,m_2^2) = \frac{1}{6-4\varepsilon}\Big[& B_0(0,m_2^2,m_2^2) - B_1(p^2,m_1^2,m_2^2) \\ & + 2m_1^2 C_0(p^2,0,p^2,m_1^2,m_2^2,m_2^2) \\ & + (p^2 - m_2^2 + m_1^2) C_1(p^2,0,p^2,m_1^2,m_2^2,m_2^2) \\ & + (p^2 - m_2^2 + m_1^2) C_2(p^2,0,p^2,m_1^2,m_2^2,m_2^2)\Big]. \end{aligned} \tag{D.21d}$$

D.3 Analytic formulae for A_0 and the massless B_0

The A_0 integral and the massless B_0 integral can be put in a closed form; we also give their expanded versions up to $\mathcal{O}(\varepsilon)$:

$$\begin{aligned} A_0(m^2)/m^2 =& -\left(\frac{4\pi\mu_{\overline{\mathrm{D}}}^2}{m^2}\right)^{\varepsilon}\Gamma(-1+\varepsilon) \\ =& \frac{1}{\varepsilon}+1+\log(4\pi)-\gamma_E+\log\left(\frac{\mu_{\overline{\mathrm{D}}}^2}{m^2}\right) \\ &+\varepsilon\left\{\frac{1}{2}\left[1+\log(4\pi)-\gamma_E+\log\left(\frac{\mu_{\overline{\mathrm{D}}}^2}{m^2}\right)\right]^2+\frac{1}{2}+\frac{\pi^2}{12}\right\} \\ &+\mathcal{O}(\varepsilon^2), \end{aligned} \tag{D.22a}$$

$$\begin{aligned} B_0(p^2,0,0) =& \left(-\frac{4\pi\mu_{\overline{\mathrm{D}}}^2}{p^2}\right)^{\varepsilon}\frac{\Gamma(\varepsilon)\Gamma^2(1-\varepsilon)}{\Gamma(2-2\varepsilon)} \\ =& \frac{1}{\varepsilon}+2+\log(4\pi)-\gamma_E+\log\left(-\frac{\mu_{\overline{\mathrm{D}}}^2}{p^2}\right) \\ &+\varepsilon\left\{\frac{1}{2}\left[2+\log(4\pi)-\gamma_E+\log\left(-\frac{\mu_{\overline{\mathrm{D}}}^2}{p^2}\right)\right]^2+2-\frac{\pi^2}{12}\right\} \\ &+\mathcal{O}(\varepsilon^2). \end{aligned} \tag{D.22b}$$

The expression for $B_0(p^2,0,0)$ is well-defined for space-like momenta $p^2<0$ only and has to be continued analytically by replacing $p^2\to p^2+\mathrm{i}\epsilon$ in order to properly treat the branch cut of the function along the positive real axis.
Two important special cases of the B_0 integral with vanishing external momentum are given by

$$\begin{aligned} B_0(0,m^2,m^2) &= (1-\varepsilon)\frac{A_0(m^2)}{m^2} \\ &= (\varepsilon-1)\left(\frac{4\pi\mu_{\overline{\mathrm{D}}}^2}{m^2}\right)^{\varepsilon}\Gamma(-1+\varepsilon), \end{aligned} \tag{D.23a}$$

$$\begin{aligned} B_0(0,m_1^2,m_2^2) &= \frac{A_0(m_1^2)-A_0(m_2^2)}{m_1^2-m_2^2} \\ &= \left(\frac{4\pi\mu_{\overline{\mathrm{D}}}^2}{m_1m_2}\right)^{\varepsilon}\Gamma(-1+\varepsilon)\frac{m_1^2(m_2/m_1)^{\varepsilon}-m_2^2(m_1/m_2)^{\varepsilon}}{m_2^2-m_1^2}. \end{aligned} \tag{D.23b}$$

E The package `ColorSimp.m`

We created the package `ColorSimp.m` to evaluate colour sums for a general number of colours, which we call N_c. Its content reads

```
Index[Colour, x_] := Symbol["Col" <> ToString[x]];
Index[Gluon, x_] := Symbol["Glu" <> ToString[x]];

SUNTSum[i_, j_, k_, l_] := 1/2 (IndexDelta[i, l] IndexDelta[j, k]
    - 1/Nc IndexDelta[i, j] IndexDelta[k, l]);

SetAttributes[IndexDelta, Orderless];

DeltaSimp =
    {IndexDelta[n_, n_] -> 1,
    IndexDelta[n_Integer, _Integer] -> 0,
    IndexDelta[x___]^n_Integer -> IndexDelta[x]};

SumOverRepl =
    {SumOver[x1_, y1_, External] -> 1,
    SumOver[x1_, y1_] SumOver[x2_, y2_]
        -> DoubleSumOver[{x1, x2}, {y1, y2}],
    SumOver[x1_, y1_] DoubleSumOver[{x2_, x3_}, {y2_, y3_}]
        -> TripleSumOver[{x1, x2, x3}, {y1, y2, y3}],
    Times[SumOver[x_, y_], z_] -> SumOver2[z, x, y],
    Times[DoubleSumOver[x_, y_], z_] -> DoubleSumOver2[z, x, y],
    Times[TripleSumOver[x_, y_], z_] -> TripleSumOver2[z, x, y]};

SumOverExp =
    {SumOver2[Times[z1_, z2_], x_, y_] /; FreeQ[z1, x]
        -> z1 SumOver2[z2, x, y],
    SumOver2[Plus[z1_, z2_], x_, y_]
        -> SumOver2[z1, x, y] + SumOver2[z2, x, y],
```

```
    DoubleSumOver2[Times[z1_, z2_], {x1_, x2_}, y_]
        /; (FreeQ[z1, x1] && FreeQ[z1, x2])
        -> z1 DoubleSumOver2[z2, {x1, x2}, y],
    DoubleSumOver2[Plus[z1_, z2_], x_, y_]
        -> DoubleSumOver2[z1, x, y] + DoubleSumOver2[z2, x, y],
    TripleSumOver2[Times[z1_, z2_], {x1_, x2_, x3_}, y_]
        /; (FreeQ[z1, x1] && FreeQ[z1, x2] && FreeQ[z1, x3])
        -> z1 TripleSumOver2[z2, {x1, x2, x3}, y],
    TripleSumOver2[Plus[z1_, z2_], x_, y_]
        -> TripleSumOver2[z1, x, y]
        + TripleSumOver2[z2, {x1, x2}, y]};

SumOverEval =
    {SumOver2[z_, x_, y_] /; FreeQ[z, x] -> z*y,
    DoubleSumOver2[z_, {x1_, x2_}, {y1_, y2_}]
        /; (FreeQ[z, x1] && FreeQ[z, x2]) -> z*y1*y2,
    TripleSumOver2[z_, {x1_, x2_, x3_}, {y1_, y2_, y3_}]
        /; (FreeQ[z, x1] && FreeQ[z, x2] && FreeQ[z, x3])
        -> z*y1*y2*y3,
    DoubleSumOver2[IndexDelta[x1_, x2_], {x1_, x2_}, {y_, y_}] -> y,
    DoubleSumOver2[SUNT[x1_, x2_, x3_] SUNT[x4_, x3_, x2_],
        {x2_, x3_}, y_] -> 1/2 IndexDelta[x1, x4],
    TripleSumOver2[SUNT[x1_, x2_, x3_] SUNT[x1_, x3_, x2_], x_, y_]
        -> 1/2 (Nc^2 - 1),
    SumOver2[IndexDelta[x1_, x3_] IndexDelta[x2_, x3_], x3_, y3_]
        -> IndexDelta[x1, x2]};
```

The replacement rules are applied to any one- or two-loop amplitude `amp` via

```
    amp = amp//.DeltaSimp//.SumOverRepl//.SumOverExp//.SumOverEval;
```

F Generation of plots

In this appendix, we explain how the different plots shown in Ch. 7 were obtained. For any given point in parameter space, we always calculate the Higgs boson mass square at the one- ($1L$) and two-loop order ($2L$) including different generations of matter:

- Only the third generation quarks (t and b) and squarks are included ($3g$).
- Quarks and squarks of all generations are included (ag).

We perform these calculations in several different limits:

- Full prediction at $\mathcal{O}(N_c)/\mathcal{O}\left(N_c^2\right)$ ($full$).
- Gaugeless limit, $\alpha_{\rm em} = 0$ (gl). We numerically take this limit by replacing $M_Z \to \widehat{M}_Z$, $M_W \to M_W(\widehat{M}_Z/M_Z)$, and $\alpha_{\rm em} \to \alpha_{\rm em}(\widehat{M}_Z/M_Z)^2$, where $\widehat{M}_Z \ll M_Z$. In scenarios 1 and 2 we use $\widehat{M}_Z = M_S/1000$, in scenario 3 $\widehat{M}_Z = \max\{|A_q|/1000, 1\text{ GeV}\}$, and in scenario 4 we set $\widehat{M}_Z = M_S/500$.
- Limit of vanishing bottom mass, $m_b = 0$ (bl). We employ this numerically by replacing $m_b \to m_b/10 = 0.418$ GeV.
- $\alpha_{\rm em} = 0$ and $m_b = 0$ ($gl + bl$). For this limit, we simply combine the aforementioned prescriptions for the gaugeless limit and the limit of vanishing bottom mass.

We use the symbol $(M^2_{h_i})^{l,g,c}$ for each of the different predictions for the squared Higgs boson masses, where

$$\begin{aligned} h_i &\in \{h, H\}, \\ l &\in \{1L, 2L\}, \\ g &\in \{3g, ag\}, \\ c &\in \{full, gl, bl, gl + bl\}. \end{aligned} \tag{F.1}$$

As the first and second generation are assumed to be massless, there is no difference between working with the third or all generations in the gaugeless limit:

$$(M^2_{h_i})^{l,3g,gl} = (M^2_{h_i})^{l,ag,gl}, \tag{F.2a}$$

$$(M^2_{h_i})^{l,3g,gl+bl} = (M^2_{h_i})^{l,ag,gl+bl}. \tag{F.2b}$$

We have used these identities to validate our implementation of the gaugeless limit. Nevertheless, we will occasionally use gaugeless results with either one or three generations. This leaves us with six predictions for the Higgs boson mass at one-loop order[16] and the same number of predictions for the two-loop masses per parameter point. We combine them to obtain all contributions we are interested in.
In the plots for the Higgs boson masses in Ch. 7 (these are Figs. 7.1, 7.3, 7.6, and 7.9), up to five curves are shown:

$$\text{cyan, solid: } M_{h_i} = \sqrt{(M^2_{h_i})^{2L,ag,full}}, \tag{F.3a}$$

$$\text{cyan, dashed: } M_{h_i} = \sqrt{(M^2_{h_i})^{2L,3g,full} - (M^2_{h_i})^{1L,3g,full} + (M^2_{h_i})^{1L,ag,full}}, \tag{F.3b}$$

$$\text{green, solid: } M_{h_i} = \sqrt{(M^2_{h_i})^{2L,ag,gl} - (M^2_{h_i})^{1L,3g,gl} + (M^2_{h_i})^{1L,ag,full}}, \tag{F.3c}$$

$$\text{green, dashed: } M_{h_i} = \sqrt{(M^2_{h_i})^{2L,3g,gl+bl} - (M^2_{h_i})^{1L,3g,gl+bl} + (M^2_{h_i})^{1L,ag,full}}, \tag{F.3d}$$

$$\text{black, solid: } M_{h_i} = \sqrt{(M^2_{h_i})^{1L,ag,full}}. \tag{F.3e}$$

When we make a prediction for the two-loop mass in any given limit and for any number of fermion generations, the same properties are also applied to the tree-level and one-loop contribution. As we are interested in estimating the size of the newly calculated two-loop corrections, we subtract the appropriate one-loop prediction from the two-loop value and add the full $\mathcal{O}(N_c)$ one-loop result, which includes all generations of matter.
In the plots for the two-loop contributions to the Higgs boson mass square (these are Figs. 7.2a, 7.4a, 7.5a, 7.7a, 7.8a, 7.10a, 7.11a), twelve combinations are possible:

$$\text{cyan, solid: } \Delta^{(2)} M^2_{h_i} = (M^2_{h_i})^{2L,ag,full} - (M^2_{h_i})^{1L,ag,full}, \tag{F.4a}$$

$$\text{cyan, dashed: } \Delta^{(2)} M^2_{h_i} = (M^2_{h_i})^{2L,3g,full} - (M^2_{h_i})^{1L,3g,full}, \tag{F.4b}$$

$$\text{magenta, solid: } \Delta^{(2)} M^2_{h_i} = (M^2_{h_i})^{2L,ag,bl} - (M^2_{h_i})^{1L,ag,bl}, \tag{F.4c}$$

$$\text{magenta, dashed: } \Delta^{(2)} M^2_{h_i} = (M^2_{h_i})^{2L,3g,bl} - (M^2_{h_i})^{1L,3g,bl}, \tag{F.4d}$$

$$\text{green, solid: } \Delta^{(2)} M^2_{h_i} = (M^2_{h_i})^{2L,ag,gl} - (M^2_{h_i})^{1L,ag,gl}, \tag{F.4e}$$

[16] 3g/full, 3g/gl, 3g/bl, 3g/gl+bl, ag/full, and ag/bl.

$$\text{green, dashed: } \Delta^{(2)} M_{h_i}^2 = (M_{h_i}^2)^{2L,3g,gl+bl} - (M_{h_i}^2)^{1L,3g,gl+bl}, \tag{F.4f}$$

$$\begin{aligned}\text{green, dotted: } \Delta^{(2)} M_{h_i}^2 = &\left[(M_{h_i}^2)^{2L,ag,gl} - (M_{h_i}^2)^{1L,ag,gl}\right] \\ &- \left[(M_{h_i}^2)^{2L,3g,gl+bl} - (M_{h_i}^2)^{1L,3g,gl+bl}\right],\end{aligned} \tag{F.4g}$$

$$\begin{aligned}\text{red, solid: } \Delta^{(2)} M_{h_i}^2 = &\left[(M_{h_i}^2)^{2L,ag,full} - (M_{h_i}^2)^{1L,ag,full}\right] \\ &- \left[(M_{h_i}^2)^{2L,ag,gl} - (M_{h_i}^2)^{1L,ag,gl}\right],\end{aligned} \tag{F.4h}$$

$$\begin{aligned}\text{red, dashed: } \Delta^{(2)} M_{h_i}^2 = &\left[(M_{h_i}^2)^{2L,3g,full} - (M_{h_i}^2)^{1L,3g,full}\right] \\ &- \left[(M_{h_i}^2)^{2L,3g,gl} - (M_{h_i}^2)^{1L,3g,gl}\right],\end{aligned} \tag{F.4i}$$

$$\begin{aligned}\text{red, dotted: } \Delta^{(2)} M_{h_i}^2 = &\left[(M_{h_i}^2)^{2L,ag,full} - (M_{h_i}^2)^{1L,ag,full}\right] \\ &- \left[(M_{h_i}^2)^{2L,3g,full} - (M_{h_i}^2)^{1L,3g,full}\right],\end{aligned} \tag{F.4j}$$

$$\begin{aligned}\text{orange, solid: } \Delta^{(2)} M_{h_i}^2 = &\left[(M_{h_i}^2)^{2L,ag,full} - (M_{h_i}^2)^{1L,ag,full}\right] \\ &- \left[(M_{h_i}^2)^{2L,ag,bl} - (M_{h_i}^2)^{1L,ag,bl}\right],\end{aligned} \tag{F.4k}$$

$$\begin{aligned}\text{orange, dashed: } \Delta^{(2)} M_{h_i}^2 = &\left[(M_{h_i}^2)^{2L,3g,full} - (M_{h_i}^2)^{1L,3g,full}\right] \\ &- \left[(M_{h_i}^2)^{2L,3g,bl} - (M_{h_i}^2)^{1L,3g,bl}\right].\end{aligned} \tag{F.4l}$$

The same twelve combinations are possible for the plots where the contributions are calculated as quantities of mass dimensions one (these are Figs. 7.2b, 7.4b, 7.5b, 7.7b, 7.8b, 7.10b, 7.11b)). Clearly, we cannot just take the square root of the expressions above, as we are interested in the difference between different Higgs boson mass predictions. We take the square roots as follows:

$$\text{cyan, solid: } \Delta^{(2)} M_{h_i} = \sqrt{(M_{h_i}^2)^{2L,ag,full}} - \sqrt{(M_{h_i}^2)^{1L,ag,full}}, \tag{F.5a}$$

$$\begin{aligned}\text{cyan, dashed: } \Delta^{(2)} M_{h_i} = &\sqrt{(M_{h_i}^2)^{2L,3g,full} - (M_{h_i}^2)^{1L,3g,full} + (M_{h_i}^2)^{1L,ag,full}} \\ &- \sqrt{(M_{h_i}^2)^{1L,ag,full}},\end{aligned} \tag{F.5b}$$

$$\begin{aligned}\text{magenta, solid: } \Delta^{(2)} M_{h_i} = &\sqrt{(M_{h_i}^2)^{2L,ag,bl} - (M_{h_i}^2)^{1L,ag,bl} + (M_{h_i}^2)^{1L,ag,full}} \\ &- \sqrt{(M_{h_i}^2)^{1L,ag,full}},\end{aligned} \tag{F.5c}$$

$$\begin{aligned}\text{magenta, dashed: } \Delta^{(2)} M_{h_i} = &\sqrt{(M_{h_i}^2)^{2L,3g,bl} - (M_{h_i}^2)^{1L,3g,bl} + (M_{h_i}^2)^{1L,ag,full}} \\ &- \sqrt{(M_{h_i}^2)^{1L,ag,full}},\end{aligned} \tag{F.5d}$$

$$\begin{aligned}\text{green, solid: } \Delta^{(2)} M_{h_i} = &\sqrt{(M_{h_i}^2)^{2L,ag,gl} - (M_{h_i}^2)^{1L,ag,gl} + (M_{h_i}^2)^{1L,ag,full}} \\ &- \sqrt{(M_{h_i}^2)^{1L,ag,full}},\end{aligned} \tag{F.5e}$$

$$\text{green, dashed: } \Delta^{(2)} M_{h_i} = \sqrt{(M^2_{h_i})^{2L,3g,gl+bl} - (M^2_{h_i})^{1L,3g,gl+bl} + (M^2_{h_i})^{1L,ag,full}} - \sqrt{(M^2_{h_i})^{1L,ag,full}}, \tag{F.5f}$$

$$\text{green, dotted: } \Delta^{(2)} M_{h_i} = \sqrt{(M^2_{h_i})^{2L,ag,gl} - (M^2_{h_i})^{1L,ag,gl} + (M^2_{h_i})^{1L,ag,full}} - \sqrt{(M^2_{h_i})^{2L,3g,gl+bl} - (M^2_{h_i})^{1L,3g,gl+bl} + (M^2_{h_i})^{1L,ag,full}}, \tag{F.5g}$$

$$\text{red, solid: } \Delta^{(2)} M_{h_i} = \sqrt{(M^2_{h_i})^{2L,ag,full}} - \sqrt{(M^2_{h_i})^{2L,ag,gl} - (M^2_{h_i})^{1L,ag,gl} + (M^2_{h_i})^{1L,ag,full}}, \tag{F.5h}$$

$$\text{red, dashed: } \Delta^{(2)} M_{h_i} = \sqrt{(M^2_{h_i})^{2L,3g,full} - (M^2_{h_i})^{1L,3g,full} + (M^2_{h_i})^{1L,ag,full}} - \sqrt{(M^2_{h_i})^{2L,3g,gl} - (M^2_{h_i})^{1L,3g,gl} + (M^2_{h_i})^{1L,ag,full}}, \tag{F.5i}$$

$$\text{red, dotted: } \Delta^{(2)} M_{h_i} = \sqrt{(M^2_{h_i})^{2L,ag,full}} - \sqrt{(M^2_{h_i})^{2L,3g,full} - (M^2_{h_i})^{1L,3g,full} + (M^2_{h_i})^{1L,ag,full}}, \tag{F.5j}$$

$$\text{orange, solid: } \Delta^{(2)} M_{h_i} = \sqrt{(M^2_{h_i})^{2L,ag,full}} - \sqrt{(M^2_{h_i})^{2L,ag,bl} - (M^2_{h_i})^{1L,ag,bl} + (M^2_{h_i})^{1L,ag,full}}, \tag{F.5k}$$

$$\text{orange, dashed: } \Delta^{(2)} M_{h_i} = \sqrt{(M^2_{h_i})^{2L,3g,full}} - \sqrt{(M^2_{h_i})^{2L,3g,bl} - (M^2_{h_i})^{1L,3g,bl} + (M^2_{h_i})^{1L,ag,full}}. \tag{F.5l}$$

The plots in Sect. 7.5 have been created in a slightly different way than the ones listed above. Fig. 7.12 was made using a fixed-order prediction and it is, hence, very similar to the ones mentioned before. The other ones were made using a fixed-point iteration (Fig. 7.13) and a subsequent appropriate subtraction (Fig. 7.14) using the same ideas as explained above.

It should also be noted that not all possible curves listed in this appendix appear in each scenario.

Bibliography

[1] ATLAS collaboration, *Observation of a new particle in the search for the Standard Model Higgs boson with the ATLAS detector at the LHC*, *Phys. Lett. B* **716** (2012) 1 [1207.7214].

[2] CMS collaboration, *Observation of a New Boson at a Mass of 125 GeV with the CMS Experiment at the LHC*, *Phys. Lett. B* **716** (2012) 30 [1207.7235].

[3] ATLAS, CMS collaboration, *Combined Measurement of the Higgs Boson Mass in pp Collisions at $\sqrt{s} = 7$ and 8 TeV with the ATLAS and CMS Experiments*, *Phys. Rev. Lett.* **114** (2015) 191803 [1503.07589].

[4] ATLAS, CMS collaboration, *Measurements of the Higgs boson production and decay rates and constraints on its couplings from a combined ATLAS and CMS analysis of the LHC pp collision data at $\sqrt{s} = 7$ and 8 TeV*, *JHEP* **08** (2016) 045 [1606.02266].

[5] ATLAS collaboration, *A detailed map of Higgs boson interactions by the ATLAS experiment ten years after the discovery*, *Nature* **607** (2022) 52 [2207.00092].

[6] CMS collaboration, *A portrait of the Higgs boson by the CMS experiment ten years after the discovery*, *Nature* **607** (2022) 60 [2207.00043].

[7] Particle Data Group collaboration, *Review of Particle Physics*, *PTEP* **2022** (2022) 083C01.

[8] H.P. Nilles, *Supersymmetry, Supergravity and Particle Physics*, *Phys. Rept.* **110** (1984) 1.

[9] H.E. Haber and G.L. Kane, *The Search for Supersymmetry: Probing Physics Beyond the Standard Model*, *Phys. Rept.* **117** (1985) 75.

[10] K. Inoue, A. Kakuto, H. Komatsu and S. Takeshita, *Low-Energy Parameters and Particle Masses in a Supersymmetric Grand Unified Model*, *Prog. Theor. Phys.* **67** (1982) 1889.

[11] S.P. Li and M. Sher, *Upper Limit to the Lightest Higgs Mass in Supersymmetric Models*, *Phys. Lett. B* **140** (1984) 339.

[12] J.F. Gunion and A. Turski, *Corrections to Higgs Boson Mass Sum Rules from the Sfermion Sector of a Supersymmetric Model*, *Phys. Rev. D* **40** (1989) 2333.

[13] M.S. Berger, *Radiative Corrections to Higgs Boson Mass Sum Rules in the Minimal Supersymmetric Extension to the Standard Model*, *Phys. Rev. D* **41** (1990) 225.

[14] Y. Okada, M. Yamaguchi and T. Yanagida, *Upper bound of the lightest Higgs boson mass in the minimal supersymmetric standard model*, *Prog. Theor. Phys.* **85** (1991) 1.

[15] J.R. Ellis, G. Ridolfi and F. Zwirner, *Radiative corrections to the masses of supersymmetric Higgs bosons*, *Phys. Lett. B* **257** (1991) 83.

[16] H.E. Haber and R. Hempfling, *Can the mass of the lightest Higgs boson of the minimal supersymmetric model be larger than m(Z)?*, *Phys. Rev. Lett.* **66** (1991) 1815.

[17] R. Barbieri and M. Frigeni, *The Supersymmetric Higgs searches at LEP after radiative corrections*, *Phys. Lett. B* **258** (1991) 395.

[18] J.R. Ellis, G. Ridolfi and F. Zwirner, *On radiative corrections to supersymmetric Higgs boson masses and their implications for LEP searches*, *Phys. Lett. B* **262** (1991) 477.

[19] A. Brignole, J.R. Ellis, G. Ridolfi and F. Zwirner, *The supersymmetric charged Higgs boson mass and LEP phenomenology*, *Phys. Lett. B* **271** (1991) 123.

[20] P.H. Chankowski, S. Pokorski and J. Rosiek, *Charged and neutral supersymmetric Higgs boson masses: Complete one loop analysis*, *Phys. Lett. B* **274** (1992) 191.

[21] A. Brignole, *Radiative corrections to the supersymmetric charged Higgs boson mass*, *Phys. Lett. B* **277** (1992) 313.

[22] A. Brignole, *Radiative corrections to the supersymmetric neutral Higgs boson masses*, *Phys. Lett. B* **281** (1992) 284.

[23] P.H. Chankowski, S. Pokorski and J. Rosiek, *Complete on-shell renormalization scheme for the minimal supersymmetric Higgs sector*, *Nucl. Phys. B* **423** (1994) 437 [hep-ph/9303309].

[24] A. Dabelstein, *The One loop renormalization of the MSSM Higgs sector and its application to the neutral scalar Higgs masses*, *Z. Phys. C* **67** (1995) 495 [hep-ph/9409375].

[25] D.M. Pierce, J.A. Bagger, K.T. Matchev and R.-j. Zhang, *Precision corrections in the minimal supersymmetric standard model*, *Nucl. Phys. B* **491** (1997) 3 [hep-ph/9606211].

[26] R. Hempfling and A.H. Hoang, *Two loop radiative corrections to the upper limit of the lightest Higgs boson mass in the minimal supersymmetric model*, *Phys. Lett. B* **331** (1994) 99 [hep-ph/9401219].

[27] S. Heinemeyer, W. Hollik and G. Weiglein, *QCD corrections to the masses of the neutral CP - even Higgs bosons in the MSSM*, *Phys. Rev. D* **58** (1998) 091701 [hep-ph/9803277].

[28] S. Heinemeyer, W. Hollik and G. Weiglein, *Precise prediction for the mass of the lightest Higgs boson in the MSSM*, *Phys. Lett. B* **440** (1998) 296 [hep-ph/9807423].

[29] R.-J. Zhang, *Two loop effective potential calculation of the lightest CP even Higgs boson mass in the MSSM*, *Phys. Lett. B* **447** (1999) 89 [hep-ph/9808299].

[30] S. Heinemeyer, W. Hollik and G. Weiglein, *The Masses of the neutral CP - even Higgs bosons in the MSSM: Accurate analysis at the two loop level*, *Eur. Phys. J. C* **9** (1999) 343 [hep-ph/9812472].

[31] J.R. Espinosa and R.-J. Zhang, *MSSM lightest CP even Higgs boson mass to O(alpha(s) alpha(t)): The Effective potential approach*, *JHEP* **03** (2000) 026 [hep-ph/9912236].

[32] M. Carena, H.E. Haber, S. Heinemeyer, W. Hollik, C.E.M. Wagner and G. Weiglein, *Reconciling the two loop diagrammatic and effective field theory computations of the mass of the lightest CP - even Higgs boson in the MSSM*, *Nucl. Phys. B* **580** (2000) 29 [hep-ph/0001002].

[33] J.R. Espinosa and R.-J. Zhang, *Complete two loop dominant corrections to the mass of the lightest CP even Higgs boson in the minimal supersymmetric standard model*, *Nucl. Phys. B* **586** (2000) 3 [hep-ph/0003246].

[34] G. Degrassi, P. Slavich and F. Zwirner, *On the neutral Higgs boson masses in the MSSM for arbitrary stop mixing*, *Nucl. Phys. B* **611** (2001) 403 [hep-ph/0105096].

[35] A. Brignole, G. Degrassi, P. Slavich and F. Zwirner, *On the O(alpha(t)**2) two loop corrections to the neutral Higgs boson masses in the MSSM*, *Nucl. Phys. B* **631** (2002) 195 [hep-ph/0112177].

[36] A. Brignole, G. Degrassi, P. Slavich and F. Zwirner, *On the two loop sbottom corrections to the neutral Higgs boson masses in the MSSM*, *Nucl. Phys. B* **643** (2002) 79 [hep-ph/0206101].

[37] A. Dedes and P. Slavich, *Two loop corrections to radiative electroweak symmetry breaking in the MSSM*, *Nucl. Phys. B* **657** (2003) 333 [hep-ph/0212132].

[38] A. Dedes, G. Degrassi and P. Slavich, *On the two loop Yukawa corrections to the MSSM Higgs boson masses at large tan beta*, *Nucl. Phys. B* **672** (2003) 144 [hep-ph/0305127].

[39] B.C. Allanach, A. Djouadi, J.L. Kneur, W. Porod and P. Slavich, *Precise determination of the neutral Higgs boson masses in the MSSM*, *JHEP* **09** (2004) 044 [hep-ph/0406166].

[40] S. Heinemeyer, W. Hollik, H. Rzehak and G. Weiglein, *High-precision predictions for the MSSM Higgs sector at O(alpha(b) alpha(s))*, *Eur. Phys. J. C* **39** (2005) 465 [hep-ph/0411114].

[41] M. Frank, L. Galeta, T. Hahn, S. Heinemeyer, W. Hollik, H. Rzehak et al., *Charged Higgs Boson Mass of the MSSM in the Feynman Diagrammatic Approach*, *Phys. Rev. D* **88** (2013) 055013 [1306.1156].

[42] W. Hollik and S. Paßehr, *Two-loop top-Yukawa-coupling corrections to the charged Higgs-boson mass in the MSSM*, *Eur. Phys. J. C* **75** (2015) 336 [1502.02394].

[43] S.P. Martin, *Complete Two Loop Effective Potential Approximation to the Lightest Higgs Scalar Boson Mass in Supersymmetry*, *Phys. Rev. D* **67** (2003) 095012 [hep-ph/0211366].

[44] S.P. Martin, *Two Loop Effective Potential for the Minimal Supersymmetric Standard Model*, *Phys. Rev. D* **66** (2002) 096001 [hep-ph/0206136].

[45] S.P. Martin, *Strong and Yukawa two-loop contributions to Higgs scalar boson self-energies and pole masses in supersymmetry*, *Phys. Rev. D* **71** (2005) 016012 [hep-ph/0405022].

[46] S.P. Martin, *Evaluation of two loop selfenergy basis integrals using differential equations*, *Phys. Rev. D* **68** (2003) 075002 [hep-ph/0307101].

[47] S.P. Martin and D.G. Robertson, *TSIL: A Program for the calculation of two-loop self-energy integrals*, *Comput. Phys. Commun.* **174** (2006) 133 [hep-ph/0501132].

[48] S. Heinemeyer, H. Rzehak and C. Schappacher, *Proposals for Bottom Quark/Squark Renormalization in the Complex MSSM*, *Phys. Rev. D* **82** (2010) 075010 [1007.0689].

[49] T. Fritzsche, S. Heinemeyer, H. Rzehak and C. Schappacher, *Heavy Scalar Top Quark Decays in the Complex MSSM: A Full One-Loop Analysis*, *Phys. Rev. D* **86** (2012) 035014 [1111.7289].

[50] T. Fritzsche, T. Hahn, S. Heinemeyer, F. von der Pahlen, H. Rzehak and C. Schappacher, *The Implementation of the Renormalized Complex MSSM in FeynArts and FormCalc*, *Comput. Phys. Commun.* **185** (2014) 1529 [1309.1692].

[51] S. Borowka, T. Hahn, S. Heinemeyer, G. Heinrich and W. Hollik, *Momentum-dependent two-loop QCD corrections to the neutral Higgs-boson masses in the MSSM*, *Eur. Phys. J. C* **74** (2014) 2994 [1404.7074].

[52] G. Degrassi, S. Di Vita and P. Slavich, *Two-loop QCD corrections to the MSSM Higgs masses beyond the effective-potential approximation*, *Eur. Phys. J. C* **75** (2015) 61 [1410.3432].

[53] J. Carter and G. Heinrich, *SecDec: A general program for sector decomposition*, *Comput. Phys. Commun.* **182** (2011) 1566 [1011.5493].

[54] S. Borowka, J. Carter and G. Heinrich, *Numerical Evaluation of Multi-Loop Integrals for Arbitrary Kinematics with SecDec 2.0*, *Comput. Phys. Commun.* **184** (2013) 396 [1204.4152].

[55] S. Borowka, T. Hahn, S. Heinemeyer, G. Heinrich and W. Hollik, *Renormalization scheme dependence of the two-loop QCD corrections to the neutral Higgs-boson masses in the MSSM*, *Eur. Phys. J. C* **75** (2015) 424 [1505.03133].

[56] S. Borowka, S. Paßehr and G. Weiglein, *Complete two-loop QCD contributions to the lightest Higgs-boson mass in the MSSM with complex parameters*, *Eur. Phys. J. C* **78** (2018) 576 [1802.09886].

[57] A. Pilaftsis, *Higgs scalar - pseudoscalar mixing in the minimal supersymmetric standard model*, *Phys. Lett. B* **435** (1998) 88 [hep-ph/9805373].

[58] D.A. Demir, *Effects of the supersymmetric phases on the neutral Higgs sector*, *Phys. Rev. D* **60** (1999) 055006 [hep-ph/9901389].

[59] A. Pilaftsis and C.E.M. Wagner, *Higgs bosons in the minimal supersymmetric standard model with explicit CP violation*, *Nucl. Phys. B* **553** (1999) 3 [hep-ph/9902371].

[60] S.Y. Choi, M. Drees and J.S. Lee, *Loop corrections to the neutral Higgs boson sector of the MSSM with explicit CP violation*, *Phys. Lett. B* **481** (2000) 57 [hep-ph/0002287].

[61] M. Carena, J.R. Ellis, A. Pilaftsis and C.E.M. Wagner, *Renormalization group improved effective potential for the MSSM Higgs sector with explicit CP violation*, *Nucl. Phys. B* **586** (2000) 92 [hep-ph/0003180].

[62] T. Ibrahim and P. Nath, *Corrections to the Higgs boson masses and mixings from chargino, W and charged Higgs exchange loops and large CP phases*, *Phys. Rev. D* **63** (2001) 035009 [hep-ph/0008237].

[63] S. Heinemeyer, *The Higgs boson sector of the complex MSSM in the Feynman diagrammatic approach*, *Eur. Phys. J. C* **22** (2001) 521 [hep-ph/0108059].

[64] M. Carena, J.R. Ellis, A. Pilaftsis and C.E.M. Wagner, *Higgs Boson Pole Masses in the MSSM with Explicit CP Violation*, *Nucl. Phys. B* **625** (2002) 345 [hep-ph/0111245].

[65] T. Ibrahim and P. Nath, *Neutralino exchange corrections to the Higgs boson mixings with explicit CP violation*, *Phys. Rev. D* **66** (2002) 015005 [hep-ph/0204092].

[66] J.R. Ellis, J.S. Lee and A. Pilaftsis, *CERN LHC signatures of resonant CP violation in a minimal supersymmetric Higgs sector*, *Phys. Rev. D* **70** (2004) 075010 [hep-ph/0404167].

[67] M. Frank, T. Hahn, S. Heinemeyer, W. Hollik, H. Rzehak and G. Weiglein, *The Higgs Boson Masses and Mixings of the Complex MSSM in the Feynman-Diagrammatic Approach*, *JHEP* **02** (2007) 047 [hep-ph/0611326].

[68] S. Heinemeyer, W. Hollik, H. Rzehak and G. Weiglein, *The Higgs sector of the complex MSSM at two-loop order: QCD contributions*, *Phys. Lett. B* **652** (2007) 300 [0705.0746].

[69] S. Heinemeyer, W. Hollik, F. Merz and S. Penaranda, *Electroweak precision observables in the MSSM with nonminimal flavor violation*, *Eur. Phys. J. C* **37** (2004) 481 [hep-ph/0403228].

[70] J. Cao, G. Eilam, K.-i. Hikasa and J.M. Yang, *Experimental constraints on stop-scharm flavor mixing and implications in top-quark FCNC processes*, *Phys. Rev. D* **74** (2006) 031701 [hep-ph/0604163].

[71] A. Brignole, *The supersymmetric Higgs boson with flavoured A-terms*, *Nucl. Phys. B* **898** (2015) 644 [1504.03273].

[72] M. Arana-Catania, S. Heinemeyer, M.J. Herrero and S. Penaranda, *Higgs Boson masses and B-Physics Constraints in Non-Minimal Flavor Violating SUSY scenarios*, *JHEP* **05** (2012) 015 [1109.6232].

[73] M.E. Gómez, T. Hahn, S. Heinemeyer and M. Rehman, *Higgs masses and Electroweak Precision Observables in the Lepton-Flavor-Violating MSSM*, *Phys. Rev. D* **90** (2014) 074016 [1408.0663].

[74] W. Hollik and S. Paßehr, *Two-loop top-Yukawa-coupling corrections to the Higgs boson masses in the complex MSSM*, *Phys. Lett. B* **733** (2014) 144 [1401.8275].

[75] W. Hollik and S. Paßehr, *Higgs boson masses and mixings in the complex MSSM with two-loop top-Yukawa-coupling corrections*, *JHEP* **10** (2014) 171 [1409.1687].

[76] T. Hahn and S. Paßehr, *Implementation of the $\mathcal{O}\left(\alpha_t^2\right)$ MSSM Higgs-mass corrections in* ***FeynHiggs***, *Comput. Phys. Commun.* **214** (2017) 91 [1508.00562].

[77] S. Paßehr and G. Weiglein, *Two-loop top and bottom Yukawa corrections to the Higgs-boson masses in the complex MSSM*, *Eur. Phys. J. C* **78** (2018) 222 [1705.07909].

[78] M.D. Goodsell and S. Paßehr, *All two-loop scalar self-energies and tadpoles in general renormalisable field theories*, *Eur. Phys. J. C* **80** (2020) 417 [1910.02094].

[79] F. Domingo and S. Paßehr, *Fighting off field dependence in MSSM Higgs-mass corrections of order $\alpha_t\,\alpha_s$ and α_t^2*, *Eur. Phys. J. C* **81** (2021) 661 [2105.01139].

[80] E.A.R. R. and R. Fazio, *High-Precision Calculations of the Higgs Boson Mass*, *Particles* **5** (2022) 53 [2112.15295].

[81] R. Barbieri, M. Frigeni and F. Caravaglios, *The Supersymmetric Higgs for heavy superpartners*, *Phys. Lett. B* **258** (1991) 167.

[82] J.R. Espinosa and M. Quiros, *Two loop radiative corrections to the mass of the lightest Higgs boson in supersymmetric standard models*, *Phys. Lett. B* **266** (1991) 389.

[83] J.A. Casas, J.R. Espinosa, M. Quiros and A. Riotto, *The Lightest Higgs boson mass in the minimal supersymmetric standard model*, *Nucl. Phys. B* **436** (1995) 3 [hep-ph/9407389].

[84] H.E. Haber and R. Hempfling, *The Renormalization group improved Higgs sector of the minimal supersymmetric model*, *Phys. Rev. D* **48** (1993) 4280 [hep-ph/9307201].

[85] M. Carena, J.R. Espinosa, M. Quiros and C.E.M. Wagner, *Analytical expressions for radiatively corrected Higgs masses and couplings in the MSSM*, *Phys. Lett. B* **355** (1995) 209 [hep-ph/9504316].

[86] M. Carena, M. Quiros and C.E.M. Wagner, *Effective potential methods and the Higgs mass spectrum in the MSSM*, *Nucl. Phys. B* **461** (1996) 407 [hep-ph/9508343].

[87] H.E. Haber, R. Hempfling and A.H. Hoang, *Approximating the radiatively corrected Higgs mass in the minimal supersymmetric model*, *Z. Phys. C* **75** (1997) 539 [hep-ph/9609331].

[88] G. Degrassi, S. Heinemeyer, W. Hollik, P. Slavich and G. Weiglein, *Towards high precision predictions for the MSSM Higgs sector*, *Eur. Phys. J. C* **28** (2003) 133 [hep-ph/0212020].

[89] S.P. Martin, *Three-loop corrections to the lightest Higgs scalar boson mass in supersymmetry*, *Phys. Rev. D* **75** (2007) 055005 [hep-ph/0701051].

[90] T. Hahn, S. Heinemeyer, W. Hollik, H. Rzehak and G. Weiglein, *High-Precision Predictions for the Light CP -Even Higgs Boson Mass of the Minimal Supersymmetric Standard Model*, *Phys. Rev. Lett.* **112** (2014) 141801 [1312.4937].

[91] P. Draper, G. Lee and C.E.M. Wagner, *Precise estimates of the Higgs mass in heavy supersymmetry*, *Phys. Rev. D* **89** (2014) 055023 [1312.5743].

[92] N. Arkani-Hamed and S. Dimopoulos, *Supersymmetric unification without low energy supersymmetry and signatures for fine-tuning at the LHC*, *JHEP* **06** (2005) 073 [hep-th/0405159].

[93] G.F. Giudice and A. Romanino, *Split supersymmetry*, *Nucl. Phys. B* **699** (2004) 65 [hep-ph/0406088].

[94] M. Carena, G. Nardini, M. Quiros and C.E.M. Wagner, *The Effective Theory of the Light Stop Scenario*, *JHEP* **10** (2008) 062 [0806.4297].

[95] M. Binger, *Higgs boson mass in split supersymmetry at two-loops*, *Phys. Rev. D* **73** (2006) 095001 [hep-ph/0408240].

[96] N. Bernal, A. Djouadi and P. Slavich, *The MSSM with heavy scalars*, *JHEP* **07** (2007) 016 [0705.1496].

[97] P.P. Giardino and P. Lodone, *Threshold Corrections to Hard Supersymmetric Relations*, *Mod. Phys. Lett. A* **29** (2014) 1450101 [1112.2635].

[98] G.F. Giudice and A. Strumia, *Probing High-Scale and Split Supersymmetry with Higgs Mass Measurements*, *Nucl. Phys. B* **858** (2012) 63 [1108.6077].

[99] E. Bagnaschi, G.F. Giudice, P. Slavich and A. Strumia, *Higgs Mass and Unnatural Supersymmetry*, *JHEP* **09** (2014) 092 [1407.4081].

[100] C. Tamarit, *Decoupling heavy sparticles in hierarchical SUSY scenarios: Two-loop Renormalization Group equations*, 1204.2292.

[101] K. Benakli, L. Darmé, M.D. Goodsell and P. Slavich, *A Fake Split Supersymmetry Model for the 126 GeV Higgs*, *JHEP* **05** (2014) 113 [1312.5220].

[102] P.J. Fox, D.E. Kaplan, E. Katz, E. Poppitz, V. Sanz, M. Schmaltz et al., *Supersplit supersymmetry*, hep-th/0503249.

[103] L.J. Hall and Y. Nomura, *A Finely-Predicted Higgs Boson Mass from A Finely-Tuned Weak Scale*, *JHEP* **03** (2010) 076 [0910.2235].

[104] M.E. Cabrera, J.A. Casas and A. Delgado, *Upper Bounds on Superpartner Masses from Upper Bounds on the Higgs Boson Mass*, *Phys. Rev. Lett.* **108** (2012) 021802 [1108.3867].

[105] G. Degrassi, S. Di Vita, J. Elias-Miro, J.R. Espinosa, G.F. Giudice, G. Isidori et al., *Higgs mass and vacuum stability in the Standard Model at NNLO*, *JHEP* **08** (2012) 098 [1205.6497].

[106] J. Pardo Vega and G. Villadoro, *SusyHD: Higgs mass Determination in Supersymmetry*, *JHEP* **07** (2015) 159 [1504.05200].

[107] E. Bagnaschi, J. Pardo Vega and P. Slavich, *Improved determination of the Higgs mass in the MSSM with heavy superpartners*, *Eur. Phys. J. C* **77** (2017) 334 [1703.08166].

[108] R.V. Harlander, J. Klappert, A.D. Ochoa Franco and A. Voigt, *The light CP-even MSSM Higgs mass resummed to fourth logarithmic order*, *Eur. Phys. J. C* **78** (2018) 874 [1807.03509].

[109] E. Bagnaschi, G. Degrassi, S. Paßehr and P. Slavich, *Full two-loop QCD corrections to the Higgs mass in the MSSM with heavy superpartners*, *Eur. Phys. J. C* **79** (2019) 910 [1908.01670].

[110] H. Bahl, I. Sobolev and G. Weiglein, *Precise prediction for the mass of the light MSSM Higgs boson for the case of a heavy gluino*, *Phys. Lett. B* **808** (2020) 135644 [1912.10002].

[111] H. Bahl, I. Sobolev and G. Weiglein, *The light MSSM Higgs boson mass for large* $\tan\beta$ *and complex input parameters*, *Eur. Phys. J. C* **80** (2020) 1063 [2009.07572].

[112] M. Carena, J. Ellis, J.S. Lee, A. Pilaftsis and C.E.M. Wagner, *CP Violation in Heavy MSSM Higgs Scenarios*, *JHEP* **02** (2016) 123 [1512.00437].

[113] N. Murphy and H. Rzehak, *Higgs-boson masses and mixings in the MSSM with CP violation and heavy SUSY particles*, *Eur. Phys. J. C* **82** (2022) 1093 [1909.00726].

[114] M. Gorbahn, S. Jager, U. Nierste and S. Trine, *The supersymmetric Higgs sector and $B - \bar{B}$ mixing for large tan β*, *Phys. Rev. D* **84** (2011) 034030 [0901.2065].

[115] H. Bahl and W. Hollik, *Precise prediction of the MSSM Higgs boson masses for low M_A*, *JHEP* **07** (2018) 182 [1805.00867].

[116] G. Lee and C.E.M. Wagner, *Higgs bosons in heavy supersymmetry with an intermediate m_A*, *Phys. Rev. D* **92** (2015) 075032 [1508.00576].

[117] H. Bahl and I. Sobolev, *Two-loop matching of renormalizable operators: general considerations and applications*, *JHEP* **03** (2021) 286 [2010.01989].

[118] P.S. Bhupal Dev and A. Pilaftsis, *Maximally Symmetric Two Higgs Doublet Model with Natural Standard Model Alignment*, *JHEP* **12** (2014) 024 [1408.3405].

[119] A.V. Bednyakov, *On three-loop RGE for the Higgs sector of 2HDM*, *JHEP* **11** (2018) 154 [1809.04527].

[120] I. Schienbein, F. Staub, T. Steudtner and K. Svirina, *Revisiting RGEs for general gauge theories*, *Nucl. Phys. B* **939** (2019) 1 [1809.06797].

[121] J. Oredsson and J. Rathsman, *$\mathbb{Z}_2$ breaking effects in 2-loop RG evolution of 2HDM*, *JHEP* **02** (2019) 152 [1810.02588].

[122] F. Herren, L. Mihaila and M. Steinhauser, *Gauge and Yukawa coupling beta functions of two-Higgs-doublet models to three-loop order*, *Phys. Rev. D* **97** (2018) 015016 [1712.06614].

[123] E. Bagnaschi, F. Brümmer, W. Buchmüller, A. Voigt and G. Weiglein, *Vacuum stability and supersymmetry at high scales with two Higgs doublets*, *JHEP* **03** (2016) 158 [1512.07761].

[124] E. Bagnaschi et al., *Benchmark scenarios for low $\tan\beta$ in the MSSM*, .

[125] H. Bahl, S. Liebler and T. Stefaniak, *MSSM Higgs benchmark scenarios for Run 2 and beyond: the low $\tan\beta$ region*, *Eur. Phys. J. C* **79** (2019) 279 [1901.05933].

[126] K. Cheung, R. Huo, J.S. Lee and Y.-L. Sming Tsai, *Dark Matter in Split SUSY with Intermediate Higgses*, *JHEP* **04** (2015) 151 [1411.7329].

[127] T. Kwasnitza and D. Stöckinger, *Resummation of terms enhanced by trilinear squark-Higgs couplings in the MSSM*, *JHEP* **08** (2021) 070 [2103.08616].

[128] H. Bahl and W. Hollik, *Precise prediction for the light MSSM Higgs boson mass combining effective field theory and fixed-order calculations*, *Eur. Phys. J. C* **76** (2016) 499 [1608.01880].

[129] H. Bahl, S. Heinemeyer, W. Hollik and G. Weiglein, *Reconciling EFT and hybrid calculations of the light MSSM Higgs-boson mass*, *Eur. Phys. J. C* **78** (2018) 57 [1706.00346].

[130] H. Bahl, *Pole mass determination in presence of heavy particles*, *JHEP* **02** (2019) 121 [1812.06452].

[131] H. Bahl, S. Heinemeyer, W. Hollik and G. Weiglein, *Theoretical uncertainties in the MSSM Higgs boson mass calculation*, *Eur. Phys. J. C* **80** (2020) 497 [1912.04199].

[132] H. Bahl, N. Murphy and H. Rzehak, *Hybrid calculation of the MSSM Higgs boson masses using the complex THDM as EFT*, *Eur. Phys. J. C* **81** (2021) 128 [2010.04711].

[133] E. Bagnaschi et al., *MSSM Higgs Boson Searches at the LHC: Benchmark Scenarios for Run 2 and Beyond*, *Eur. Phys. J. C* **79** (2019) 617 [1808.07542].

[134] I. Sobolev, *Precise predictions for Higgs physics in supersymmetric models*, Ph.D. thesis, Hamburg U., 2020. 10.3204/PUBDB-2020-02962.

[135] P. Athron, J.-h. Park, T. Steudtner, D. Stöckinger and A. Voigt, *Precise Higgs mass calculations in (non-)minimal supersymmetry at both high and low scales*, *JHEP* **01** (2017) 079 [1609.00371].

[136] F. Staub and W. Porod, *Improved predictions for intermediate and heavy Supersymmetry in the MSSM and beyond*, *Eur. Phys. J. C* **77** (2017) 338 [1703.03267].

[137] P. Athron, M. Bach, D. Harries, T. Kwasnitza, J.-h. Park, D. Stöckinger et al., *FlexibleSUSY 2.0: Extensions to investigate the phenomenology of*

SUSY and non-SUSY models, *Comput. Phys. Commun.* **230** (2018) 145 [1710.03760].

[138] T. Kwasnitza, D. Stöckinger and A. Voigt, *Improved MSSM Higgs mass calculation using the 3-loop FlexibleEFTHiggs approach including x_t-resummation*, *JHEP* **07** (2020) 197 [2003.04639].

[139] R.V. Harlander, J. Klappert and A. Voigt, *The light CP-even MSSM Higgs mass including N^3LO+N^3LL QCD corrections*, *Eur. Phys. J. C* **80** (2020) 186 [1910.03595].

[140] P. Slavich et al., *Higgs-mass predictions in the MSSM and beyond*, *Eur. Phys. J. C* **81** (2021) 450 [2012.15629].

[141] M. Planck, *Ueber das Gesetz der Energieverteilung im Normalspectrum*, *Annalen Phys.* **4** (1901) 553.

[142] A. Einstein, *Über einen die Erzeugung und Verwandlung des Lichts betreffenden heuristischen Gesichtspunkt*, *Annalen Phys.* **17** (1905) 132.

[143] L.-V.P.R. de Broglie, *Recherches sur la théorie des quanta*, *Annals Phys.* **2** (1925) 22.

[144] A. Einstein, *Zur Elektrodynamik bewegter Körper*, *Annalen Phys.* **17** (1905) 891.

[145] A. Einstein, *Ist die Trägheit eines Körpers von seinem Energieinhalt abhängig?*, *Annalen Phys.* **18** (1905) 639.

[146] M.E. Peskin and D.V. Schroeder, *An Introduction to Quantum Field Theory*, Addison-Wesley, Reading, USA (1995).

[147] W. Pauli and F. Villars, *On the Invariant Regularization in Relativistic Quantum Theory*, *Rev. Mod. Phys.* **21** (1949) 434.

[148] A.A. Slavnov, *Invariant regularization of non-linear chiral theories*, *Nucl. Phys. B* **31** (1971) 301.

[149] G. 't Hooft and M.J.G. Veltman, *Regularization and Renormalization of Gauge Fields*, *Nucl. Phys. B* **44** (1972) 189.

[150] C. Ford and C. Wiesendanger, *Multi-scale Renormalization*, *Phys. Lett. B* **398** (1997) 342 [hep-th/9612193].

[151] D. Stöckinger, *Regularization by Dimensional Reduction: Consistency, Quantum Action Principle, and Supersymmetry*, *JHEP* **03** (2005) 076 [hep-ph/0503129].

[152] W. Siegel, *Supersymmetric Dimensional Regularization via Dimensional Reduction*, *Phys. Lett. B* **84** (1979) 193.

[153] R. Gupta, *Introduction to lattice QCD: Course*, in *Les Houches Summer School in Theoretical Physics, Session 68: Probing the Standard Model of Particle Interactions*, pp. 83–219, 7, 1997 [hep-lat/9807028].

[154] A. Einstein, *Die Grundlage der allgemeinen Relativitätstheorie*, *Annalen Phys.* **49** (1916) 769.

[155] S.W. Hawking, *Zeta Function Regularization of Path Integrals in Curved Space-Time*, *Commun. Math. Phys.* **55** (1977) 133.

[156] D. Iellici and V. Moretti, *Zeta function regularization and one loop renormalization of field fluctuations in curved space-times*, *Phys. Lett. B* **425** (1998) 33 [gr-qc/9705077].

[157] P. Athron, J.-h. Park, D. Stöckinger and A. Voigt, *FlexibleSUSY—A spectrum generator generator for supersymmetric models*, *Comput. Phys. Commun.* **190** (2015) 139 [1406.2319].

[158] M. Sperling, *Renormierung von Vakuumerwartungswerten in spontan gebrochenen Eichtheorien*, diplomarbeit, Dresden, Tech. U., 2013.

[159] J. Collins, *Foundations of perturbative QCD*, vol. 32, Cambridge University Press (11, 2013).

[160] T. Hahn, *LoopTools 2.15 User's Guide*, .

[161] S. Paßehr, *Two-Loop Corrections to the Higgs-Boson Masses in the Minimal Supersymmetric Standard Model with CP-Violation*, Ph.D. thesis, Munich, Tech. U., 2014.

[162] F.J. Dyson, *The S matrix in quantum electrodynamics*, *Phys. Rev.* **75** (1949) 1736.

[163] E. Fuchs and G. Weiglein, *Breit-Wigner approximation for propagators of mixed unstable states*, *JHEP* **09** (2017) 079 [1610.06193].

[164] A. Freitas, W. Hollik, W. Walter and G. Weiglein, *Electroweak two loop corrections to the $M_W - M_Z$ mass correlation in the standard model*, *Nucl. Phys. B* **632** (2002) 189 [hep-ph/0202131].

[165] A. Denner and S. Dittmaier, *The complex-mass scheme for perturbative calculations with unstable particles*, *Nucl. Phys. B Proc. Suppl.* **160** (2006) 22 [hep-ph/0605312].

[166] A. Denner and J.-N. Lang, *The Complex-Mass Scheme and Unitarity in perturbative Quantum Field Theory*, *Eur. Phys. J. C* **75** (2015) 377 [1406.6280].

[167] F. Domingo and S. Paßehr, *Towards Higgs masses and decay widths satisfying the symmetries in the (N)MSSM*, *Eur. Phys. J. C* **80** (2020) 1124 [2007.11010].

[168] H.A. Rzehak, *Zwei-Schleifen-Beiträge im supersymmetrischen Higgs-Sektor*, dissertation, Munich Tech. U., 6, 2005.

[169] H. Bahl, J. Braathen and G. Weiglein, *Theoretical concepts and measurement prospects for BSM trilinear couplings: a case study for scalar top quarks*, 2212.11213.

[170] R.D. Peccei and H.R. Quinn, *CP Conservation in the Presence of Instantons*, *Phys. Rev. Lett.* **38** (1977) 1440.

[171] R.D. Peccei and H.R. Quinn, *Constraints Imposed by CP Conservation in the Presence of Instantons*, *Phys. Rev. D* **16** (1977) 1791.

[172] S. Dimopoulos and S.D. Thomas, *Dynamical relaxation of the supersymmetric CP violating phases*, *Nucl. Phys. B* **465** (1996) 23 [hep-ph/9510220].

[173] M. Drees, R.M. Godbole and P. Roy, *Theory and Phenomenology of Sparticles: An account of four-dimensional N=1 supersymmetry in High Energy Physics*, World Scientific Publishing Co. Pte. Ltd. (2004).

[174] G. Weiglein, R. Scharf and M. Böhm, *Reduction of general two loop selfenergies to standard scalar integrals*, *Nucl. Phys. B* **416** (1994) 606 [hep-ph/9310358].

[175] A. Denner, *Techniques for calculation of electroweak radiative corrections at the one loop level and results for W physics at LEP-200*, *Fortsch. Phys.* **41** (1993) 307 [0709.1075].

[176] S. Eidelman and F. Jegerlehner, *Hadronic contributions to g-2 of the leptons and to the effective fine structure constant alpha (M(z)**2)*, *Z. Phys. C* **67** (1995) 585 [hep-ph/9502298].

[177] A. Bharucha, A. Fowler, G. Moortgat-Pick and G. Weiglein, *Consistent on shell renormalisation of electroweakinos in the complex MSSM: LHC and LC predictions*, *JHEP* **05** (2013) 053 [1211.3134].

[178] G. Degrassi, P. Gambino and P.P. Giardino, *The $m_W - m_z$ interdependence in the Standard Model: a new scrutiny*, *JHEP* **05** (2015) 154 [1411.7040].

[179] S. Bauberger, *Two-loop contributions to muon decay*, Ph.D. thesis, Würzburg U., 1997.

[180] M. Awramik, M. Czakon, A. Onishchenko and O. Veretin, *Bosonic corrections to Delta r at the two loop level*, *Phys. Rev. D* **68** (2003) 053004 [hep-ph/0209084].

[181] S. Dittmaier, *Electric charge renormalization to all orders*, *Phys. Rev. D* **103** (2021) 053006 [2101.05154].

[182] S. Hessenberger, *Two-loop corrections to electroweak precision observables in Two-Higgs-Doublet-Models*, Ph.D. thesis, Munich, Tech. U., 2018.

[183] A. Freitas and D. Stöckinger, *Gauge dependence and renormalization of tan beta*, in *10th International Conference on Supersymmetry and Unification of Fundamental Interactions (SUSY02)*, pp. 657–661, 10, 2002 [hep-ph/0210372].

[184] A. Freitas and D. Stöckinger, *Gauge dependence and renormalization of tan beta in the MSSM*, *Phys. Rev. D* **66** (2002) 095014 [hep-ph/0205281].

[185] N. Baro, F. Boudjema and A. Semenov, *Automatised full one-loop renormalisation of the MSSM. I. The Higgs sector, the issue of tan(beta) and gauge invariance*, *Phys. Rev. D* **78** (2008) 115003 [0807.4668].

[186] L.-H. Wan, W.-G. Ma, R.-Y. Zhang and Y. Jiang, *Electroweak corrections to the charged Higgs boson decay into chargino and neutralino*, *Phys. Rev. D* **64** (2001) 115004 [hep-ph/0107089].

[187] M. Frank, S. Heinemeyer, W. Hollik and G. Weiglein, *FeynHiggs1.2: Hybrid MS-bar / on-shell renormalization for the CP even Higgs boson sector in the MSSM*, hep-ph/0202166.

[188] H. Bahl, J. Braathen and G. Weiglein, *External leg corrections as an origin of large logarithms*, *JHEP* **02** (2022) 159 [2112.11419].

[189] J. Küblbeck, M. Böhm and A. Denner, *Feyn Arts: Computer Algebraic Generation of Feynman Graphs and Amplitudes*, *Comput. Phys. Commun.* **60** (1990) 165.

[190] T. Hahn, *Generating Feynman diagrams and amplitudes with FeynArts 3*, *Comput. Phys. Commun.* **140** (2001) 418 [hep-ph/0012260].

[191] T. Hahn and M. Perez-Victoria, *Automatized one loop calculations in four-dimensions and D-dimensions*, *Comput. Phys. Commun.* **118** (1999) 153 [hep-ph/9807565].

[192] T. Hahn, S. Paßehr and C. Schappacher, *FormCalc 9 and Extensions*, *PoS* **LL2016** (2016) 068 [1604.04611].

[193] G. Weiglein, R. Mertig, R. Scharf and M. Böhm, *Computer algebraic calculation of two loop selfenergies in the electroweak standard model*, in *2nd International Workshop on Software Engineering, Artificial Intelligence and Expert Systems for High-energy and Nuclear Physics*, 5, 1995.

[194] S. Heinemeyer, W. Hollik and G. Weiglein, *FeynHiggs: A Program for the calculation of the masses of the neutral CP even Higgs bosons in the MSSM*, *Comput. Phys. Commun.* **124** (2000) 76 [hep-ph/9812320].

[195] T. Hahn, S. Heinemeyer, W. Hollik, H. Rzehak and G. Weiglein, *FeynHiggs: A program for the calculation of MSSM Higgs-boson observables - Version 2.6.5*, *Comput. Phys. Commun.* **180** (2009) 1426.

[196] H. Bahl, T. Hahn, S. Heinemeyer, W. Hollik, S. Paßehr, H. Rzehak et al., *Precision calculations in the MSSM Higgs-boson sector with FeynHiggs 2.14*, *Comput. Phys. Commun.* **249** (2020) 107099 [1811.09073].

[197] M.D. Schwartz, *Quantum Field Theory and the Standard Model*, Cambridge University Press (3, 2014).

[198] K.E. Williams, H. Rzehak and G. Weiglein, *Higher order corrections to Higgs boson decays in the MSSM with complex parameters*, *Eur. Phys. J. C* **71** (2011) 1669 [1103.1335].

[199] A. Pilaftsis, *CP odd tadpole renormalization of Higgs scalar - pseudoscalar mixing*, *Phys. Rev. D* **58** (1998) 096010 [hep-ph/9803297].

[200] H.E. Haber, *The Status of the minimal supersymmetric standard model and beyond*, *Nucl. Phys. B Proc. Suppl.* **62** (1998) 469 [hep-ph/9709450].

[201] Particle Data Group collaboration, *Review of Particle Physics*, *PTEP* **2020** (2020) 083C01.

[202] M. Steinhauser, *Leptonic contribution to the effective electromagnetic coupling constant up to three loops*, *Phys. Lett. B* **429** (1998) 158 [hep-ph/9803313].

[203] U. Langenfeld, S. Moch and P. Uwer, *Measuring the running top-quark mass*, *Phys. Rev. D* **80** (2009) 054009 [0906.5273].

[204] B.A. Kniehl and O.L. Veretin, *Low-mass Higgs decays to four leptons at one loop and beyond*, *Phys. Rev. D* **86** (2012) 053007 [1206.7110].

[205] F. Jegerlehner, M.Y. Kalmykov and B.A. Kniehl, *On the difference between the pole and the $\overline{MS}$ masses of the top quark at the electroweak scale*, *Phys. Lett. B* **722** (2013) 123 [1212.4319].

[206] D. Meuser and A. Voigt, *Investigating multiple solutions to boundary value problems in constrained minimal and non-minimal SUSY models*, *Eur. Phys. J. C* **79** (2019) 821 [1907.07686].

[207] A. Dabelstein, *Fermionic decays of neutral MSSM Higgs bosons at the one loop level*, *Nucl. Phys. B* **456** (1995) 25 [hep-ph/9503443].

[208] H.E. Logan and S.-f. Su, *Associated Production of $H^{\pm}$ and $W^{\mp}$ in High-Energy e^+e^- Collisions in the Minimal Supersymmetric Standard Model*, *Phys. Rev. D* **66** (2002) 035001 [hep-ph/0203270].

Eidesstattliche Versicherung / Declaration on oath

Hiermit versichere ich an Eides statt, die vorliegende Dissertationsschrift selbst verfasst und keine anderen als die angegebenen Hilfsmittel und Quellen benutzt zu haben.

Hamburg, den 12. Juli 2023

Unterschrift der Doktorandin / des Doktoranden